NASA CR-121022

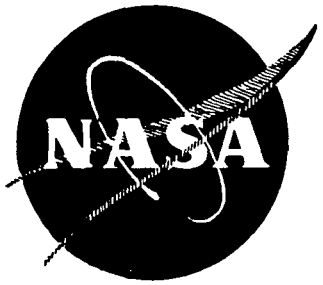

FINAL REPORT

Development Of Fused Slurry Silicide Coatings For Tantalum Re-Entry Heat Shields

by

R. V. Warnock and A. R. Stetson

SOLAR DIVISION OF INTERNATIONAL HARVESTER COMPANY

SAN DIEGO, CALIFORNIA

September 1972

prepared for

NATIONAL AERONAUTICS AND SPACE ADMINISTRATION

NASA LEWIS RESEARCH CENTER

CONTRACT NAS3-14315

John P. Merutka, Project Manager

NOTICE

This report was prepared as an account of government-sponsored work. Neither the United States, nor the National Aeronautics and Space Administration (NASA), nor any person acting on behalf of NASA:

A.) Makes any warranty or representation, expressed or implied, with respect to the accuracy, completeness, or usefulness of the information contained in this report, or that the use of any information, apparatus, method, or process disclosed in this report may not infringe privately owned rights; or

B.) Assumes any liabilities with respect to the use of, or for damages resulting from the use of any information, apparatus, method or process disclosed in this report.

As used above, "person acting on behalf of NASA" includes any employee or contractor of NASA, or employee of such contractor, to the extent that such employee or contractor of NASA, or employee of such contractor prepares, disseminates, or provides access to, any information pursuant to his employment or contract with NASA, or his employment with such contractor.

1. Report No.	2. Government Accession No.	3. Recipient's Catalog No.
CR-121022		

4. Title and Subtitle	5. Report Date
DEVELOPMENT OF FUSED SLURRY SILICIDE COATINGS FOR TANTALUM RE-ENTRY HEAT SHIELDS	September 21, 1972
	6. Performing Organization Code

7. Author(s)	8. Performing Organization Report No.
R. V. Warnock and A. R. Stetson	RDR-1685-7
	10. Work Unit No.

9. Performing Organization Name and Address	11. Contract or Grant No.
Solar Division of International Harvester Company 2200 Pacific Highway San Diego, California 92138	NAS3-14315
	13. Type of Report and Period Covered
12. Sponsoring Agency Name and Address	Contractor Report
National Aeronautics and Space Administration Washington, D.C. 20546	14. Sponsoring Agency Code

15. Supplementary Notes

Project Manager, John P. Merutka, NASA Lewis Research Center, Cleveland, Ohio

16. Abstract

A fused slurry silicide coating was developed to provide atmospheric re-entry protection for the 90Ta-10W alloy. Overlaying the silicide with a highly refractory glass greatly improved total lifetime and reliability of the coating system. Low-pressure, slow-cycle lifetimes in excess of 100 cycles were consistently recorded for 1700°K - 13 and 1300 N/m^2 test conditions. A minimum of 25 cycles was obtained for 1810°K - 1300 N/m^2 conditions. About 50 simulated re-entry cycles (variable temperature, pressure and stress) were endured by coated 1-inch x 4-inch miniature heat shield panels when exposed to a maximum of 1700°K and either internal or external pressure conditions.

17. Key Words (Suggested by Author(s))	18. Distribution Statement
Oxidation resistant coatings Tantalum alloys Fused slurry silicide coatings Heat shields	Unclassified - unlimited

19. Security Classif. (of this report)	20. Security Classif. (of this page)	21. No. of Pages	22. Price*
Unclassified	Unclassified	178	$3.00

* For sale by the National Technical Information Service, Springfield, Virginia 22151

FOREWORD

This is the Final Technical Report on NASA-Lewis Research Center Contract NAS3-14315 and covers all experimental work performed on the program.

This contract was initiated between NASA-Lewis Research Center and the Solar Division of International Harvester Company for the development of fused slurry silicide coatings for 90Ta-10W alloy. Responsible Solar personnel were Mr. Richard V. Warnock, principal investigator, and Mr. Alvin R. Stetson, technical program director. Mr. John P. Merutka of NASA-Lewis served as Project Manager.

Solar's internal report number is RDR 1685-7.

ABSTRACT

A fused slurry silicide coating was developed to provide atmospheric re-entry protection for the 90Ta-10W alloy. Overlaying the silicide with a highly refractory glass greatly improved total lifetime and reliability of the coating system. Low-pressure, slow-cycle lifetimes in excess of 100 cycles were consistently recorded for 1700° F - 13 and 1300 N/m^2 test conditions. A minimum of 25 cycles was obtained for 1810° K - 1300 N/m^2 conditions. About 50 simulated re-entry cycles (variable temperature, pressure and stress) were endured by coated 1-inch x 4-inch miniature heat shield panels when exposed to a maximum of 1700° K and either internal or external pressure conditions.

CONTENTS

Page Intentionally Left Blank

ILLUSTRATIONS

ILLUSTRATIONS (Cont)

ILLUSTRATIONS (Cont)

ILLUSTRATIONS (Cont)

ILLUSTRATIONS (Cont)

TABLES

TABLES (Cont)

TABLES (Cont)

1

SUMMARY

Development of improved fused slurry silicide coatings for tantalum alloys was the basic program goal.

A complex slurry (Si-20Ti-10Cr-4Mo-4W-2V) was developed yielding a coating which performed well when low-pressure, slow-cycle oxidation tested at 1700°K - 13 N/m^2, 1700°K - 1300 N/m^2 and 1810°K - 1300 N/m^2.

Development and application of a highly refractory and stable glass overlay for the silicide resulted in a coating system which never experienced a failure when exposed for up to 100 cycles to 1700°K and 13 or 1300 N/m^2. Better performance from the plain silicide than from the glass overlaid silicide was observed when tested at 1810°K and 1300 N/m^2. Twenty-four to 63 cycle lifetimes were recorded for the silicide coating, while the vitreous overlaid system survived a maximum of about 30 such cycles.

Exposure of intentionally defected samples was employed to ascertain the effects on the substrate of coating damage. Vitreous overlaid coupons performed significantly better than coupons with only the silicide layer.

Simulated atmospheric re-entry exposure of miniature heat shield panels was performed to 1700°K using either an internal or external pressure profile. Stress levels which resulted in panel deformation were found to accelerate coating degradation.

Mechanical properties of the substrate were retained or slightly increased after low-pressure, slow-cycle testing. Microhardness values for the substrate showed only small increases with increased exposure times for each set of test conditions. A ductile-brittle bend transition temperature of 200°K or lower was determined for low-pressure, slow-cycle exposed specimens.

At the initiation of this program, state-of-the-art fused slurry silicide coatings for tantalum alloys could survive from zero to 10 low pressure, slow cycles to any of the conditions employed throughout this program.

2

INTRODUCTION

Various methods including pack, fluidized bed, fused salt electrodeposition, sintered slurry and fused slurry have been studied as means of applying simple and complex silicides to tantalum alloys. Pack siliciding was extensively investigated and yielded the best first generation coatings. Control of coating composition and difficulty of process scaleup caused this technique to be largely abandoned. The slurry applied, sintered modifier plus pack siliciding approach has yielded longer lifetimes than any other known system. Application was by the vacuum sintering of tungsten, molybdenum, titanium and vanadium powders and subsequent pack siliciding. Protection for greater than 1000 hours at 1590°K and atmospheric pressure (Ref. 1) and for 100 plus cycles to 1810°K (50 hours at 1810°K) and 1300 N/m^2 pressure have been recorded.

The fused slurry application method employs various silicon-metal eutectics to promote melting during application and yields coatings which necessarily contain some dissolved substrate material. Overall coating composition is not as well controlled as for the sintered slurry case; however better edge, faying surface, and internal surface coverage can be obtained with current application techniques. Lives in excess of 150 hours at 1366°K and "hours" at 1920°K have been reported for the Si-20Ti-10Mo (R512C) coating on tantalum alloys (Ref. 2,3). Outstanding performance by fused slurry silicides on columbium alloys has been obtained in very recent work (Ref. 4).

The tantalum alloy, 90Ta-10W, may in the future be used in the fabrication of those areas of a reusable space shuttle vehicle which will experience temperatures to about 1800°K. The objective of this program was to develop fusion silicide-type coatings for high-temperature protection of fabricated panels and to determine that these coatings would afford protection from a re-entry environment for a minimum of 100 cycles.

The fused slurry method for the application of the coating was selected because experimental work had shown that this type of coating provides the most reliable coverage of edges and internal and faying surfaces. Available coatings have not proven adequate to the requirements for the space shuttle. This program, therefore, aimed at improving the current technology by providing modified slurries that would approach the protective properties of previously developed sintered coatings while maintaining the good flow characteristics of the fused slurry coatings.

Two approaches were investigated in the development of improved fusion coating systems. The first concept (SA series) utilized silicon-metal eutectics to dissolve various amounts of tungsten, molybdenum and vanadium. The second approach (DAM series) investigated employed a duplex processing cycle. The initially applide coating relied on iron-molybdenum and iron-tungsten minimum melting points to provide flow. Once the silicon-free modifier alloy had been fused onto the surface, a fusion silicide coating (DAS series) was applied to convert the modifier alloy to a complex silicide.

The program was divided into six tasks as shown below:

- Task I - Coating Composition Development
- Task II - Re-Entry Simulation Testing
- Task III - Coating Improvement
- Task IV - Reporting
- Task V - Vitreous Overlay Study
- Task VI - Plasma Tunnel Test Specimens

Task I included extensive low-pressure, slow-cycle (LP-SC) testing to 1700 and 1810°K. Two coatings were selected from Tasks I, III or V for use in Task II. Re-entry testing in Task II employed a miniature heat shield specimen and included the simultaneous variation of temperature, pressure, and stress levels. Improved coating compositions were to be developed in Task III. Evaluation was by low-pressure (13 N/m^2 and 1300 N/m^2), slow-cycle testing, re-entry cycle exposure, and bend and tensile testing. Creep testing and emittance measurements completed the task. Task V developed very stable, viscous and high-melting glasses for application over previously developed fusion silicide coatings. This concept was also evaluated with the aid of low-pressure, slow-cycle testing. Fabrication and coating of specimens for plasma arc tunnel testing was the only activity in Task VI.

Many of the dimensions and units used in this report conform to the International System of Units as adopted by NASA. A number of conversion factors between this and the more commonly used systems of units are noted below:

UNIT CONVERSIONS

	S. I.	Common
Linear Distance	25.4×10^{-6} m	0.001 inch
Angular Measurement	1 radian	57.4 degrees
Temperature	1700°K	2600°F
	1810°K	2800°F
Pressure	1300 N/m^2	10 mm Hg
	13 N/m^2	0.1 mm Hg
	1.3×10^{-2} N/m^2	10^{-4} mm Hg
Weight/Thickness	1 kg/m^2	100 mg/cm^2
Tensile Strength	6.89 MN/m^2	1 ksi

3

EXPERIMENTAL

3.1 COATING DEVELOPMENT

All materials, equipment and experimental activities are described in this section.

3.1.1 Coating Compositions

The initial selection of single-step (SA) coating compositions was based on the near eutectic Si-20Ti and Si-20Fe binaries and the low-melting Si-20Cr-10Ti ternary system. Double-cycle alloy coatings (DAM) were related to minimum melting compositions in the Fe-Mo and Fe-W systems. Systematic modification of these starting systems with additional quantities of Mo, Ti, V and W was effected to yield more refractory final compositions. Siliciding agents (DAS) for the Mo and W based alloy coatings (DAM) were selected for their relatively low melting temperatures. Table I shows all original coating compositions investigated for applicability. The SA-1 composition is equivalent to the R512C* coating and was to serve as the baseline coating throughout the program.

3.1.2 Materials

Tantalum-10 tungsten alloy was specified by NASA-Lewis Research Center for use throughout the program. Two heats of the nominally 3.3×10^{-4} meter thick alloy were purchased from the Wah Chang Albany Corporation. Vendor-supplied analytical data for each heat number are shown in Tables II and III. All specimens used in Tasks I, V, VI and for miniature heat shield fabrication used material from heat number 620053. Tensile test coupons used in Task III employed material from heat number 630034. Figure 1 shows the typical appearance of the as-received alloy.

Chemicals used throughout the program are listed in Table IV together with the supplier and pertinent analytical data.

---

*Originally developed by the High Temperature Composites Laboratory of GTE Sylvania, now known as HiTemCo, a wholly owned subsidiary of DeWiant Corp.

TABLE I

COATING COMPOSITIONS FOR EVALUATION

Coating	Composition (w/o)
SA-1	Si-20Ti-10Mo
SA-2	Si-20Fe-10Mo
SA-3	Si-20Fe-4Mo-4W-2V
SA-4	Si-20Fe-7Mo-7W-3V
SA-5	Si-20Fe-10Mo-10W-5V-5Ti
SA-6	Si-20Cr-10Ti-10Mo
SA-7	Si-20Cr-10Ti-10Mo-4V
SA-8	Si-20Cr-10Ti-16W-4V
SA-9	Si-20Cr-10Ti-10Mo-10W-5V
SA-10	Si-20Ti-4Mo-4W-2V
SA-11	Si-20Ti-7Mo-7W-3V
SA-12	Si-20Ti-10Mo-10W-5V
DAM-1	Fe-40Mo-3Ti-3V
DAM-2	Fe-40Mo-6Ti-6V
DAM-3	Fe-30W-3Ti-3V
DAM-4	Fe-30W-6Ti-6V
DAM-5	Fe-30Mo-10W-6Ti-6V
DAM-6	Fe-20Mo-15W-6Ti-6V
DAM-7	Fe-30Mo-10W-3Ti-3V
DAM-8	Fe-20Mo-15W-3Ti-3V
DAS-1	Pure Si
DAS-2	Si-20Fe
DAS-3	Si-20Cr-5Ti
DAS-4	Si-20Cr-20Fe

TABLE II

HEAT ANALYSIS
Ta-10W INGOT 620053

Composition in Percent		
	Top	Bottom
W	9.2	9.8
Ta	Balance	
Impurity Content, ppm		
Al	<20	<20
C	40	30
Cb	400	250
Fe	<40	<40
H	4.2	4.1
Hf	<500	<500
Mg	<20	<20
Mn	<20	<20
Mo	<20	<20
N	6	9
Ni	<20	<20
O	<50	<50
Pb	<20	<20
Si	<40	<40
Ti	<50	<50
V	<20	<20
Zr	<500	<500
Cr	<20	<20
Cu	<40	<40
Hardness in BHN		
Range	183-200	
Average	192	

TABLE III

HEAT ANALYSIS, Ta-10W INGOT 630034

Ingot Chemistry
Composition in Percent

	Top	Bottom
W	9.0	10.0
Ta	Balance	

Impurity Content, ppm

	Top	Bottom
C	<30	<30
Cb	600	560
Fe	<40	<40
H	1.7	1.7
Mo	<20	<20
N	22	20
Ni	<20	<20
O	<50	<50

Product Analysis, ppm

	Sample #1	Sample #2
H	<1.0	<1.0
Q	<50	<50
N	30	15

ASTM Grain Size

Sample	Average
Top Long	8.5
Bottom Long	8.5
Top Rolling Plane	8.0
Bottom Rolling Plane	8.0

Bend Test Results at R.T.

1T Radius
Sample #1 - dye penetrant inspection of bend area showed no cracking.
Sample #2 - dye penetrant inspection of bend area showed no cracking.

Tensile Test Results at R.T.

Sample #1	Ultimate Tensile Strength, psi	Yield Strength 0.2% Offset	Elongation In Percent
Trans 1	93,600	81,000 psi	21.0
Trans 2	94,000	81,300 psi	22.0

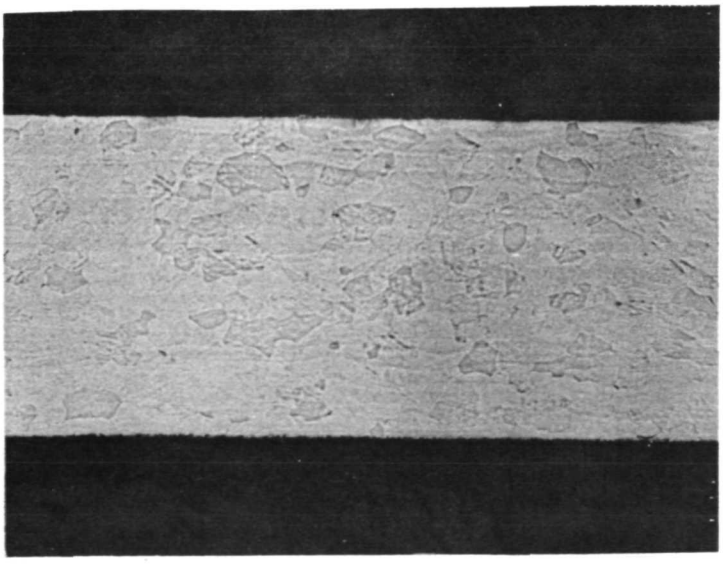

90Ta-10W Alloy

Etchant: Lactic-HF-HNO_3

Magnification: 125X

Rolling direction is perpendicular to plane of paper.

FIGURE 1. AS-RECEIVED 90Ta-10W ALLOY

TABLE IV

COATING MATERIALS, SOURCES AND ANALYSIS

Material	Supplier	Grade or Lot No.	Solar Analysis Oxygen (w/o)	Vendor Analysis Oxygen (w/o)
Al_2O_3	Alcoa	A-14	--	--
$BaCO_3$	Baker	Reagent	--	--
B_2O_3	Pacific Coast Borax Co.	Tech.	--	--
$CaCO_3$	Baker	Reagent	--	--
Cr powder	Union Carbide	128-P4G	--	0.5 to 1.0
Cr_2O_3	McGean Chemical	Ceramic	--	--
Fe powder	Glidden	26186	0.08, 0.18	--
$MgCO_3$	Baker	Reagent	--	--
Mo powder	General Electric	ID70-3-81	0.09, 0.10	0.15
Si powder	Foote Mineral	710	--	--
SiO_2	Ottawa Silica Co.	390-SIL-CO-SIL	--	--
Fused SiO_2	Thermo Materials Corporation	Glasrock Foam No. 25	--	--
$SrCO_3$	Baker	Reagent	--	--
Ti sponge	OMC	IT6240-H440	0.06	0.05
V chips	Atomergic	C4465	0.15	0.16
W powder	General Electric	U4.5-7750	0.066	0.038
Xylene		Technical	--	--
Ethylcellulose		N-200	--	--
MPA-60	Baker Castor Oil	--	--	--

Past experience has shown it best to introduce both titanium and vanadium into slurry coatings as the respective hydrides. This approach decreases both the possibility of the finely divided metal powders becoming oxidized during handling in air and eases the difficulty of comminution. Hydriding runs were performed to convert the titanium sponge and vanadium chips to their respective hydride powders. Techniques developed during a previous NASA sponsored program were employed (Ref. 1).

3.1.3 Slurry and Specimen Preparation

Coating slurries were prepared by mixing together 0.5 kg of coating powders and sufficient vehicle to yield a 2.5 to 1 liquid to solids volume ratio. The vehicle used for all slurries was prepared by dissolving 0.025 kg of ethyl cellulose in 1×10^{-3} m^3 of xylene. Each slurry was ball milled for 3600 seconds in a grinding jar and was subsequently stored in a sealed glass bottle. Application to all flat test specimens was by spraying.

Test coupons were prepared by shearing, drilling, machining and numbering. Completed specimens were radiused by exposing in a vibratory finisher for 6×10^4 seconds. Grit blasting and cleaning in acetone immediately preceded weighing and spray coating.

3.1.4 Initial Firing and Flow Tests

SA Series Coatings

Twelve SA-series slurries were prepared as described above, applied to ten 0.0127 x 0.0254 x 0.00033 meter coupons each and fired for 3600 seconds at 1.3×10^{-2} N/m^2 and temperatures of 1625 and 1875°K. Table V contains numerical data for these coupons, and Figure 2 shows the range of appearances encountered.

Three of the Si-Fe based coatings (SA-2,3,4) exhibited satisfactory flow when fired at 1625 and 1692°K. Higher firing temperatures yielded very rough and generally unsatisfactory coatings. The highly modified Si-Fe based SA-5 fired well up to 1753°K. Silicon-titanium-chromium based coatings (SA-6,7,8,9) showed generally poor flow characteristics. Only SA-6 flowed well when fired at either 1818 or 1875°K. The other three coatings (SA-7,8,9) showed either partial or no coating flow. The control coating (SA-1) and SA-10, 11 and 12 were all derived from the Si-Ti system. SA-1 appeared to flow satisfactorily when fired at 1750, 1818 and 1875°K. Of the SA-10, 11 and 12 group, only SA-10 flowed sufficiently well to warrant further investigation.

Coating weight losses during firing were determined for most systems and are included in Table V. All coating systems showed increased weight losses with increased firing temperatures. Weight change data for SA-1, 10, 11 and 12 indicate about a 20 percent loss at 1750°K, about a 30 percent loss at 1818°K, and about a 40 percent loss at 1875°K. Silicon vaporization probably accounted for essentially all of the weight loss experienced by these four Si-Ti eutectic based coatings. On this assumption, insufficient silicon would remain after firing for 1 hour at 1875°K to have converted the modifier elements to the disilicides. Since some substrate was observed to be consumed, only M_5Si_3 or lower type silicides would be present.

Little weight loss data during firing were accumulated for the Si-Fe eutectic based coatings (SA-2,3,4 and 5). The volatility of iron and silicon is similar; it is, therefore, incorrect to assume that weight losses are due to silicon volatility alone. Excessive vaporization and interdiffusion of silicon would again lead to formation of the less desirable lower silicides, i.e., M_5Si_3 and MSi.

Losses during firing appear highest for Si-20Cr-10Ti based coatings (SA-6,7, 8 and 9). This is probably explained by the fact that chromium is the most volatile element included in the SA type coatings. Weight losses ranged from about 28 percent for 1750°K through nearly 50 percent for 1 hour 1875°K firing of these coatings.

TABLE V

FIRING CHARACTERISTICS OF SA SERIES COATINGS

Coating	Temp. (°K)	Weight Loss (%)	Comments
SA-1	1625	ND	No flow, loose powder
(Si-20Ti-10Mo)	1692	4	Some flow, segregated
	1753	15, 26	Fair flow, smooth
	1818	22	Fair flow, smooth, easily scratched
	1875	ND	Flowed, smooth, easily scratched
SA-2	1625	ND	Flowed, smooth
(Si-20Fe-10Mo)	1692	ND	Flowed, smooth
	1753	ND	Flowed, porous
	1818	ND	Flowed, rough
	1875	ND	Flowed, very rough
SA-3	1625	ND	Flowed, slightly rough surface
(Si-20Fe-4Mo-4W-2V)	1692	ND	Flowed, slightly rough surface
	1753	ND	Reacted, very rough surface
	1818	ND	Reacted, very rough surface
	1875	ND	Reacted, very rough surface
SA-4	1625	ND	Flowed, slightly rough surface
(Si-20Fe-7Mo-7W-3V)	1692	ND	Good flow, some porosity
	1753	ND	Flowed, rough surface
	1818	ND	Flowed, rough surface
	1875	ND	Reacted, very rough surface
SA-5	1753	15, 24	Good flow, slight roughness
(Si-20Fe-10Mo-10W-5V-5Ti)	1794	11	Fair flow, rough surface
SA-6	1750	27	Some flow, rough surface
(Si-20Cr-10Ti-10Mo)	1818	46, 38	Flowed, slightly rough surface
	1875	47	Flowed, slightly rough surface
SA-7	1750	26	Sintered powder
(Si-20Cr-10Ti-10Mo-4V)	1818	42	Some flow, some sintered powder
	1875	53	Some flow, some loose powder
SA-8	1750	30	Some flow, some loose powder
(Si-20Cr-10Ti-16W-4V)	1818	47	Some flow, some loose powder
	1875	49	Some flow, some loose powder
SA-9	1750	29	No flow, loose powder
(Si-20Cr-10Ti-10Mo-10W-5V)	1818	48	No flow, loose powder
	1875	48	No flow, loose powder
SA-10	1750	6	Some flow, rough, easily scratched
(Si-20Ti-4Mo-4W-2V)	1818	31, 40	Some flow, rough
	1875	47	Flowed, slightly rough surface
SA-11	1750	16	Some flow, some loose powder
(Si-20Ti-7Mo-7W-3V)	1818	30	Some flow, some loose powder
	1875	40	Some flow, some sintered powder
SA-12	1750	20	No flow, loose powder
(Si-20Ti-10Mo-10W-5V)	1818	33	No flow, loose powder
	1875	40	No flow, loose powder

ND - Not Determined

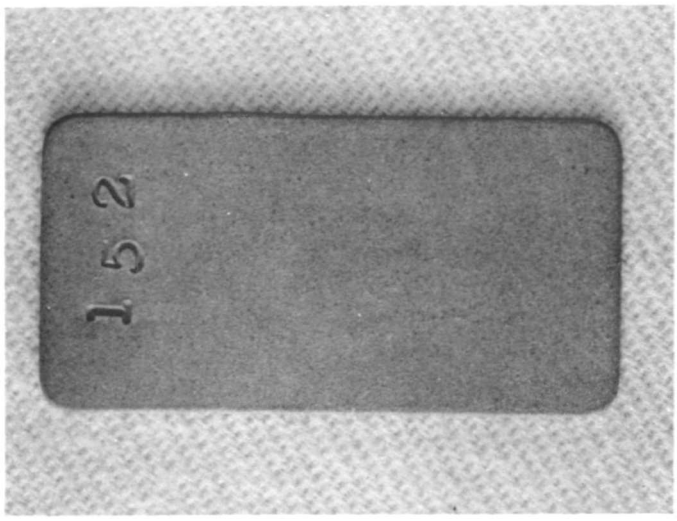

Part A

Excellent Flow

SA-3, 3600 Seconds, 1692°K

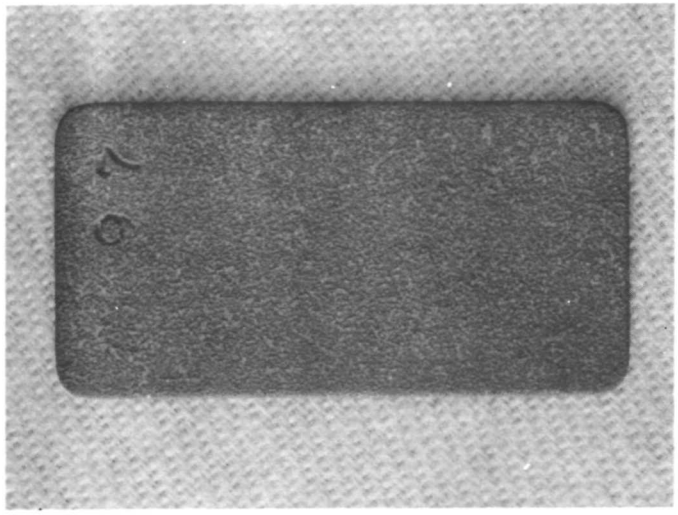

Magnification: 3X

Part B

Fair Flow

SA-1, 3600 Seconds, 1692°K

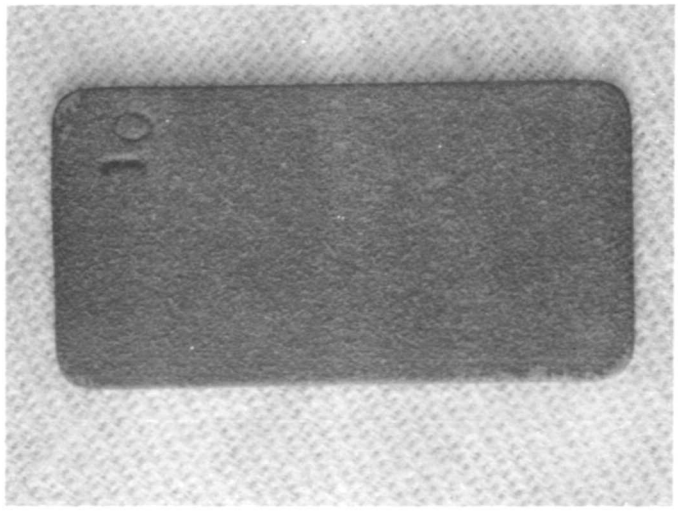

Part C

No Flow

SA-12, 3600 Seconds, 1818°K

FIGURE 2. SURFACE APPEARANCE OF FIRED COATINGS SHOWING EXCELLENT (A), FAIR (B) AND POOR (C) FLOW

It is probable that greater than 50 percent of these weight losses are accounted for by chromium vaporization. Significant amounts of silicon are also expected to have been lost and to have reduced the quantity of disilicides possibly present in the final composition.

The above data and calculated results suggested that shortened firing cycles might yield potentially more protective coatings while still maintaining adequate flow characteristics.

Short-time firing runs were conducted with selected SA series coatings (one from each basic group). Resultant data are shown in Table VI. Comparison of these data with those reported in Table V indicates that the 300-second firing cycles reduced the weight loss for each basic coating type by about 50 percent over that which was experienced during a 3600-second run. The 900-second firing cycles also decreased the weight loss experienced by the SA-6 and 10 coating types.

TABLE VI

WEIGHT LOSS DATA FOR SHORT-TIME FIRING OF SA COATINGS

Coating	Firing Time (seconds)	Temperature (°K)	Pressure (N/m^2)	Weight Loss (%)
SA-6	900	1865	1.3×10^{-2}	27
SA-10	900	1865	1.3×10^{-2}	38
SA-4	300	1675	1.3×10^{-2}	16
SA-6	300	1810	1.3×10^{-2}	18
SA-10	300	1810	1.3×10^{-2}	19

Figure 3 shows the structure of the SA-4, 6 and 10 coatings after firing for 300 seconds. The structure of SA-4 appeared less well developed when fired for 300 seconds than when fired for 3600 seconds. Both SA-6 and 10 exhibited typical fused slurry silicide structures and did not appear less well developed when fired for 300 seconds than for 3600 seconds. Decreasing the firing times yielded a thinner "diffusion zone" just above the substrate.

Another Si-20Cr-10Ti based SA-type coating was prepared at the request of the NASA project manager in order to better determine the influence of a 10 percent molybdenum versus a 4Mo-4W-2V addition to a basic SA-series system. The new coating was designated SA-13 and had the composition Si-20Cr-10Ti-4Mo-4W-2V.

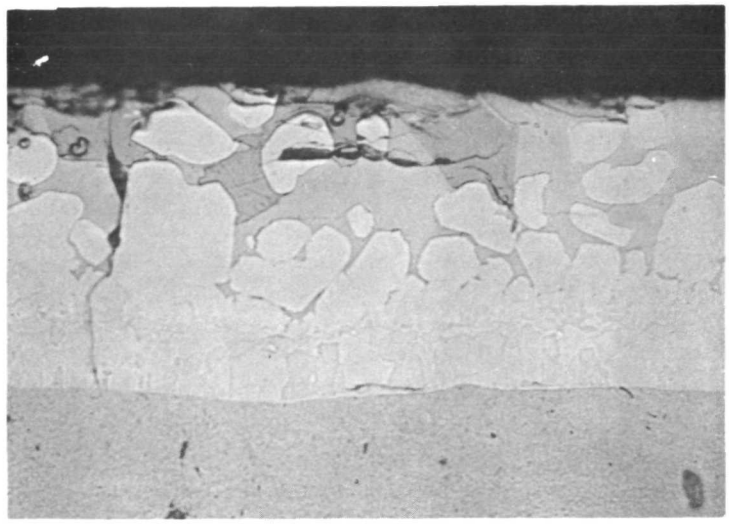

A

SA-4

1675° K - 1.3 x 10^{-2} N/m^2

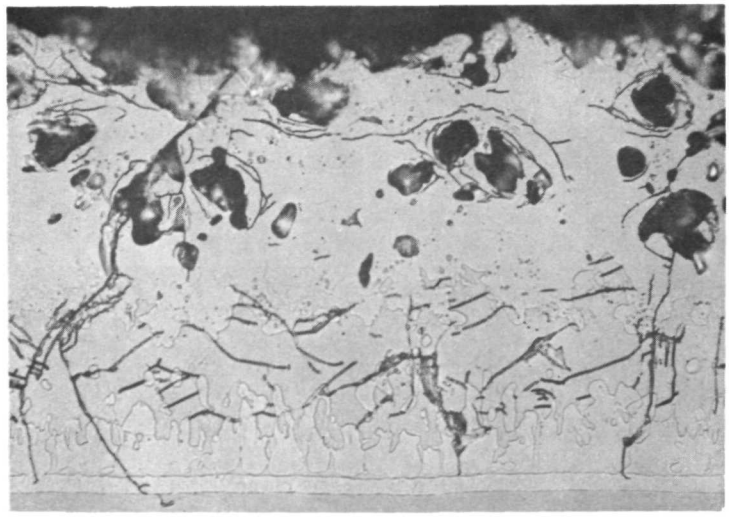

B

SA-6

1810° K - 1.3 x 10^{-2} N/m^2

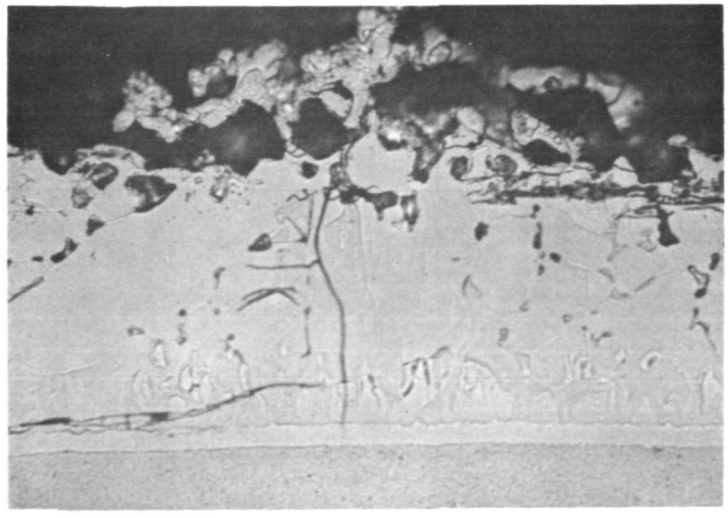

C

SA-10

1810° K - 1.3 x 10^{-2} N/m^2

Etchant: Lactic-HF-HNO_3

Magnification: 500X

FIGURE 3. MICROSTRUCTURE OF SA-4(A), SA-6(B) AND SA-10(C) AFTER 300-SECOND FIRINGS

Firing for 300 seconds at 1810°K and 1.3×10^{-2} N/m^2 (same cycle as SA-6) yielded good coating flow and a weight loss during firing of 16 percent.

Seven SA-series coatings were recommended to NASA for the initial low-pressure, slow-cycle oxidation screening test. Selected coatings and processing cycles are shown in Table VII.

TABLE VII

NASA APPROVED SA SERIES COATINGS AND APPLICATION CYCLES

Coating	Firing Cycle
SA-1 (Si-20Ti-10Mo)	Sylvania Supplied
SA-2 (Si-20Fe-10Mo)	300 s - 1675°K - 1.3×10^{-2} N/m^2
SA-3 (Si-20Fe-4Mo-4W-2V)	300 s - 1675°K - 1.3×10^{-2} N/m^2
SA-5 (Si-20Fe-10Mo-10W-5V-5Ti)	300 s - 1755°K - 1.3×10^{-2} N/m^2
SA-6 (Si-20Cr-10Ti-10Mo)	300 s - 1810°K - 1.3×10^{-2} N/m^2
SA-10 (Si-20Ti-4Mo-4W-2V)	300 s - 1810°K - 1.3×10^{-2} N/m^2
SA-13 (Si-20Cr-10Ti-4Mo-4W-2V)	300 s - 1810°K - 1.3×10^{-2} N/m^2

DAM Series Coatings

Eight coupons were spray coated with each DAM-type coating and were fired for 3600 seconds at 1.3×10^{-2} N/m^2 and 1694 to 1859°K. One specimen of each coating type was only half coated to permit better assessment of flow characteristics. Table VIII contains data from these first firings.

Those compositions which contained both tungsten and molybdenum (DAM-5, 6, 7, 8) exhibited generally better flow than did the systems containing only molybdenum (DAM-1, 2) or tungsten (DAM-3, 4). Firing at 1804°K defined two coatings (DAM-6, 8) with excellent flow and a number of other compositions with adequate flow. Weight losses during fusion were presumed to be due essentially to the loss of iron. Fusion at 1804°K apparently eliminated 76-93 percent of the originally present iron from each composition.

Metallographic analyses were performed on DAM-1, 2, 3, 6, 7 and 8 after firing for 3600 seconds at 1804°K and 1.3×10^{-2} N/m^{-2}. Both DAM-1 and 2 (molybdenum based) showed extensive void areas within the coatings. The majority of each of these two coatings appeared suspended above the substrate with virtually no contact points.

TABLE VIII

FIRING CHARACTERISTICS OF DAM SERIES COATINGS

Coating	Firing Temperature (°K)	Weight Loss (%)	Comments
DAM-1	1694	27	Slight flow, porous, powdery speckles
(54Fe-40Mo-3Ti-3V)	1749	41	Some flow, powdery speckles
	1804	41	Fair flow, few speckles
	1859	45	Fair flow, speckled porous
DAM-2	1694	28	No flow, easily scraped off
(48Fe-40Mo-6Ti-6V)	1749	32	No flow, porous, powdery speckles
	1804	40	Fair flow, porous, few powdery speckles
	1859	42	Poor flow, speckled, porous
DAM-3	1694	48	No flow, loose powder
(64Fe-30W-3Ti-3V)	1749	54	Slight flow, porous, powdery speckles
	1804	55	Fair flow, speckled but not powdery
	1859	53	Fair flow, some powder, mottled
DAM-4	1694	42	Slight flow, easily scraped off
(58Fe-30W-6Ti-6V)	1749	45	Slight flow, powdery speckles
	1804	54	Some flow, powdery speckles
	1859	52	Poor flow, mottled, fragile
DAM-5	1694	26	Slight flow, porous, easily scraped off
(48Fe-30Mo-10W-6Ti-6V)	1749	35	Some flow, porous, easily scraped off
	1804	41	Some flow, porous, easily scraped off
	1859	43	Fair flow, porous, metallic
DAM-6	1694	40	Porous material over flowed layer
(53Fe-20Mo-15W-6Ti-6V)	1749	43	Fair flow, metallic, few speckles
	1804	44	Excellent flow, smooth, metallic
	1859	47	Good flow, slightly rough, metallic
DAM-7	1694	29	Some flow, porous, easily scraped off
(54Fe-30Mo-10W-3Ti-3V)	1749	41	Some flow, porous
	1804	45	Good flow, slight porosity, metallic
	1859	47	Excellent flow, metallic, strong
DAM-8	1694	39	Some flow, porous, easily scraped off
(59Fe-20Mo-15W-3Ti-3V)	1749	46	Fair flow, porous, easily scraped off
	1804	50	Excellent flow, smooth, metallic
	1859	53	Excellent flow, smooth, metallic

The tungsten based DAM-3 appeared free from large voids but exhibited some evidence for bisque tearing. Coatings which contained both molybdenum and tungsten were intermediate in appearance and contained some voids. Figure 4 shows an example of the appearance of the most severe case of coating-substrate separation (DAM-2) together with examples of DAM-3 and 8.

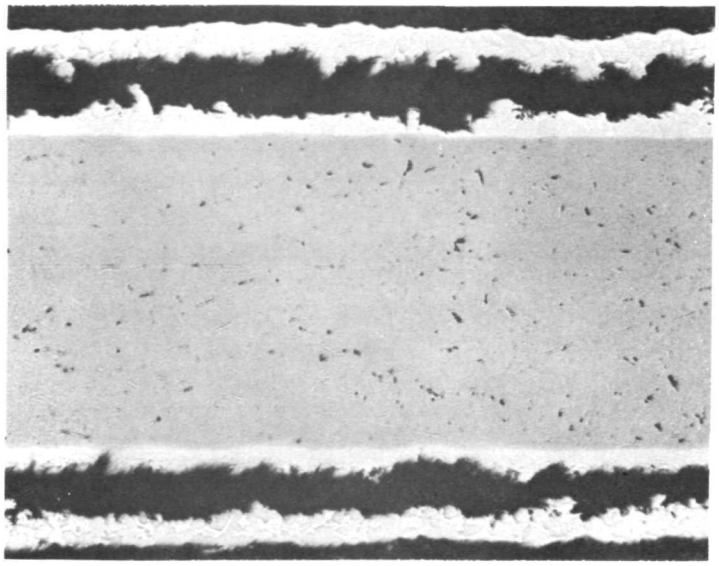

DAM-2

Etchant: Unetched

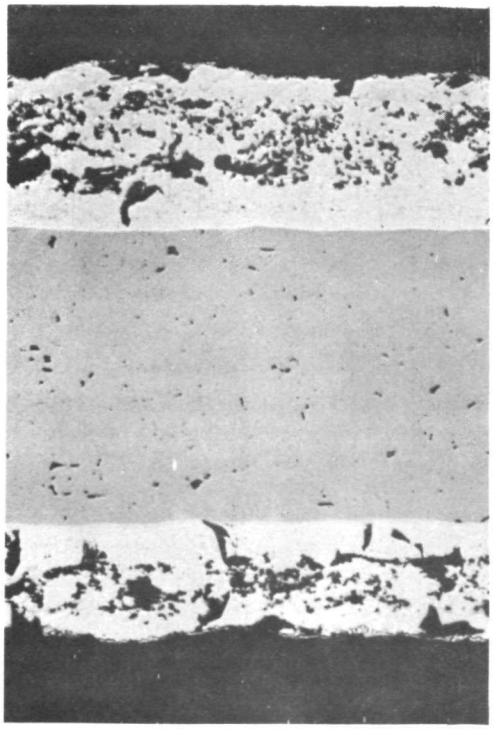

DAM-3

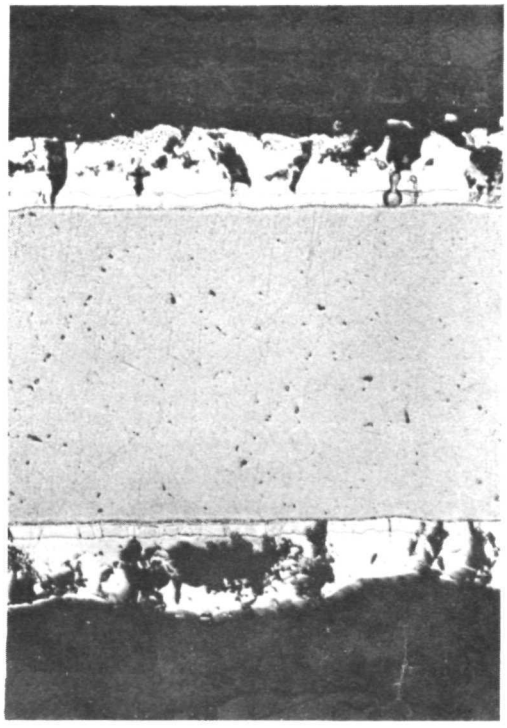

DAM-8

Magnification: 125X

FIGURE 4. DAM SERIES COATING MICROSTRUCTURES AFTER 3600 SECONDS-1804°K-1.3 x 10^{-2} N/m^2 FIRING

It was initially suspected that slow dissolution of molybdenum powder might permit liquid Mo-Fe alloy to run away from large molybdenum powder particles before complete dissolution could occur. Substitution of finer molybdenum and tungsten powders into the slurry had no influence on the occurrence of coating voids. It was found that longer firing cycles (10,800 seconds) aggravated the coating void problem, while 300-second firings improved the situation.

Examination of the vapor pressure versus temperature data for iron and the metallography for the entire DAM coating series suggested that the source of the void problem was the high vapor pressure of iron. Every firing cycle employed for the DAM coating series was found to permit boiling of iron. Vacuum firing conditions (1.3×10^{-2} N/m^2) were believed to result in very high Fe vaporization rates, rapid compositional changes near the coating surface, solidification of the resultant low-iron surface coating and coating deformation and separation by entrapped iron vapors.

A number of DAM-2 and 3 coated 90Ta-10W specimens were fired for short-time, high-pressure cycles. Data from these runs are shown in Table IX. The vacuum furnace was alternately pumped below 10^{-2} N/m^2 and backfilled with argon to the desired pressure. No improvement in coating appearance resulted from 13 N/m^2 firings. Fusion at 130 N/m^2 produced no improvement in the microscopic appearance of DAM-2, but did yield a dense DAM-3 coating. Centerline substrate hardness measurements showed that firing at 130 N/m^2 argon pressure caused some substrate hardening and was, therefore, undesirable.

TABLE IX

SHORT-TIME, HIGH-PRESSURE FIRING OF DAM-2 AND DAM-3 COATINGS

Coating	Temperature (°K)	Time (seconds)	Pressure N/m^2	Weight Loss (%)
DAM-2	1773	300	13	13
DAM-2	1802	300	130	3
DAM-3	1818	300	13	36
DAM-3	1810	300	130	31

Fusion and flow studies of the DAM-type coatings were concluded with the selection of the DAM-1,6,7 and 8 compositions for further study. DAM-3 was added at the request of the NASA project manager. Table X shows the selected firing conditions for each DAM composition.

TABLE X

NASA APPROVED DAM COATINGS AND APPLICATION CYCLES

Coating	Firing Cycle
DAM-1	3600 seconds - 1810°K - 1.3×10^{-2} N/m^2
DAM-3	3600 seconds - 1810°K - 1.3×10^{-2} N/m^2
DAM-6	3600 seconds - 1810°K - 1.3×10^{-2} N/m^2
DAM-7	3600 seconds - 1810°K - 1.3×10^{-2} N/m^2
DAM-8	3600 seconds - 1810°K - 1.3×10^{-2} N/m^2

DAS Series Coatings

Each DAS-type siliciding agent was applied to five DAM-1, 3 and 7 coated coupons in a quantity twice as large as would be required to convert the DAM modifier alloy to disilicide. This was expected to provide sufficient silicon to allow for (1) vaporization during firing, and (2) substrate siliciding as well as (3) the siliciding of the modifier alloy. The DAS-1 coated specimens were fired for 300 seconds at 1755° K and 1.3×10^{-2} N/m^2. All DAS-2, 3 and 4 coatings were fired for 1800 seconds at 1675° K and 1.3×10^{-2} N/m^2. Table XI contains data relevant to the various DAM + DAS coating combinations prepared and fired.

TABLE XI

FIRING DATA FOR DAS-1, 2, 3 AND 4 COATINGS OVER DAM-1, 3 AND 7 MODIFIERS

	Average DAS Weight Loss During Firing (%)	Comment
DAM-1 (Fe-40Mo-3Ti-3V) + DAS-1 (pure Si)	20	Good edges, support rod marks
+ DAS-2 (Si-20Fe)	13	Few edge cracks, slight support rod marks
+ DAS-3 (Si-20Cr-5Ti)	19	Corner splits, rough, porous
+ DAS-4 (Si-20Cr-20Fe)	18	Few edge cracks, porous, support rod marks
DAM-3 (Fe-30W-3Ti-3V) + DAS-1	20	Good edges, non-porous, massive support rod fillets
+ DAS-2	10	Good edges, smooth, metallic, large support rod fillets
+ DAS-3	20	Good edges, large support rod fillets
+ DAS-4	17	Good edges, smooth, massive support rod fillets
DAM-7 (Fe-30Mo-10W-3Ti-3V) + DAS-1	17	Few edge cracks, porous
+ DAS-2	13	Good edges, porous, smooth
+ DAS-3	17	Few edge cracks, rough, porous
+ DAS-4	19	Fair edges, support rod marks, porous

Metallographic analyses of as-prepared DAM-1 and 7 plus DAS-1, 2, 3 and 4 coated specimens revealed that the DAS-4 siliciding agent consumed large quantities of substrate alloy. These first DAM-DAS coatings ranged to twice as thick as the program goal of 0.00010 meter. About 0.000254 meter of unaffected substrate remained under the DAM-DAS-1, 2, 3 combinations while only about 0.00020 meter of 90Ta-10W remained under the DAM + DAS-4 systems. The DAM-1 and 7 plus DAS-3 coated specimens appeared rougher than the other coating combinations investigated.

Physical appearance and metallographic analyses were believed insufficient data on which to base selection of the best DAM-DAS combinations for initial low-pressure, slow-cycle oxidation testing. A number of DAM-DAS systems were, therefore, selected for 1700° K furnace testing at atmospheric pressure. The selections were made to include at least one example of each DAS coating and to exclude all DAM-DAS combinations which were shown to fire poorly (i.e., poor edges, severe support rod marks). The selected specimens experienced a number of 1, 16 and 64 hour - 1700° K - atmospheric pressure cycles. Data from these tests are shown in Table XII. All specimens showed increased roughness with increased exposure time. DAS-1 and 2 silicided coupons demonstrated both the best overall appearance and the longest lifetimes of the various combinations investigated. These two siliciding agents were recommended for use on DAM coated specimens which would undergo low-pressure, slow-cycle evaluation.

TABLE XII

1700° K FURNACE OXIDATION OF SELECTED DAM-DAS SYSTEMS

Coating	Total Exposure (hrs)	Comment
DAM-1 (Fe-40Mo-3Ti-3V) + DAS-1 (pure Si)	11(1 hr) + 2(16 hr) + 1(64 hr)	Removed from test at 107 hrs.
-2 (Si-20Fe)	"	"
-4 (Si-20Cr-20Fe)	7(1 hr) + 2(16 hr)	Edge failure, 23-39 hrs.
DAM-3 (Fe-30W-3Ti-3V) + DAS-4	11(1 hr) + 2(16 hr)	Failure due to defect in DAM-3 layer, 43 hrs.
DAM-7 (Fe-30Mo-10W-3Ti-3V) + DAS-1	11(1 hr) + 2(16 hr) + 1(64 hr)	Removed from test at 107 hrs.
-2	"	"
-3(Si-20Cr-5Ti)	7(1 hr) + 2(16 hr)	Total failure, 23-39 hrs.
-4	"	Edge failure, 23-39 hrs.

3.1.5 Screening of Initial Coating Compositions

The principal oxidation test to be used throughout the program was low-pressure, slow-cycle (LP-SC) exposure for up to 100 cycles. A test facility was designed and constructed to perform oxidation tests at 1700 and 1810° K while the ambient pressure was maintained at 13 or 1300 N/m^2. Three Pt-20Rh resistance-type furnaces were constructed and placed in a large steel tank. A mechanism was designed

and built to cycle coated specimens into and out of the furnaces every 2940 seconds. The resultant time/temperature profile is shown in Figure 5. Insulated shutters covered each furnace as soon as the specimens were removed for the cooling part of each cycle. Figure 6 shows a furnace schematic together with the interior of the steel chamber, the completed furnaces, and pressure control instrumentation. Not shown are the timers and temperature controllers.

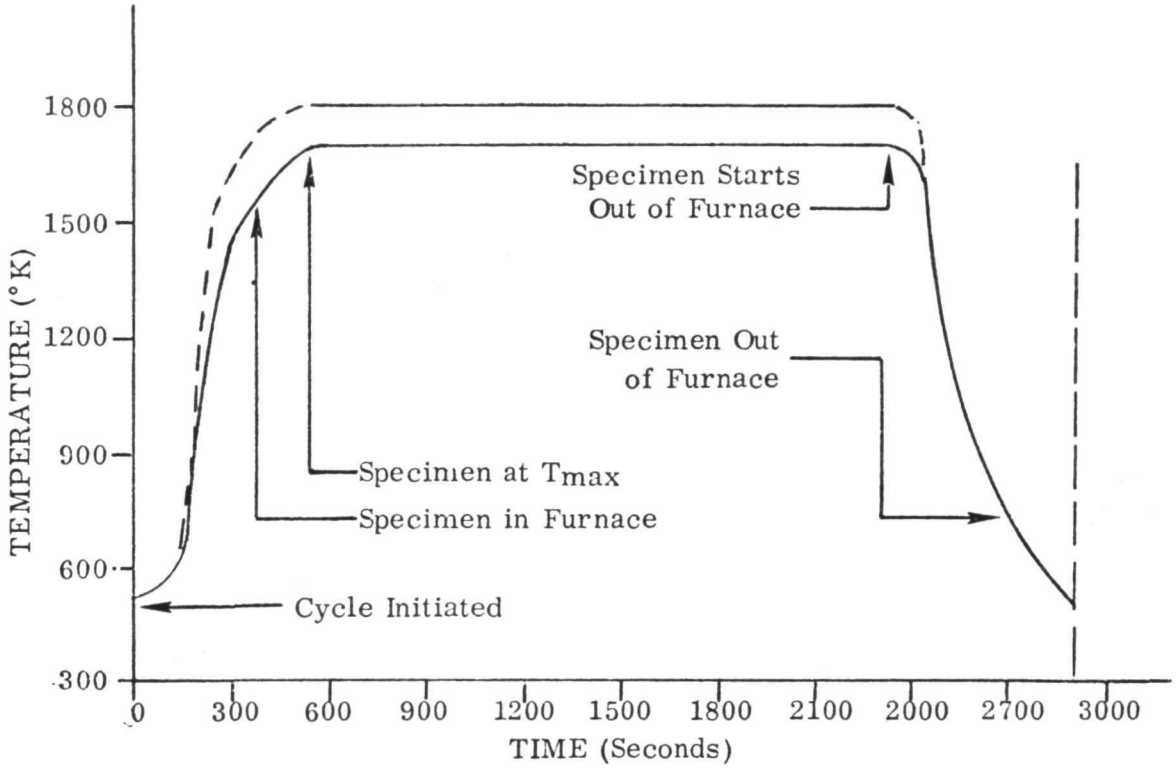

FIGURE 5. TIME-TEMPERATURE PROFILES FOR THE LOW-PRESSURE, SLOW-CYCLE TEST

Five bend test specimens (0.0127 x 0.0.762 x 0.00032 meter) were coated with each of the selected SA-series and DAM + DAS type coatings. In addition, Sylvania-prepared R512C (SA-1) coated coupons were obtained and placed in test to provide base-line data and a comparison with previous work. Tables XIII and XIV contain data on the preparation and firing of these specimens.

It was required that each selected coating be LP-SC tested in both the intentionally defected and the non-defected conditions. Intentional defecting was accomplished by grit blasting a centrally located 0.0015 meter diameter hole through the coating so as to expose the substrate. The size of the defect was controlled by grit blasting through an 0.0015 meter hole in a copper mask. Visual inspection was used to determine that all coating material had been removed from the intentionally defected area.

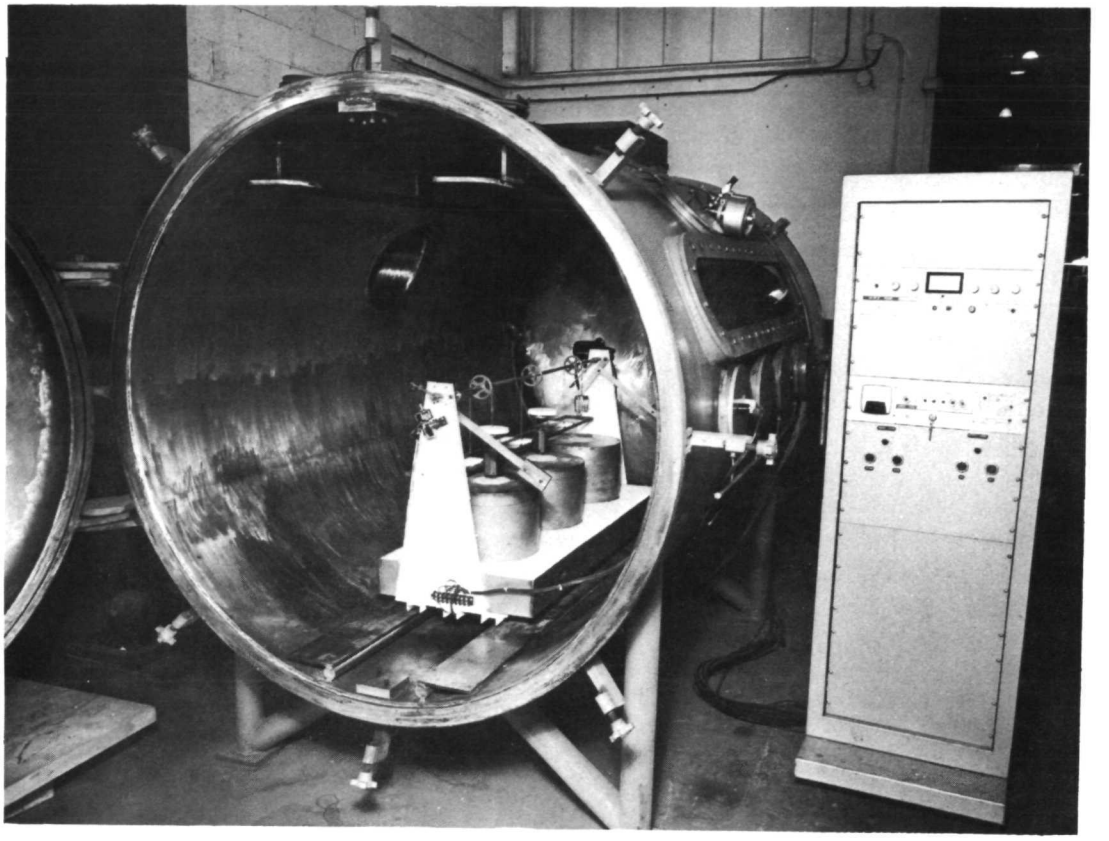

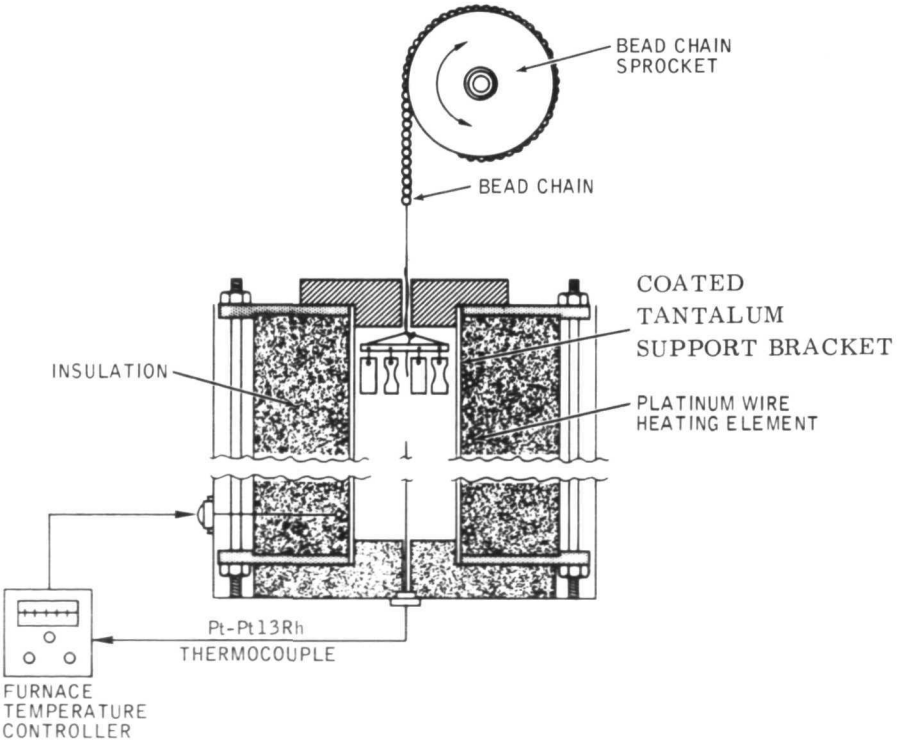

FIGURE 6. LOW-PRESSURE, SLOW-CYCLE TEST FACILITY

TABLE XIII

SA SERIES COATED LOW-PRESSURE, SLOW-CYCLE TEST COUPONS

Coating	Weight Loss, % (Range, Average)	Fired Weight Range (kg/m^2)
SA-2	12-14, 13	0.298 - 0.330
SA-3	12-16, 15	0.305 - 0.344
SA-5	11-14, 12	0.290 - 0.345
SA-6	15-24, 19	0.241 - 0.314
SA-10	17-24, 21	0.251 - 0.327
SA-13	22-25, 24	0.253 - 0.297

TABLE XIV

DAM-DAS COATED LOW-PRESSURE, SLOW-CYCLE TEST COUPONS

Coating	DAM Wt. Loss % (Range, Average)	DAS Wt. Loss % (Range, Average)	Final Coating Weight (kg/m^2)
DAM-1 + DAS-1	36-44, 41	18-21, 20	0.429 - 0.512
DAM-1 + DAS-2	36-44, 41	18-22, 20	0.503 - 0.530
DAM-3 + DAS-1	49-54, 53	12-15, 14	0.447 - 0.501
DAM-6 + DAS-1	44-46, 45	19	0.509 - 0.521
DAM-6 + DAS-2	44-46, 45	14-17, 15	0.602 - 0.610
DAM-7 + DAS-1	41-46, 44	13-20, 19	0.508 - 0.547
DAM-7 + DAS-2	41-46, 44	11-21, 17	0.573 - 0.617
DAM-8 + DAS-1	41-49, 46	19	0.466 - 0.545
DAM-8 + DAS-2	41-49, 46	11-20, 16	0.561 - 0.660

Eight fused slurry silicide coated specimens were placed in each furnace and were exposed in the LP-SC facility at 1700° K and 1300 N/m^2 until 100 cycles had been completed or until visual evidence of substrate oxide indicated failure. A few specimens had to be removed from test because severe bending and twisting occurred which prevented further cycling. Specimens were weighed before exposure and after 1, 10, 23, 45 and 100 cycles of testing. One example of each selected coating composition was exposed in the as-prepared and another in the as-intentionally defected condition. Defected and non-defected specimens were exposed in different furnaces to prevent possible contamination of non-defected specimens by oxidation products from failing intentionally defected specimens.

Table XV summarizes the results obtained from the first LP-SC screening tests. Those coatings which showed little or no tendency to glaze during oxidation also exhibited generally poor performance and virtually no tolerance for defects. Of the SA-series coatings, SA-5 developed a thick layer of glass and SA-13 generated a thin vitreous surface layer. The DAS-2 silicided DAM coatings developed copious quantities of fluid glass. DAS-1 silicided DAM alloys generated less glass than DAS-2 silicided systems and showed no tendency for the glass to flow during test exposure. These initial test results strongly emphasized the importance of forming a vitreous surface layer during oxidation.

The only coating to survive 100 cycles without failure was SA-5, the most highly modified composition based on the Si-Fe system. The next best performance (43 cycles) for a non-defected specimen was registered by SA-13, a modification of the Si-20Cr-10Ti system. Also exceeding 40 cycles were the non-defected DAM-8 + DAS-2 and the intentionally defected DAM-1, 6 and 7 + DAS-2 specimens. Neither coating based on the Si-Ti system (R512C ≡ SA-1, SA-10) developed a glazed surface nor survived beyond 10 test cycles.

Figure 7 shows the macroscopic and microscopic appearance of the SA-5 coated specimen which survived 100 low-pressure, slow cycles. The coating glazed and turned a dark red color after the first few cycles of exposure. Further darkening occurred throughout the test period. The original coating was about 120×10^{-6} meter thick and increased to about 210×10^{-6} meter by the end of testing. Good side-to-side coating thickness uniformity was observed. A total of about 50×10^{-6} meter of substrate was lost during testing as a result of coating/substrate interdiffusion. About 220×10^{-6} meter of the substrate remained after test and showed no visual evidence for oxygen contamination. The centerline hardness of the SA-5 coated specimen increased from 285-299 KHN (100 g load) in the as-prepared condition to 418-450 KHN (100 g load) in the exposed condition. As-received substrate material (90Ta-10W) showed a hardness of 261-281 KHN (100 g load). The tested specimen was placed in a 4T bend test fixture and was observed to deflect approximately 0.35 radian before fracturing. All as-coated systems (SA and DAM-DAS) sustained 1.6 radian permanent bends without substrate cracking.

TABLE XV

1700°K - 1300 N/m^2 LP-SC TEST RESULTS FROM INITIAL SCREENING TEST

Coating Type	Defected	Cycles	Failure Mode
SA-1	Yes	2	0.003m hole, defected area
SA-1	No	10	Edge, twisted
SA-2	Yes	1	0.003m hole, defected area
SA-2	No	17-23	Twisted, spalling
SA-3	Yes	1	0.003m hole, defected area
SA-3	No	10	Edges
SA-5	Yes	2	0.003m hole, defected area
SA-5	No	100	Not failed
SA-6	Yes	2	0.003m hole, defected area
SA-6	No	24-30	Edges, corner
SA-10	Yes	2	0.003m hole, defected area
SA-10	No	10	Corner
SA-13	Yes	2	0.002m hole, defected area
SA-13	No	43	Edge
DAM-1 + DAS-1	Yes	2	0.009m hole, defected area
DAM-1 + DAS-1	No	24-30	Edge
DAM-3 + DAS-1	Yes	17-23	Twisted, edges
DAM-3 + DAS-1	No	10	Edge, twisted
DAM-6 + DAS-1	Yes	3	0.012m hole, defected area
DAM-6 + DAS-1	No	24-30	Edge, corner
DAM-7 + DAS-1	Yes	3	0.012m hole, defected area
DAM-7 + DAS-1	No	6	Corner
DAM-8 + DAS-1	Yes	3	0.009m hole, defected area
DAM-8 + DAS-1	No	24-30	Corner
DAM-1 + DAS-2	Yes	43	Twisted
DAM-1 + DAS-2	No	17-23	Edges, twisted
DAM-6 + DAS-2	Yes	57	Edge by defect
DAM-6 + DAS-2	No	17-23	Twisted, edges
DAM-7 + DAS-2	Yes	45	Twisted
DAM-7 + DAS-2	No	10	Corner
DAM-8 + DAS-2	Yes	1	0.002m hole, defected area
DAM-8 + DAS-2	No	40	Twisted, corner

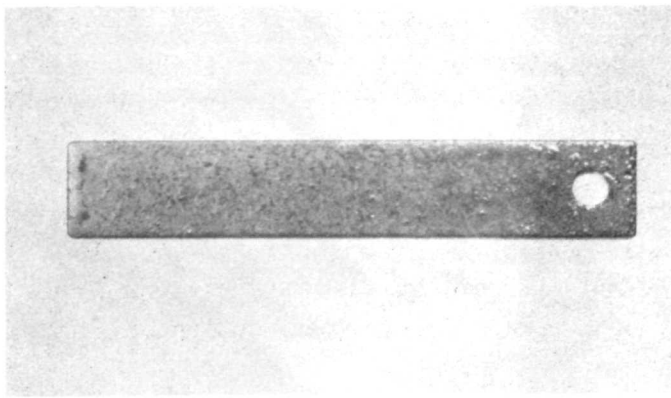

SA-5

Magnification: 1X

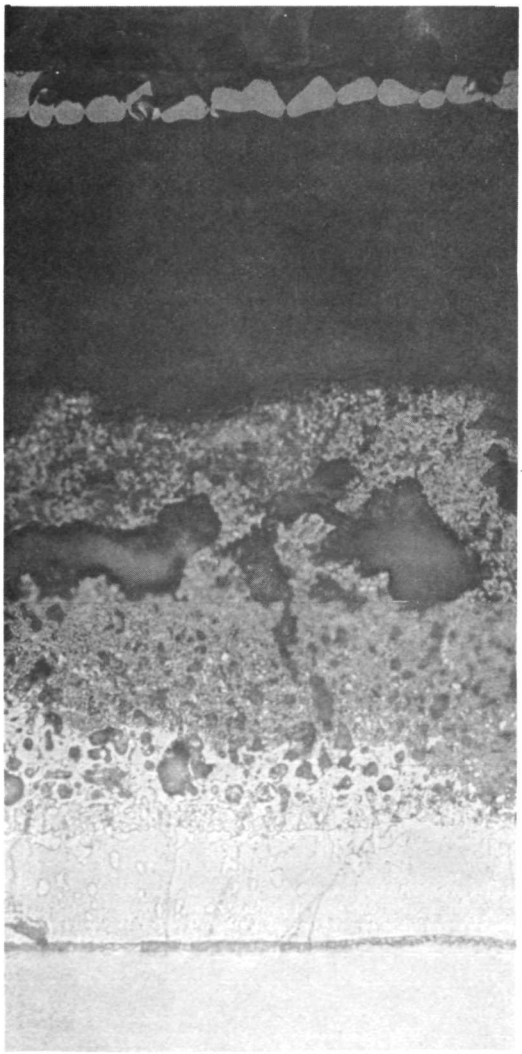

SA-5

Etchant: Lactic-HF-HNO_3

Magnification: 500X

FIGURE 7. SA-5 MACRO AND MICROSTRUCTURE AFTER 100 LOW-PRESSURE, SLOW CYCLES TO 1700°K AND 1300 N/m^2

Figure 8 shows the macro and microscopic appearance of the SA-13 coated specimen which survived 43 cycles of testing. The coating exhibited a slight tendency to glaze, turned brown after one cycle and darkened to a charcoal brown by the end of 43 cycles. Side-to-side coating thickness uniformity was good. About 18 x 10^{-6} meter of substrate was lost to interdiffusion during the 43 cycles of testing and about 250 x 10^{-6} meter of apparently unaffected substrate remained. The substrate hardness was 297-322 KHN (100 g load) for the exposed specimen as compared to 285-298 KHN (100 g load) for as-coated specimens. A 4T bend test revealed that the tested specimen would withstand a permanent 1.6 radian bend at 300° K without any substrate cracking.

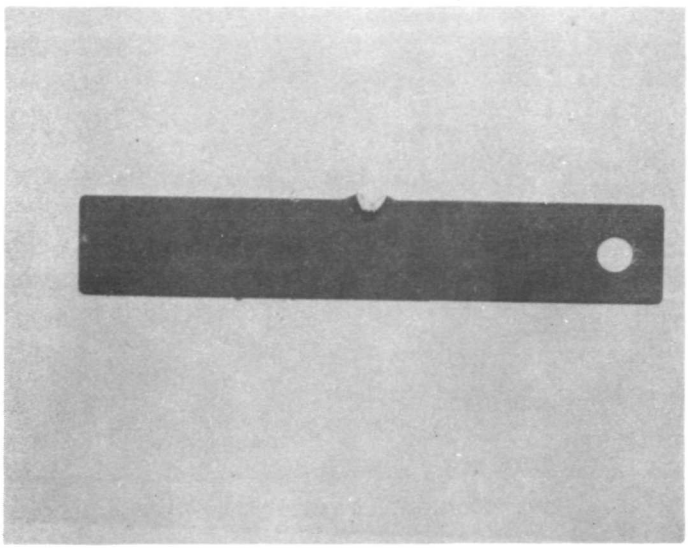

SA-13

Magnification: 1X

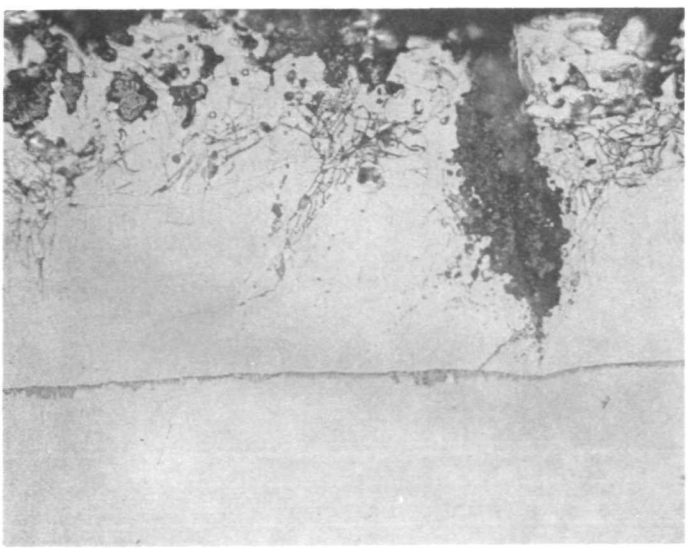

SA-13

Etchant: Lactic-HF-HNO_3

Magnification: 500X

FIGURE 8. SA-13 MACRO AND MICROSTRUCTURE AFTER 43 LOW-PRESSURE, SLOW CYCLES TO 1700° K AND 1300 N/m^2

Shown in Figure 9 are the macro and microstructure appearance of the DAM-6 + DAS-2 coating system after 57 cycles of exposure. The cross section shown was located 0.0315 meter below the top of the specimen. Exposure for one cycle turned the coating gray; continued cycling developed a thick, wrinkled glaze and a dull black color. The extent of the glass formation, the side-to-side coating thickness variation and the unaffected appearance of the substrate are best observed in the 125X photograph. About 210 x 10^{-6} meter of substrate remained after testing. The centerline substrate hardness for an as-coated DAM-6 + DAS-2 specimen was 289-303 KHN (100 g load) while that of the exposed coupon was 364-444 KHN (100 g load). Insufficient material was available to gain any indication of as-tested specimen ductility.

Figure 10 includes the macro appearance and microstructure of a DAM-7 + DAS-2 coated coupon which survived 45 test cycles. The coating turned gray during the first cycle and then gradually glazed and blackened during subsequent cycling. The intentionally defected area turned shiny black and raised during the first exposure cycle. The defected area grew into a large pimple which caused the specimen to bend away from the defect. A glaze developed over the entire specimen during the first few cycles and is visible in the photomicrograph. About 210 x 10^{-6} meter of substrate remained at the end of 45 low-pressure slow cycles.

The progressive deterioration which resulted from an unhealed, intentionally induced defect may be seen in Figure 11. Each specimen was defected by grit blasting an 0.0015 meter diameter hole through the coating so as to expose the substrate. The top specimen in Figure 11 shows the appearance of an unhealed, defected area after experiencing one cycle to 1700° K and 1300 N/m. The central and lower specimens show the effect of one and two additional cycles to 1700° K. Further exposure generally resulted in "burn-off" of the lower end of the coupon.

Metallographic analyses were completed on two intentionally defected and exposed specimens which did not immediately fail. Figures 12 and 13 show cross-sectional views through the defected area of a DAM-3 + DAS-1 and a DAM-7 + DAS-2 coated specimen. The lack of any silicide coating and the presence of flowed glass over the defect in the DAM-3 + DAS-1 coated specimen is evident. The extent of the obviously affected substrate zone (under DAM-3 + DAS-1) was determined to be a circle, approximately concentric about the defect and of about 0.0035 meter diameter. No glass is apparent in the defected area of the DAM-7 + DAS-2 coated specimen. The obviously affected substrate zone measured about 0.0055 meter in diameter for this specimen.

Weight gain versus time data for selected specimens are shown plotted in Figure 14. The SA-5 and DAM + DAS-2 coated specimens experienced the highest weight gains recorded. Taken as a group, these specimens showed an approximately parabolic time versus weight gain relationship. The DAM + DAS-1 coated specimens

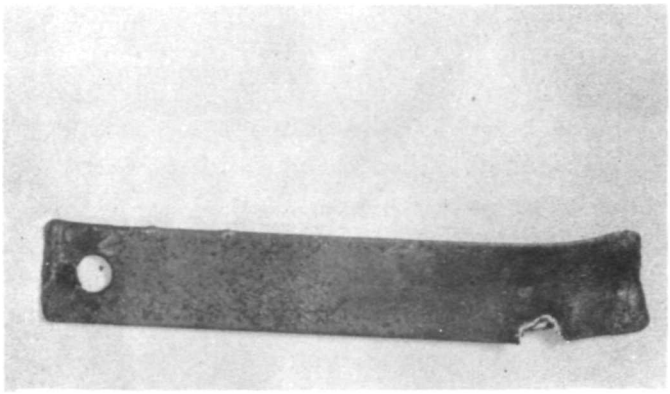

DAM-6 + DAS-2

Magnification: 1X

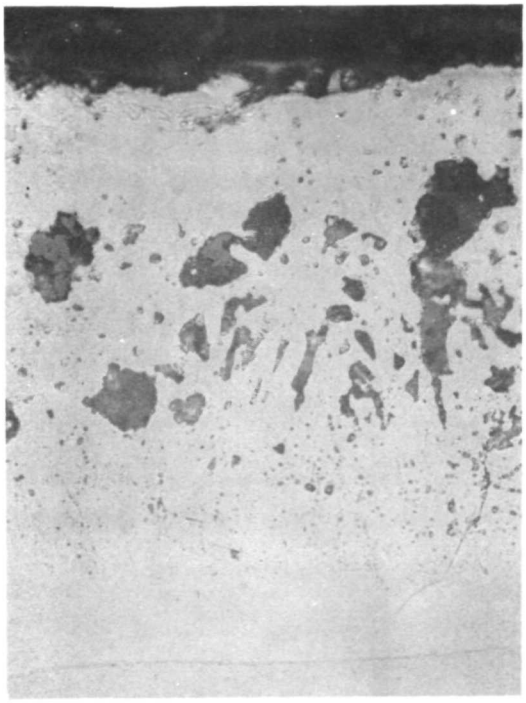

DAM-6 + DAS-2

Etchant: Lactic-HF-HNO_3

Magnification: 500X

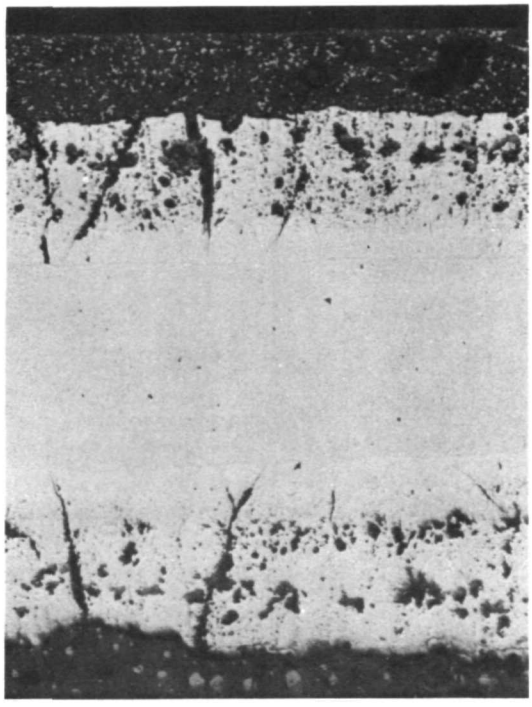

DAM-6 + DAS-2

Etchant: Lactic HF-HNO_3

Magnification: 125X

FIGURE 9. DAM-6 + DAS-2 MACRO AND MICROSTRUCTURE AFTER 57 LOW-PRESSURE, SLOW CYCLES TO 1700° K AND 1300 N/m^2

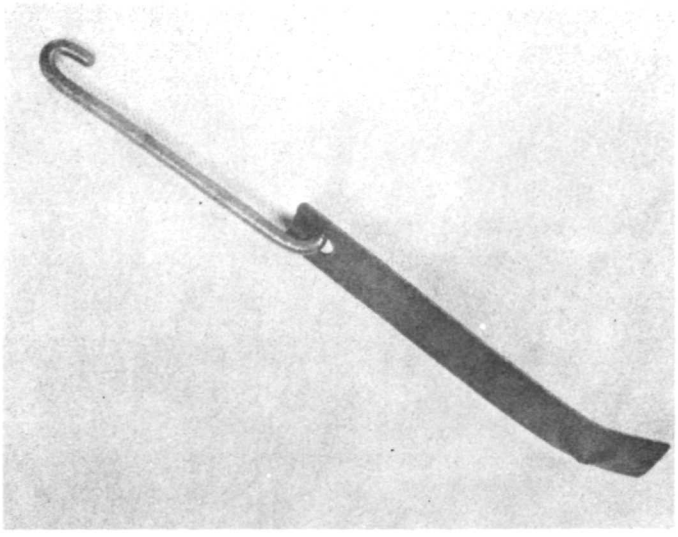

DAM-7 + DAS-2

40 Cycles

Magnification: 0.75X

Note Defected Area

DAM-7 + DAS-2

45 Cycles

Etchant: Lactic - HF - HNO_3

Magnification: 500X

FIGURE 10. DAM-7 + DAS-2 MACRO AND MICROSTRUCTURE AFTER 45 LOW-PRESSURE, SLOW CYCLES TO 1700°K AND 1300 N/m^2

did not glaze as heavily as the DAM + DAS-2 coated specimens and also showed approximately parabolic kinetics. The remaining SA series coatings and DAM-1 + DAS-1 exhibited little tendency to glaze and also approximated parabolic kinetics.

Table XVI summarizes the hardness and bend ductility data obtained from specimens coated with the originally selected 15 coating compositions. Bend data

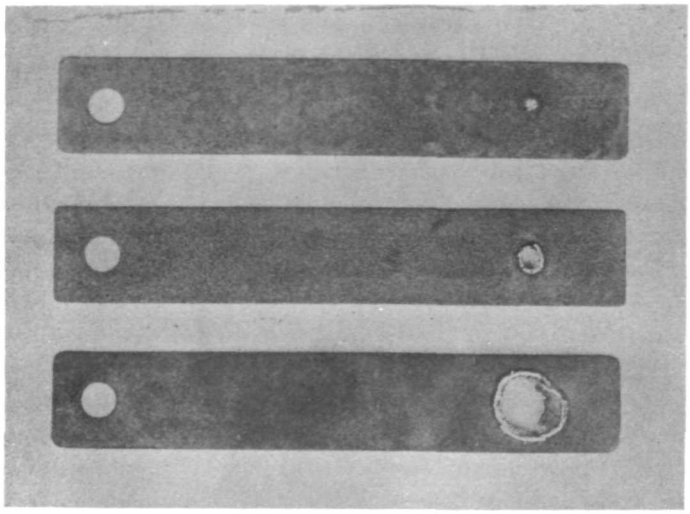

Top - 1 Cycle, 1700°K, 1300 N/m^2

Center - 2 Cycles, 1700°K, 1300 N/m^2

Bottom - 3 Cycles, 1700°K, 1300 N/m^2

FIGURE 11. PROGRESSIVE DAMAGE DUE TO AN INTENTIONALLY INDUCED DEFECT

noted in Table XVI were obtained by hand-bending coupons in a room temperature, 4T bend fixture. The approximate angle of fracture was noted for those specimens which cracked. A 1.6 radian notation means that the coupon was permanently bent 1.6 radians without cracking.

An explanation was sought for the high hardness values and lack of ductility exhibited by some specimens. It appeared possible that either iron from the coatings or oxygen from the test atmosphere might be responsible for the deterioration of the substrate mechanical properties. Specimens were prepared for vacuum fusion, X-ray fluorescent and microprobe analyses. The vacuum fusion and X-ray fluorescent samples were grit blasted to remove all coating and were then etched in H_2SO_4-HNO_3-HF until a smooth, polished, metallic surface resulted.

Microprobe analysis of the substrate under the SA-5, SA-13, and DAM-16 + DAS-2 coatings showed no etectable iron in either the as-prepared or as-exposed conditions. Both the SA-5 and DAM-6 + DAS-2 coatings were shown to contain iron in the as-prepared condition. Data for the as-prepared DAM-6 + DAS-2 coating indicated the possibility of $TaFe_2$ at the coating/substrate interface and also suggested iron segregation within the coating. The segregation probably occurred at phase boundaries within the coating and may have resulted from incomplete dissolution of tungsten or molybdenum powder particles during fusion. Low-pressure, slow-cycle exposure at1700°K and 1300 N/m^2 permitted the iron in DAM-6 + DAS-2 to diffuse throughout the coating and thereby eliminate high-iron concentration areas. Iron scans were run on SA-13 to provide background data only, since SA-13 is an iron-free coating.

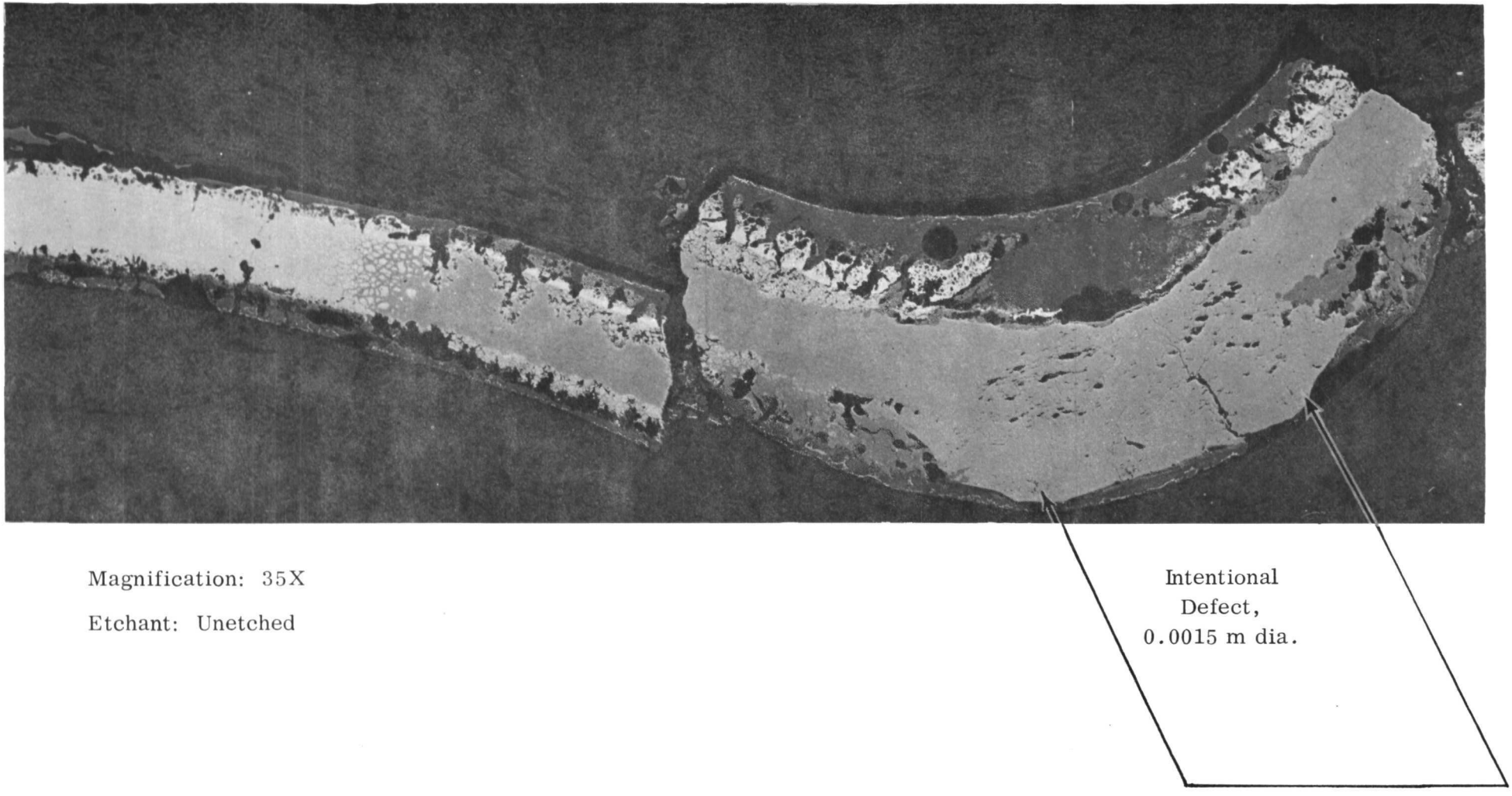

FIGURE 12. CROSS SECTION OF DAM-3 + DAS-1 INTENTIONALLY DEFECTED AREA AFTER 23 CYCLES TO 1700° K AND 1300 N/m^2

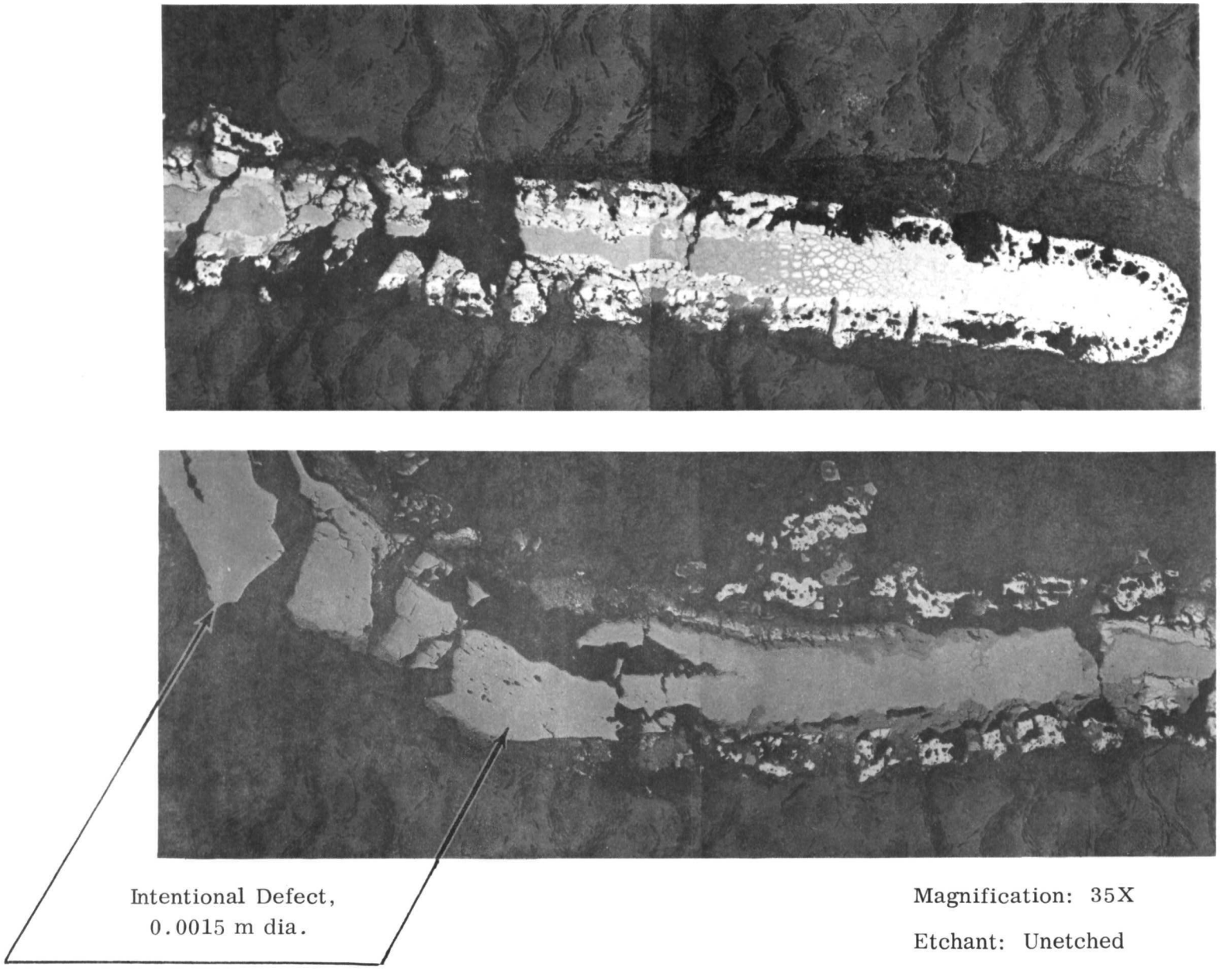

FIGURE 13. CROSS SECTION OF DAM-7 + DAS-2 INTENTIONALLY DEFECTED AREA AFTER 57 CYCLES TO 1700°K AND 1300 N/m^2

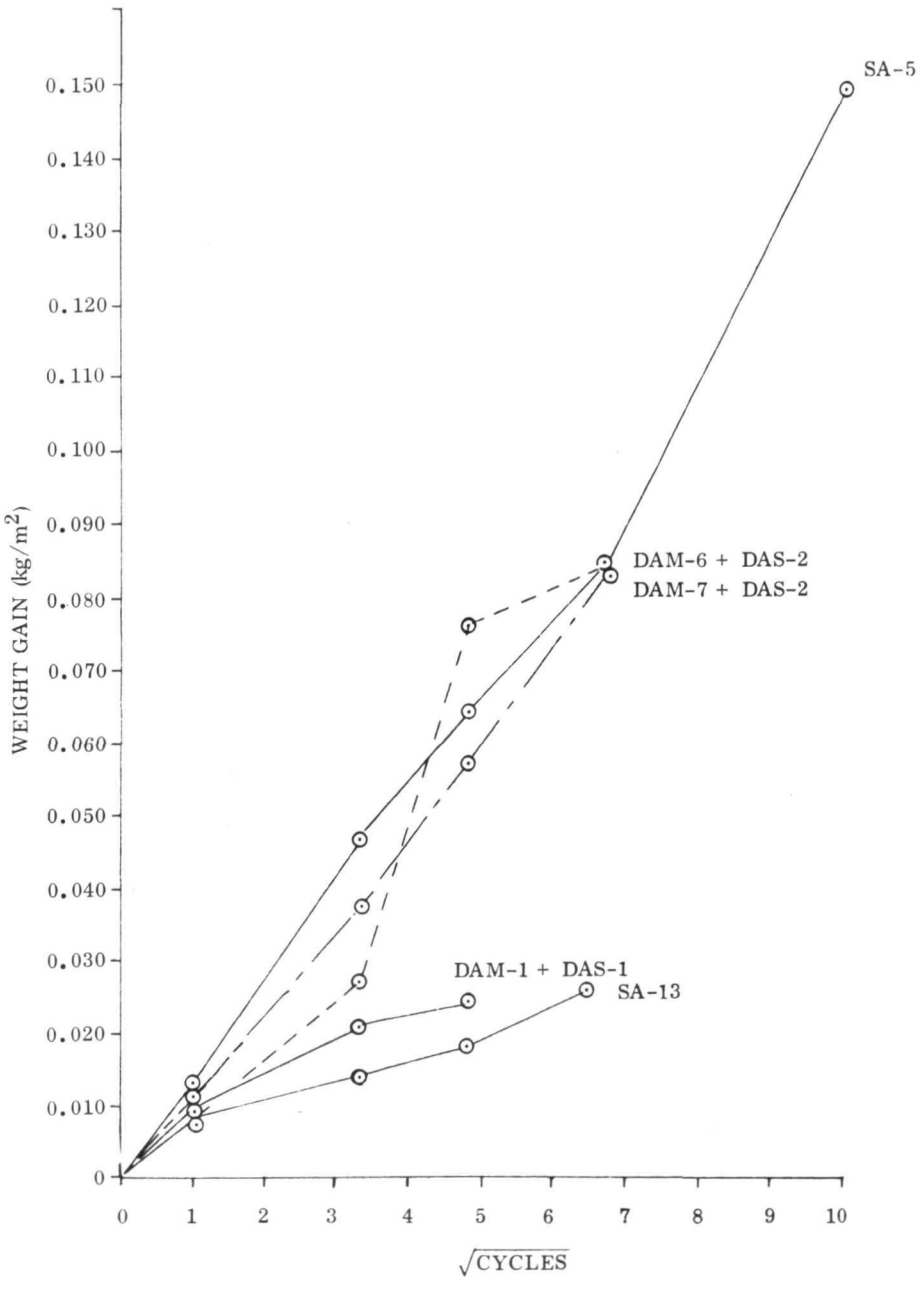

FIGURE 14. WEIGHT GAIN VS $\sqrt{\text{TIME}}$ FOR SELECTED COATING SYSTEMS

X-ray fluorescent analyses of the substrate under LP-SC exposed, SA-5 (100 cycles), SA-13 (43 cycles), and DAM-7 + DAS-2 (45 cycles) coatings showed no iron or silicon present.

Vacuum fusion analyses for oxygen were conducted on substrate material from LP-SC exposed SA-5 (100 cycles), SA-13 (43 cycles) and DAM-7 + DAS-2 (45 cycles) specimens. Since no iron was observed in the above substrates, it was expected that

TABLE XVI

HARDNESS AND BEND DATA FOR SELECTED COATING COMPOSITIONS

Specimen Type	Cycles	Substrate Hardness (100 g KHN)	Bend Angle (radian)
90Ta-10W	0	261-281	1.6
All, as-coated	0	265-303	1.6
SA-5	100	418-450	0.3 deflection
SA-10	10	--	1.6
SA-13	43	297-322	1.6
DAM-1 + DAS-1	30	313-339	1.6
DAM-6 + DAS-1	30	310-341	1.0, cracked
DAM-7 + DAS-1	6	--	1.0, cracked
DAM-8 + DAS-1	30	--	0.5, cracked
DAM-1 + DAS-2	43	378-425	--
DAM-6 + DAS-2	23	364-444	--
DAM-6 + DAS-2	57	363-402	--
DAM-7 + DAS-2	10	--	1.6
DAM-7 + DAS-2	45	331-364	--
DAM-8 + DAS-2	40	396-480	0.8-1.6, cracked

oxygen content would explain the ductility or lack of ductility observed for various specimens and would also correlate with the measured hardness data. Table XVII contains the analytical data. Figure 15 shows a plot of this hardness versus oxygen content data and includes similar data for pure tantalum for comparison. The hardness values taken from the literature are for pure tantalum and for a 50 g load rather than for a 100 g load (Ref. 5). This difference is unimportant for the present comparison which is concerned with the trend and not with the absolute hardness values. The reason for brittle substrates under some of the exposed coatings appeared due to substrate contamination by oxygen.

Nondestructive test techniques including visual examination and thermoelectric probe and Dermitron eddy current measurements were performed on each test specimen.

TABLE XVII

VACUUM FUSION ANALYSIS OF LOW-PRESSURE, SLOW-CYCLE EXPOSED SUBSTRATES

Coating	No. of Cycles	Hardness KHN (100 g)	Oxygen (w/o)
As-received 90Ta-10W	0	261-281	0.0136
SA-5	100	418-450	0.064
SA-13	43	297-322	0.038
DAM-7 + DAS-2	45	331-364	0.062

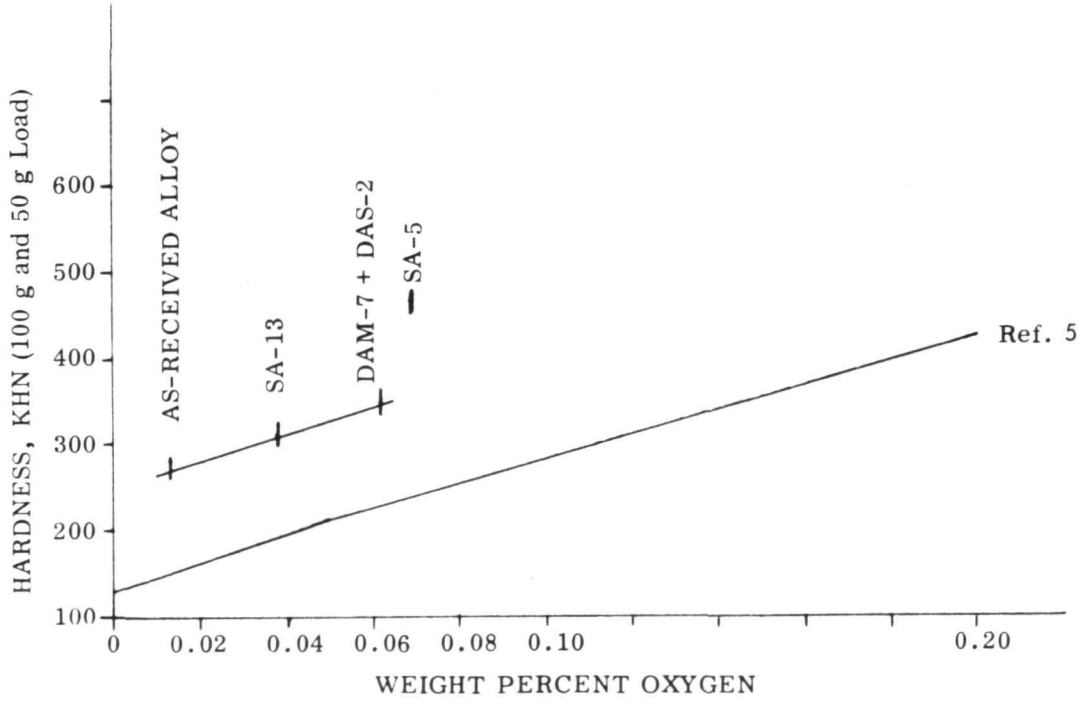

FIGURE 15. SUBSTRATE OXYGEN CONTENT VERSUS SUBSTRATE HARDNESS

A low magnification examination (7-30X) was used to inspect all specimen corners, edges and surfaces. A "map" of all visible defects (cracks, support rod marks) and appearance variations was made for each specimen which was to be low-pressure, slow-cycle oxidation tested.

The thermoelectric inspection of edges and corners was performed using an Ungar soldering iron and a Hewlett-Packard auto-ranging digital voltmeter (DVM). The "common" lead from the DVM was connected to the room temperature specimen and the VDC lead from the DVM was connected to a wedge-shaped copper tip on the soldering iron. The heated soldering iron was held against the selected area on the specimen for 10 seconds before a reading was obtained from the DVM. The copper tip was cleaned frequently to eliminate tip oxidation products. Thermoelectric readings generally remained constant within about ±30 percent for a given contact point. Slight variations in the contact point resulted in large fluctuations of the thermoelectric reading. Of the 32 specimens examined, two yielded positive thermoelectric values, 12 yielded mixed values, and 18 yielded negative thermoelectric values. Mixed readings were mainly obtained for the DAM-DAS systems. These coatings are applied in two steps and may be more subject to composition variations than the SA-series coatings. The SA-2, 3, 5, 6 and 13 coatings produced negative values for all thermoelectric measurements.

Eddy current thickness measurements were obtained using a Dermitron Eddy Current Thickness instrument. All measurements were made relative to the coating thickness versus Dermitron response curve shown in Figure 16. This curve was generated by adjusting the Dermitron to read zero for the 90Ta-10W alloy and 0.080 for a 0.400 kg/m^2 thick SA-3 coating. Intermediate data points were determined to define the response curve. Probe D and the Operate-3 mode were used. This Dermitron setting was selected to permit reading of all coatings without changing the Dermitron calibration. Since coating composition varied from sample to sample, the Dermitron response was not necessarily comparable for different coating types. This procedure was expected to provide an indication of inconsistencies between specimens coated with the same coating or between opposing sides of any specific coupon.

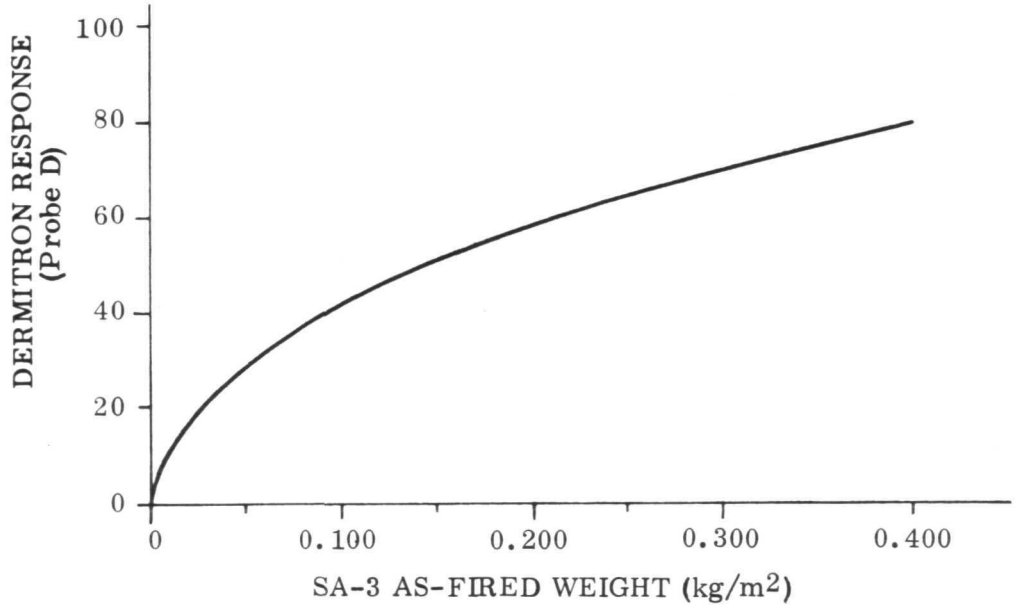

FIGURE 16. COATING THICKNESS VS DERMITRON RESPONSE

Figure 17 shows the format used for recording NDT data and a typical set of data. Table XVIII includes a correlation between all NDT data and the observed performance of each low-pressure, slow-cycle oxidation tested specimen. Almost no relation between lifetime and NDT data was observed.

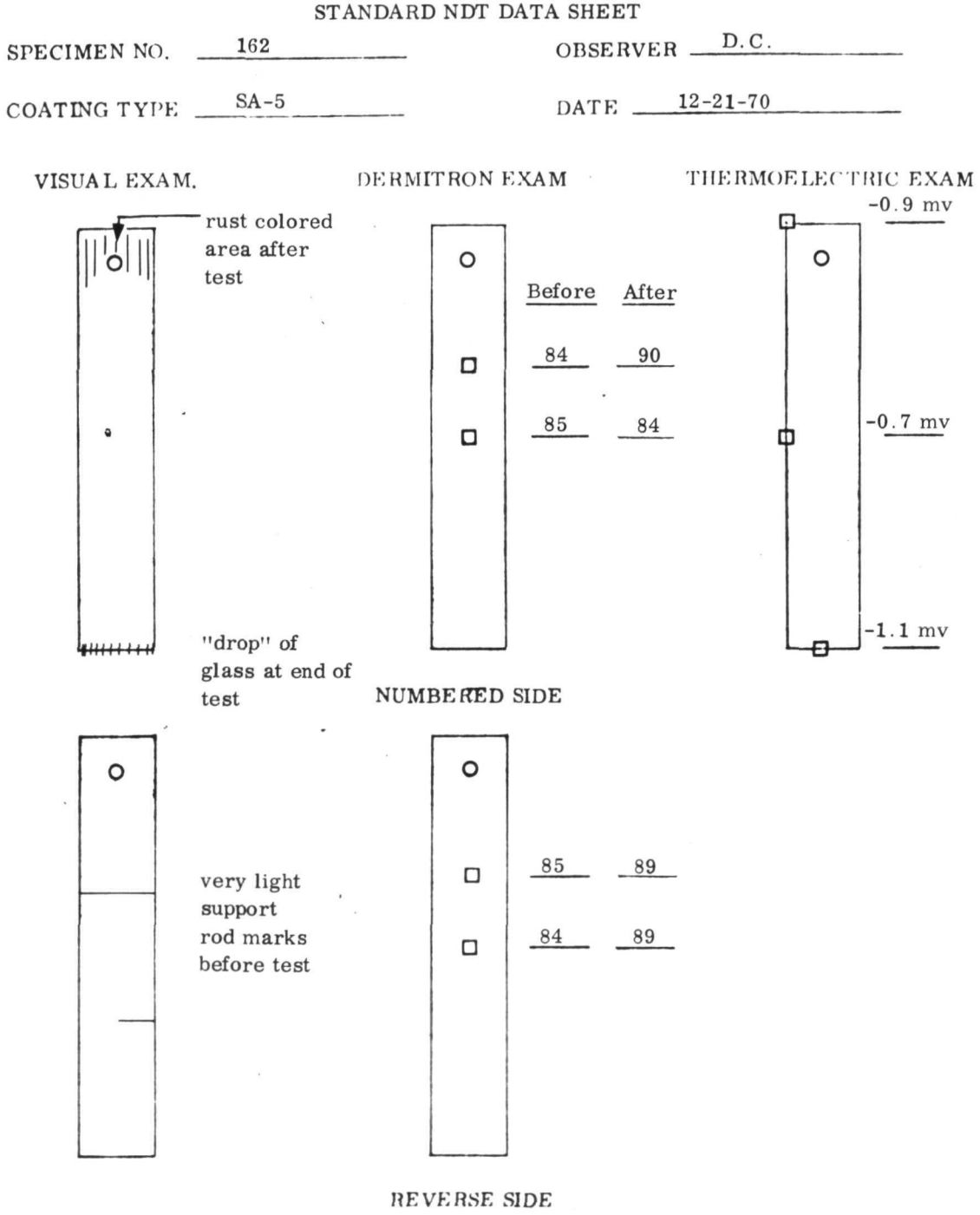

FIGURE 17. FORMAT USED FOR RECORDING NDT DATA AND A TYPICAL SET OF DATA

TABLE XVIII

NDT DATA CORRELATION

Specimen	Thermoelectric	Dermitron	Visual
SA-1 *	N.M.	N.M.	F.D.
"	N.M.	N.M.	N.C.
SA-2 *	N.M.	N.M.	F.D. support rod marks → edge failures
"	N.M.	N.C.	N.C.
SA-3 *	Readings more neg. than -2.6mv → failures	N.M.	F.D., enlarged corners → corner failures
"	N.C.	N.M.	N.C.
SA-5 *	N.M.	N.M.	F.D.
"	N.M.	N.M.	N.F.
SA-6 *	N.M.	N.M.	N.C.
"	N.M.	N.M.	N.C.
SA-10 *	N.M.	N.M.	F.D.
"	N.M.	N.M.	N.C.
SA-13 *	N.M.	N.M.	F.C.
"	Most neg. reading → failed edge	N.M.	N.C.
DAM-1 + DAS-1 *	N.M.	N.M.	F.D., surface cracks near defect → severe failure
"	N.C.	N.M.	N.C.
DAM-3 + DAS-1 *	N.C.	Side to side thickness possibly related to bending	N.C.
"	N.M.	N.C.	N.C.
DAM-6 + DAS-1 *	N.M.	N.M.	F.D.
"	Least neg. reading → failure at corner	N.M.	N.C.
DAM-7 + DAS-1 *	N.M.	N.M.	F.D.
"	N.M.	N.M.	N.C.
DAM-8 + DAS-1 *	N.M.	N.M.	F.C.
"	N.M.	N.M.	N.C.
DAM-1 + DAS-2 *	Most neg. reading → edge failure	Side to side thickness variation possibly related to bending	Support rod marks possibly related to bending
"	N.M.	Side to side thickness variation possibly related to bending	N.C.
DAM-6 + DAS-2 *	N.M.	N.M.	N.C.
"	N.C.	N.M.	Possible edge failures and bending at support marks
DAM-7 + DAS-2 *	N.M.	N.M.	F.D.
"	N.M.	N.M.	F.C.
DAM-8 + DAS-2 *	Positive reading correlated with metallic area, no failure	N.M.	F.D.
"	Positive reading → edge failure, most neg. reading → corner failure	N.M.	N.C.

N.M. = No measurement in failed area
N.C. = No correlation between observation and failure
N.F. = No Failure
* Intentionally defected, F.D. = Failed at intentional defect

3.1.6 Selection and Testing of Three Coating Compositions

Based on the application characteristics, performance in 1700°K - 1300 N/m^2 LP-SC testing, and the preceding analytical data and mechanical properties, three coating systems were selected for further study. These were: SA-5, SA-13 and DAM-7 + DAS-2. Three Sylvania applied coatings, R512A, R512C and R512K, were also included in the testing to provide baseline data and a comparison with previous work. The selected coatings were applied, NDT examined, low-pressure, slow-cycle tested to 1700°K and 1810°K at 1300 N/m^2, and subsequently tensile or bend tested.

Specimen Preparation

All required specimens were either prepared (SA-5, SA-13, DAM-7 + DAS-2) or purchased (R512A, C, K) from Sylvania. A total of 20 bend and 12 tensile specimens per coating were needed to complete the scheduled 1700 and 1810°K - 1300 N/m^2 low-pressure, slow-cycle testing. Design of the tensile coupon is shown in Figure 18.

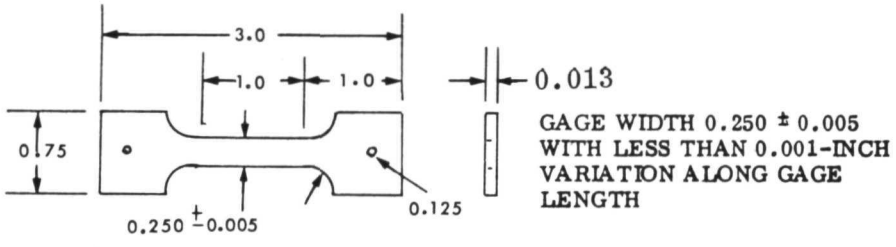

FIGURE 18. TENSILE TEST SPECIMEN FOR LP-SC EXPOSURE

TABLE XIX

FIRING RESULTS FOR NASA-SOLAR COATINGS

Coating	No. Spec. Fired	Wt. Loss % (Range, Ave.)	Coating Weight Range (kg/m^2)
SA-5	26	14-22, 19	0.255-0.332
SA-5	6	10-17, 14	0.281-0.331
SA-13	6	25-28, 26	0.255-0.286
SA-13	26	20-27, 24	0.233-0.292
DAM-7	12	40-44, 42	0.246-0.287
DAM-7	20	38-48, 44	0.247-0.289
DAS-2	12	14-21, 19	0.269-0.312
DAS-2	20	14-31, 24	0.234-0.293

Table XIX contains firing data relevant to the NASA-Solar coatings. All firing cycles were as previously employed. Specimens coated with each different composition were fired in two separate runs. The data of Table XIX, therefore, reflect run-to-run weight loss and coating weight variations, as well as specimen-to-specimen variations. Very minor temperature or pressure differences between firing runs showed no correlation with specimen weight change data for different firing runs.

Data relative to the three Sylvania applied coatings (R512A, C, K) are shown in Table XX. No information on the firing cycles used to apply these coatings was available. The consistency of the specimen-to-specimen weight gain for each Sylvania coating type was excellent and is believed due to extensive NDT evaluation of the as-applied coating bisque.

TABLE XX

WEIGHT GAIN DATA FOR SYLVANIA APPLIED COATINGS

Coating	No. of Specimens	Coating Weight Range (kg/m^2)
R512A	26	0.230-0.261
R512C (SA-1)	26	0.228-0.256
R512K	26	0.233-0.259

All coated specimens were pre-oxidized in a furnace for one hour at 1700° K and atmospheric pressure before being placed into LP-SC testing. This procedure is desirable because it permits the development of a thin oxide or glass layer before extensive exposure to low (about 1000° K) temperature occurs. This technique has been found effective in reducing or eliminating early low-temperature failures in other silicide coatings and is normally performed at Solar.

Intentional Defecting

One bend specimen/coating was intentionally defected by drilling a 0.00132 meter hole through the specimen and one specimen/coating was intentionally defected by removing a 0.00033 meter and a 0.00132 meter diameter area of coating from the specimen surface. Figure 19 shows the appearance of these three defect conditions. These defected specimens were low-pressure, slow-cycle exposed until the appearance of substrate oxide. Equivalent bend specimens were low-pressure, slow-cycled exposed for 20 cycles, defected as above, and further exposed until failure occurred. Failed specimens were bent through the intentionally defected areas.

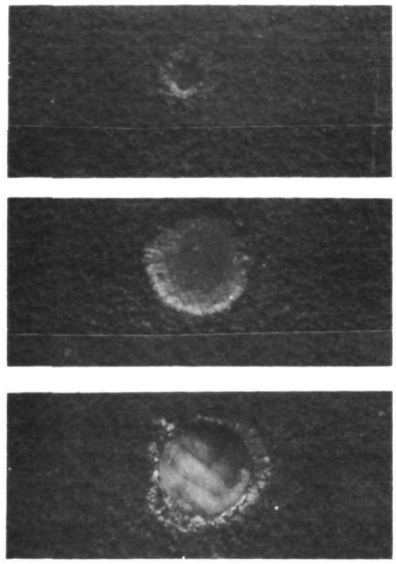

1T Surface Defect

4T Surface Defect

4T Hole Defect

Magnification: 9X

FIGURE 19. INTENTIONALLY FORMED DEFECTS

LP-SC Exposure

Low-pressure, slow-cycle testing was performed as previously described. Tables XXI and XXII contain exposure data for the six coating systems in the non-defected condition, while Tables XXIII and XXIV contain similar data for intentionally defected coupons. All nondefected test coupons were exposed first, and, as a consequence of the results, some coating systems were not tested in the intentionally defected conditions.

The SA-5 coated specimens did not perform as well as was expected from the initial work. The single specimen which was previously tested for 100 cycles to 1700° K without failure developed a thick layer of glass and a dark red color after the first few cycles. Only two of eight specimens showed similar glazing tendencies during this 1700° K - 1300 N/m^2 test series. The other SA-5 coated specimens turned black and developed a relatively thin glass layer when exposed. The "black" SA-5 coated specimens failed after 44, 45, 47 and 62 cycles, while the "red" SA-5 specimens failed after 58 and 86 cycles. Exposure to the 1810° K LP-SC condition resulted in 14 to 25 cycle lifetimes for the SA-5 composition. The specimens glazed heavily and displayed a red-brown or brown color.

Coupons coated with the SA-13 exhibited lifetimes from 40 to 86 cycles in length when exposed at 1700° K and 1300 N/m^2. This was considerably better than the first test sequence which indicated a 43-cycle lifetime for the SA-13 composition. All specimens used in the present test series turned "milk chocolate" brown at first and gradually darkened with increasing exposure. None of the coupons developed an obvious glaze. The color change and glazing tendency of the present set of SA-13

TABLE XXI

TEST RESULTS FOR 1700° K - 1300 N/m^2 LOW-PRESSURE, SLOW-CYCLE EXPOSED SPECIMENS

Specimen No.	Coating Type	Cycles	Comments
11(T)	SA-5	22	Removed for test, black, light glaze.
29(B)	SA-5	22	Removed for test, black, light glaze.
133(B)	SA-5	44	Edge failures, black, light glaze.
51(T)	SA-5	45	Edge failure, black, light glaze.
175(B)	SA-5	47	Removed for test, some deformation, black, light glaze
43(T)	SA-5	58	Corner failure, brown, heavy glaze.
189(B)	SA-5	62	Edge failure, black, light glaze.
40(T)	SA-5	86	Removed for test, some deformation, red-brown, heavy glaze.
44(T)	SA-13	22	Removed for test, brown, no glaze.
104(B)	SA-13	22	Removed for test, brown, no glaze.
7(T)	SA-13	40	Corner failure, brown, no glaze.
211(B)	SA-13	47	Removed for test, brown, no glaze.
37(T)	SA-13	58	Edge failures, brown, no glaze.
1(T)	SA-13	62	Edge failures, brown, no glaze.
192(B)	SA-13	84	Edge failure, brown, no glaze.
219(B)	SA-13	86	Edge failures, brown, no glaze.
3(T)	DAM-7+DAS-2	20	Removed for test, black and brown, medium glaze.
3(B)	DAM-7+DAS-2	20	Removed for test, black, light glaze.
18(T)	DAM-7+DAS-2	49	Removed for test, black, medium glaze.
151(B)	DAM-7+DAS-2	49	Removed for test, black and brown, medium glaze.
45(T)	DAM-7+DAS-2	59	Edge failure, black and brown, medium glaze.
48(B)	DAM-7+DAS-2	64	Edge failure, black, light glaze
28(T)	DAM-7+DAS-2	100	Removed for test, black and brown, medium glaze.
185(B)	DAM-7+DAS-2	100	Removed for test, black and brown, medium glaze.
35(T)	R512A	10	All coatings delaminated by the sixth cycle.
36(T)	R512A	10	Edge and corner failures occurred by the
48(T)	R512A	10	tenth cycle on all specimens. All coupons
218(B)	R512A	10	were tan colored and unglazed.
223(B)	R512A	10	
253(B)	R512A	10	
254(B)	R512A	10	
4(T)	R512C	6	All coatings failed at the edges by the sixth
8(T)	R512C	6	cycle. Most specimens were severely
10(T)	R512C	6	deformed. All coupons were gray-green
7(B)	R512C	6	colored and unglazed.
9(B)	R512C	6	
13(B)	R512C	6	
16(B)	R512C	6	
20(T)	R512K	4	All specimens failed by the fifth cycle.
21(T)	R512K	5	Most were also deformed. All specimens
22(T)	R512K	4	were charcoal gray colored and unglazed.
147(B)	R512K	5	
150(B)	R512K	5	
153(B)	R512K	5	
155(B)	R512K	4	

T = Tensile specimen
B = Bend specimen

TABLE XXII

RESULTS FOR 1810° K - 1300 N/m^2 LOW-PRESSURE, SLOW-CYCLE EXPOSED SPECIMENS

Specimen No.	Coating Type	Cycles	Comments
88(B)	SA-5	14	Corner failure, rough, medium brown glaze.
210(B)	SA-5	14	Corner failure, rough, red-brown glaze.
30(T)	SA-5	15	Edge and surface failure, brown, medium glaze.
49(T)	SA-5	16	Edge failure, brown, medium glaze.
14(T)	SA-5	18	Corner failure, heavy red glaze.
53(T)	SA-5	19	Edge failures, heavy red-brown glaze.
212(B)	SA-5	22-25	Corner failure, deformed, brown glaze.
124(B)	SA-5	22-25	Edge failure, black, medium glaze.
39(T)	SA-13	20	Removed for test, charcoal brown, no glaze.
42(T)	SA-13	24	Edge failure, charcoal brown, slight glaze.
169(B)	SA-13	25	Removed for test, black, slight glaze.
38(T)	SA-13	25	Edge failure, black, no glaze.
50(T)	SA-13	26	Edge failure, charcoal brown, slight glaze.
44(B)	SA-13	51	Removed for test, black, medium glaze.
171(B)	SA-13	53*	Corner failure, black, light glaze.
11(B)	SA-13	63	Corner failures, black, medium glaze.
232(B)	DAM-7+DAS-2	20	Removed for test, rough, black and brown, light glaze.
6(T)	DAM-7+DAS-2	20	Removed for test, rough, patch brown glaze.
25(B)	DAM-7+DAS-2	28	Corner failure, black and brown, slight glaze.
209(B)	DAM-7+DAS-2	28	Edge failure, rough, black, light glaze.
231(B)	DAM-7+DAS-2	28	Edge failure, black, slight glaze.
41(T)	DAM-7+DAS-2	29	Corner failure, brown, heavy patchy glaze.
23(T)	DAM-7+DAS-2	34	Edge failure, brown, medium patchy glaze.
27(T)	DAM-7+DAS-2	44-57	Edge failure, brown, heavy glaze.
32(T)	R512A	8	Edge failures, gray-brown, no glaze.
29(T)	R512A	8	Edge failures, gray-brown, slight glaze.
204(B)	R512A	9	Edge failures, green and black, slight glaze.
206(B)	R512A	9	Edge failures, green and black, slight glaze.
217(B)	R512A	9	Edge failures, brown and black, slight glaze.
213(B)	R512A	14	Edge failures, green and black, slight glaze.
17(B)	R512C	2	Edge failures, black and gray, slight glaze.
24(B)	R512C	2	Edge failures, black and gray, slight glaze.
60(B)	R512C	2	Edge failures, black and gray, slight glaze.
64(B)	R512C	2	Edge failures, black and gray, slight glaze.
109(B)	R512K	1	Edge failures, gray-black, no glaze.
116(B)	R512K	1	Edge failures, gray-black, no glaze.
117(B)	R512K	1	Edge failures, gray-black, no glaze.
121(B)	R512K	1	Edge failures, gray-black, no glaze.

T = Tensile specimen
B = Bend specimen

*Specimen hit edge of furnace - probably chipped.

TABLE XXIII

TEST RESULTS FOR INTENTIONALLY DEFECTED 1700°K - 1300 N/m^2 LOW-PRESSURE, SLOW-CYCLE EXPOSED SPECIMENS

Specimen	Coating	Defect	Total Cycles	Cycles After Defect	Comment
72	SA-5	4T hole	1	1	Substrate oxide at defect.
73	SA-5	1T and 4T surface	2	2	Hole at 4T site; 1T site okay.
137	SA-5	4T hole	23	--	Failed before being defected.
152	SA-5	1T and 4T surface	20	3	Hole at 4T site; oxide at 1T site.
247	SA-13	4T hole	2	2	Substrate oxide at defect.
130	SA-13	1T and 4T surface	2	2	Hole at 4T site; 1T site okay.
235	SA-13	4T hole	21	1	Substrate oxide at defect.
63	SA-13	1T and 4T surface	23	3	Hole at 4T site; oxide at 1T site.
76	DAM-7+ DAS-2	4T hole	1	1	Substrate oxide at defect.
127	DAM-7+ DAS-2	1T and 4T surface	2	2	Hole at 4T site; 1T site healed.
113	DAM-7+ DAS-2	4T hole	21	1	Substrate oxide at defect.
220	DAM-7+ DAS-2	1T and 4T surface	23	3	Hole at 4T site, 1T site healed.

TABLE XXIV

TEST RESULTS FOR INTENTIONALLY DEFECTED 1810°K - 1300 N/m^2 LOW-PRESSURE, SLOW-CYCLE EXPOSED SPECIMENS

Specimen	Coating	Defect	Total Cycles	Cycles After Defect	Comments
106(B)	SA-13	4T hole	1	1	Substrate oxide, 0.004 m hole
251(B)	SA-13	1T and 4T spot	1	1	Oxide pimple at 1T and 4T spot
163(B)	SA-13	4T hole	21	1	Substrate oxide, 0.003 m hole
193(B)	SA-13	1T and 4T spot	21	1	Oxide pimple at 1T and 4T spot
266(B)	DAM-7+DAS-2	4T hole	1	1	Substrate oxide, 0.004 m hole
47(B)	DAM-7+DAS-2	1T and 4T spot	--	--	Failed in pre-oxidation
170(B)	DAM-7+DAS-2	4T hole	21	1	Substrate oxide 0.004 m hole
199(B)	DAM-7+DAS-2	1T and 4T spot	21	1	0.002 m hole at 4T spot, oxide pimple at 1T spot

coated specimens was the same as was observed in the initial evaluation. Exposure to the 1810° K test cycle caused all SA-13 coated coupons to turn black and to slowly develop a translucent, milky white glaze. Lifetimes ranged from 24-63 cycles and glazing was heavier at the bottom than at the top of the specimens.

Appearance of the 1700° K exposed DAM-7 + DAS-2 coated specimens was similar to the previously tested, nondefected coupon. The specimens displayed a rough surface, mottled black and brown coloration, and areas of heavy and light glazing. Marks from the support rods used during the firing of the specimens were normally the most heavily glazed areas. None of the tested specimens developed the very heavy, fluid layer of glass previously observed on a DAM-7 + DAS-2 coated specimen which withstood forty-five 1700° K - 1300 N/m^2 cycles. Only two of the present eight specimens failed during testing. These failures occurred after 50 and 64 cycles. All other 1700° K specimens lasted the scheduled 25, 50 or 100 cycles. Exposure to the 1810° K LP-SC profile reduced the life expectancy of a DAM-7 + DAS-2 coated coupon to a maximum of about 44-57 cycles. The outward appearance (color and glazing) of the coating was the same as for 1700° K exposure.

Exposure of the Sylvania applied R512A coating to the 1700° K - 1300 N/m^2 LP-SC test resulted in severe delamination of the coating after the first five or six cycles. Failure of all specimens occurred by the tenth cycle. Every R512A coated coupon turned a light tan color and showed no evidence for surface glass formation. Testing with the 1810° K - 1300 N/m^2 LP-SC profile caused the R512A coated specimens to fail in the 8-14 cycle range. The specimens turned dark brown or black and in some instances showed green colored areas. A slight tendency to glaze was observed.

Sylvania applied R512C coatings experienced failure by the sixth 1700° K - 1300 N/m^2 cycle. The coupons displayed a gray-green color and developed no obvious glaze. In addition to edge failures, most specimens also deformed during testing. Failure after the second cycle to 1810° K was observed for all R512C coupons. Each specimen developed gray and black colored areas and showed a limited tendency to glaze.

Exposure to the 1700° K - 1300 N/m^2 LP-SC profile failed all R512K coated coupons by the fifth cycle. The coating turned charcoal gray, did not develop a glazed surface, and became quite rough. Most coupons were severely deformed. Failure of the R512K coating occurred during the first cycle to 1810° K. Each specimen displayed a charcoal black, unglazed surface appearance.

Tensile Test Data

Room temperature tensile tests were conducted in an Instron Tensile Machine with uncoated, as-coated and exposed specimens. Generated data are shown in

Table XXV. The ultimate and yield strength values are based on the dimensions of the coupons before coating. It was found that 12 specimens from the original batch of 72 tensile test coupons escaped pre-coating measurement. The nominal gage width and thickness were used to calculate the strength data for each of these specimens. Samples were strained at a constant rate of 0.05 inch/minute over a 1-inch gage length. A clamp-on extensometer fed an x-y recorder and provided the data necessary to determine the percent elongation and the yield strength (0.2 percent offset). Elongation was also determined by measuring the pre- and post-test distances between two scribe marks on each specimen.

The data for uncoated 90Ta-10W alloy correspond reasonably well to published data determined from recrystallized 254 x 10^{-6} meter thick stock (Ref. 5) and to vendor supplied data (Table III). Unexposed coated specimens were found to elongate about 13-16 percent as compared with about 24 percent for uncoated material. Single SA-5 and DAM-7 + DAS-2 coated coupons elongated only 5.8 and 7.8 percent, respectively. Exposure to the 1700° K - 1300 N/m^2 LP-SC condition caused a further decrease in the ability of the substrate to elongate. The SA-5, SA-13 and DAM-7 + DAS-2 coated specimens elongated about 7-13 percent after 20-100 exposure cycles. No trend of decreased ability to elongate with increased exposure time was evident from the limited data. Exposure to the 1810° K - 1300 N/m^2 condition resulted in elongation values of 4-7 percent, 7-9 percent, and approximately zero percent, respectively, for SA-5, SA-13 and DAM-7 + DAS-2 coated specimens. Little or no ability to elongate was observed for any exposed R512A, C or K coated specimen.

Strength values for the as-coated specimens were approximately equal to the uncoated specimen values. Exposure to the 1700° K test profile also had little influence on observed ultimate and yield strengths of the SA-5, SA-13 or DAM-7 + DAS-2 coated coupons. Cycling to 1810° K caused embrittlement and loss of strength by the DAM-7 + DAS-2 coated substrate, but not by the SA-5 or SA-13 coated specimens.

Bend Test Data

With only one bend test coupon available for each exposure condition, it was necessary to employ a progressive bend test in order to determine approximate ductile brittle bend transition temperatures (DBBTT). Each specimen was placed in the bend test fixture (Fig. 20) and was bent at room temperature (295° K) over a 4T radius (T = material thickness) until a 0.17 radian deflection was attained. Every specimen which withstood the room temperature deflection was then subjected to a 0.35 radian deflection at 244° K. The specimens were next subjected to a 0.53 radian deflection at 200° K. All specimens which survived this test level were subsequently deflected 1.83 radians at 82° K. This final deflection yielded an approximately 1.6 radian permanent bend if the specimen did not fracture. Only the uncoated and as-coated coupons withstood bending at the 82° K level. Most coated and exposed SA-5, SA-13 and DAM-7 + DAS-2 coupons withstood the 0.53 radian deflection at 200° K

TABLE XXV

ROOM TEMPERATURE TENSILE DATA AFTER LP-SC EXPOSURE AT 1700 OR 1810°K AND 1300 N/m^2

Specimen Number	Coating	Exposure (cycles/°K)	Yield MN/m^2	Ultimate MN/m^2	Elongation (percent)
0	Uncoated	0	503	589	25.0
00	Uncoated	0	560	664	23.0
Ref. 5	Uncoated	0	519	611	19.0
9*	SA-5	0	534	605	15.6
34*	SA-5	0	545	619	5.8
11*	SA-5	22/1700	583	630	12.0
51*	SA-5	45/1700	615	653	9.0
40	SA-5	86/1700	567	607	10.0
49*	SA-5	16/1810	575	609	4.0
53*	SA-5	18/1810	560	599	7.0
5*	SA-13	0	551	621	15.6
52*	SA-13	0	562	625	16.4
44	SA-13	22/1700	562	605	8.5
7	SA-13	40/1700	595	651	13.0
1	SA-13	62.1700	580	629	11.8
39*	SA-13	20/1810	575	617	7.0
38*	SA-13	25/1810	550	596	9.0
15	DAM-7 + DAS-2	0	534	566	7.8
19	"	0	533	591	14.6
3	"	20/1700	581	609	6.8
18	"	49/1700	555	579	12.3
28	"	100/1700	557	591	8.5
6	"	20/1810	-	556	0.6
23	"	34/1810	-	432	0.3
33	R512A	0	483	563	13.4
48	R512A	10/1700	-	176	0.3
32	R512A	8/1810	-	316	4.0(a)
16		0	545	631	14.6
26	R512K	0	525	608	16.1
22	R512K	4/1700	-	225	1.0

* Based on nominal cross sectional area.

(a) Questionable value.

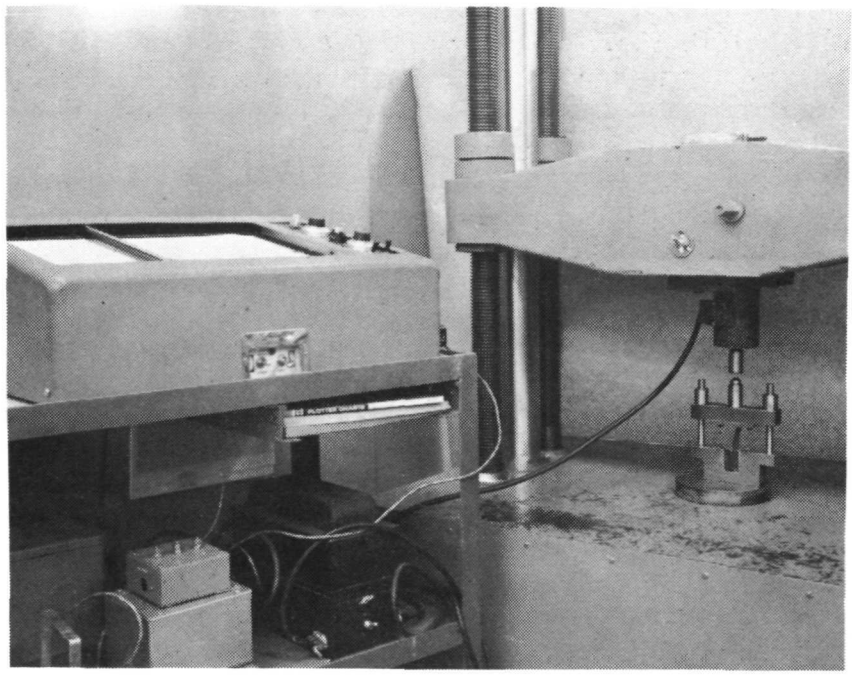

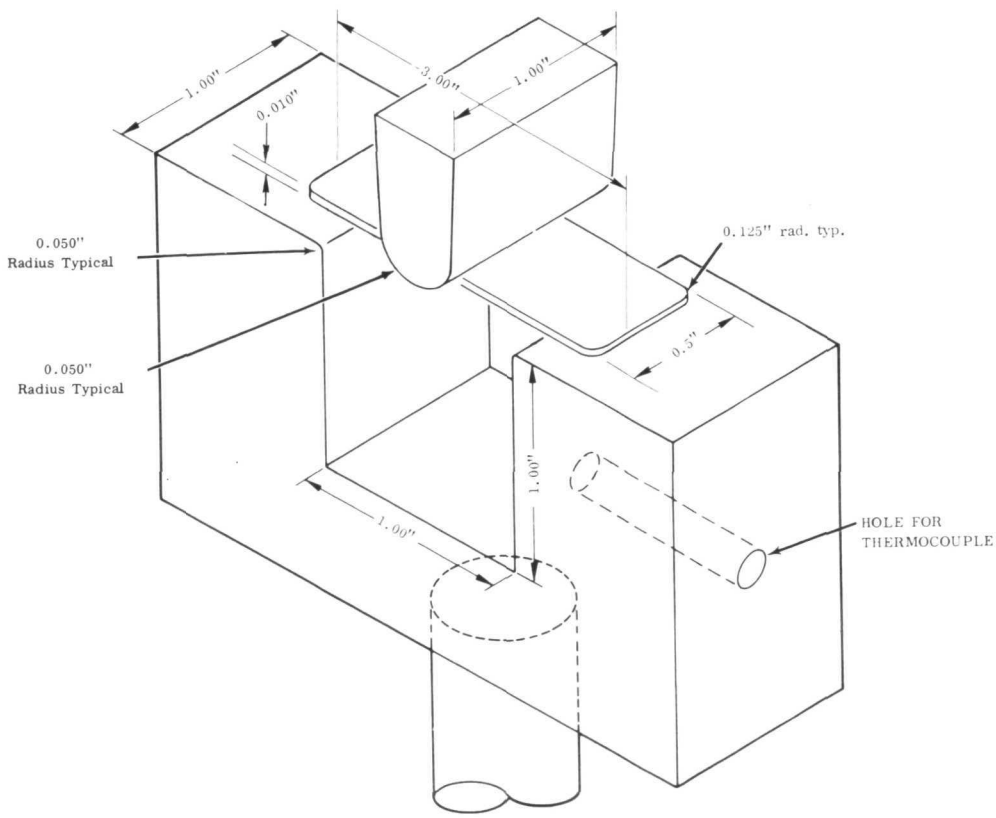

FIGURE 20. BEND TEST FIXTURE AND LOAD DEFLECTION RECORDER

but fractured during the 1.83 radian deflection at 82°K. The majority of LP-SC exposed R512A, C and K coated specimens fractured during the room temperature deflection. Many of the intentionally defected and exposed specimens withstood the 0.53 radian deflection at 200°K. Intentionally defected specimens were not bent at 82°K after it had been shown that no nondefected and exposed coupon would sustain bending at this temperature. Table XXVI contains data for all nondefected coupons, and Table XXVII contains data for the intentionally defected specimens.

Analytical Data

Extensive metallographic analyses of the tested specimens were performed to aid in defining the effects of oxidation on the coating and substrate. Substrate microhardness values, diffusion zone thicknesses, weight changes during LP-SC testing and X-ray diffraction (XRD) and electron microprobe (EMP) analyses were also conducted.

Figure 21 shows a macroscopic view, and Figures 22, 23 and 24 detail the microscopic appearance of R512A, C and K coated samples after 1700 and 1810°K - 1300 N/m^2 LP-SC exposure. While the Sylvania applied coatings experienced early failures, it should be remembered that these coatings were first generation systems and were not fully developed during an adequate research effort. No claims by Sylvania indicated that particularly long lifetimes should be expected from these coatings when applied to tantalum alloys and tested in the 1700 and 1800°K range.

Microscopic appearances of lightly and heavily glazed, 1700°K - 1300 N/m^2 exposed SA-5 coatings are shown in Figure 25. The variable appearance of the SA-5 coated, LP-SC exposed specimens is possibly related to the weight loss during fusion. Those specimens which lost 11-15 weight percent during fusion tended to glaze heavily, while those coupons which lost about 16-22 weight percent during fusion developed a thin glaze and a black color during testing. Less of the "black" than of the "red-brown" coating was consumed during testing as is seen by the relative quantities of surface glass and the frequency of glass-filled "holes" (Fig. 25). Edges of the heavily glazed coupon were observed to be nearly free of the thick glass layer.

The macro and microscopic appearance of SA-5 coated coupons after 15-19 LP-SC's to 1810°K and 1300 N/m^2 are shown in Figure 26. Of particular interest was the tendency for this coating to form bubbles in the heavy red-brown glaze. This suggested the possibility of vaporization from within the coating of constituents or reaction products such as MoO_3, WO_3 or SiO. Comparison of Figure 25, Part B, with Figure 26, Part B, shows a similar degree of coating consumption during 58 cycles to 1700°K and during 19 cycles to 1810°K. The glass on these coupons appears to be multi-phased rather than homogeneous.

TABLE XXVI

BEND TEST DATA FOR NON-DEFECTED COUPONS AFTER 1300 N/m^2 LP-SC

Specimen Number	Coating	Exposure (cycles/°K)	Test Temperature			
			295°K	244°K	200°K	82°K
567	Uncoated	0	B	B	B	B
621	Uncoated	0	B	B	B	B
90	SA-5	0	B	B	B	B
198	SA-5	0	B	B	B	B
29	SA-5	22/1700	B	B	B	F
175	SA-5	47/1700	B	F	-	-
210	SA-5	14/1810	B	B	B	F
159	SA-13	0	B	B	B	B
245	SA-13	0	B	B	B	B
104	SA-13	22/1700	B	B	B	F
211	SA-13	47/1700	B	B	B	F
219	SA-13	86/1700	B	B	B	F
169	SA-13	25/1810	B	B	B	F
171	SA-13	53/1810	B	B	B	F
11	SA-13	63/1810	B	B	B	F
33	DAM-7+DAS-2	0	B	B	B	B
119	DAM-7+DAS-2	0	B	B	B	B
3	DAM-7+DAS-2	20/1700	B	B	B	F
151	DAM-7+DAS-2	49/1700	B	B	B	F
185	DAM-7+DAS-2	100/1700	B	B	B	F
232	DAM-7+DAS-2	20/1810	B	B	B	F
25	DAM-7+DAS-2	28/1810	B	B	B	F
184	R512A	0	B	B	B	B
223	R512A	10/1700	B	B	B	F
217	R512A	9/1810	B	B	B	F
67	R512C	0	B	B	B	B
7	R512C	6/1700	F	-	-	-
123	R512K	0	B	B	B	B
155	R512K	4/1700	F	-	-	-

B = Deflected without cracking or fracturing

F = Fractured

TABLE XXVII

BEND TEST DATA FOR INTENTIONALLY DEFECTED COUPONS AFTER 1300 N/m^2 LP-SC

Specimen Number	Coating	Defect Type	Exposure (cycles/°K)	Test Temperature			
				295°K	244°K	200°K	82°K
72	SA-5	4T hole	1/1700	B	B	B	NT
73	SA-5	1T spot	2/1700	B	B	B	NT
73	SA-5	4T spot	2/1700	B	B	B	NT
152	SA-5	1T spot	20+3/1700	B	B	F	-
152	SA-5	4T spot	20+3/1700	B	B	B	NT
247	SA-13	4T hole	2/1700	B	B	B	NT
235	SA-13	4T hole	20+1/1700	B	B	B	NT
130	SA-13	1T spot	2/1700	B	B	B	NT
130	SA-13	4T spot	2/1700	B	B	B	NT
63	SA-13	1T spot	20+3/1700	B	B	B	NT
63	SA-13	4T spot	20+3/1700	B	B	B	NT
106	SA-13	4T hole	1/1810	B	B	B	NT
163	SA-13	4T hole	20+1/1810	B	B	B	NT
251	SA-13	1T spot	1/1810	B	B	B	NT
251	SA-13	4T spot	1/1810	B	B	B	NT
193	SA-13	1T spot	20+1/1810	B	B	B	NT
193	SA-13	4T spot	20+1/1810	B	B	B	NT
76	DAM-7+DAS-2	4T hole	1/1700	B	B	F	-
113	DAM-7+DAS-2	4T hole	20+1/1700	B	B	F	-
127	DAM-7+DAS-2	1T spot	2/1700	B	B	B	NT
127	DAM-7+DAS-2	4T spot	2/1700	B	B	B	NT
220	DAM-7+DAS-2	1T spot	20+3/1700	B	B	B	NT
220	DAM-7+DAS-2	4T spot	20+3/1700	B	B	B	NT
266	DAM-7+DAS-2	4T hole	1/1810	B	B	B	NT
170	DAM-7+DAS-2	4T hole	20+1/1810	F	-	-	-
199	DAM-7+DAS-2	1T spot	20+1/1810	B	B	F	-
199	DAM-7+DAS-2	4T spot	20+1/1810	B	B	F	-

B = Defected without cracking or fracturing

F = Fractured

NT = Not tested

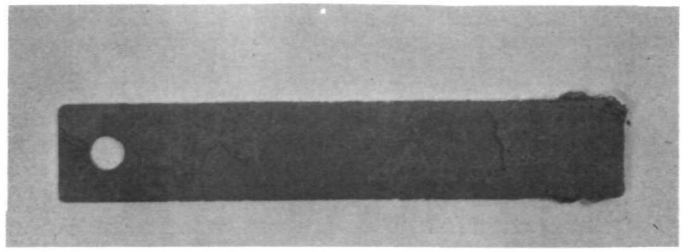

R512A

Exposure: 10 Cycles, 1700°K-
1300 N/m^2

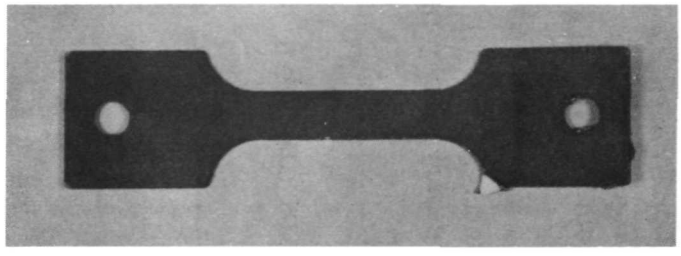

R512C

Exposure: 6 Cycles, 1700°K -
1300 N/m^2

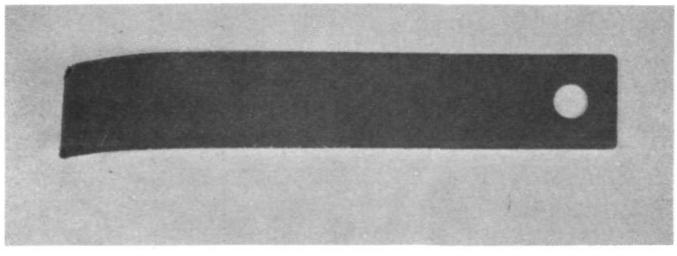

R512K

Exposure: 5 Cycles, 1700° K -
1300 N/m^2

Magnification: 1X

FIGURE 21. TYPICAL FAILURES FOR SYLVANIA APPLIED COATINGS

Figure 27 exhibits the microstructure of the SA-13 coating after 22 and 86 LP-SC's to 1700° K. Almost no oxide or glass is evident on the surface of either specimen; however expansion cracks were all observed to contain coating oxidation products. The diffusion zone under the applied portion of the coating appeared to be made up of two layers rather than one, as was seen under the SA-5 coatings. The outer layer in the diffusion zone was formed during fusion and did not appear to change during 1700° K testing. Many small coating cracks run approximately parallel to the coating-substrate interface but not at the interface.

A thick layer of glass is seen to have formed on the surface of the SA-13 coating during the 1810° K exposure, Figure 28. This glass appears multi-phased and seems to permeate most of the pores and cracks which developed in the coating. The diffusion zone of the coating contained two or more phases but consisted of only one layer in contrast to the two-layer diffusion zone seen in the as-coated and 1700° K

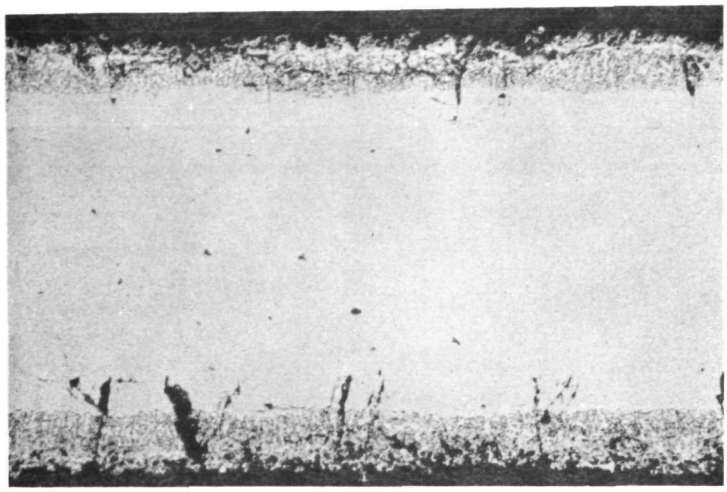

Specimen No. 176(B)

As-Received

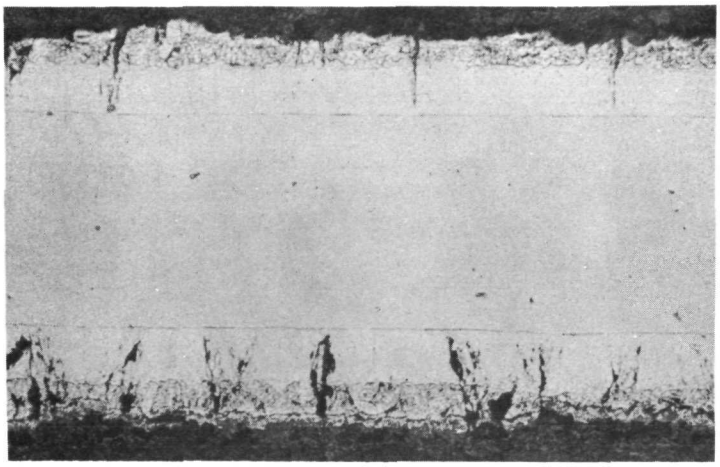

Specimen No. 253(B)

10 LP-SC's to 1700° K

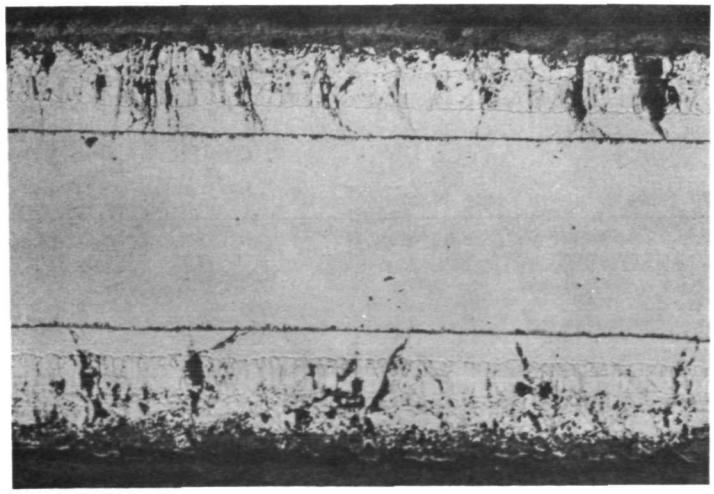

Specimen No. 213(B)

14 LP-SC's to 1810° K

Etchant: HF-HNO_3-Lactic

Magnification: 125X

FIGURE 22. AS-RECEIVED AND EXPOSED R512A COATED SPECIMENS

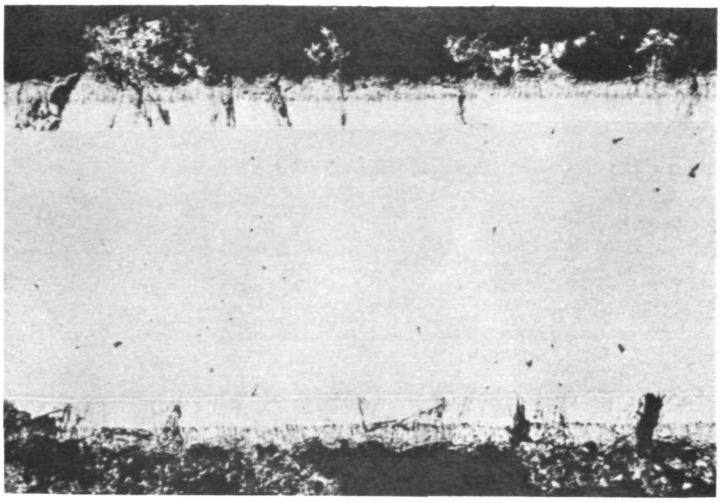

Specimen No. 68(B)

As-Received

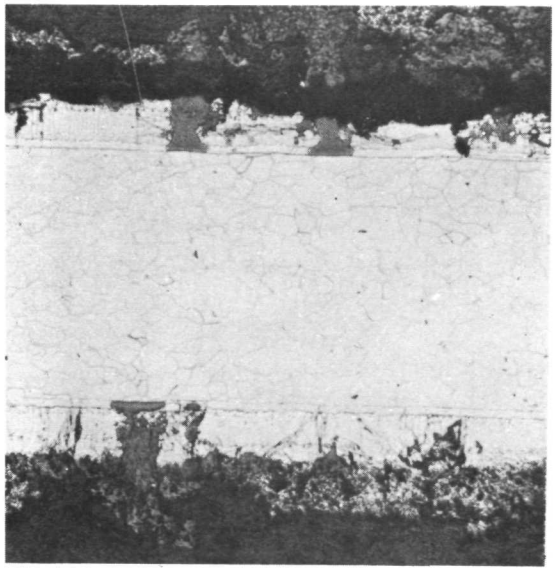

Specimen No. 16(B)

6 LP-SC's to 1700° K

Etchant: $HF-HNO_3$-Lactic

Magnification: 125X

FIGURE 23. AS-RECEIVED AND EXPOSED R512C COATED SPECIMENS

tested coupons. The growth of a columnarly structured compound is evident at the lowest silicon activity interface, probably indicating the growth of a lower tantalum silicide such as Ta_2Si.

Figure 29 shows the microscopic details of the DAM-7 + DAS-2 coating after 20 (Part A) and 100 (Part B) LP-SC's to 1700° K and 1300 N/m^2. The glass layer is multi-phased. A single and apparently two-phased diffusion zone divided the applied coating from the residual substrate. As with SA-13, there were many short coating cracks just above the diffusion zone.

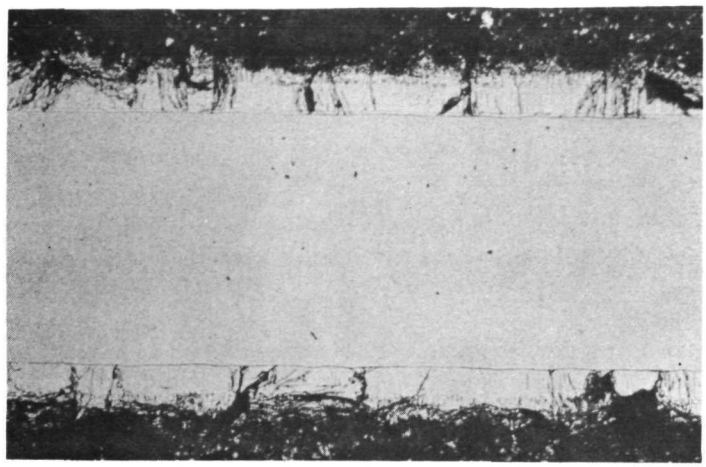

Specimen No. 131(B)

As-Received

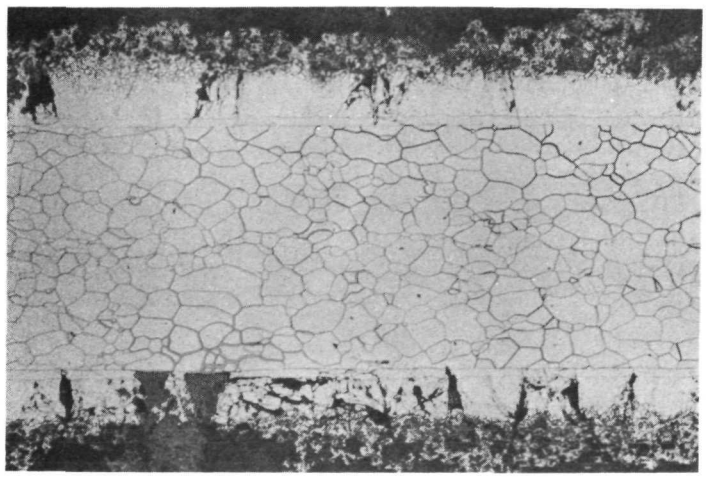

Specimen No. 155(B)

4 LP-SC's to 1700° K

Etchant: HF-HNO_3-Lactic

Magnification: 125X

FIGURE 24. AS-RECEIVED AND EXPOSED R512K COATED SPECIMENS

After 1810° K LP-SC exposure, the DAM-7 + DAS-2 coating features are shown in Figure 30. The glass layer on these specimens looks quite similar to that seen on the 1700° K exposed coupons. Again, the diffusion zone appeared two-phased and also of similar structure to that seen under the 1700° K exposed specimens.

Coated specimens were deliverately defected by grit blasting 1T and 4T (T = substrate alloy thickness) holes through the coating or by drilling a 4T hole through the entire specimen. Coated and intentionally defected examples of the SA-13 coating system were chosen for metallographic analysis to determine the effect of LP-SC exposure on substrate properties. Figure 31 shows the cross-sectional appearance of a 4T spot defect after 2 LP-SC's to 1700° K (Part A) and after 1 LP-SC to 1810° K (Part B). In each case, the coating defect was placed on the specimen surface nearest the top of the page. The original defect was 1320 x 10^{-6} meter in diameter and approximately doubled during the exposure. The oxide "pimple" which generally formed during the first test cycle is evident on the 1810° K exposed coupon. A similar "pimple" formed on the 1700° K specimen and subsequently spalled off.

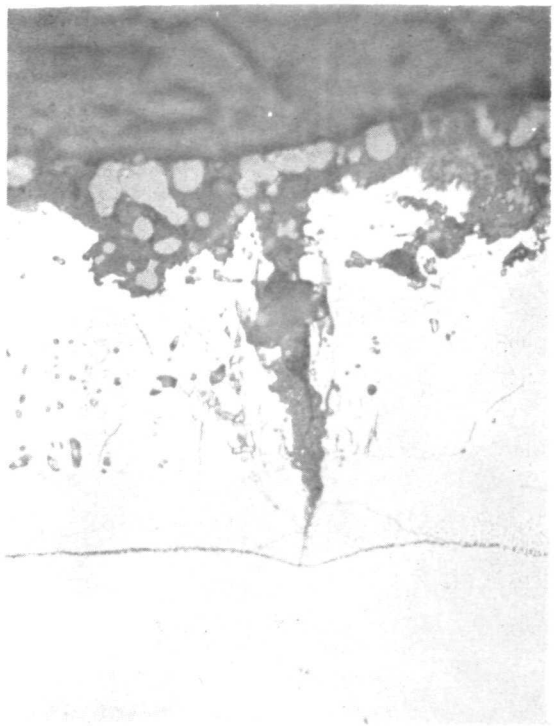

Part A - Lightly Glazed

Specimen No. 189(B)

62 LP-SC's

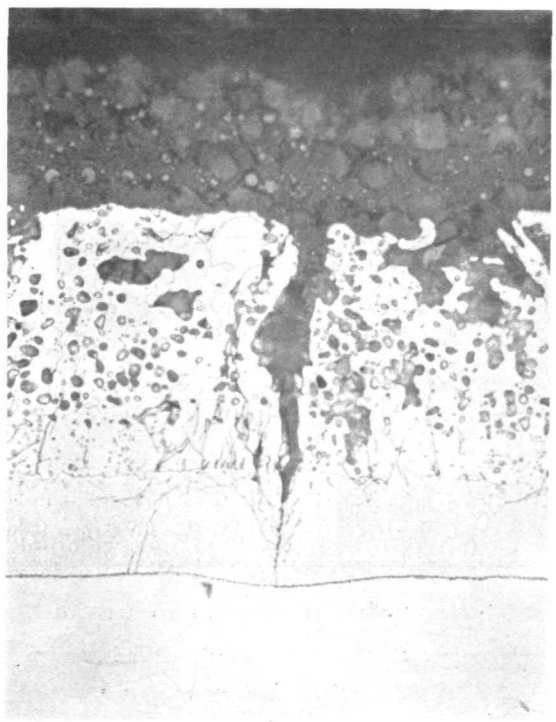

Part B - Heavily Glazed

Specimen No. 43(T)

58 LP-SC's

Etchant: $HF-HNO_3$-Lactic

Magnification: 500X

FIGURE 25. SA-5 MICROSTRUCTURE AFTER LP-SC EXPOSURE AT 1700°K AND 1300 N/m^2

Part A

Specimen No. 14(T)

15 LP-SC's

Magnification: 1X

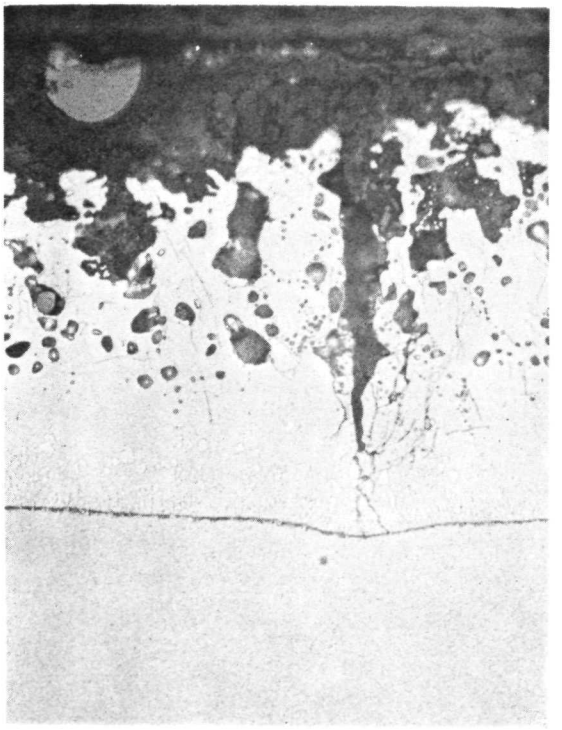

Part B

Specimen No. 53(T)

19 LP-SC's

Etchant: HF-HNO_3-Lactic

Magnification: 500X

FIGURE 26. SA-5 MACRO AND MICROSTRUCTURE AFTER LP-SC EXPOSURE AT 1810°K AND 1300 N/m^2

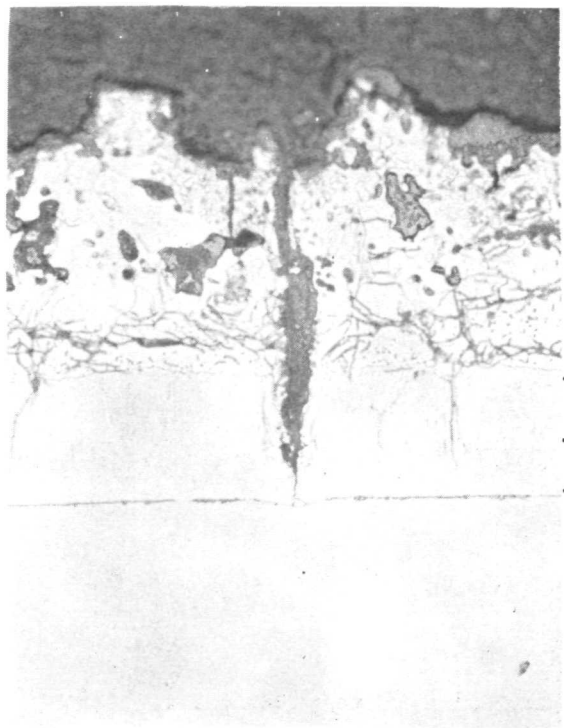

Part A

Specimen No. 104(B)

22 LP-SC's

Columnar growth layer

Two-phased substrate silicide

Part B

Specimen No. 219(B)

86 LP-SC's

Columnar growth layer

Two-phased substrate silicide

Etchant: $HF-HNO_3$-Lactic

Magnification: 500X

FIGURE 27. SA-13 MICROSTRUCTURE AFTER LP-SC EXPOSURE AT 1700°K AND 1300 N/m^2

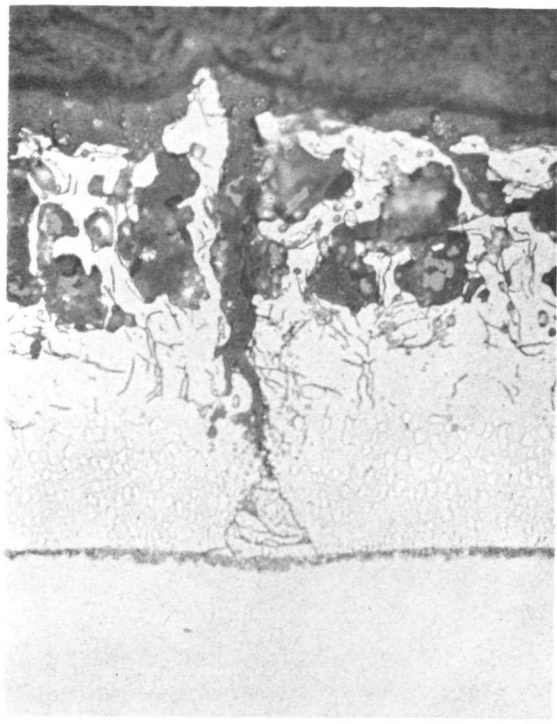

Part A

Specimen No. 39(T)

20 LP-SC's

No remaining columnar layer

Two-phased substrate silicide

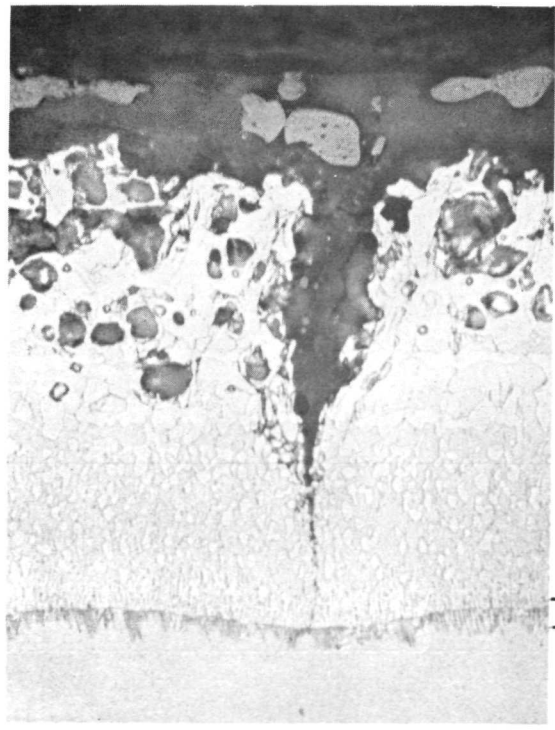

Part B

Specimen No. 11(B)

63 LP-SC's

Two-phased substrate silicide

Ta_2Si or ?

Etchant: $HF-HNO_3$-Lactic

Magnification: 500X

FIGURE 28. SA-13 MICROSTRUCTURE AFTER LP-SC EXPOSURE AT 1810°K AND 1300 N/m^2

Part A

Specimen No. 3(T)

20 LP-SC's

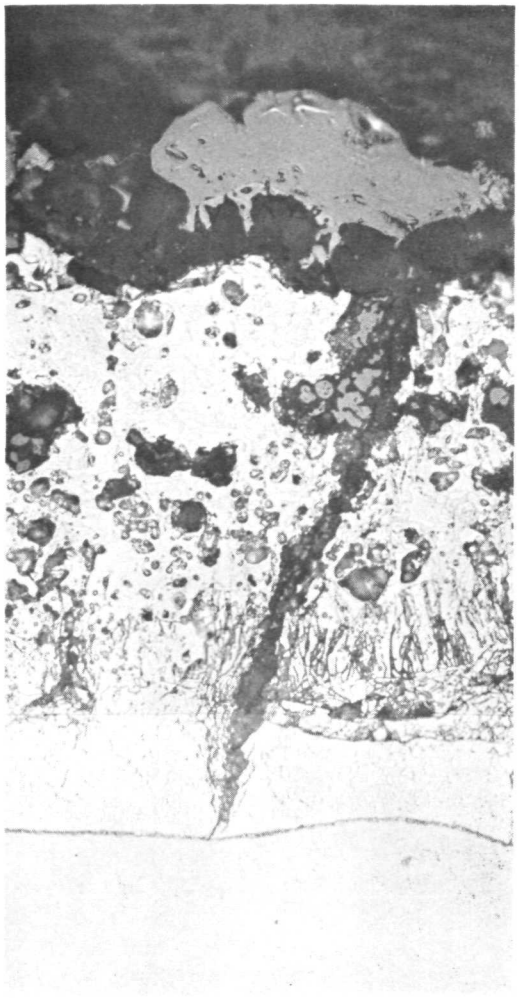

Part B

Specimen No. 28(T)

100 LP-SC's

Etchant: $HF-HNO_3$-Lactic

Magnification: 500X

FIGURE 29. DAM-7 + DAS-2 MICROSTRUCTURE AFTER LP-SC EXPOSURE AT 1700°K AND 1300 N/m^2

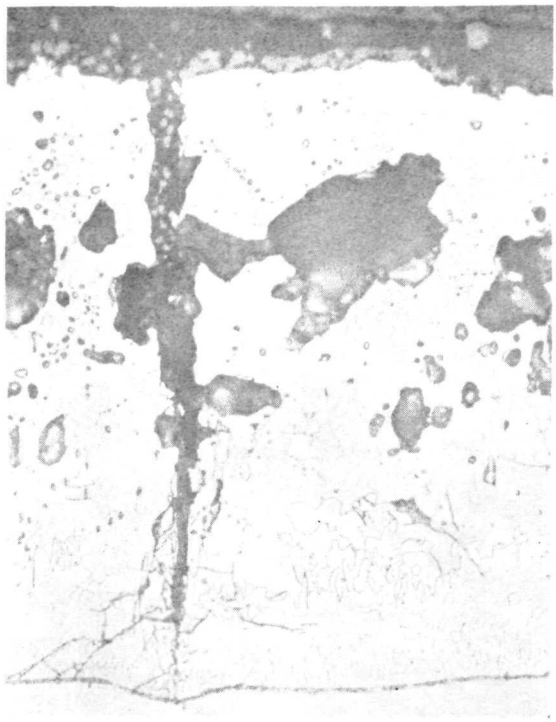

Part A

Specimen No. 25(B)

28 LP-SC's

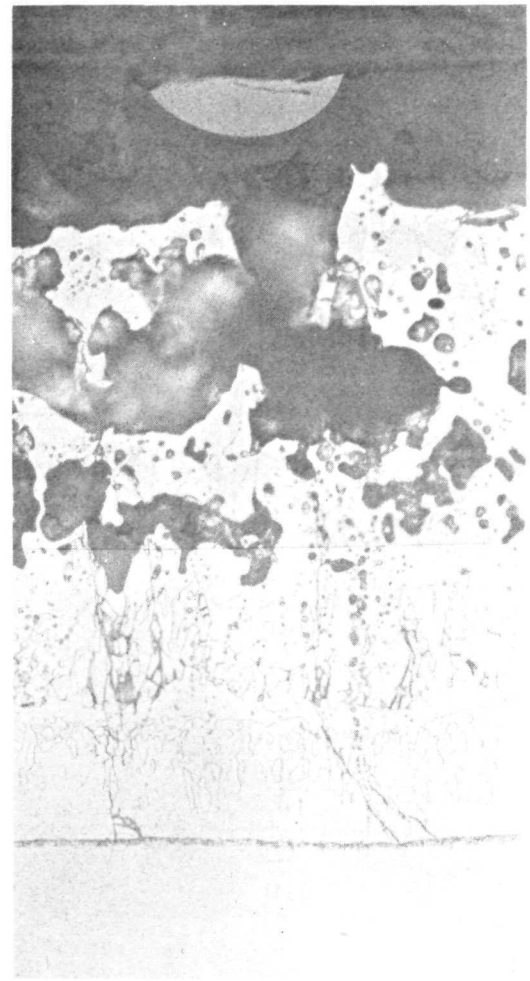

Part B

Specimen No. 27(T)

57 LP-SC's

Etchant: HF-HNO_3-Lactic

Magnification: 500X

FIGURE 30. DAM-7 + DAS-2 MICROSTRUCTURE AFTER LP-SC EXPOSURE AT 1810°K AND 1300 N/m^2

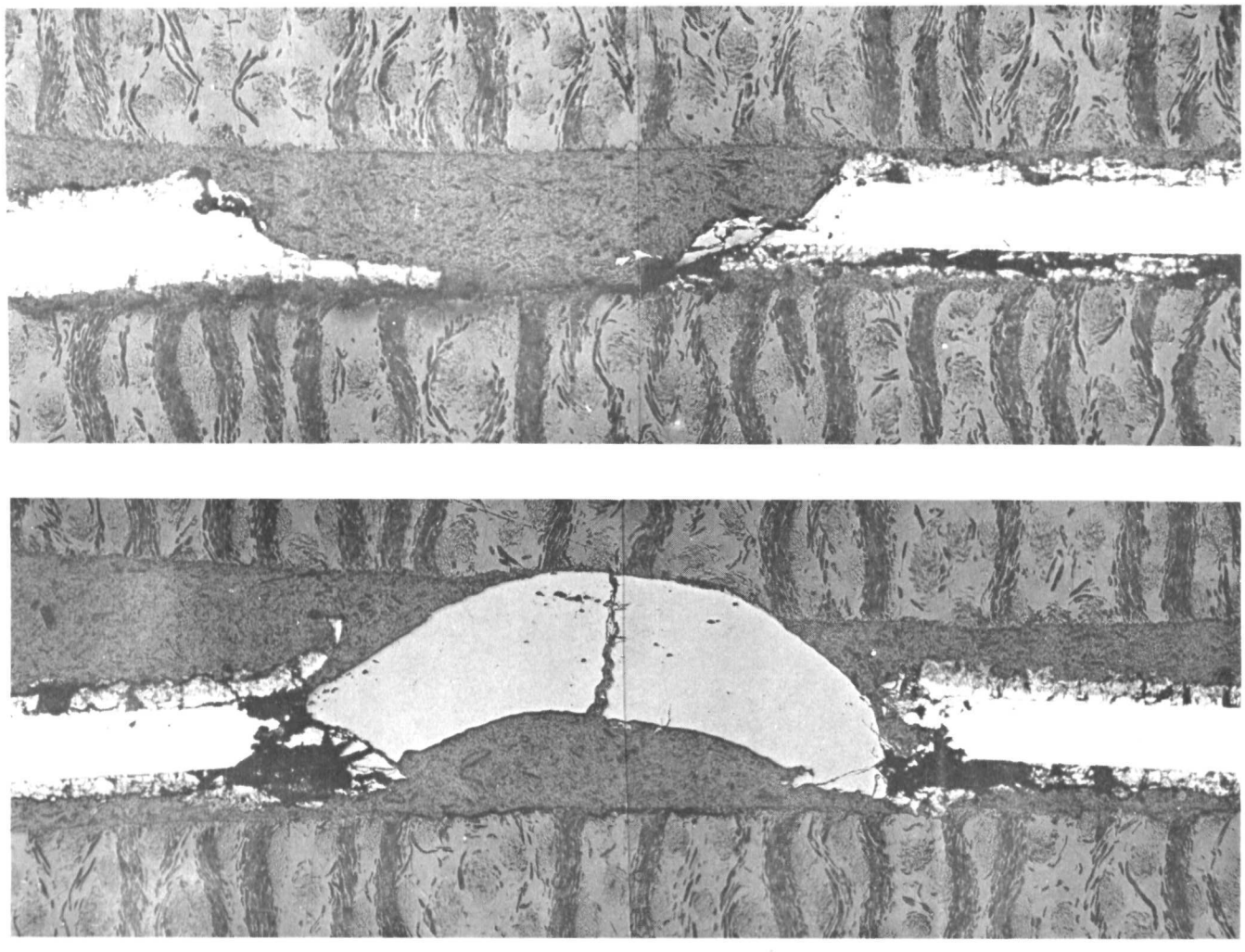

Part A

Specimen No. 130(B)

2 LP-SC's to 1700° K

4T Spot Defect

Part B

Specimen No. 251(B)

1 LP-SC to 1810° K

4T Spot Defect

Etchant: HF-HNO_3-Lactic

Magnification: 35X

FIGURE 31. 4T SPOT DEFECTED SPECIMENS, SA-13 COATING, AFTER LP-SC EXPOSURE AT 1700 OR 1810°K AND 1300 N/m^2

Figure 32 shows the macro and microscopic appearance of coupons which were defected with a 1320 x 10^{-6} meter hole and subsequently LP-SC exposed. A single cycle to 1700° K did not obviously fail the specimen, while one cycle to 1810° K nearly burned the specimen in half. Two cycles to 1700° K and 1300 N/m^2 obviously caused severe damage. Figure 33 diagrams substrate centerline microhardness data for each specimen shown in Figure 32. Comparison of these data with data for protected areas showed that substrate hardening occurred up to about 1250-1500 x 10^{-6} meter back from the edge of the final hole.

Data in Table XXVIII show the approximate diameter of the area of substrate affected by 4T spot and hole defects. The hole defect is seen to be much the more serious defect for SA-13 coated coupons. In spite of the appearance of the defected specimens, bend ductility was not lost, as was shown by the data of Table XXVII. This coating (SA-13) exhibited no ability to self heal and these data, therefore, may represent the maximum amount of substrate damage that might be expected for these test conditions.

TABLE XXVIII

TOTAL AREA INFLUENCED BY INTENTIONALLY PRODUCED DEFECTS IN SA-13 COATING

Defect Type	Exposure (cycles/°K/N/m^2)	Approximate Diameter of Affected Region (meter)
4T Spot	2/1700/1300	0.5 x 10^{-3}
4T Hole	2/1700/1300	3 x 10^{-3}
4T Spot	1/1810/1300	0.5 x 10^{-3}
4T Hole	1/1810/1300	11 x 10^{-3}

Measurements of the quantity/side of substrate material consumed during LP-SC exposure were made and are shown in Figure 34. Both diffusion zone thickness and residual substrate thickness measurements were used to define these plots. The data do not pass through the 0, 0 point because a thin M_5Si_3 layer is formed during formation of the coating. Table XXIX defines the amount of substrate consumed during the fusion processes for each coating. Total substrate consumption at any time during test may be determined by combining the appropriate values from Figure 34 and Table XXIX.

Hardness measurements for LP-SC exposed coupons are graphed in Figure 35 to show the effect of increasing exposure times. All readings were taken in duplicate,

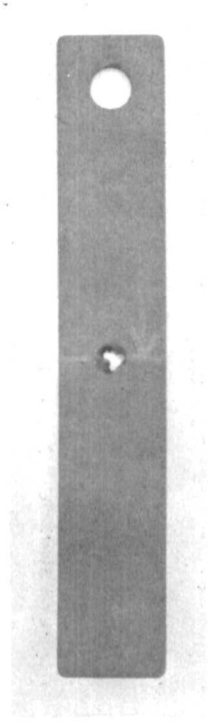

Mag: 1X

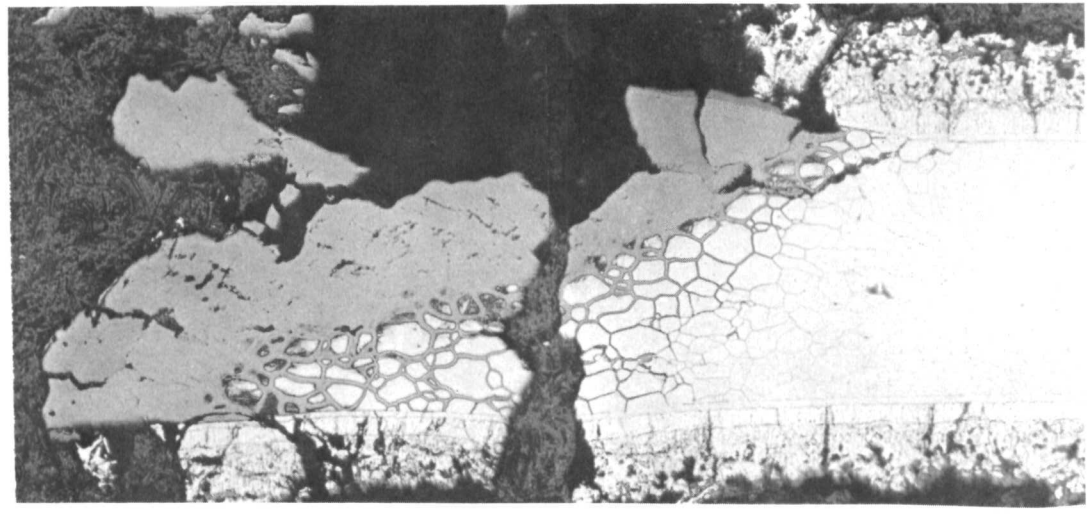

Part A

Specimen No. 247(B)

2 LP-SC's to 1700° K

4T Hole Defect

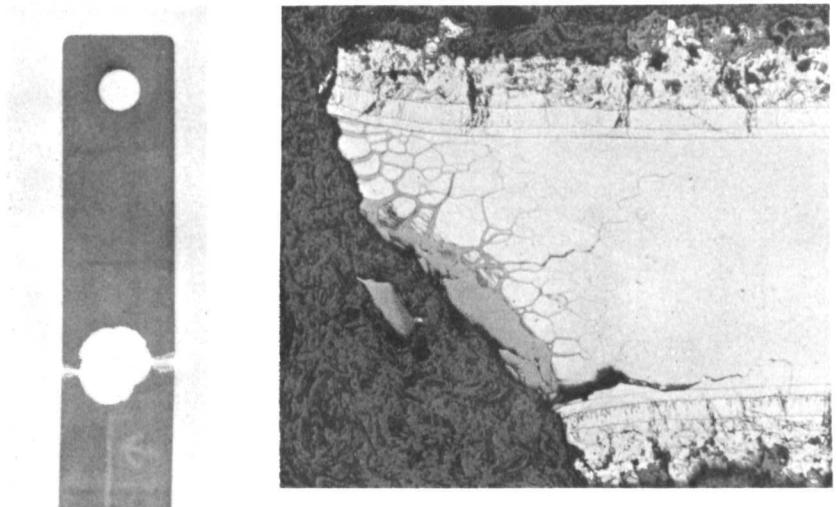

Part B

Specimen No. 106(B)

1 LP-SC to 1810° K

4T Hole Defect

Etchant: HF-HNO_3-Lactic

Magnification: 125X

Mag: 1X

FIGURE 32. 4T HOLE DEFECTED SPECIMENS (SA-13 COATING) AFTER LP-SC EXPOSURE AT 1700 OR 1810° K AND 1300 N/m^2

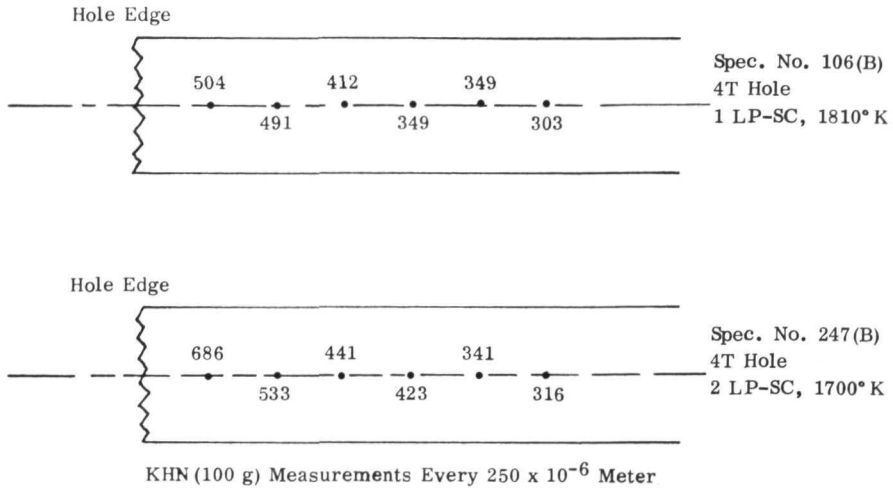

FIGURE 33. DIAGRAM OF MICROHARDNESS MEASUREMENTS FROM INTENTIONALLY DEFECTED, SA-13 COATED, SPECIMENS AFTER 1700 AND 1810°K - 1300 N/m^2 LP-SC EXPOSURE

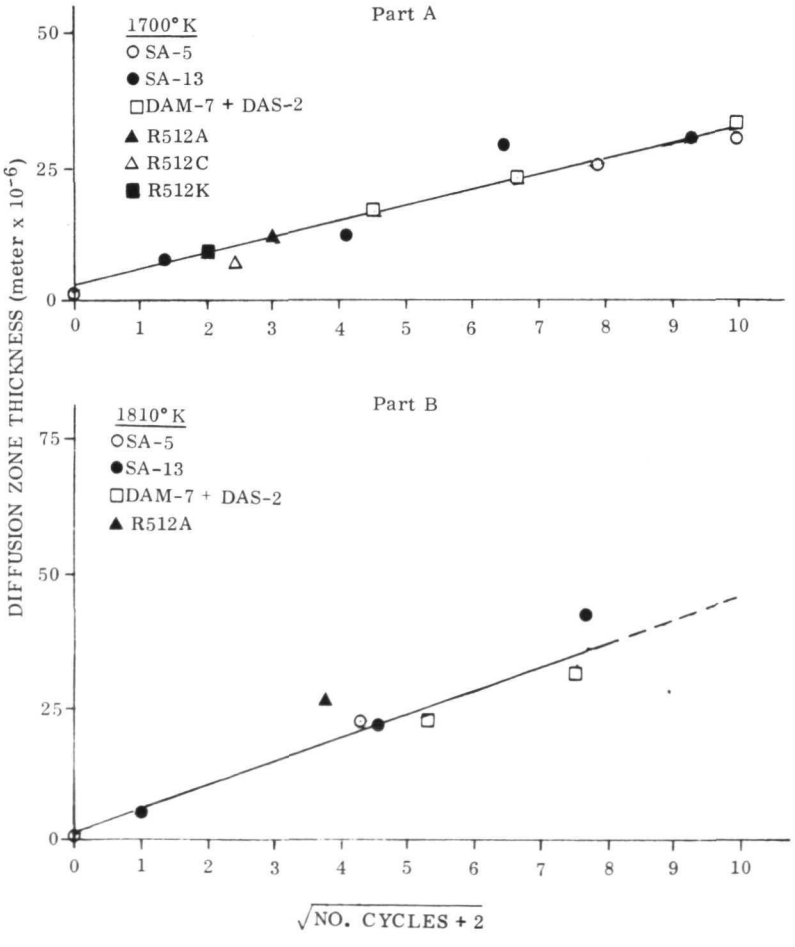

FIGURE 34. DIFFUSION ZONE THICKNESS VS EXPOSURE TIME

TABLE XXIX

SUBSTRATE CONSUMPTION DURING FUSION
FOR TYPICAL THICKNESS COATINGS

Coating	Consumed Substrate (meter x 10^{-6})
SA-5	35
SA-13	35
DAM-7 + DAS-2	30
R512A	36
R512C	23
R512K	25

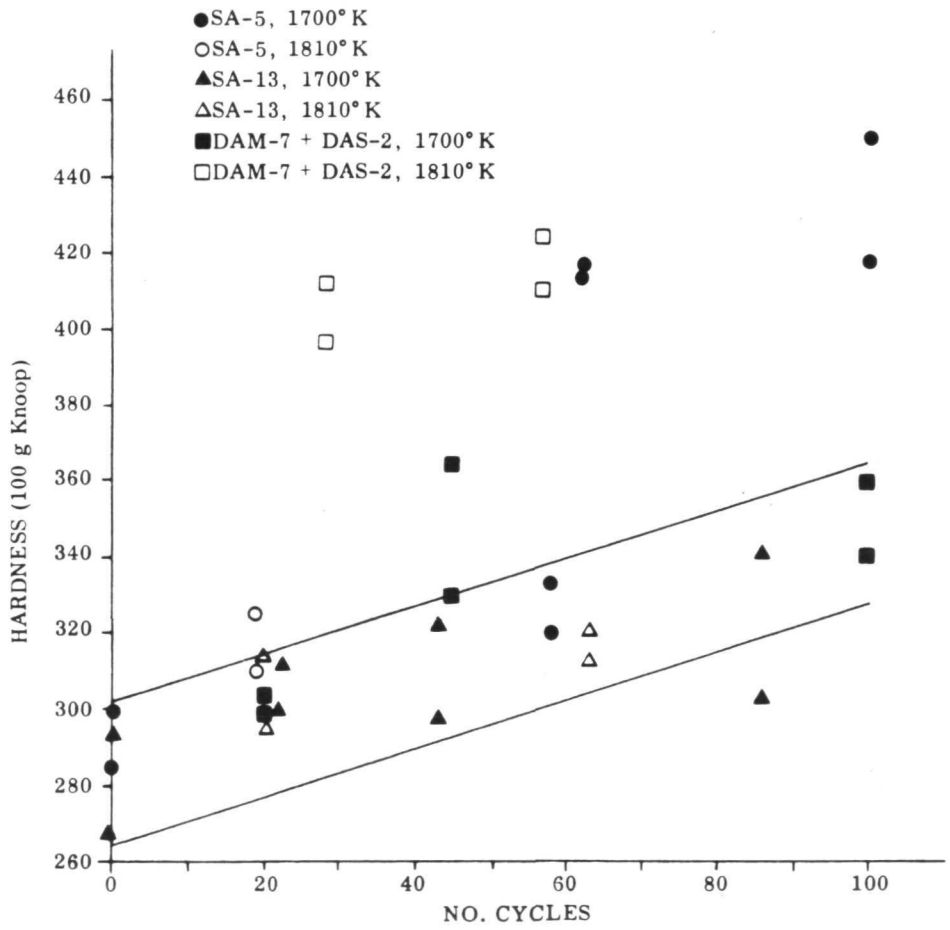

FIGURE 35. SUBSTRATE CENTERLINE HARDNESS VALUES FOR 1300 N/m^2 LP-SC EXPOSED SPECIMENS

were located on the centerline of the residual substrate, and are for areas which were apparently protected. Hardness values for SA-5 coated coupons are scattered and may be influenced by the fact that two "types" (heavily glazed, red-brown versus lightly glazed, black) of coupons are included in the data. Heavily glazed coupons tended to be longer lived than the lightly glazed, black specimens, but also exhibited much the higher substrate hardness values. Insufficient data were available to determine the influence of 1810° K exposure on SA-5 coated substrates. SA-13 coated specimens showed a gradual and nearly linear increase in substrate hardness with increasing exposure times. This coating better preserved the substrate mechanical properties than either the SA-5 or DAM-7 + DAS-2 coating. The available data show that substrate hardness under the SA-13 coating was not influenced by increasing the test temperature from 1700 to 1810° K. Exposure at 1810° K resulted in much more rapid hardening than was caused by 1700° K exposure of DAM-7 + DAS-2 coated specimens.

Comparison of the substrate hardness values of Figure 35 with the bend test data (Table XXVI) implies that a DBBTT below 200° K may be expected if the substrate hardness is below about 400 KHN (100 g). Reference to Figure 15 shows that this hardness level corresponds to about 500-1000 ppm oxygen in the substrate.

Weight change data for the 1700 and 1810° K LP-SC tested SA-5, SA-13 and DAM-7 + DAS-2 specimens are shown in Figures 36, 37 and 38. The number of cycles was increased by two in every case to include the effect of the one-hour - 1700° K pre-oxidation exposure prior to initiation of testing. The solid line drawn through 1700° K data bars (Fig. 36) represents the performance of those SA-5 specimens which were heavily glazed and red-brown in color. The coupons which were black and lightly glazed did not appear to oxidize according to a parabolic rate law. Individual data points are shown for the 1810° K data because widely variable weight changes were noted for different specimens. At least one specimen experienced a small weight loss during the 1810° K exposure. Very small weight changes were recorded for the SA-13 coated specimens. No significant difference was evident between the 1700 and 1810° K data until about 50 exposure cycles. At this point, the 1810° K coupons began to lose weight. Neither the 1700 nor the 1810° K exposed specimens appeared to follow parabolic kinetics.

Relatively close adherence to a parabolic rate law was observed for 1700° K tested DAM-8 + DAS-2 coated coupons. Oxidation at 1810° K was more rapid than at 1700° K and may also conform to parabolic kinetics.

Surface X-ray diffraction (XRD) analyses were performed to assist in defining the composition of the protective glass layer on a 100-cycle - 1700° K - 1300 N/m^2 exposed, DAM-7 + DAS-2 coated coupon and on 63-cycle - 1810° K - 1300 N/m^2 exposed, exposed, SA-13 coated specimen. Table XXX contains the findings of these analyses. Additional weak and unidentified lines were present in the diffraction pattern from the SA-13 coated specimen.

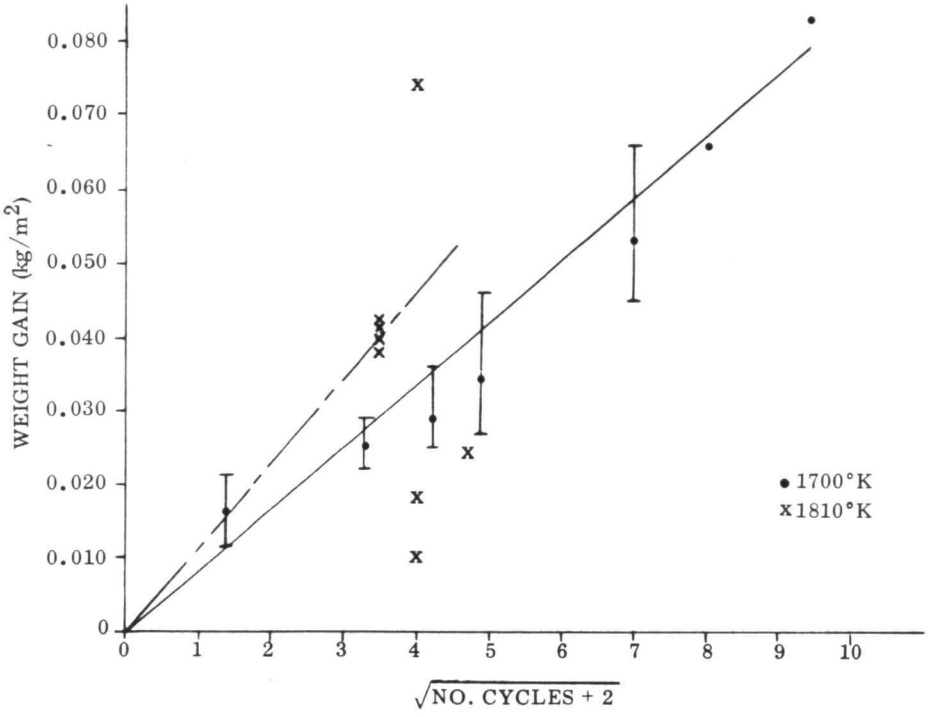

FIGURE 36. WEIGHT CHANGE DATA FOR 1300 N/m^2 LP-SC EXPOSED SA-5 COATING

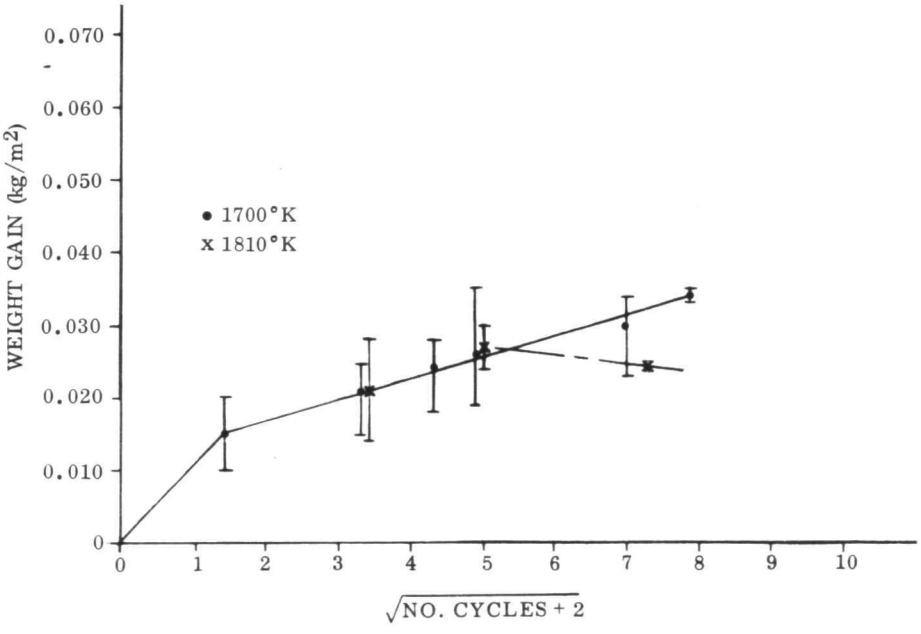

FIGURE 37. WEIGHT CHANGE DATA FOR 1300 N/m^2 LP-SC EXPOSED SA-13 COATING

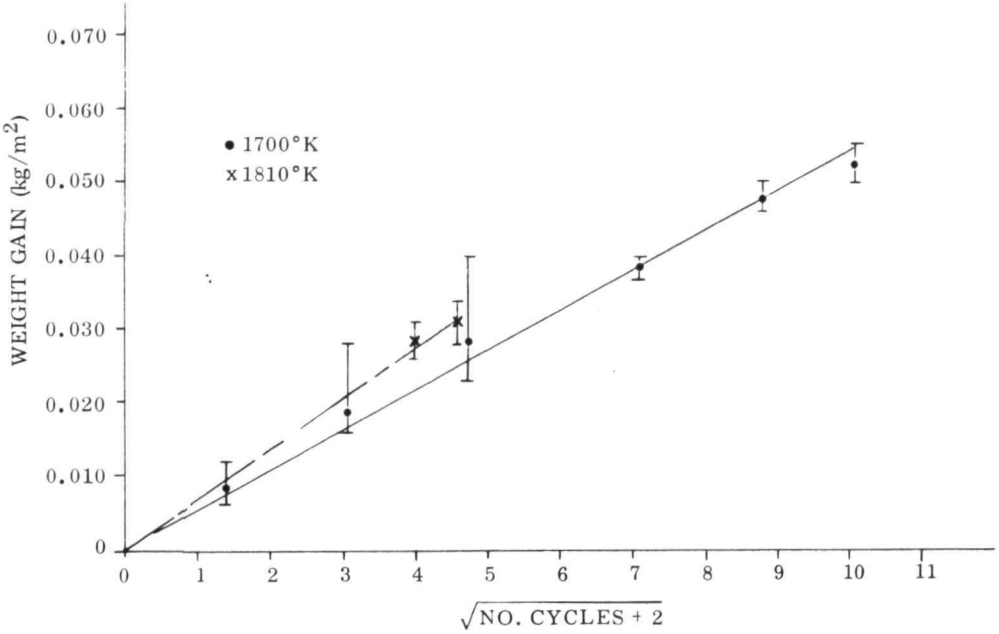

FIGURE 38. WEIGHT CHANGE DATA FOR 1300 N/m^2 LP-SC EXPOSED DAM-7 + DAS-2 COATING

TABLE XXX

X-RAY DIFFRACTION ANALYSES FOR LP-SC EXPOSED SA-13 AND DAM-7 + DAS-2 COATED SPECIMENS

Coating Type	Exposure Cycles/°K/N/m^2	Major Compounds Present	Minor Compounds Possibly Present
SA-13	63/1810/1300	SiO_2 (cristobalite) TiO_2 (rutile)	Cr_2O_3 $TiSi_2$ Ti_5Si_3
DAM-7 + DAS-2	100/1700/1300	SiO_2 (cristobalite) Fe_2O_3 (hematite) Fe_3O_4 (magnetite)	None

Electron microprobe (EMP) analyses were also conducted on the two XRD analyzed coatings. Analyses for eight elements were conducted on selected areas within the coating. The data presented are an average for visually identical areas on each side of each coupon. Figure 39 and Table XXXI show the typical location and quantity (atomic percent) of the various elements present in the SA-13 coating after 63 cycles to 1810° K and 1300 N/m^2. The approximate diameter of the area covered by the EMP beam was 3×10^{-6} meter.

Spot 1 in Figure 39 is probably a mixture of Ta_2O_5, Cr_2O_3 and TiO_2 with traces of SiO_2 present. Support for the presence of Cr_2O_3 and TiO_2 is provided by the XRD data; however no tantalum oxides were observed by XRD analysis. The large range for chromium occurs because chromium was concentrated within the small, dark areas of the particle identified as Spot 1. These particles appear to contain either two or three different phases. The mutual solubility of Ta_2O_5, Cr_2O_3 and TiO_2 is unknown but presumably low, since each crystallizes with a different structure. The vitreous layer identified by Spot 2 is most probably a mixture of SiO_2 and Ta_2O_5. Two phases appear present in this vitreous area and may consist of crystalline SiO_2 (cristobalite) and vitreous SiO_2 plus dissolved tantalum oxide. Cristobalite was positively identified by XRD. The total quantity of elements (Si plus Ta) observed in Spot 2 type areas was too low to produce known compounds with the amount of oxygen found by difference. Spot 3 is an area within the originally applied coating and is probably a mixture of disilicides of tantalum, tungsten and molybdenum. Regions in this area of the coating appear to contain four "phases". One "phase" (large dark areas) appears to be voids, while another phase (few small dark areas) is an oxide of titanium. The remaining light gray areas may be $TaSi_2$ and $MoSi_2 + WSi_2$. Molybdenum and tungsten disilicides crystallize in the same structural type and have nearly identical lattice parameters; $TaSi_2$ forms a different crystal type. More silicon than can be accounted for by the disilicides was found in this region. Spot 4 represents coating areas believed to have been just below the original coating/substrate interface. The tantalum-to-tungsten ratio in these areas is nearly the same as for the as-received alloy and supports the supposition. This region probably contains a mixture of the M_5Si_3 type silicides and may also contain some disilicides. Small amounts of chromium and titanium were detected and suggest the possibility of limited diffusion into the growing M_5Si_3 region by these elements. Three or more phases are present. These might be accounted for by an α $Ta_5Si_3 + W_5Si_3 + Cr_5Si_3$ region, a β Ta_5Si_3 region and possibly a disilicide region. The possible presence of a disilicide is suggested because insufficient metallic elements are present to account for the apparent quantity of silicon as M_5Si_3 compounds and because one phase in Spot 4 may be continuous with a phase in Spot 3. Coating areas represented by Spot 5 differ only slightly from Spot 4 type areas. No metallic elements but tantalum and tungsten were detected and the ratio between these two elements was the same as for the original substrate. The quantity of silicon present was again too high to be accounted for by M_5Si_3 silicides. The material balance total was only about 92 percent. It seems more probable that the computer program does not adequately correct the raw data for the various absorption coefficients than that some disilicide is present in this region.

TABLE XXXI

EMP DATA FOR EXPOSED SA-13 COATING

Spot Number	Atomic Percent							
	Cr	Mo	O*	Si	Ta	Ti	V	W
1	5-25	<0.1	40-85	0.5	8	4.9	<0.1	<0.1
2	<0.1	<0.1	75	24	0.4	0.1	<0.1	<0.1
3	<0.1	2.0	--	74	19.7	0.1	<0.1	4.0
4	0.5	<0.1	--	47	47.8	0.2	<0.1	4.4
5	<0.1	<0.1	--	46	47	<0.1	<0.1	5.3

*Determined by difference

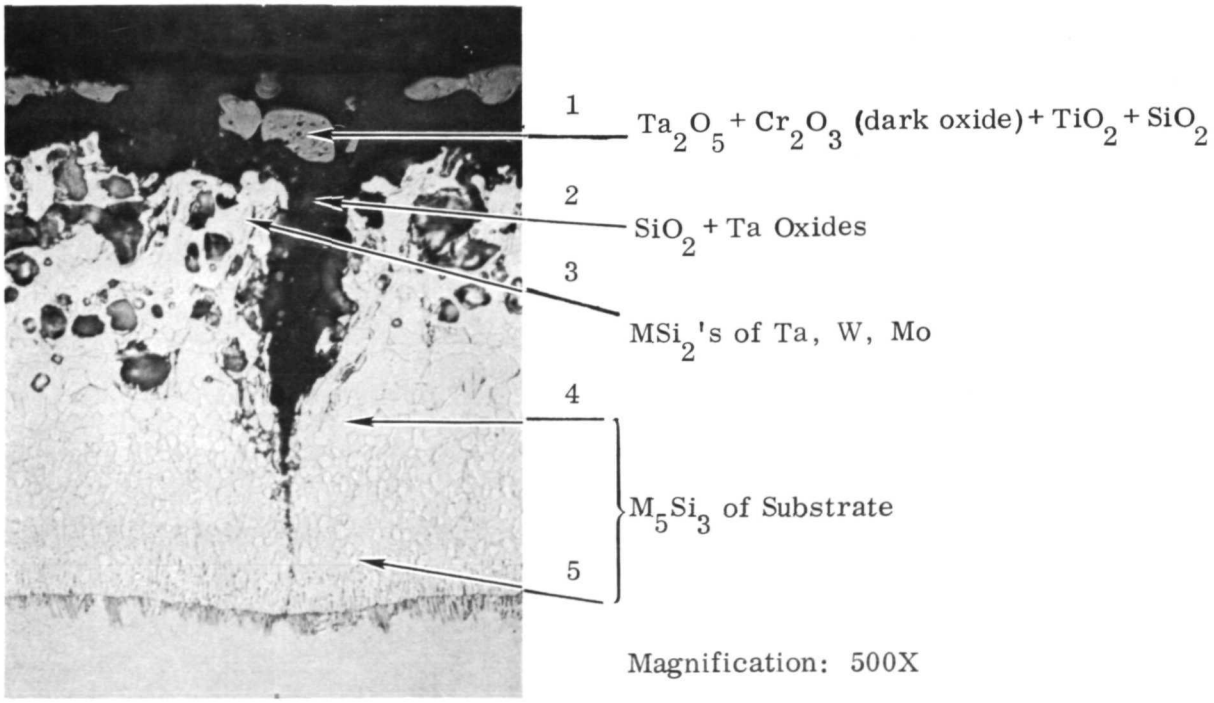

FIGURE 39. TYPICAL LOCATION FOR EMP ANALYSES OF SA-13 AFTER 63 LP-SC's TO 1810°K AND 1300 N/m^2

Table XXXII and Figure 40 contain the EMP data and locate typical analyzed areas in the exposed DAM-7 + DAS-21 coating. Spot 1 in Figure 40 contains two or more phases and may consist of Ta_2O_5 and Fe_2O_3. The XRD data provide support for Fe_2O_3 but not for any tantalum oxides. These two oxides (Ta_2O_5 and Fe_2O_3) crystallize with different structures but are also reported to form the complex oxide $FeTaO_4$. The quantity of metallic elements observed in Spot 1 is not sufficient to account for all of the oxygen indicated by difference. Spot 2 represents the vitreous phase of the oxidized coating. This phase is believed to be largely SiO_2 containing a small amount of dissolved iron oxides. Diffraction data definitely indicate the presence of cristobalite (SiO_2). The glass has undergone some crystallization into cristobalite. The coating areas represented by Spot 3 are within the originally deposited coating and probably consist of mixed tantalum, tungsten and molybdenum disilicides plus a small amount of an iron compound. Iron monosilicide (FeSi) is the most stable of the various possible iron silicides. This portion of the coating appears to contain three phases in addition to some voids. The two major phases may be $TaSi_2$ and WSi_2 + $MoSi_2$. If present, FeSi might be a separate phase from either of the above phases because it crystallizes with a different structure. Spot 4 is the area just above the original coating/substrate interface. An EMP X-ray image scan for iron showed an as-prepared DAM-7 + DAS-2 coating to contain considerable iron in this area but none in the substrate. A large amount of iron was also observed after LP-SC exposure. It appears probable that a layer of $TaFe_2$ was formed when the DAM-7 layer was fused onto the substrate. Subsequent siliciding may or may not have converted the $TaFe_2$ to silicides. Based on melting points, the order of stability for probable compounds in this area is $TaSi_2 > TaFe_2 > FeSi$. The quantity of silicon present is not sufficient to convert the metallic elements to disilicides. This area of the coating is multiphased and may contain the iron-tantalum intermetallic compound as well as a complex mixture of silicides. Spot 5 is nearly identical to Spot 5 in Figure 39 and appears to be a mixture of Ta_5Si_3 and W_5Si_3. The tantalum/tungsten ratio in this area is equal to that for the substrate alloy. A small amount of iron in this region suggests the diffusion of iron into the M_5Si_3 region.

Procedures identical with those previously reported were again employed to obtain the required visual, thermoelectric and eddy current thickness NDT data. Relatively few instances of correlation between failures and NDT measurements were observed. Table XXXIII contains data for all SA-5, SA-13 and DAM-7 + DAS-2 coated and tested specimens. Data for the R512A, R512C and R512K coatings were not tabulated because of the gross coating failures.

Six SA-5 coated specimens experienced failures in areas which had been surveyed by the thermoelectric technique. The thermoelectric measurements ranged from +0.4 mv to -1.3 mv for all SA-5 coated specimens. All but two values were negative. Areas which were measured with the thermoelectric probe and which subsequently experienced a failure also registered thermoelectric values over the entire

TABLE XXXII

EMP DATA FOR LP-SC EXPOSED DAM-7 + DAS-2 COATING

Spot Number	Atomic Percent							
	Fe	Mo	O*	Si	Ta	Ti	V	W
1	7.3	<0.1	81	0.4	11.3	<0.1	<0.1	<0.1
2	0.4	<0.1	68	32	<0.1	<0.1	<0.1	<0.1
3	3	17	--	68	7.7	<0.1	<0.1	4.4
4	30	0.5	--	40	26	<0.1	<0.1	3
5	0.6	<0.1	--	44	50	<0.1	<0.1	5.2

*Determined by difference

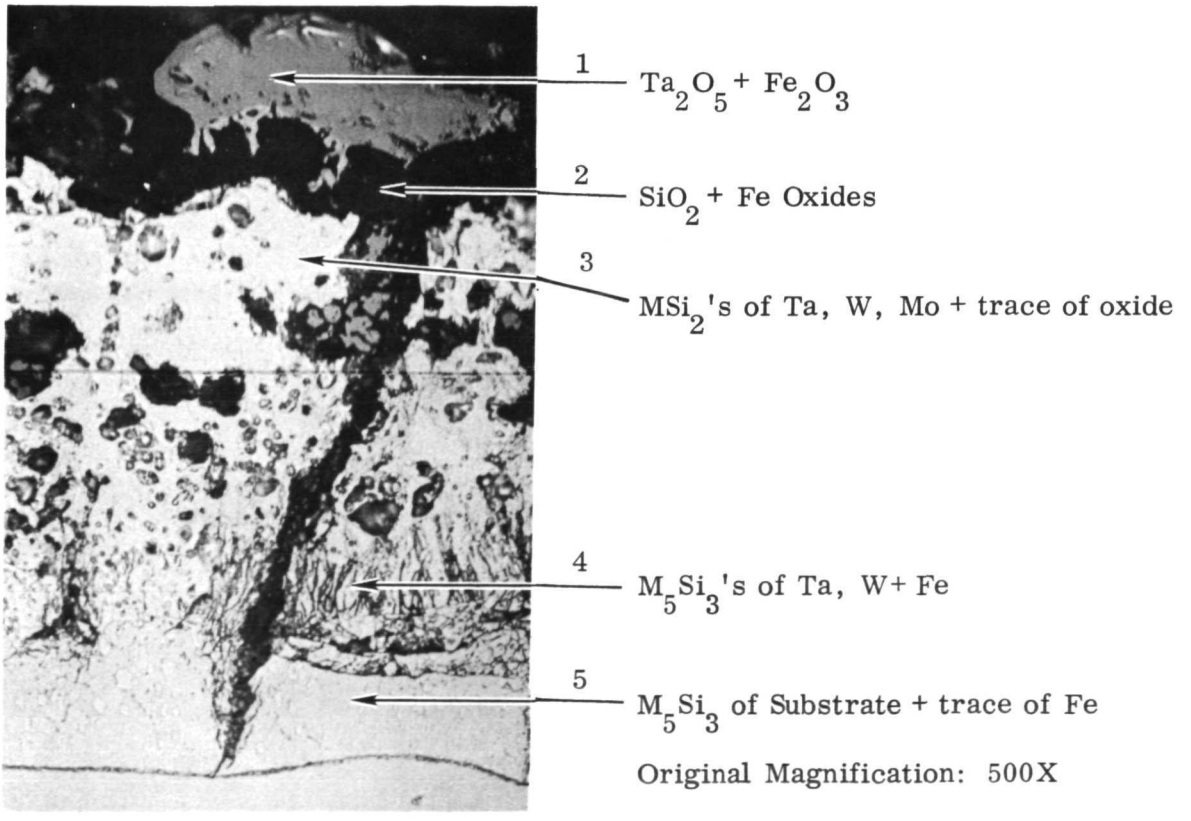

FIGURE 40. TYPICAL LOCATION FOR EMP ANALYSES OF DAM-7 + DAS-2 AFTER 100 LP-SC's TO 1700° K AND 1300 N/m^2

TABLE XXXIII

NDT DATA CORRELATION

Specimen No.	Coating	Thermo-electric	Dermitron	Visual
11(T)	SA-5	NF	NF	NF
14(T)	SA-5	MS	NM	NC
30(T)	SA-5	NM	NM	NC
40(T)	SA-5	NM	NM	NC
43(T)	SA-5	NM	NM	NC
49(T)	SA-5	MS	NM	NC
51(T)	SA-5	NM	NM	NC
53(T)	SA-5	NM	NM	NC
29(B)	SA-5	NF	NF	NF
88(B)	SA-5	NM	NM	NC
124(B)	SA-5	MS	NM	C
133(B)	SA-5	MS	NM	C
137(B)	SA-5	NM	NM	C
175(B)	SA-5	NM	NM	C
189(B)	SA-5	MS	NM	C
210(B)	SA-5	MS	NM	NC
212(B)	SA-5	NM	NM	NC
1(T)	SA-13	NM	NM	NC
7(T)	SA-13	NM	NM	NC
37(T)	SA-13	NM	NM	NC
38(T)	SA-13	NF	NF	NF
39(T)	SA-13	NF	NF	NF
42(T)	SA-13	MS	NM	NC
44(T)	SA-13	NF	NF	NF
50(T)	SA-13	NM	NM	NC
11(B)	SA-13	NM	NM	NC
44(B)	SA-13	MS	NM	NC
104(B)	SA-13	NF	NF	NF
169(B)	SA-13	NF	NF	NF
171(B)	SA-13	NM	NM	NC
192(B)	SA-13	MS	NM	NC
211(B)	SA-13	NF	NF	NF
219(B)	SA-13	NM	NM	NC
3(T)	DAM-7+DAS-2	NF	NF	NF
6(T)	DAM-7+DAS-2	NF	NF	NF
18(T)	DAM-7+DAS-2	NF	NF	NF
23(T)	DAM-7+DAS-2	NM	NM	NC
27(T)	DAM-7+DAS-2	MS	NM	NC
28(T)	DAM-7+DAS-2	NF	NF	NF
41(T)	DAM-7+DAS-2	NM	NM	NC
45(T)	DAM-7+DAS-2	NM	NM	NC
3(B)	DAM-7+DAS-2	NF	NF	NF
25(B)	DAM-7+DAS-2	NM	NM	NC
48(B)	DAM-7+DAS-2	NM	NM	NC
151(B)	DAM-7+DAS-2	NF	NF	NF
185(B)	DAM-7+DAS-2	NF	NF	NF
209(B)	DAM-7+DAS-2	MS	NM	NC
231(B)	DAM-7+DAS-2	MS	NM	NC
232(B)	DAM-7+DAS-2	NF	NF	NF

C = Possible correlation between measurement and failure.
NF= No failure.
NC= No correlation between measurement and failure.
NM= No measurement in failed area.
MS = Measurement at failure site.

+0.4 mv to -1.3 mv range. No single thermoelectric value or limited range of values was common to the observed failure sites. Thermoelectric readings identical with those from failure sites were observed for many other specimens which did not experience failure in the measured area.

Three SA-13 coated specimens failed in areas which had been measured with the thermoelectric device. All measurements on SA-13 coatings ranged from +0.2 mv to -1.4 mv. All but one of the thermoelectric readings were negative. Failed areas registered thermoelectric values between -0.5 and -1.1 mv. Many unfailed areas also registered thermoelectric values within the -0.5 to -1.1 mv range. Again, no single thermoelectric value or range of values was unique to only failed areas. However, the data for SA-13 coated specimens may suggest that thermoelectric values more positive than -0.5 mv are indicative of failure-free performance.

Three DAM-7 + DAS-2 coated specimens developed edge failures in areas which had been surveyed with the thermoelectric device. Thermoelectric values were observed to range from +1.7 to -1.1 mv. Edge failures were observed in areas which had produced thermoelectric readings of +1.5, -0.3 and -0.5 mv. Unfailed areas on other specimens also yielded identical thermoelectric values plus many other readings within the +1.5 or -0.5 mv range. It does not appear that any thermoelectric value or range of values (for DAM-7 + DAS-2) can be said to correspond to either subsequent failure or nonfailure.

When taken together, the thermoelectric data for SA-5, SA-13 and DAM-7 + DAS-2 coated coupons show only that edge failures occurred where 12 of 144 thermoelectric measurements were made. In no instance was it possible to show that a specific thermoelectric value would definitely indicate the probability of an edge failure. It is possible to interpret the observed data as indicating that the thermoelectric technique, as employed in this program, may be responsible for the edge failures which occurred in measured areas.

There were no definite instances of eddy current measurements and failure site correlation. This does not indicate that the method is valueless but rather that virtually no surface failures were encountered. Almost all failures occurred at edges or corners.

Visual inspection was the method of greatest value employed in this program. Only a few instances of correlation between pre-test visual observations and failure modes were observed. This is partially attributable to the fact that all specimens were visually sorted before being considered for testing. Obvious defects such as cracks or chips eliminated a specimen from being tested. Were this not the case, a much better visual versus performance correlation would undoubtedly have occurred.

3.1.7 Modification and Testing of Two Coatings

Low-pressure, slow-cycle testing at 13 N/m^2 and 1700 and 1810° K was the next test condition to be investigated. Data from the preceding tests were reviewed and two coatings, SA-13 and DAM-7 + DAS-2, were selected for this activity.

LP-SC Exposure at 1700 and 1810° K and 13 N/m

Specimens were prepared as before and were entered into test. Tables XXXIV and XXXV contain the 1700 and 1810° K - 13 N/m^2 pressure test data for the SA-13 and DAM-7 + DAS-2 coating types. The coatings withstood the 1810° K - 13 N/m^2 test condition for less than 10 cycles. Weight loss data (average and range) at 1810° K are shown in Figure 41 and exhibit the general trend expected from comparison of the test conditions (temperature and pressure) with the "active" and "passive" oxidation regions defined by Bartlett (Ref. 6). The test conditions were well within the "active" region for the most stable MSi_2 and M_5Si_3 type silicides. This is also the case for the 1700° K - 13 N/m^2 conditions; however only the DAM-7 + DAS-2 coating exhibited "active" type oxidation (Fig. 41). The SA-13 coating system initially displayed "active" oxidation but changed to "passive" type oxidation after about five test cycles.

Analytical Data

Metallographic analysis of the two coating systems readily showed the difference between specimens which experienced "active" vs "passive" oxidation. Figure 42 shows SA-13 microstructural aspects and hardness values after different exposure levels at 1700° K and 13 N/m^2. The protective surface oxide did not appear vitreous and was only about twice as thick after 98 test cycles as after 6 cycles. The quantity of originally applied coating was seen to decrease in thickness and increase in porosity with increased exposure. When combined with the low surface oxide growth rate and the weight change data (Fig. 41), this indicates that coating degradation probably conforms to a reaction such as

$$5MSi_2 + 7SiO_2 \rightarrow M_5Si_3 + 14SiO(g) \qquad (1)$$

which yields the gaseous product SiO. The same reaction undoubtedly accounted for the very rapid coating degradation seen in Figure 43 where 10 LP-SC's to 1810° K and 13 N/m^2 are seen to have completely consumed the SA-13 coating.

Shown in Figure 44 are the effects on DAM-7 + DAS-2 of 1700 and 1810° K LP-SC exposure at 13 N/m^2. Reaction (1) is again believed responsible for the observed degradation.

Intentionally defected examples of SA-13 coated coupons were also LP-SC exposed at 1700° K and 13 N/m^2. Defects included 1T and 4T spots and 4T holes

TABLE XXXIV

1700° K LP-SC TESTING OF SA-13 AND DAM-7 + DAS-2 AT 13 N/m^2

Specimen No.	Coating	Cycles	Comments
107(T)	DAM-7 + DAS-2	7	Black, deformed at lower end of specimen, severe weight losses.
89(T)		8	
97(T)		8	
100(T)		8	
734(B)		8	
790(B)		8	
820(B)		8	
835(b)		8	
126(T)	SA-13	20	Removed from test, green and brown.
830(B)		20	Removed from test, green and brown.
75(T)		24	Failed, edge, green and brown.
92(T)		24	Failed, surface, green and brown.
86(T)		50	Removed for test, green and brown.
813(B)		50	Removed for test, brown.
819(B)		98	Failed, side edge, dark brown
842(B)		98	Failed, lower surface, brown & green

TABLE XXXV

1810° K LP-SC TESTING OF SA-13 AND DAM-7 + DAS-2 AT 13 N/m^2

Specimen No.	Coating	Cycles	Comments
785(B)	DAM-7 + DAS-2	5	Dull black, deformed at lower end, severe weight losses.
88(T)		6	
133(T)		6	
140(T)		6	
142(T)		6	
704(B)		6	
804(B)		6	
852(B)		6	
147(T)	SA-13	6	Blue-black to black, deformed at lower edge, severe weight losses.
809(B)		8	
837(B)		9	
127(T)		9	
137(T)		9	
138(T)		9	
798(B)		10	
802(B)		10	

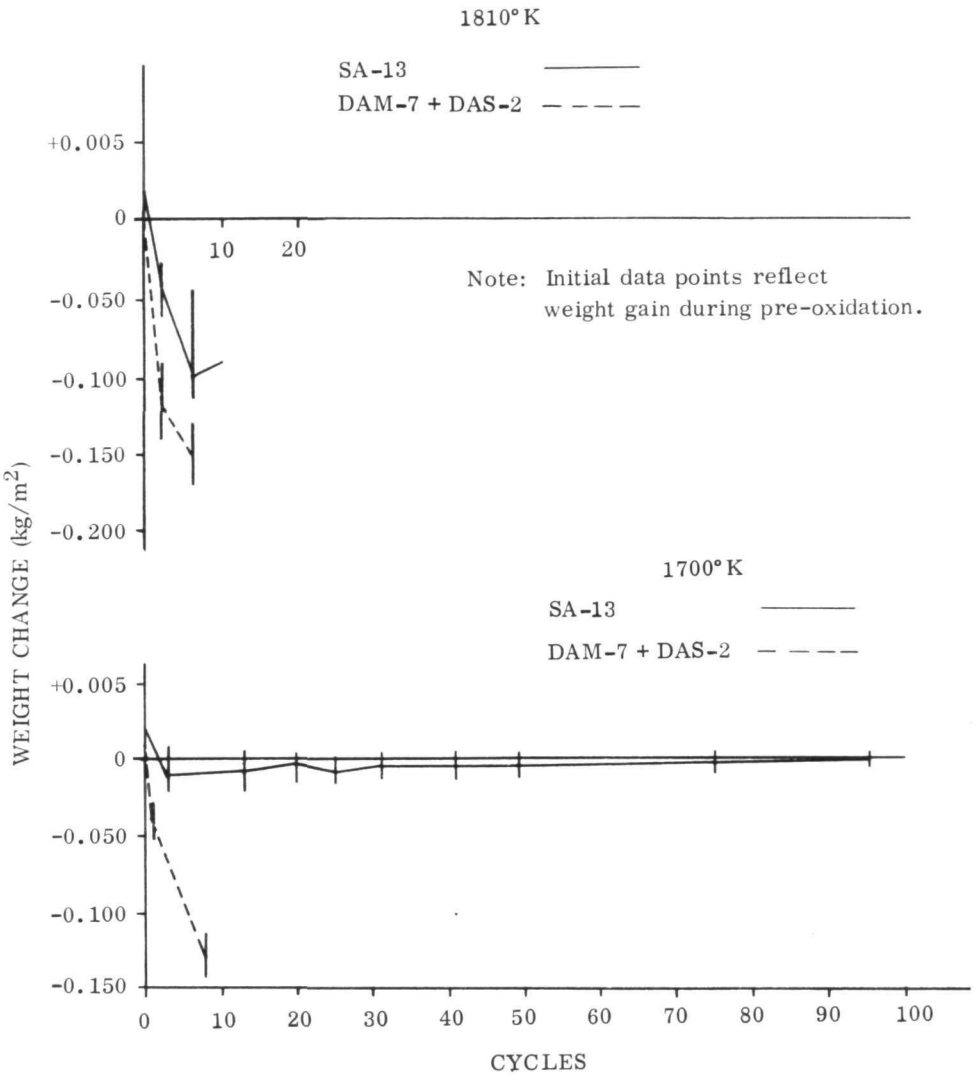

FIGURE 41. WEIGHT CHANGE DATA FOR 13 N/m^2 LP-SC EXPOSED SA-13 AND DAM-7 + DAS-2 COATINGS

(T = material thickness) and were placed in "new" coupons and coupons which had already experienced 20 test cycles. Failure was defined as the first appearance of substrate oxide or sufficient deformation to prevent further testing. Table XXXVI contains data for the exposed specimens. It is unfortunate that the spot-defected coupons each failed in an area other than the intentional defect, since the spot defect does not appear very serious at 13 N/m^2.

Both hole-defected specimens failed at the hole. Figure 45 shows the macro and microscopic appearance of the 1 and 4T spot-defected specimen which sustained 6 LP-SC's after defecting. A surface failure at a support rod site is visible on the reverse side of the specimen and was sufficiently close to the 4T spot defect to require that the specimen be removed from test in order to prevent contamination of the

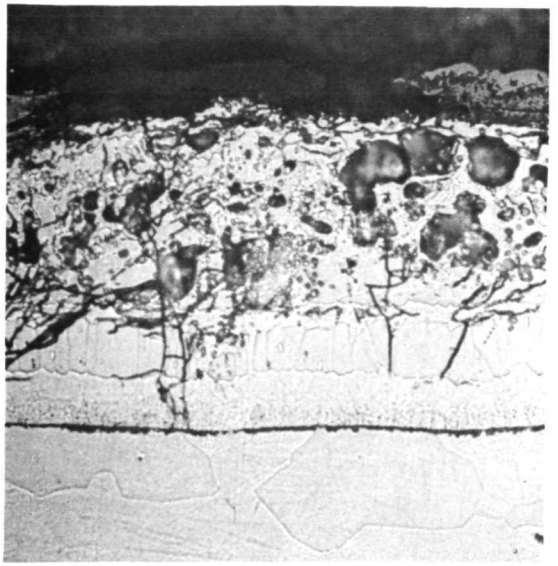

Specimen No. 821

6 LP-SC

℄ Hardness = 271 KHN (100 g)

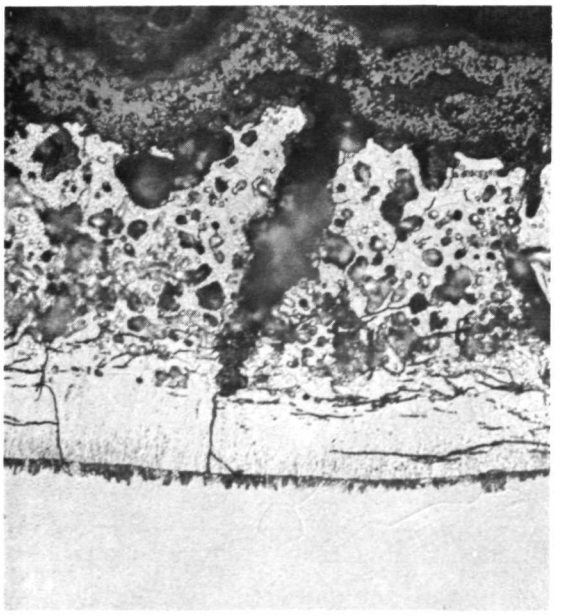

Specimen No. 75

24 LP-SC

℄ Hardness = 250-254 KHN (100 g)

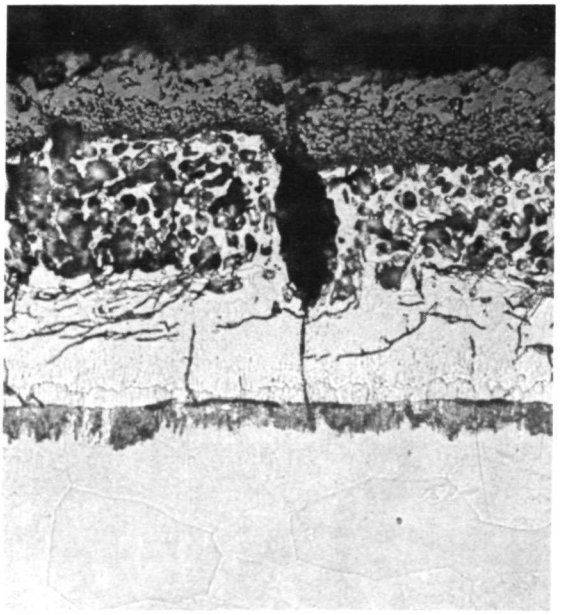

Specimen No. 819

98 LP-SC

℄ Hardness = 246-290 KHN (100 g)

Etchant: HF-HNO_3-Lactic
Magnification: 500X

FIGURE 42. SA-13 MICROSTRUCTURE AFTER LP-SC EXPOSURE AT 1700°K AND 13 N/m^2

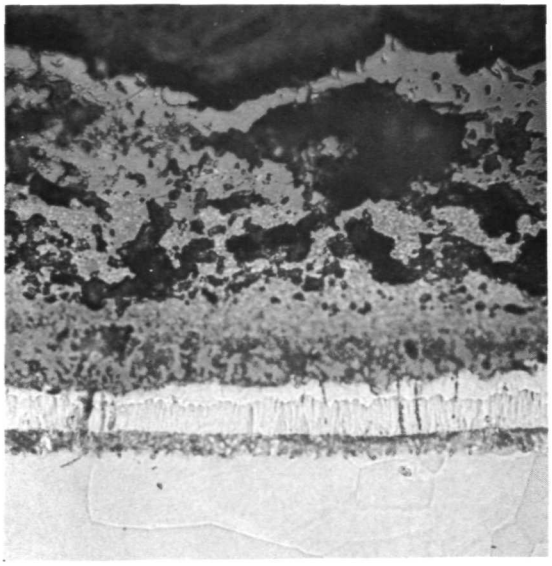

Specimen No. 798

10 LP-SC

Etchant: HF-HNO_3-Lactic

Magnification: 500X

FIGURE 43. SA-13 MICROSTRUCTURE AFTER LP-SC EXPOSURE AT 1810°K AND 13 N/m^2

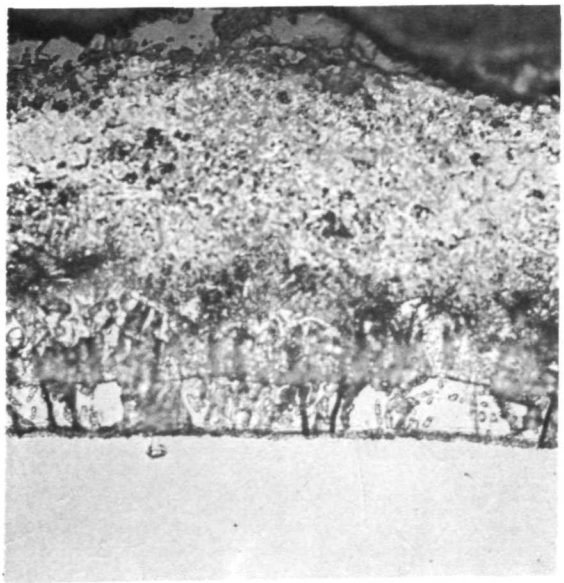

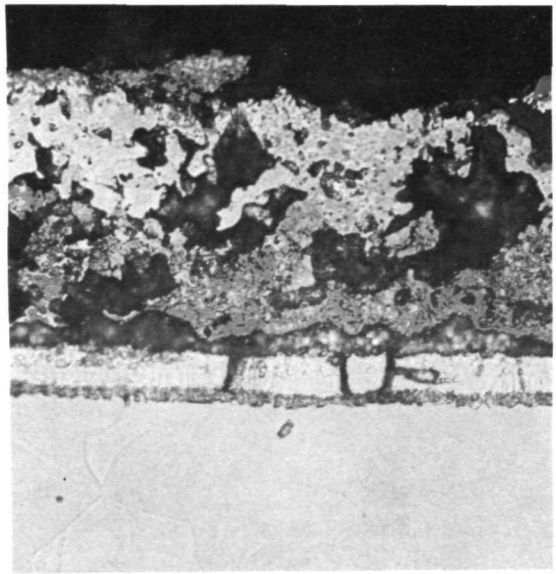

Specimen No. 820

8 LP-SC - 1700° K

Specimen No. 88

6 LP-SC - 1810°K

Etchant: HF-HNO_3-Lactic

Magnification: 500X

FIGURE 44. DAM-7 + DAS-2 MICROSTRUCTURE AFTER LP-SC EXPOSURE AT 1700°K OR 1810° K AND 13 N/m^2

TABLE XXXVI

1700° K, 1300 N/m^2 EXPOSED, INTENTIONALLY DEFECTED SA-13 COATED SPECIMENS

Specimen Number	Defect Type	Initial Exposure	Exposure After Defecting	Comments
821	1 & 4T spot	0	6	Intentional defects o.k., support mark failure
792	4T hole	0	3	Failed at hole
806	1 & 4T spot	20	5	Intentional defects o.k., edge failure
803	4T hole	20	1	Failed at hole

substrate near the intentional defect. The cross-sectional view of the 1T spot indicates that a small layer of the diffusion zone may not have been removed during defecting. This was not the case for the 4T spot. Exfoliation was observed on all 4T hole defected coupons but was not present at any of the spot defects which were exposed at 1700° K and 13 N/m^2. Figure 46 shows the appearance of a 4T hole defect after 3 LP-SC's to 1700° K and 13 N/m^2. The hole was partially filled with oxide and had decreased from 1.3×10^{-3} to 1×10^{-3} meter diameter.

Microhardness values determined for the substrate near the intentionally introduced defects are diagrammed in Figure 47. The diagrams are drawn to scale on the horizontal plane only. Hardness values were determined every 250×10^{-6} meter along the centerline of the substrate for all defects and also on the defect centerline for the 1T spot defect. The original size of the spot defects is drawn to the same scale as the points indicating hardness data locations.

X-ray diffraction and fluorescent analyses were performed on one of the SA-13 coated coupons which completed 98 LP-SC's to 1700° K and 13 N/m^2. The XRF data were used to help narrow the choice of possibly present compounds and to identify impurities. An XRD pattern was also obtained from an unexposed SA-13 coated specimen. Table XXXVII contains the identified XRD data for both specimens, and Table XXXVIII includes a listing of unidentified lines in each pattern. None of the major lines in the XRD pattern for the LP-SC exposed coating could be identified and four of the higher intensity lines from the as-prepared coupon also remain unidentified.

4T SPOT 1T SPOT

Defected Side

Magnification: 1X

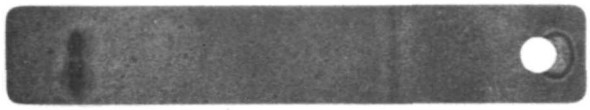

Reverse Side

Magnification: 1X

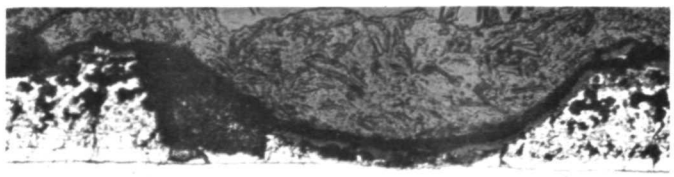

1T Spot

Specimen No. 821

6 LP-SC

Etchant: HF-HNO_3-Lactic

Magnification: 125X

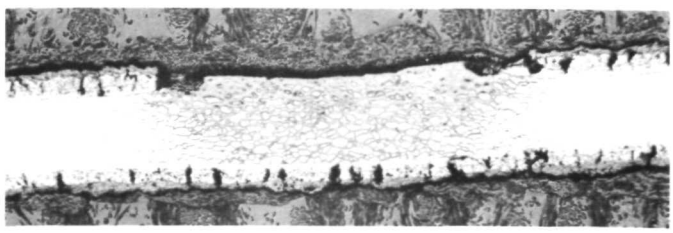

4T Spot

Specimen No. 821

6 LP-SC

Etchant: HF-HNO_3-Lactic

Magnification 35X

FIGURE 45. 1T AND 4T SPOT DEFECTED SPECIMENS, SA-13 COATING, AFTER LP-SC EXPOSURE AT 1700°K AND 13 N/m^2

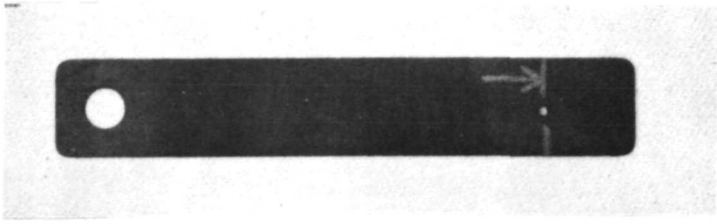

Specimen No. 721

Magnification: 1X

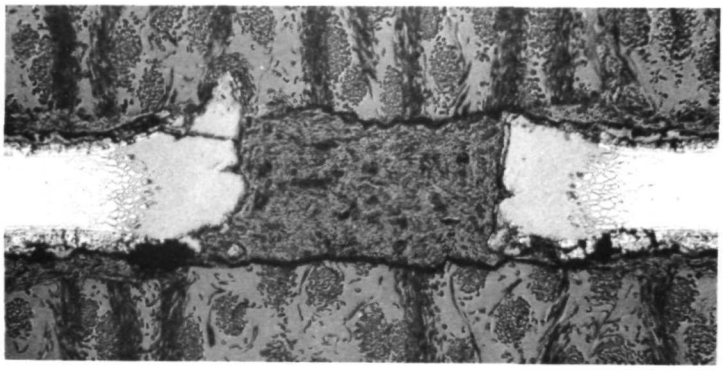

4T Hole

3 LP-SC

Etchant: HF-HNO_3-Lactic

Magnification: 35X

FIGURE 46. 4T HOLE DEFECTED SPECIMEN, SA-13 COATING, AFTER LP-SC EXPOSURE AT 1700° K AND 13 N/m^2

Included in Table XXXIX are results from the qualitative XRF analyses together with estimated quantities of the various elements. Elements observed in the exposed coating and regarded as contaminants include aluminum, barium, iron, strontium, and zirconium. The aluminum and iron can be accounted for by known impurities in the silicon.

These XRD data are seen to correlate reasonably well with previously obtained XRD results (Table XX) which showed SiO_2 and TiO_2 definitely present and Cr_2O_3, $TiSi_2$ and Ta_5Si_3 as possibly present in a 63 LP-SC, 1810° K, 1300 N/m^2 exposed SA-13 coating. Only a few minor lines were unidentified in the previous work. The XRF results from the just completed work support the earlier EMP data which showed tantalum present in the outer areas of the exposed coating.

3.2 COATING IMPROVEMENTS

The initial test results from the program emphasized one very important fact: those coatings which developed no adherent oxide layer failed rapidly.

The coating compositions which slowly oxidized to form thin, vitreous surface layers offered the longest lives and best substrate protection of all systems developed. For substantial life, a silicide coating must form oxidation products which will fill or seal cracks that develop within the silicide layer and which will aid in reducing the

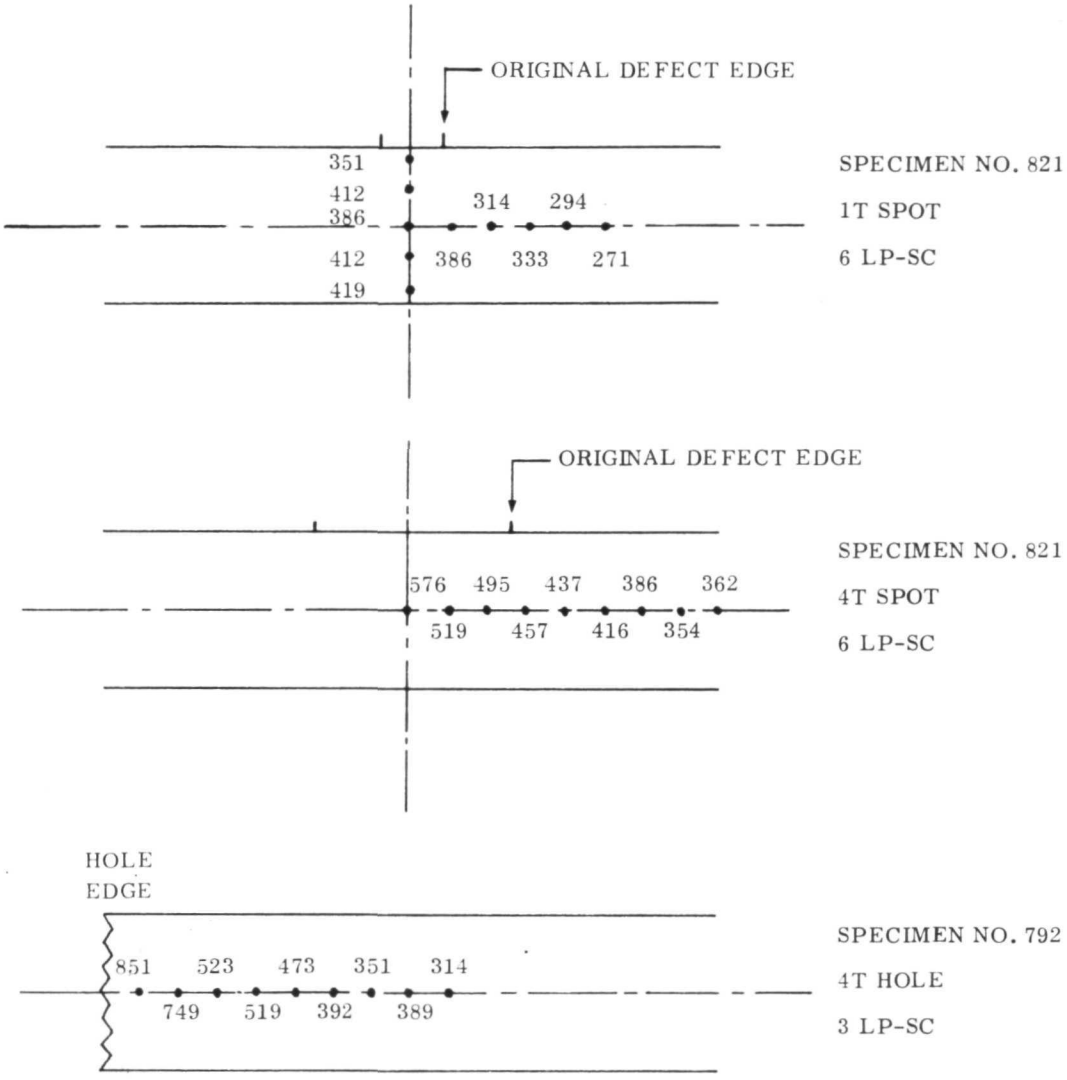

FIGURE 47. DIAGRAM OF MICROHARDNESS MEASUREMENTS FROM INTENTIONALLY DEFECTED SPECIMENS AFTER 1700°K - 13 N/m^2 LP-SC EXPOSURE

subsequent rate of attack on the remaining silicides. Other systems which developed excessive amounts of vitreous oxides also failed prematurely and afforded less resistance to substrate degradation than was desired.

Two approaches were adopted for the improvement of the developed coating systems. These included (1) modification of the basic silicide to promote more desirable glazing characteristics, and (2) development of a vitreous overlay to be applied over the already developed SA-13 silicide coating.

TABLE XXXVII

X-RAY DIFFRACTION DATA FOR LP-SC EXPOSED AND UNEXPOSED SA-13 COATINGS

	Possible Compounds
Specimen 18 (unexposed)	WSi_2
	$MoSi_2$
	$TiSi_2$
	Ta_5Si_3
	(hexagonal & tetragonal)
	Cr_3Si
Specimen 819 (98 LP-SC, 1700°K, 13 N/m^2)	SiO_2(cristobalite)
	Cr_2O_3
	Ta_5Si_3
	Al_2SiO_5 (kyanite)

TABLE XXXVIII

UNIDENTIFIED XRD LINES, SA-13 COATING

Specimen 18 (unexposed)	Specimen 819 (98LP-SC, 1700°K, 13 N/m^2)
4.09	*4.06
3.26	*3.27
3.18	3.15
2.95	2.96
2.85	2.85
2.52	*2.52
2.34	*2.31
2.22	2.21
*2.04	2.04
2.00	2.02
1.91	1.94
*1.51	1.50
1.40	1.40
1.36	*1.37
*1.26	1.26
*1.18	1.18
1.12	1.11
1.07	1.09
1.05	1.05
1.04	1.03
0.94	0.95
0.93	0.94
0.90	0.90
0.89	*0.88
0.86	0.85
0.83	*0.83

*Lines of major importance

TABLE XXXIX

QUALITATIVE XRF ANALYSIS OF LP-SC
EXPOSED SA-13 COATING

Element	Estimated Percent*
Al	2-3
Cr	5
Fe	0.2
Mo	1
Si	28
Ta	60
Ti	3-4

*Values are on a metallic basis and are believed accurate within a factor of two.

3.2.1 Silicide Coating Composition Modifications

Coating modifications were based on the SA-5 and SA-13 single-cycle slurries and on DAM-1 + DAS and DAM + DAS-2 double-cycle systems. Compositions based on SA-5 were designated SA-51, 52 and 53 and were formulated with the objective of reducing the glazing tendency of SA-5 and of increasing the substrate ductility after oxidation. Increased titanium and decreased vanadium contents were expected to favor less glazing while increased molybdenum and tungsten contents should increase refractoriness.

Variations of SA-13 were designed to slightly increase the glazing tendency of this coating. The approaches included lowered titanium plus increased vanadium and the substitution of iron for titanium. Two titanium-free compositions were also evaluated.

Duplex DAM-1, 6, 7 and 8 coatings were modified by siliciding with an agent (DAS-21) containing less iron than DAS-2. The effort was intended to reduce the fluidity of the vitreous oxidation product by eliminating some iron from the coating. The modification to DAM-1 (DAM-11) was an attempt to provide an increased ability to glaze when compared to that shown by the DAM-1 + DAS-1 system. Table XL defines all of the modified coating system compositions.

TABLE XL

MODIFIED COATING COMPOSITIONS

Coating	Composition
SA-51	Si-20Fe-12Mo-12W-8Ti-4V
SA-52	Si-20Fe-10Mo-10W-8Ti-3V
SA-53	Si-20Fe-12Mo-12W-4Ti-5V
SA-131	Si-20Cr-8Ti-4Mo-4W-4V
SA-132	Si-15Cr-12Ti-4Mo-4W-4V
SA-133	Si-18Cr-9Ti-4Mo-4W-6V
SA-134	Si-20Cr-4Mo-4W-2V
SA-135	Si-20Cr-10Fe-4Mo-4W-2V
SA-136	Si-18Cr-4Mo-4W-6V
SA-137	Si-18Cr-9Fe-4Mo-4W-6V
DAM-11	Fe-40Mo-2Ti-5V
DAS-21	Si-5Fe

Test Firing

Each new SA-series coating was prepared as previously described and was applied to five coupons for the test firing. Table XLI summarizes the resultant data for SA-type coatings. Six coupons per DAM coating type were prepared and fired for 3600 seconds at 1810° K and 1.3×10^{-2} N/m^2. The DAM-1, 6, 7 and 8 coatings experienced weight losses within the range previously experienced. The new DAM-11 alloy lost 41 weight percent during firing, a value equivalent to that for the parent alloy DAM-1. All five alloy coatings were smooth, slightly porous, and metallic in appearance.

Initial DAS-21 firings were for 1800 seconds at 1.3×10^{-2} N/m^2 pressure and either 1700 or 1728° K. Weight losses (DAS-21) were near 20 percent for the 1700° K firing and 30 percent for the 1728° K firing cycle. Edges tended to be severely cracked after the higher firing temperature and slightly cracked after the lower temperature firing. The firing cycle used for DAS-1 (300 seconds at 1728° K plus 300 seconds at 1672° K and 1.3×10^{-2} N/m^2) was tried with DAS-21 and found to be the most satisfactory of the cycles investigated. The DAM + DAS-21 coated coupons tend to have poorer edges than the DAM + DAS-2 coated specimens.

TABLE XLI

FIRING CHARACTERISTICS FOR MODIFIED SA-TYPE COMPOSITIONS

Coating	Temp. (°K)	Time (sec)	Pressure (N/m^2)	Wt. Loss (%)	Comments
SA-51	1755	300	$1.3x10^{-2}$	15	Smooth, good flow
	1810	300	$1.3x10^{-2}$	22	Crystalline surface; flow not as good as 1755°K
SA-52	1755	300	$1.3x10^{-2}$	13	Smooth, dense, large support rod marks
	1810	300	$1.3x10^{-2}$	25	Porous, support rod marks present
SA-53	1755	300	$1.3x10^{-2}$	16	Smooth, medium support marks
SA-131	1810	300	$1.3x10^{-2}$	33	Good flow, smooth, dense
SA-132	1810	300	$1.3x10^{-2}$	21-28	Good flow, smooth, dense
SA-133	1810	300	$1.3x10^{-2}$	18	Smooth surface, large support marks
SA-134	1810	300	$1.3x10^{-2}$	28	Poor flow
SA-135	1810	300	$1.3x10^{-2}$	30	Smooth, good flow
SA-136	1810	300	$1.3x10^{-2}$	29	Smooth surface, edge cracks
SA-137	1810	300	$1.3x10^{-2}$	27	Smooth, good flow

LP-SC Exposure

Five coupons were prepared and coated with each coating modification. Tables XLII and XLIII contain firing and thickness data for the various coating systems. Low-pressure, slow-cycle exposure at 1700°K and 1300 N/m^2 was employed to evaluate four coupons of each coating type. Table XLIV contains the results from the LP-SC testing and shows that none of the newer compositions was an improvement over the parent coating.

None of the three modifications (SA-51, 52, 53) to the SA-5 coating achieved 1700°K LP-SC lifetimes equivalent to the original composition. The weight loss during firing for the SA-51 and 52 coatings suggested, based on comparison with SA-5 data, that extensive glazing could be expected. Again, by comparison with SA-5 firing data, the SA-53 modification was expected to yield lightly glazed coupons. Virtually no glazing was observed for any of the LP-SC exposed, modified SA-5 coatings. Figure 48 shows the microscopic appearance of an SA-52 coated specimen after 5 LP-SC's to 1700°K. The appearance of SA-51 and SA-53 coated coupons was similar. The surface oxide appears porous and has apparently not sealed the expansion cracks in the SA-51 and SA-52 silicides. Some cracks in the SA-53 coating contained oxides, but a

TABLE XLII

FIRING DATA FOR SA TEST SPECIMENS

Coating	Wt. Loss (%) (range, ave.)	Coating Weight (kg/m^2)
SA-51	8-12, 11	0.292 - 0.324
SA-52	6-11, 9	0.295 - 0.337
SA-53	8-17, 14	0.255 - 0.306
SA-53	14-17, 16	0.259 - 0.305
SA-131	19-26, 23	0.258 - 0.285
SA-132	21-28, 23	0.261 - 0.298
SA-133	15-20, 18	0.288 - 0.314
SA-135	27-31, 29	0.225 - 0.257
SA-136	27-32, 30	0.215 - 0.248
SA-137	27-30, 28	0.224 - 0.262

TABLE XLIII

FIRING DATA FOR DAM-DAS TEST SPECIMENS

Coating	DAM Wt. Loss (%) (Range, Ave.)	DAS Wt. Loss (%) (Range, Ave.)	Final Coating Weight (kg/m^2)
DAM-1 + DAS-21	39-43, 42	10-14, 12	0.395 - 0.417
DAM-6 + DAS-21	40-41, 41	15-18, 17	0.378 - 0.429
DAM-7 + DAS-21	39-43, 41	18-20, 19	0.388 - 0.416
DAM-8 + DAS-21	42-47, 45	19-22, 20	0.338 - 0.401
DAM-11 + DAS-1	39-44, 41	17-25, 22	0.403 - 0.444

TABLE XLIV

TEST RESULTS FOR 1700° K - 1300 N/m^2 LP-SC EXPOSED COATING MODIFICATIONS

Specimen Number	Coating	Cycles	Comment
66	SA-51	0	Total failure during pre-oxidation
78	SA-51	0	Total failure during pre-oxidation
91	SA-51	0	Total failure during pre-oxidation
111	SA-51	5	EEF, no glaze, black
256	SA-51	22	SF, EEF, slight glaze, black
32	SA-52	5	EEF, no glaze, black
40	SA-52	5	EEF, no glaze, black
70	SA-52	5	EEF, no glaze, black
157	SA-52	5	EEF, no glaze, black
561	SA-53	13	EEF, black, no glaze
630	SA-53	14	EEF, black, slight glaze
563	SA-53	16	SEF, black, rough, slight glaze
626	SA-53	20	EEF, black, rough, no glaze
132	SA-131	22	SF, deformed, no glaze, brown
208	SA-131	22	EEF, no glaze, dark brown
229	SA-131	22	EEF, no glaze, dark brown
258	SA-131	28-33	Support hook failure, specimen lost
554	SA-132	22	Removed for test, no glaze, brown
598	SA-132	28-33	Support hook failure, specimen lost
604	SA-132	28-33	EEF, no glaze, dark brown
613	SA-132	39	EEF, no glaze, dark brown
612	SA-133	13	EEF, brown, no glaze
641	SA-133	14	EEF, brown, no glaze
644	SA-133	17	SF, charcoal brown, no glaze
562	SA-133	20-28	EEF, brown, slight glaze
762	SA-135	6	SF, brown, no glaze, surface spalling
656	SA-135	9	SF, brown, deformed, surface spalling
732	SA-135	9	EEF, brown, surface spalling
778	SA-135	9	SEF, brown, surface spalling
569*	SA-136	20-21	EEF, SEF, Charcoal brown, no glaze
712*	SA-136	20-21	EEF, SEF, Charcoal brown, no glaze
760*	SA-136	20-21	EEF, SEF, Charcoal brown, no glaze
766*	SA-136	20-21	EEF, SEF, Charcoal brown, no glaze
759	SA-137	9	SF, charcoal brown, deformed
782	SA-137	13	SF, charcoal black, deformed
763	SA-137	16	EEF, brown, spalling surface
670*	SA-137	17	SF, brown, spalling surface
662	DAM-1+DAS-21	9	EEF, black, slight glaze
710	DAM-1+DAS-21	16	SEF, black, slight glaze
731	DAM-1+DAS-21	16	EEF, black, slight glaze
721	DAM-1+DAS-21	22	SEF, black, slight glaze
593	DAM-6+DAS-21	13	EEF, black, light glaze
672	DAM-6+DAS-21	14	EEF, black, light glaze
678	DAM-6+DAS-21	18	EEF, black, light glaze
556	DAM-6+DAS-21	58	EEF, black, light glaze
591	DAM-7+DAS-21	12	EEF, SF, black, slight glaze
650	DAM-7+DAS-21	12	SF, black, slight glaze
695	DAM-7+DAS-21	28	Removed from test, black, slight glaze
674	DAM-7+DAS-21	39-44	SEF, black, light glaze
559	DAM-8+DAS-21	5	EEF, black, light glaze
675	DAM-8+DAS-21	6	EEF, black-brown, medium glaze
552	DAM-8+DAS-21	9	EEF, black-brown, medium glaze
642	DAM-8+DAS-21	13	SEF, black-brown, medium glaze
572	DAM-11+DAS-1	7	EEF, black, slight glaze
542	DAM-11+DAS-1	8	EEF, black, slight glaze
596	DAM-11+DAS-1	8	EEF, SEF, black, slight glaze
625	DAM-11+DAS-1	16	SEF, black, slight glaze

EEF = End edge failure
SEF = Side edge failure
SF = Surface failure

*Specimens cooled to about 1420°K during sixteenth cycle when power lead to furnace failed.

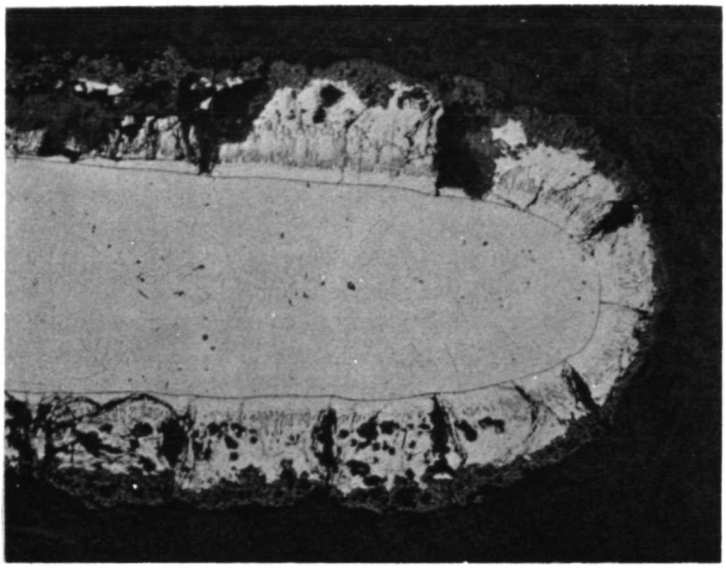

Specimen No. 40

5 LP-SC's

Etchant: $HF-HNO_3$-Lactic

Magnification: 125X

FIGURE 48. SA-52 MICROSTRUCTURE AFTER LP-SC EXPOSURE AT 1700°K AND 1300 N/m^2

vitreous layer was not present. Figure 48 and other photomicrographs showed the SA-51 and SA-52 coated specimens to have thin top and bottom edge coatings.

The SA-13 coating modifications may be considered in three groups. Those systems with minor chromium, titanium and vanadium concentration variations included SA-131, 132 and 133. The SA-134 and 136 coatings are variations of the SA-13 and SA-133 compositions but were titanium-free. Compositions identified as SA-135 and 137 were also similar to SA-13 and SA-133 but had iron substituted for titanium in each case.

Figure 49 displays the microscopic features of an SA-132 coating after 33 LP-SC's to 1700° K and 1300 N/m^2. Expansion cracks and small pores within the coating are seen to contain a two- or more phased oxide. The presence of a continuous vitreous surface layer is not evident in Figure 49. However, the SA-132 coated specimens were not "dusty" on the surface and showed no tendency toward surface spalling. Intact areas of the SA-131 and 133 coatings showed a similar appearance to that of Figure 49. Some surface problems were noted on two of the SA-131 composition coupons and were the result of porosity, possibly caused by incomplete fusion.

Specimens coated with the SA-135 and 137 compositions tended to have porous surfaces after fusion. The appearance was that which might result from boiling, sudden freezing and bubble entrapment. Both coating systems developed loose, brown, spalling oxide surfaces during LP-SC exposure. Figure 50 clearly shows the resultant rapid SA-137 coating consumption level after only 13 LP-SC's to 1700° K and 1300 N/m^2.

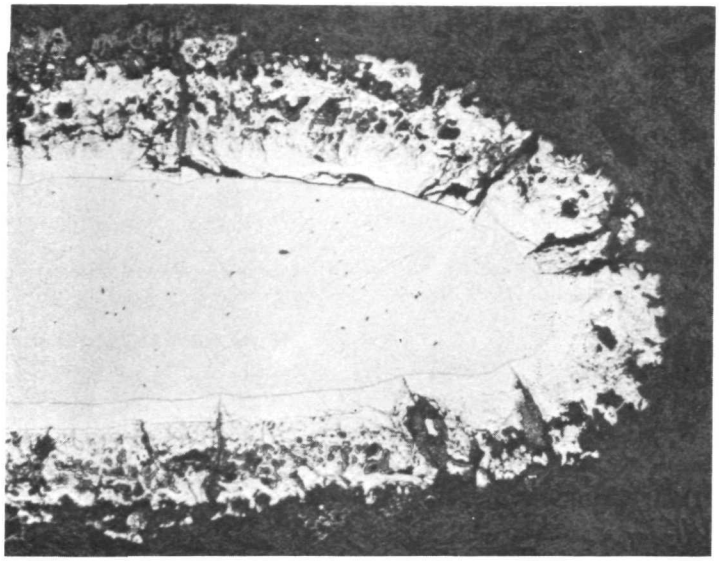

Specimen No. 604

33 LP-SC's

Etchant: HF-HNO_3-Lactic

Magnification: 125X

FIGURE 49. SA-132 MICROSTRUCTURE AFTER LP-SC EXPOSURE AT 1700° K AND 1300 N/m^2

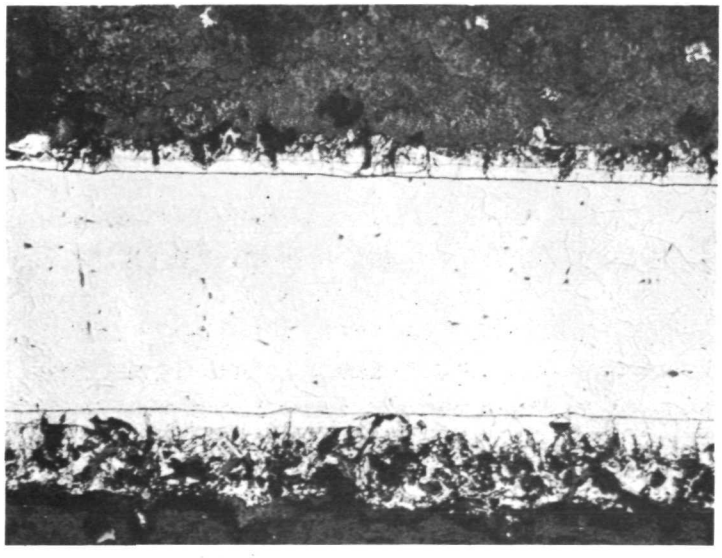

Specimen No. 782

13 LP-SC's

Etchant: HF-HNO_3-Lactic

Magnification: 125X

FIGURE 50. SA-137 MICROSTRUCTURE AFTER LP-SC EXPOSURE AT 1700° K AND 1300 N/m^2

All SA-136 coated coupons exhibited thick and thin areas of coating at the specimen edges and suggested possible bisque tearing during firing. Pre-oxidation of SA-136 coupons yielded a medium gray rather than brown surface oxide. Exposure in the LP-SC rig at 1700° K darkened the color to charcoal brown and developed a slightly powdery surface on two specimens. Figure 51 shows the cross-sectional appearance of an SA-136 coated specimen after 21 LP-SC's. Coating pores and expansion cracks are seen to be filled. However, examination of the surface layer shows the oxide to be porous and discontinuous.

As previously noted, all DAM + DAS-21 coating modifications were directed toward increasing the refractoriness and reducing the glazing characteristics of the coatings. Only the DAM-11 + DAS-1 system sought to increase glazing. Comparison of data from Task I specimens with that of Table XLIV indicates that the modified original systems (DAM-1 + DAS-21 and DAM-11 = DAS-1) were not as good as the original systems (DAM-1 + DAS-1, DAM-1 + DAS-2). Considerably less glass formed on the DAS-21 silicided specimens than on DAS-2 silicided coupons. No appreciable difference in glass forming tendency was observed between the DAM-1 and DAM-11 modifier alloys. The DAM-8 + DAS-21 modification exhibited much poorer performance than either DAM-8 + DAS-1 or DAM-8 + DAS-2. Glazing of DAM-8 + DAS-21 was light to medium, similar to DAM-8 + DAS-1 and less than for DAM-8 + DAS-2. The best of both the DAM-6 and -7 + DAS-21 modifications lasted approximately the same number of cycles as the original DAM-6 and -7 + DAS-2 systems. Lighter glazing was generally noted for the modified coatings than for the original compositions. The coatings were characteristically rougher than the SA-series coatings. All suffered from minor to severe edge cracking, and all developed a black surface after LP-SC exposure.

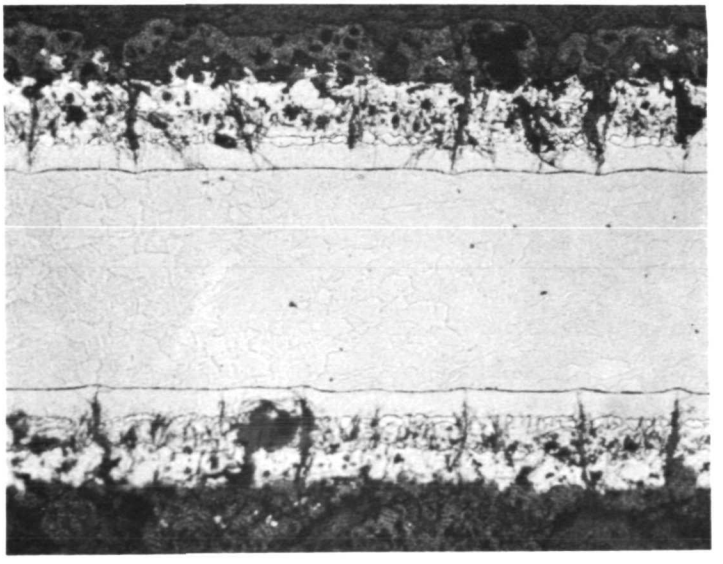

Specimen No. 569

21 LP-SC's

Etchant: $HF-HNO_3$-Lactic

Magnification: 125X

FIGURE 51. SA-136 MICROSTRUCTURE AFTER LP-SC EXPOSURE AT 1700° K AND 1300 N/m^2

Figure 52 includes examples of the modified DAM + DAS coatings after 8 to 58 LP-SC's to 1700° K. The DAM-11 + DAS-1 (Part A) coating was very porous. Extreme porosity is characteristic of the DAM-1 alloy layer. Part B of Figure 52 was included to show the surface roughness encountered in many of the DAM + DAS-21 coating combinations. Growth of a continuous oxide phase on the coating surface was indicated for the DAM-7 + DAS-21 combination. Comparison of Part C of Figure 52 with Figure 9 dramatically shows the decreased glazing tendency of DAM-6 + DAS-21 over DAM-6 + DAS-2. The DAM-6 + DAS-2 coupon gained 84 kg/m^2 after 45 LP-SC's to 1700° K, while the DAM-6 + DAS-21 specimen gained approximately 45 kg/m^2 during the same exposure.

Diffusion zone thickness data from the modified coatings are shown in Figure 53. These data were plotted to include the 1-hour - 1700° K pre-oxidation cycle received by all specimens prior to entering test. These substrate consumption data agree well with similar previously obtained data (Fig. 34).

Average weight gain data during 1700° K LP-SC exposure for the modified coating compositions are shown in Figure 54. The relatively high weight gain for SA-135 and 137 reflects the observation that a loose, porous oxide formed at the coating surface. The slower than parabolic kinetics rate shown by SA-131, 132 and 133 are typical of, and nearly identical to, previously reported SA-13 data.

3.2.2 Vitreous Overlays

Development of a thin vitreous layer over a silicide coating appears necessary for extended lifetimes at elevated temperatures. Unfortunately, this glassy layer must be formed at the expense of some of the silicide coating and, therefore, may contain oxides of each element present in the silicide. Current silicide coatings are quite complex and generally contain a number of different transition metals. Transition elements are noteworthy for their multiple valence states and ability to form defect oxide systems. The availability of numerous valence states provides a means of transporting oxygen through a surface oxide layer according to reactions such as:

$$\text{Surface} \quad 2Fe^{2+} + 1/2\,O_2 \rightarrow 2Fe^{3+} + O^{2-}$$

$$\text{Interface} \quad \frac{1}{n}M + Fe^{3+} \rightarrow Fe^{2+} + \frac{1}{n}M^{n+}.$$

Formation of defect oxide structures can also greatly enhance the transport rate for oxide or metal ions through that oxide.

Development of glasses which would be stable when in contact with silicides and which were formulated from materials possessing only a single, stable, oxidation state was undertaken as a means of significantly improving silicide coating performance. Constituents were essentially limited to such glass formers as SiO_2 and B_2O_3

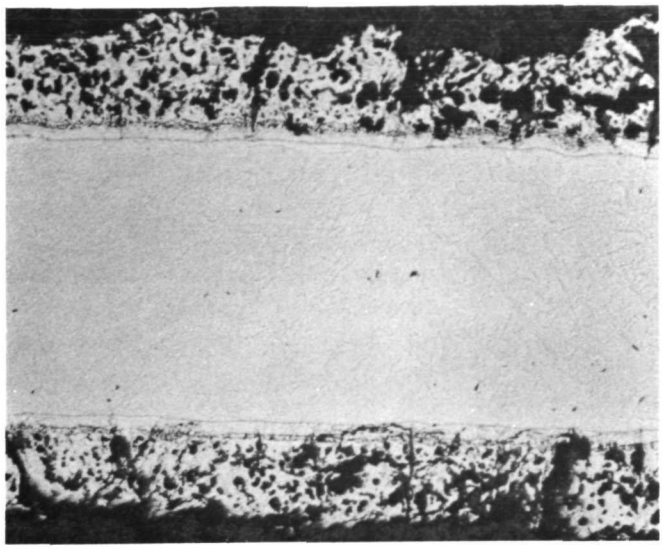

PART A

DAM-11 + DAS-1 Specimen No. 596

8 LP-SC's

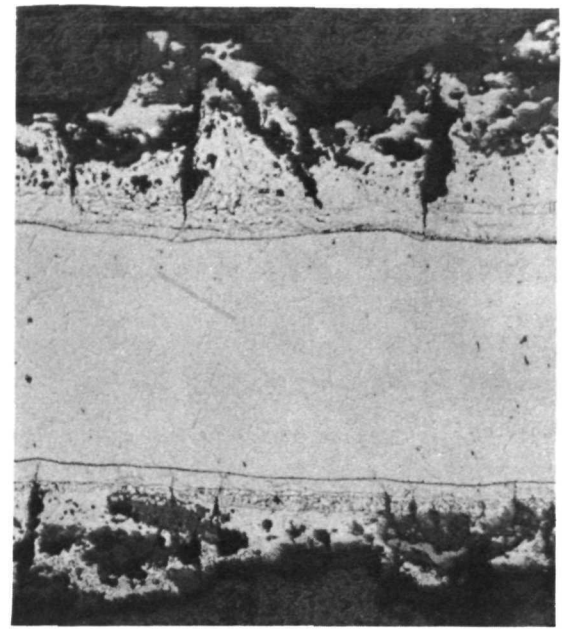

PART B

DAM-7 + DAS-21 Specimen No. 695

28 LP-SC's

Note Surface Roughness

Magnification: 125X

Etchant: $HF-HNO_3$-Lactic

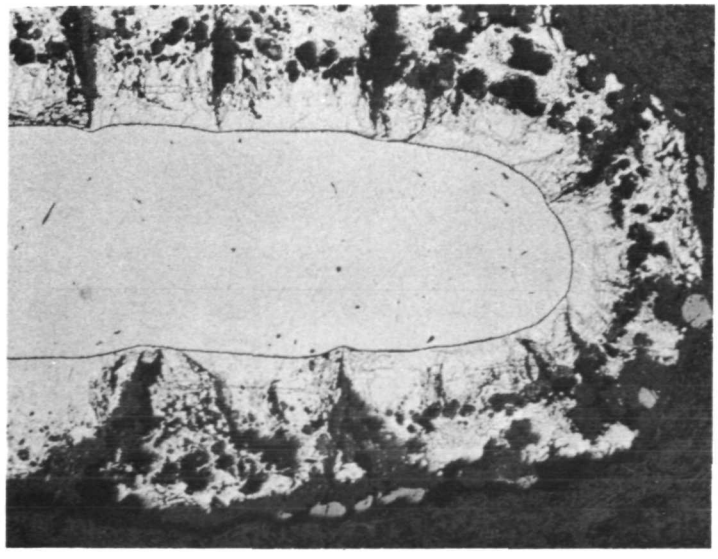

PART C

DAM-6 + DAS-21

Specimen No. 556

58 LP-SC's

FIGURE 52. DAM + DAS MICROSTRUCTURES AFTER LP-SC EXPOSURE AT 1700°K AND 1300 N/m^2

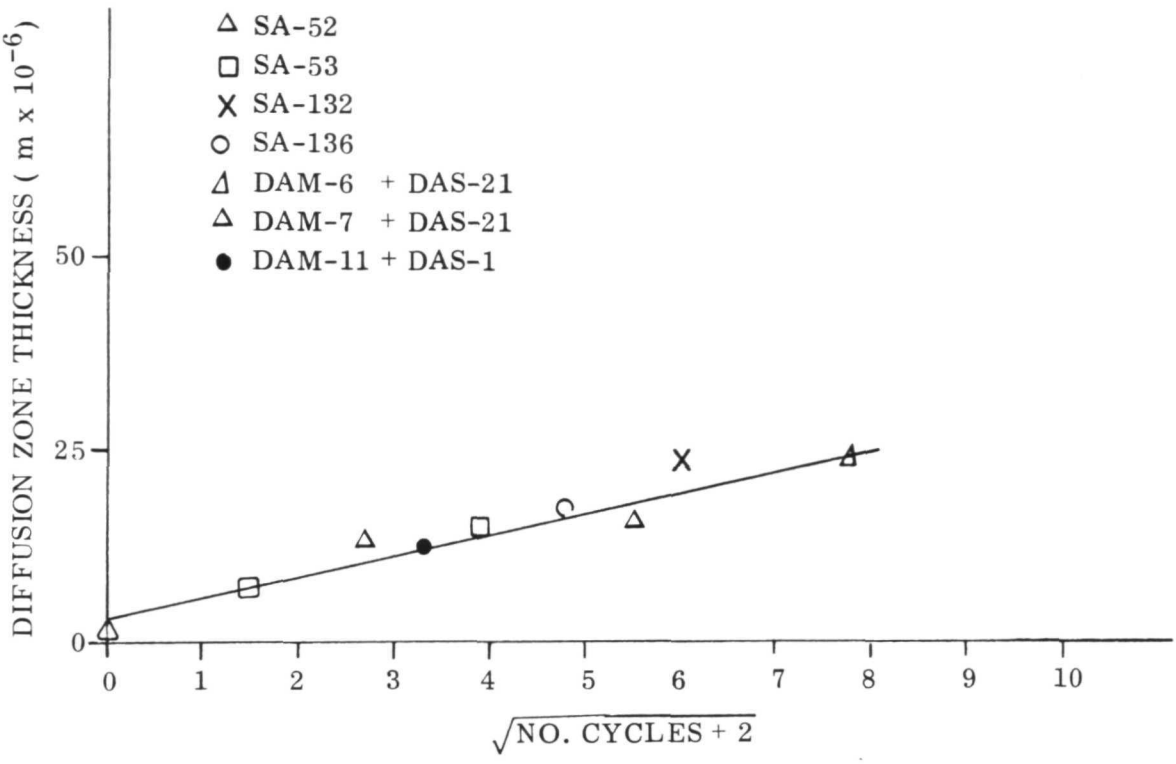

FIGURE 53. DIFFUSION ZONE THICKNESS VERSUS EXPOSURE AT 1700°K AND 1300 N/m^2

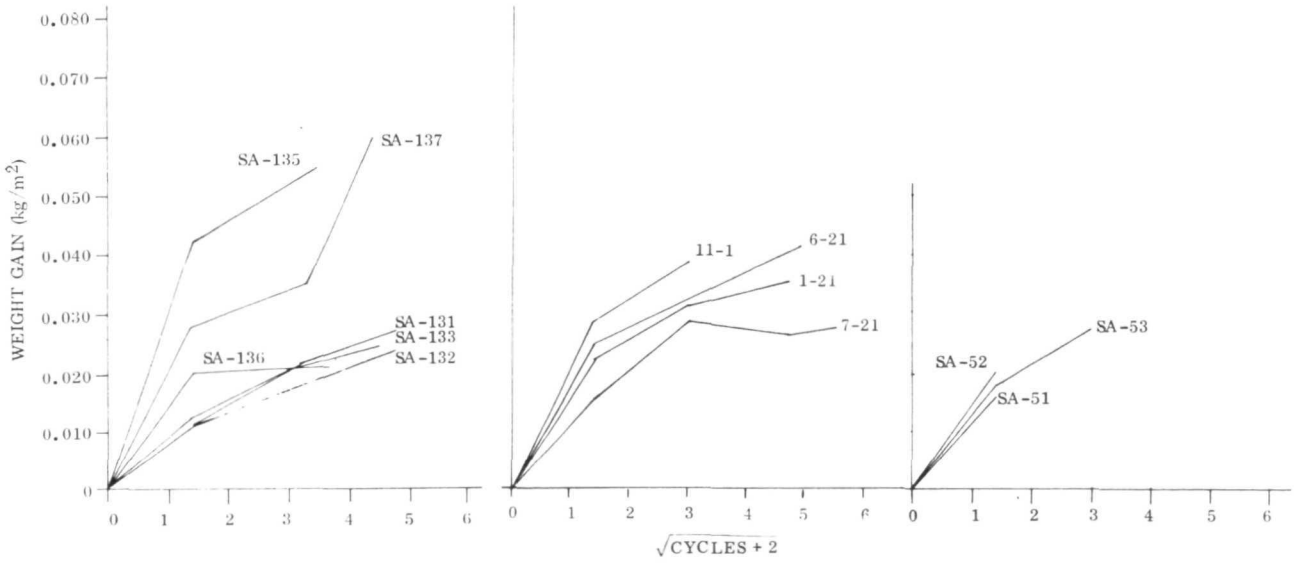

FIGURE 54. WEIGHT CHANGE DATA FOR 1700° K - 1300 N/m^2 LP-SC EXPOSED MODIFIED COATINGS

plus the alkaline earth oxides. Twenty glass compositions (Table XLV) were selected for preparation and evaluation.

TABLE XLV

VITREOUS OVERLAY COMPOSITIONS

Name	Glass Former, w/o (x SiO_2-yB_2O_3)	Modifier Al_2O_3	Fluxes			
			BaO	SrO	CaO	MgO
GN-1	90-(90SiO_2-10B_2O_3)	-	7	2	0.5	0.5
-2	80-	-	14	4	1	1
-3	75-	-	17.5	5	1.25	1.25
-4	80-	-	14	-	5	1
-5	80-	-	15	4	1	-
-6	78-	2	14	4	1	1
-7	75-	5	14	4	1	1
-8	70-	5	17.5	5	1.25	1.25
-9	80-	-	20	-	-	-
-10	80-	2	18	-	-	-
-11	60-	-	28	8	2	2
-12	60-	-	30	8	2	-
-13	43-	-	22	6	14.5	14.5
-14	51-	-	25	7	17	-
-15	90-(80SiO_2-20B_2O_3)	-	7	2	0.5	0.5
-16	51-(90 SiO_2-10B_2O_3)	-	25	7	17	-
-17	47-(90SiO_2-10B_2O_3)	-	38.5	-	14.5	-
-18	47SiO_2	-	38.5	-	14.5	-
-19	42-(90SiO_2-10B_2O_3)	5	38.5	-	14.5	-
-20	49-(90SiO_2-10B_2O_3)	2	25	7	17	-

Glass Preparation

Smelting of the glasses was initiated in a resistance heated platinum crucible; however hot spots developed in the crucible walls and ultimately caused crucible failure. The maximum attainable temperature in the 0.02 liter capacity platinum crucible was about 1850°K. Smelting was continued in a gas-fired smelter using a high-silica, clay-bonded crucible. This smelter had a maximum use temperature of near 1755°K and could accommodate a 1 kg charge. Any glass selected for use in the program had to be smelted in the gas-fired apparatus in order to obtain sufficient quantities for evaluation. Initial smelting was, therefore, performed at temperatures attainable by the gas-fired smelter.

As noted in Table IV, alkaline earth carbonates were used for preparation of the glasses. Slow decomposition of the carbonates during smelting promotes good constituent mixing through constant stirring. Table XLVI contains observations from the first effort to smelt each glass. These data eliminated compositions GN-1 to 10 and GN-15 from further consideration.

TABLE XLVI

SMELTING OF VITREOUS OVERLAYS

Composition	Smelter Temp. (°K)	Observation
GN-1	1755	Too refractory to pour or sample.
-2*	1845	White, able to sample, unable to pour.
-3*	1835	White, able to sample, unable to pour.
-4*	1870	Too refractory to sample or pour.
-5*	1870	Too refractory to sample or pour.
-6	1755	White, scraped out of crucible.
-7*	1835	Clear, crucible failed.
-8*	1820	Clear, unable to sample.
-9	1800	Too refractory to pour or sample
-10	1800	Too refractory to pour or sample
-11	1755	White, poured
-12*	1700	White, sampled
-13	1645	Clear, poured, sampled.
-14	1645	Clear, sampled, poured.
-15	1800	Too refractory to pour or sample.
-16	1600	Clear, poured
-17	1650	Clear, poured
-18	1600	Clear, poured
-19	1630	Clear, poured
-20	1600	Clear, poured

*Performed in resistance heated Pt crucible.

Softening Temperatures

A softening point determination was performed on the GN-11, 14, 16, 17, 18, 19 and 20 systems. Approximately 0.15 meter long by 0.001 meter diameter glass rods were pulled from each glass when in the molten state. These rods were held by one end and were heated for 900 seconds at various temperatures until sagging occurred. The temperature at which sagging occurred was defined as the softening point. These

data are shown in Table XLVII. Relatively little difference was observed between the various glass compositions.

TABLE XLVII

GLASS SOFTENING TEMPERATURES

Glass	Temp. (°K)
GN-11	1030
-14	1010
-16	1000
-17	1010
-18	1010
-19	1010
-20	980

Devitrification

The effect of heating and cooling on devitrification (crystallization) was determined for the GN-11, 14, 16, 17, 18, 19 and 20 glass compositions. Small pieces of each glass were supported on microquartz and were heated to 1260° K, held for 1800 seconds, and cooled to room temperature. This was repeated to a total of 4 cycles. Table XLVIII contains data on the appearance of each glass after 0, 1, 2, 3 and 4 heating and cooling cycles. The GN-11 glass appeared to be a crystalline material after only one cycle to 1260° K and was also found to crumble rather than fracture like a glass. All other compositions appeared to retain the properties of a glass, with GN-16 and GN-19 showing the least tendency to devitrify.

Expansion Measurements

Linear expansions were determined for the GN-11, 12, 14, 16, 18, 19 and 20 composition glasses and for 90Ta-10W alloy with the aid of a fused silica dilatometer. Basically, the apparatus provides a means of comparing the change in length of a cylindrical specimen with the change in length of a fused silica tube which surrounded the specimen. The specimen was supported by the bottom of the fused silica tube and was contacted above by a fused silica rod. The difference between the elongation of the specimen and the fused silica tube opposite the specimen was measured by a micrometer which could be read to the nearest 2.54×10^{-7} meter. A weak spring and an LVDT were used to assure uniform pressure on the specimen from measurement to measurement and to check the zero point between measurements. Temperature measurement was by a chromel-alumel thermocouple attached to the fused silica tube. The thermocouple bead was within about 1×10^{-3} meter of the specimen.

TABLE XLVIII

DEVITRIFICATION OF GN-SERIES GLASSES

Glass	CYCLE				
	0	1	2	3	4
GN-11	milky white	opaque white	opaque white	opaque white	opaque white
-14	pale green, clear	pale green, cloudy	pale green, cloudy	pale green, opaque	nearly white, opaque
-16	clear, colorless	clear, colorless	cloudy, colorless	cloudy, colorless	cloudy, colorless
-17	clear, colorless	clear, colorless	cloudy, colorless	cloudy, white	cloudy, white
-18	clear, colorless	slightly cloudy, colorless	cloudy, white	opaque, white	opaque, white
-19	clear, colorless	clear, colorless	clear, colorless	clear, colorless	cloudy, colorless
-20	clear, colorless	clear, colorless	cloudy, colorless	cloudy, colorless	cloudy, white

Calibration of the fused silica dilatometer was accomplished by measuring the expansion of an NBS supplied platinum rod with a known length and expansion coefficient. Between 300 and 900° K, extension of the standard, as measured, was in agreement with the known expansion data for the platinum.

Specimens to be used for expansion measurements were prepared by casting a finely milled slip of each glass. The slip was poured into a glass tube, compacted by centrifuging, extruded from the glass mold, vacuum dried to remove excess vehicle (xylene + ethyl cellulose), and was finally sintered in air above the softening temperature. Each sintered glass rod was cut to about 0.0254 meter in length and was then measured with a micrometer to the nearest $\pm 7.6 \times 10^{-6}$ meter. Expansion measurements were made during heating and cooling in the room temperature to 870° K temperature range for the GN-11, 12, 14, 16, 18, 19 and 20 glasses and for the 90Ta-10W alloy. An argon atmosphere was used while measurements were performed on the 90Ta-10W alloy. Measured expansions are graphed versus temperature in Figure 55 together with known values for pure tantalum and fused silica.

Only GN-11 had an expansion rate lower than that of the 90Ta-10W alloy. The GN-14, 16, 18, 19 and 20 compositions were all found to expand about 25 percent faster than 90Ta-10W. The expansion data for GN-14, 18 and 20 were indistinguishable and were only slightly lower than for GN-19. The GN-16 system showed an

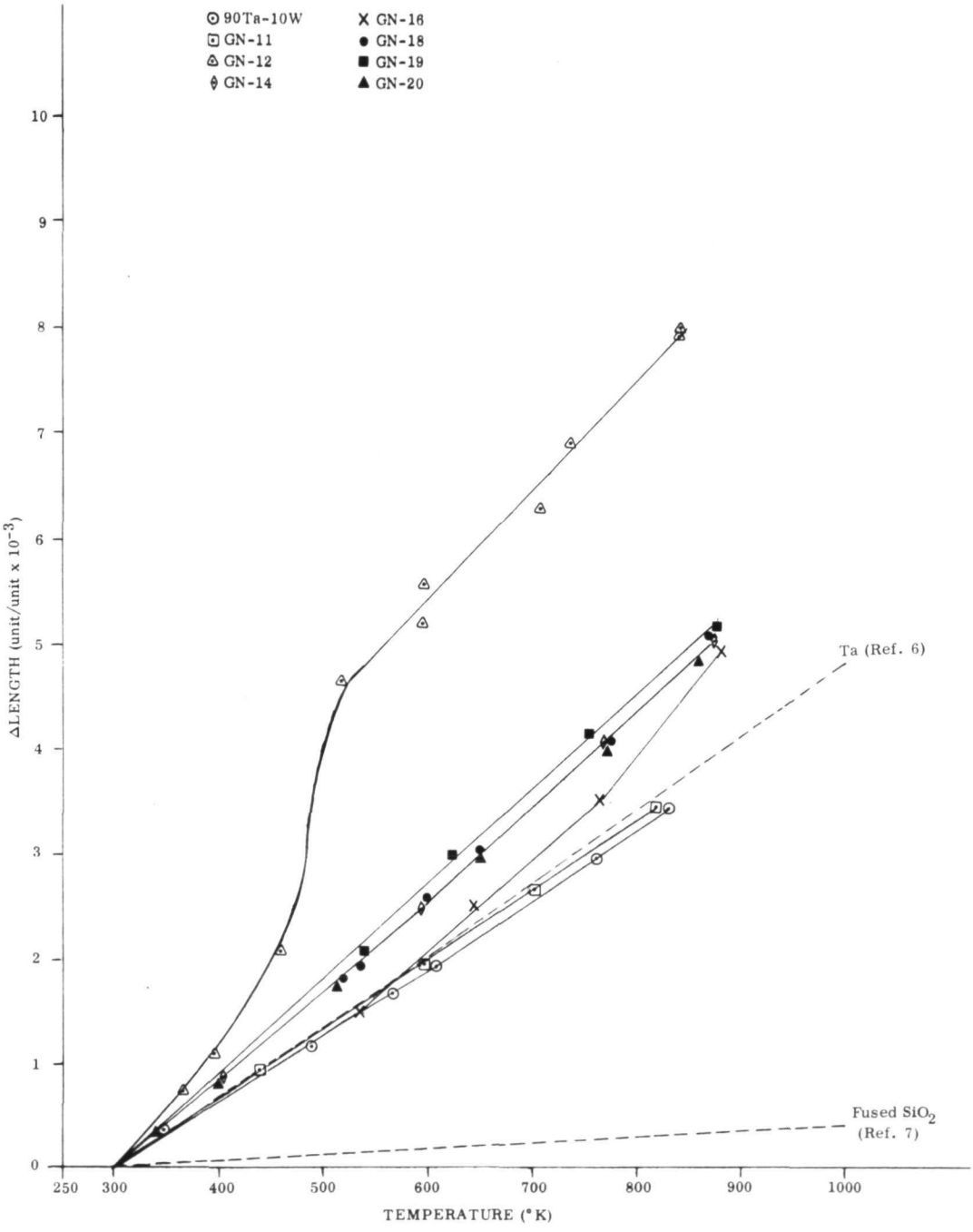

FIGURE 55. EXPANSION OF GN-SERIES GLASSES

increasing expansion rate with increasing temperature. A very high and non-linear expansion rate was determined for the GN-12 system and was verified with a second specimen. With the exception of GN-12, higher silica levels in the glasses led to lower expansions.

Coating Preparation

Relative devitrification rates and expansion data provided the basis for selection of GN-16 and GN-19 for development into overlay coatings. The original plan was to employ only Cr_2O_3 as a mill addition to each of five glass compositions. Chromium oxide is nearly insoluble in silica glasses and serves to physically restrict flow of a glass. Facility limitations precluded smelting of sufficiently refractory glasses and necessitated the use of fused silica mill additions as a means of obtaining the desired high silica glass content and resultant refractoriness and immobility. This approach permitted the deliberate variation of glass properties so as to obtain a quite fluid glass which might exhibit excellent self-healing characteristics or a very refractory and immobile system which would remain firmly in place at the highest exposure temperatures.

Various quantities of fused silica and Cr_2O_3 were added to the GN-16 and GN-19 frits and were ball-milled for 6 hours in xylene. Sufficient ethyl cellulose was added to yield a 1/2 percent binder level. These coatings were then applied to scrap SA-13 coated coupons and were fired in air. Table XLIX contains resultant data.

All fired specimens which were overlayed with a SiO_2 modified glass exhibited a chromium oxide (Cr_2O_3) green color rather than the usual milk chocolate brown of the oxidized SA-13 coating. The Cr_2O_3 modified glasses appeared very dark green or black after firing. Vitreous overlays containing SiO_2 mill additions were observed to contain numerous expansion cracks.

It was, therefore, suspected that the fused silica used as a mill addition might have contained some quartz or cristobalite. An X-ray diffraction analysis was performed on the fused silica and yielded no diffraction pattern. This confirmed that only vitreous silica was present.

Expansion measurements were performed on the GN-19D coating. The specimens were prepared by slip casting, centrifuging, drying, and were then sintered for 1800 seconds at about 1520°K. Figure 56 shows the measured expansion data together with data for the basic GN-19 glass, the 90Ta-10W alloy and the linear expansion for cristobalite (calculated from volume expansion data in Ref. 7). These data show that the glasses which result from substantial mill additions of fused silica to the GN-series glasses experience a high expansion rate in the low temperature range. Above about 600°K, the expansion rates of GN-19D and of 90Ta-10W are nearly equal. The shape

TABLE XLIX

FIRING OF VITREOUS OVERLAY COATINGS

Coating	Composition (w/o)			Firing Temp. (°K)	Firing Time(sec)	Comments
	Frit	SiO_2	Cr_2O_3			
GN-16A	100	--	--	1255	1800	Sintered
GN-16B	55	45	--	1700	1800	Partially fused
GN-16C	62	38	--	1700	1800	Fused
GN-16-4Cr	71	--	29	1700	1800	Fused, bubbled
GN-16-6Cr	62	--	38	1700	1800	Fused, rough
GN-16-10Cr	50	--	50	1700	1800	Fused, smooth
GN-19A	100	--	--	1145	1800	Spalled
GN-19A	100	--	--	1255	1800	Sintered
GN-19B	38	62	--	1700	1800	Partially sintered
GN-19C	56	44	--	1700	1800	Fused
GN-19D	50	50	--	1700	1800	Partially fused
GN-19-10Cr	50	--	50	1700	1800	Fused, smooth

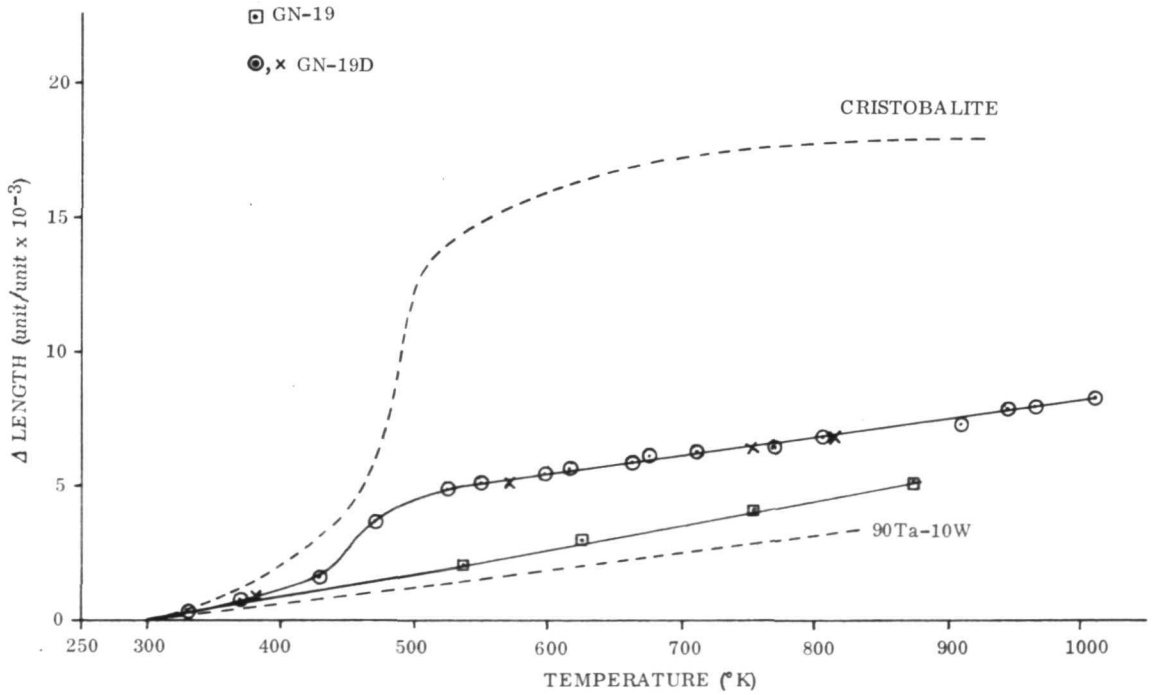

FIGURE 56. EXPANSION OF GN-19 SERIES COATINGS

of the expansion curve for GN-19D is believed to indicate the presence of some cristobalite. This suggests that expansion cracks in a vitreous overlay of a GN-series glass plus a SiO_2 mill addition will open and remain open below the temperature at which the cristobalite expansion rate changes with respect to the 90Ta-10W expansion rate. Though not the most theoretically desirable situation, this is probably harmless because it occurs below about 500° K.

Selection of vitreous overlay coatings and firing cycles were made from Table XLIX data and are shown in Table L.

TABLE L

SELECTED VITREOUS OVERLAYS

Coating	Composition	Firing Conditions	Thickness (kg/m^2)
GN-16C	62 frit-38SiO_2	1800 sec. - 1700° K	0.050
GN-19C	56 frit-44SiO_2	1800 sec. - 1700° K	0.050
GN-19D	50 frit-50SiO_2	1800 sec. - 1700° K	0.050
GN-16-10Cr	50 frit-50Cr_2O_3	1800 sec. - 1700° K	0.050
GN-19-10Cr	50 frit-50Cr_2O_3	1800 sec. - 1700° K	0.050

LP-SC of Vitreous Overlaid Specimens

A total of 160 SA-13 coated bend test specimens were required for 1700 and 1810° K LP-SC testing at 13 and 1300 N/m^2 and subsequent bend testing. Two hundred specimens were prepared, coated, fired and divided into groups for subsequent vitreous overlay application. About 20 of the 200 coated specimens were rejected for visible coating flaws and another 15 were rejected for abnormal weight losses during fusion. Forty SA-13 coated bend test coupons were overlaid with 0.050 ± 0.010 kg/m^2 of each of the five glasses listed in Table L. Low-pressure, slow-cycle exposure was performed at 1700 and 1810° K and 13 N/m^2 on all five coatings in the intentionally defected and nondefected conditions. Again, failure was defined as the first appearance of substrate oxide. Exposure at 1700 and 1810° K and 1300 N/m^2 was limited to two selected vitreous overlays, GN-16C and GN-19D. Test data are shown in Tables LI, LII, LIII and LIV.

As previously reported, the SA-13 silicide assumed a mottled brown and green colored surface during 1700° K - 13 N/m^2 exposure. Glass overlaid SA-13 coupons developed a gray to black color during similar exposure. Testing at 1810° K and 13 N/m^2 caused all coupons to display a dull, black, porous surface after only one test cycle.

TABLE LI

1700°K LP-SC EXPOSURE OF VITREOUS OVERLAY COATINGS AT 13 N/m^2

Spec.No.	Coating	Cycles	Comments
757	SA-13 + GN16C	19	Removed, gray, glazed, bubbles
903		52	Removed, gray, glazed, bubbles
937		100	Removed, gray, glazed, bubbles
978		100	Removed, gray, glazed, bubbles
984	SA-13 + GN-16-10Cr	27	Removed, black, smooth, shiny
931		48	Failed, lower edge, black, smooth, shiny
665		100	Removed, black, smooth, shiny
864		100	Removed, black, smooth, shiny
975	SA-13 + GN-19C	9	Failed, surface, gray, glazed, bubbles
922		27	Removed, black, glazed, bubbles
679		48	Removed, black, glazed, bubbles
875		100	Removed, gray, glazed, bubbles
979	SA-13 + GN-19D	27	Removed, black, glazed, bubbles
707		48	Removed, black, glazed, bubbles
880		100	Removed, black, glazed, bubbles
950		100	Removed, black, glazed, bubbles
925	SA-13 + GN-19-10Cr	27	Removed, black, shiny
878		38-44	Failed, lower edge, black, shiny
660		48	Removed, black, smooth, shiny
755		64	Failed, lower edge, black, smooth, shiny

TABLE LII

1810°K LP-SC EXPOSURE OF VITREOUS OVERLAY COATINGS AT 13 N/m^2

Specimen Number	Coating	Cycles	Comments
682	SA-13 + GN16C	6	All specimens turned dull black after one cycle and showed no indication of any glass on the surface after the first cycle. Failure was by severe deformation.
753		6	
911		6	
976		6	
828	SA-13 + GN16-10Cr	5	
905		5	
909		5	
972		5	
668	SA-13 + GN19C	3	
761		3	
914		3	
980		3	
743	SA-13 + GN19D	6	
901		6	
935		6	
987		6	
688	SA-13 + GN19-10Cr	5	
872		5	
899		5	
948		5	

TABLE LIII

1700°K - 13 N/m^2 LP-SC EXPOSURE OF DEFECTED VITREOUS OVERLAID COUPONS

Specimen No.	Coating SA-13 + Overlay	Defect Type	Cycles	Comments
658	GN-16C	4T hole	8	
667	"	1&4T spots	8	Raised area of each spot
669	GN-16-10Cr	4T hole	3	0.004 meter hole
685	"	1&4T spots	6	Severe deformation at 4T spot
702	GN-19C	4T hole	2	0.001 meter hole
655	"	1&4T spots	8	Raised area at 4T spot
671	GN-19D	4T hole	6	0.002 meter hole
661	"	1&4T spots	6	Raised area at each hole
594	GN-19-10Cr	4T hole	3	0.003 meter hole
677	"	1&4T spots	4	Deformed at 4T spot

TABLE LIV

1700 AND 1810°K LP-SC EXPOSURE OF VITREOUS OVERLAY COATINGS AT 1300 N/m^2

Specimen No.	Coating	Temp. (°K)	Cycles	Comments
941	SA-13 + GN-16C	1700	10	Heavily glazed, light tan, severely bubbled glass, extensive glass flow.
840		1700	20	
912		1700	20	
932		1700	20	
723		1810	12	
867		1810	12	
862		1810	13	
906		1810	13	
729	SA-13 + GN-19D	1700	20	
756		1700	20	
859		1700	20	
861		1700	20	
974		1810	10	
107		1810	13	
926		1810	13	
974		1810	13	

Both coating reliability and specimen lifetime at 1700° K and 13 N/m^2 were significantly improved by addition of the vitreous overlays to the SA-13 silicide system. For instance, seven of ten glass overlaid coupons scheduled to be tested for 100 LP-SC's to 1700° K and 13 N/m^2 achieved that level while no plain SA-13 coupons survived beyond 98 test cycles.

Performance at 1810° K and 13 N/m^2 was poor and was in line with predicitions from kinetic and thermodynamic data. These results suggest that silica glass is unstable with respect to decomposition or evaporation at this pressure/temperature condition. The previously noted reaction (see page 78) between an MSi_2 silicide and SiO_2 would also occur.

Defected specimens were exposed at 1700° K and 13 N/m^2 but not at 1810° K. This low-pressure level (13 N/m^2) promoted considerable substrate hardening and deformation near an intentional defect but did not develop large growths of oxide. As a consequence, determination of failure of the defected coupons was largely subjective rather than quantitative.

As noted in Table LIV, all "1700° K" and "1810° K" - 1300 N/m^2 exposed, vitreous overlaid specimens glazed very heavily, exhibited extensive glass flow and failed within 20 cycles. This was neither expected nor reasonable in view of the performance recorded at 13 N/m^2. Also, atmospheric pressure firing of the glasses at 1700° K for up to 16 hours had not produced specimen failure or any appreciable glass flow. Metallographic analyses were performed on four coupons. Diffusion zone (M_5Si_3) thickness data were obtained and indicated that the "1700° K" specimens had been exposed at about 1800° K and that the "1810° K" specimens were exposed near 1840° K.

All of the 1300 N/m^2 pressure level coupons were tested in a single furnace with the "1810° K" samples being run first. A post test check of the furnace control thermocouple revealed a broken protection tube and a 78° K low reading at 1590° K. This furnace control thermocouple was new at the start of the "1810° K" exposures. The cracked Al_2O_3 protection tube probably permitted contamination of the thermocouple by volatile coating oxidation products.

Bend Test Data

It was previously demonstrated that only uncoated or as-prepared SA-13 coated coupons could withstand a 1.84 radian bend over a 4T (T = material thickness) radius punch at 82° K (Table XXVI). Most LP-SC exposed specimens were able to sustain such a bend at 200° K. As a consequence, the glass overlaid specimens were not evaluated at the 82° K temperature level. A progressive bend test was employed in which all coupons were deflected 0.18 radian at 295° K. If inspection revealed no cracking, the

coupon was subsequently bent through 1.84 radians to yield a permanent bend of about 1.6 radians. Data from the tests are tabulated in Tables LV and LVI. As may be seen from Table LV, all 1700° K - 13 N/m^2 exposed coupons exhibited a DBBTT of 200° K or lower. Similar results were observed for the few coupons which had been exposed at 1300 N/m^2 and either "1700° K" or "1810° K". Nearly all intentionally defected coupons either cracked or fractured when bent at 200° K (Table LVI). Previously tested, intentionally defected coupons (Table XXX) were generally observed to bend at 200° K but after only 1 or 2 LP-SC exposures instead of 3 to 8.

Analytical

Weight change data for the 1700 - 13 N/m^2 exposed samples are shown in Figure 57. Previously reported data (Fig. 41) showed the SA-13 silicide to experience an active/passive transition after about 5 test cycles and to slowly gain weight thereafter. Glass overlaid SA-13 samples lost weight at a decreasing rate with increasing exposure time, but never actually gained weight during equivalent testing. Data for 1810° K - 13 N/m^2 testing were not plotted because of extreme irregularities. Losses as high as 0.140 kg/m^2 (50 percent of the coating) were observed during the first test cycle.

Shown in Figure 58 are weight change data for the glass overlaid coupons which were tested at 1300 N/m^2 and near 1840 instead of 1810° K. These weight gains are similar to those recorded for the SA-13 silicide when tested at 1810° K and 1300 N/m^2.

Figure 59 shows the appearance of SA-13 + GN-19D coated coupons after 27, 48 and 100 LP-SC exposures at 1700° K and 13 N/m^2. Substrate centerline hardness values are included with this figure and show the 90Ta-10W alloy to be slightly softer after 100 test cycles than in the as-received condition. Comparison of this figure with Figure 42 (SA-13, 1700° K - 13 N/m^2 data) shows the glass overlay to have reduced the silicide coating consumption rate and to have better preserved the substrate properties (lower hardness values) than SA-13 without an overlay.

An example of the microscopic appearance of the GN-16C overlaid coating after 1840° K - 1300 N/m^2 exposure is shown in Figure 60. The glass overlay appeared noteworthy for the lack of opaque oxide phases customarily observed. A surface X-ray diffraction pattern was obtained from this specimen and showed only a trace of cristobalite (SiO_2). The exposure temperature was above that for the TiO_2-SiO_2 eutectic and may have permitted dissolution of TiO_2. An X-ray fluorescent scan of the glass surface detected all of the glass constituent elements, all coating elements but vanadium, and traces of zirconium, iron and aluminum.

Appearance characteristics of 4T hole and 4T spot defects are shown in Figure 61. Sectioning through the center of the 4T hole was not possible and this view does not, therefore, encompass the full extent of the substrate damage. Damage was

TABLE LV

BEND TEST DATA FOR NONDEFECTED SA-13 PLUS VITREOUS OVERLAID COUPONS

Specimen No.	Coating (SA-13 + Overlay)	Pressure (N/m^2)	Exposure (cycles/°K)	Test Temperature	
				295°K	200°K
881	16C	-	-	B	B
757		13	19/1700	B	B
903		13	52/1700	B	B
978		13	100/1700	B	B
890		1300	30/1700	B	B
906		1300	13/1810	B	B
717	16-10Cr	-	-	B	B
984		13	27/1700	B	B
931		13	48/1700	B	B
665		13	100/1700	B	B
719	19C	-	-	B	B
922		13	27/1700	B	B
679		13	48/1700	B	B
875		13	100/1700	B	B
920	19D	-	-	B	B
979		13	27/1700	B	B
707		13	48/1700	B	B
950		13	100/1700	B	B
861		1300	20/1700	B	B
907		1300	13/1810	B	B
693	19-10Cr	-	-	B	B
925		13	27/1700	B	F
660		13	48/1700	B	F

B = Bent without cracking
F = Fractured

TABLE LVI

BEND TEST DATA FOR INTENTIONALLY DEFECTED SA-13 PLUS VITREOUS OVERLAID COUPONS

Specimen No.	Coating SA-13 + Overlay	Defect Type	Pressure (N/m^2)	Exposure (cycles/°K)	Test Temperature	
					295°K	200°K
881	16C	4T hole	13	2/1700	B	C
667		1T spot	13	8/1700	B	F
667		4T spot	13	8/1700	B	C
669	16-10Cr	4T hole	13	3/1700	B	C
702	19C	4T hole	13	2/1700	B	C
655		1T spot	13	8/1700	B	B
655		4T spot	13	8/1700	B	F
671	19D	4T hole	13	6/1700	B	C
661		1T spot	13	6/1700	B	C
661		4T spot	13	6/1700	B	F
594	19-10Cr	4T hole	13	3/1700	B	C

B = Bent without cracking
C = Cracked
F = Fractured

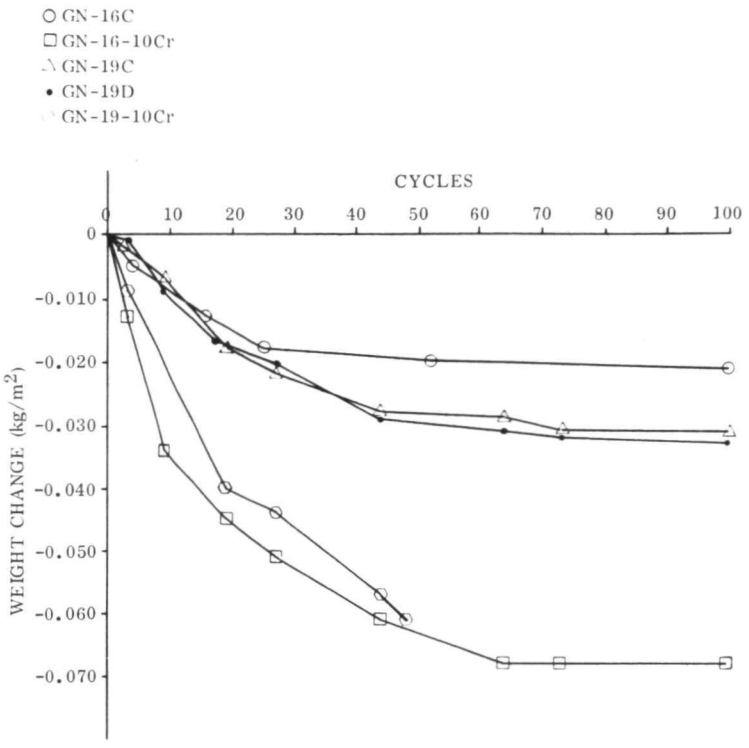

FIGURE 57. WEIGHT CHANGE DATA FOR 1700°K - 13 N/m^2 EXPOSED VITREOUS OVERLAY COATINGS

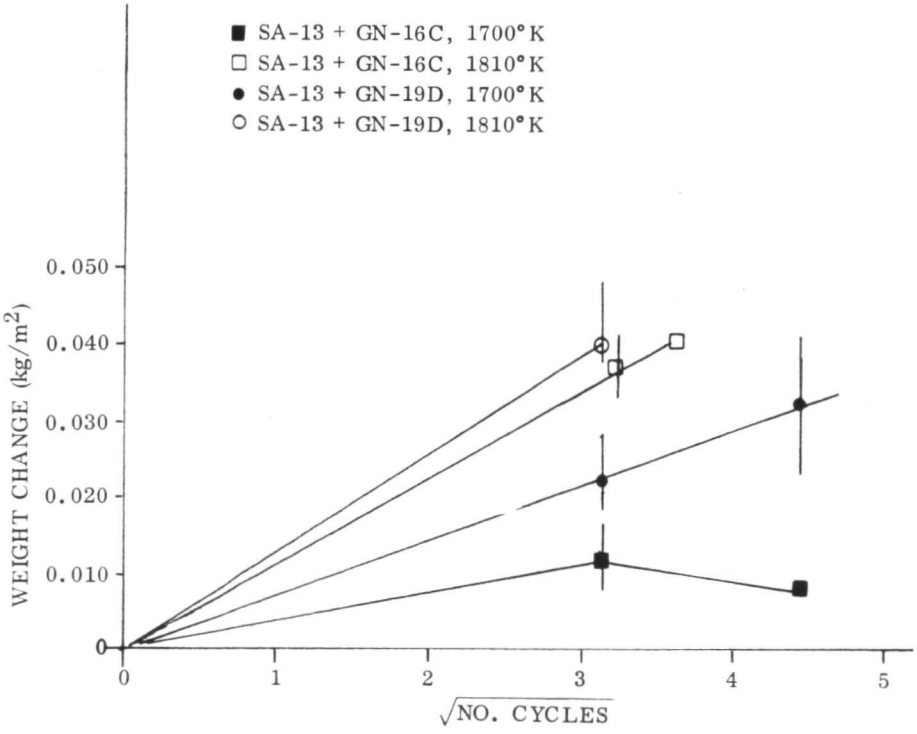

FIGURE 58. WEIGHT CHANGE DATA FOR 1700 OR 1810°K - 1300 N/m^2 LP-SC EXPOSED VITREOUS OVERLAY COATINGS

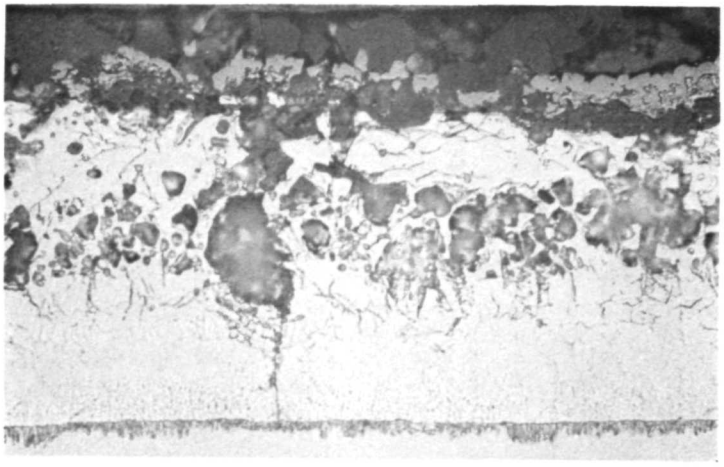

Specimen No. 979

27 LP-SC

Substrate ℄ Hardness:

236-252 KHN (100 g load)

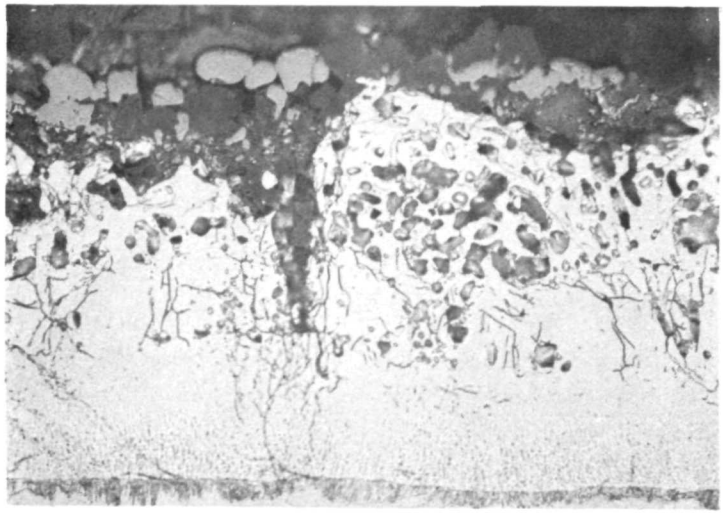

Specimen No. 707

48 LP-SC

Substrate ℄ Hardness:

238-250 KHN (100 g load)

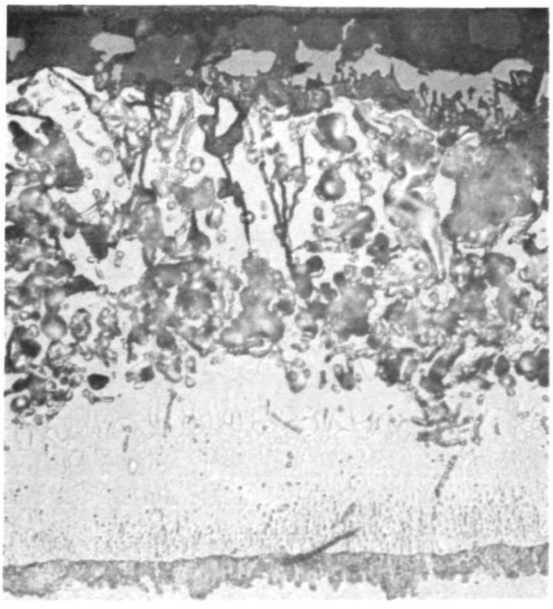

Specimen No. 880

100 LP-SC

Substrate ℄ Hardness:

242-249 KHN (100 g load)

Magnification: 500X

Etchant: HF-HNO_3-Lactic

FIGURE 59. SA-13 + GN-19D MICROSTRUCTURE AFTER LP-SC EXPOSURE AT 1700°K AND 13 N/m^2

Specimen No. 867

12 LP-SC

Magnification: 500X

Etchant: HF-HNO_3-Lactic

FIGURE 60. SA-13 + GN-16C MICROSTRUCTURE AFTER LP-SC EXPOSURE AT 1840° K AND 1300 N/m^2

estimated to spread over an 8.5×10^{-3} meter diameter area. Substrate hardening beneath the 4T spot defect is diagrammed in Figure 62. Measurements were made every 250×10^{-6} meter and defined a damaged area of 5×10^{-3} meter diameter.

3.3 COATING EVALUATION

Advanced methods of coating evaluation included: (1) plasma arc tunnel exposure; (2) simulated atmospheric re-entry; (3) further LP-SC exposure followed by elevated temperature testing; (4) total hemispherical emittance measurements; and (5) creep measurements. Both the SA-13 and SA-13 + GN-19D coatings were evaluated in most of the above tests.

3.3.1 Plasma Arc Tunnel Tests

Exposure of coated tantalum alloy samples to pressure, temperature and enthalpy levels believed representative of atmospheric re-entry was scheduled by NASA-Lewis midway through the present program. Two sets of SA-13 coated parts were prepared from 90Ta-10W alloy according to NASA supplied specifications and were forwarded to NASA-Lewis Research Center. Figures 63 and 64 show the samples. Exposure of the metallic test samples and other parts was performed by Aerotherm under contract NAS2-6445. A final report entitled "The Effect of High Mass Flow on

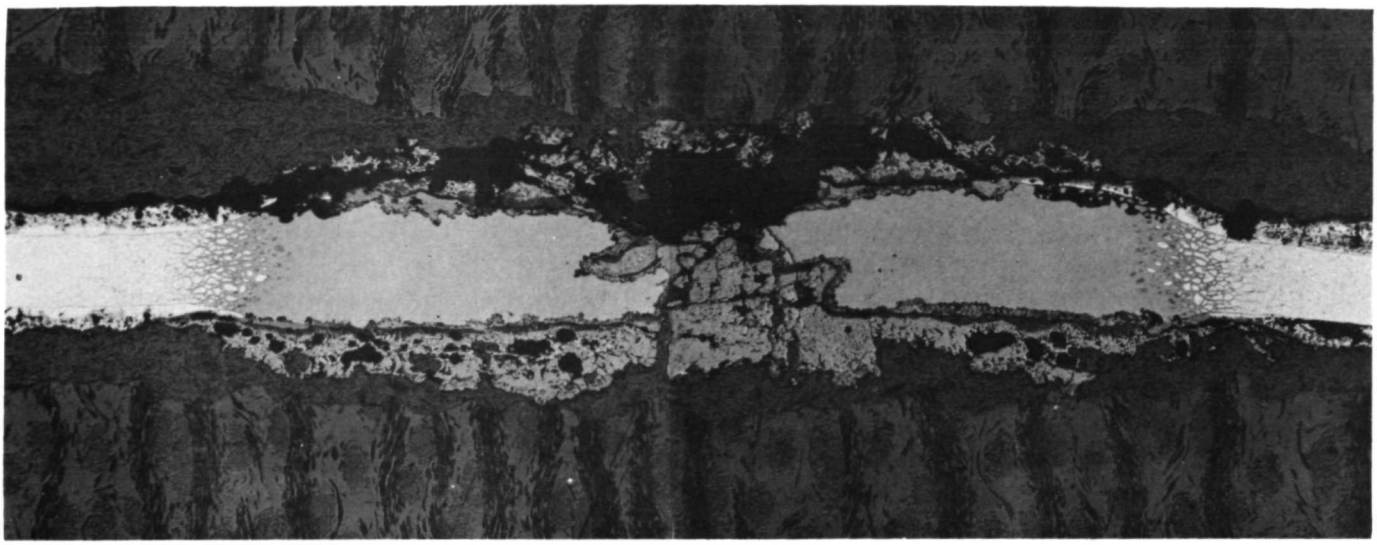

4T Hole Defect Specimen No. 671 6 LP-SC

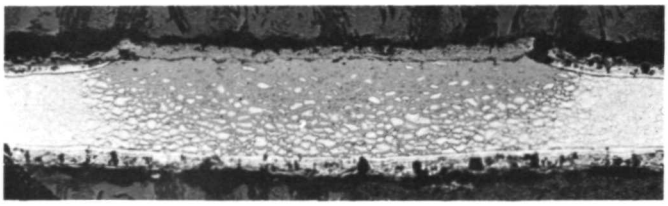

4T Spot Defect Specimen No. 661 6 LP-SC

Magnification: 35X

Etchant: $HF-HNO_3$-Lactic

FIGURE 61. 4T HOLE SPOT DEFECTED SPECIMEN, SA-13 + GN-19D COATING, AFTER LP-SC EXPOSURE AT 1700° K AND 13 N/m^2

Coated Columbium and Tantalum Alloys" was not available when this report went to print. That report will be issued by NASA-Lewis at a later date.

3.3.2 Atmospheric Re-Entry Simulation

An existing re-entry simulator was modified to permit simultaneous variation of temperature, pressure and stress level on a scaled miniature heat shield panel (MHS). Rib stiffened heat shield panels (Fig. 65) were fabricated from 90Ta-10W alloy using the continuous seam diffusion bonding technique. Coating methods were developed to permit reliable MHS panel protection.

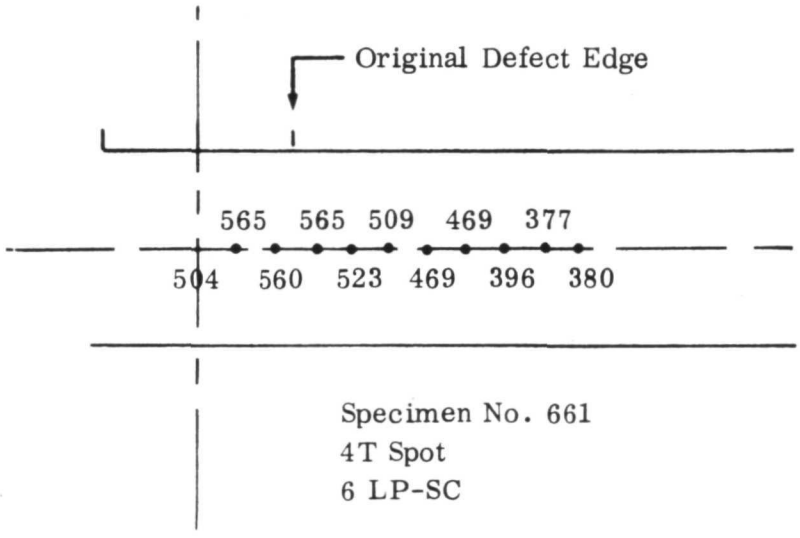

FIGURE 62. DIAGRAM OF MICROHARDNESS MEASUREMENTS FROM AN INTENTIONALLY DEFECTED SPECIMEN AFTER 1700°K - 13 N/m^2 LP-SC EXPOSURE

Equipment

Re-entry simulation for the coated miniature heat shield panels consisted of simultaneously exposing the specimens to a controlled temperature, air pressure and stress as a function of time. Tests were performed in one of Solar's re-entry simulators especially modified to accept the 1- x 4-inch MHS panels. Figure 66 shows an overall view of the test rig, and Figures 67 and 68 provide detailed views of the heating system and the stressing mechanism.

The simulated re-entry test profiles (pressure, stress and temperature vs time) are shown in Figure 69. These profiles were prepared from information furnished by the NASA Program Manager for use in this program. The temperatures, however, have been changed to reflect the higher temperature capability of the tantalum alloy over the previously tested columbium alloys.

The temperature profile was achieved by means of a preshaped temperature-time program cam operating on an electronic temperature controller and silicon-controlled rectifiers. The test panel was heated with twelve 1200-watt clear quartz tubular lamps enclosed in a water-cooled, 4-inch diameter, gold-plated reflector assembly. A thermocouple adjacent to the surface of the test panel furnished the feedback signal to the temperature control system.

The pressure was controlled in the chamber by means of an automatic pressure controller operating in conjunction with a gauge controller and servo controlled leak valve. This servo controlled leak valve was actuated by the pressure controller which

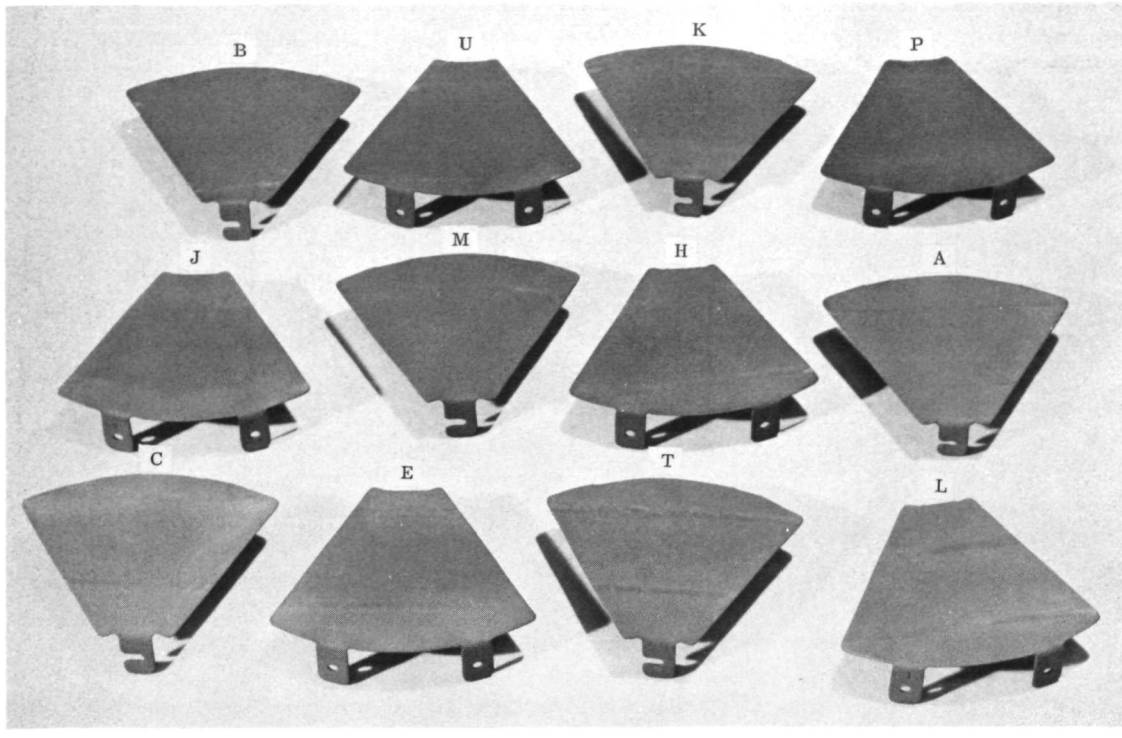

FIGURE 63. METALLIC TEST SAMPLES

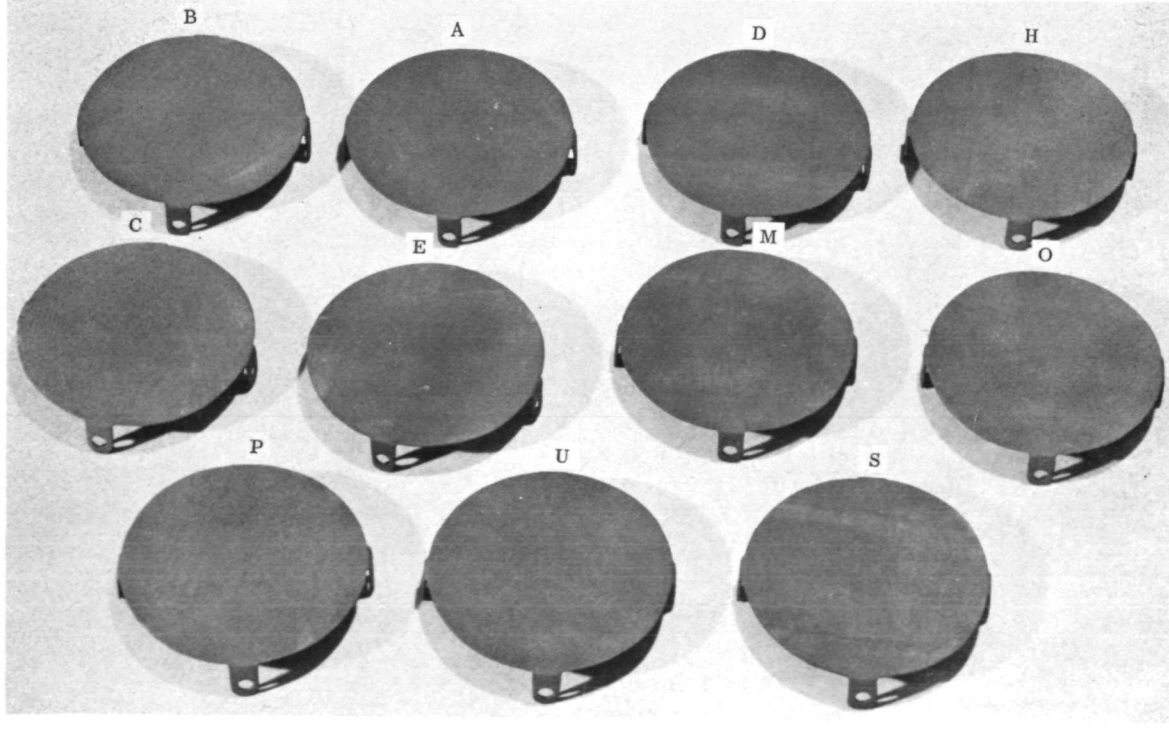

FIGURE 64. SINGLE PIECE STAGNATION MODEL SAMPLES

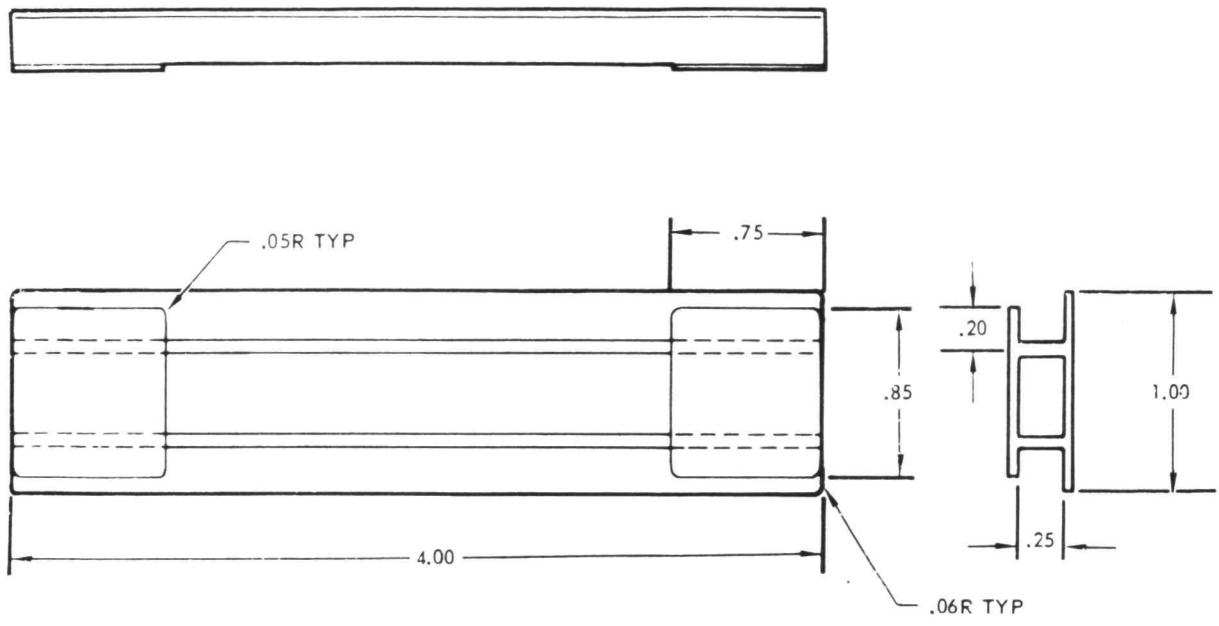

FIGURE 65. RIB STIFFENED HEAT SHIELD PANEL

FIGURE 66. RE-ENTRY SIMULATOR

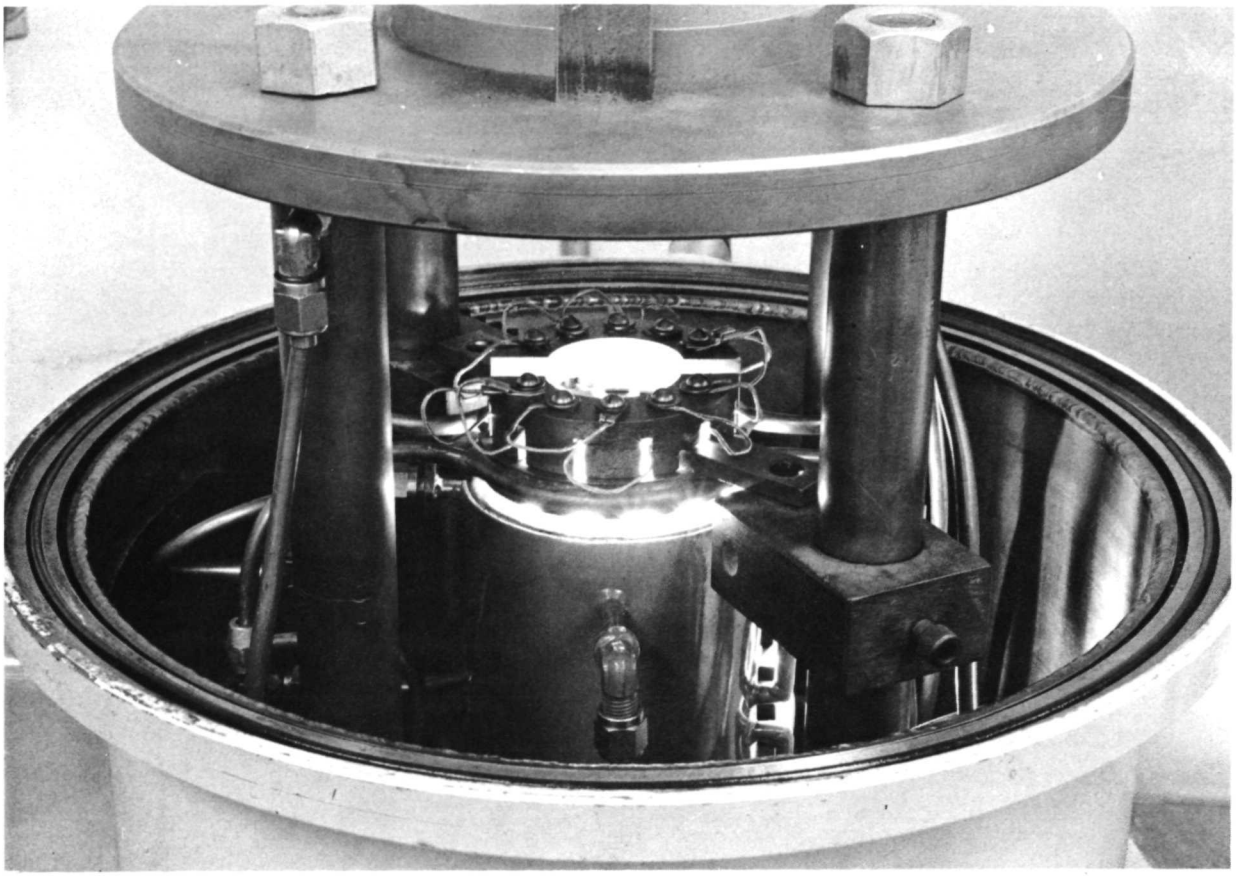

FIGURE 67. RE-ENTRY SIMULATOR CHAMBER, LOADING MECHANISM REMOVED

in turn was programmed by a preshaped pressure (vacuum)-time program on a Data Trak Programmer. A 15 cfm mechanical vacuum pump was used to evacuate the test chamber and could achieve a minimum pressure of about 0.7 N/m^2.

The programmed load applied during testing was obtained from a pneumatic linear actuator located in the lower compartment of the re-entry simulator. Loads to the four-point bending fixture were measured by means of a load cell mounted in series with the loading mechanism. The load cell furnished the feedback signal to the load control system. Any difference between the specimen load and the programmed load was automatically corrected in the control system by regulating the amount of air to the actuator with an electric-to-pneumatic converter.

The MHS panel was stressed using a four-point bending fixture. This method of loading placed the heat shield specimens in bending which is typical of flight behavior. The fixture straps and rods were fabricated from 90Ta-10W alloy and were protected with either the Solar NS-4 coating or the SA-13 silicide developed during this program. Figure 70 shows an assembled fixture and panel.

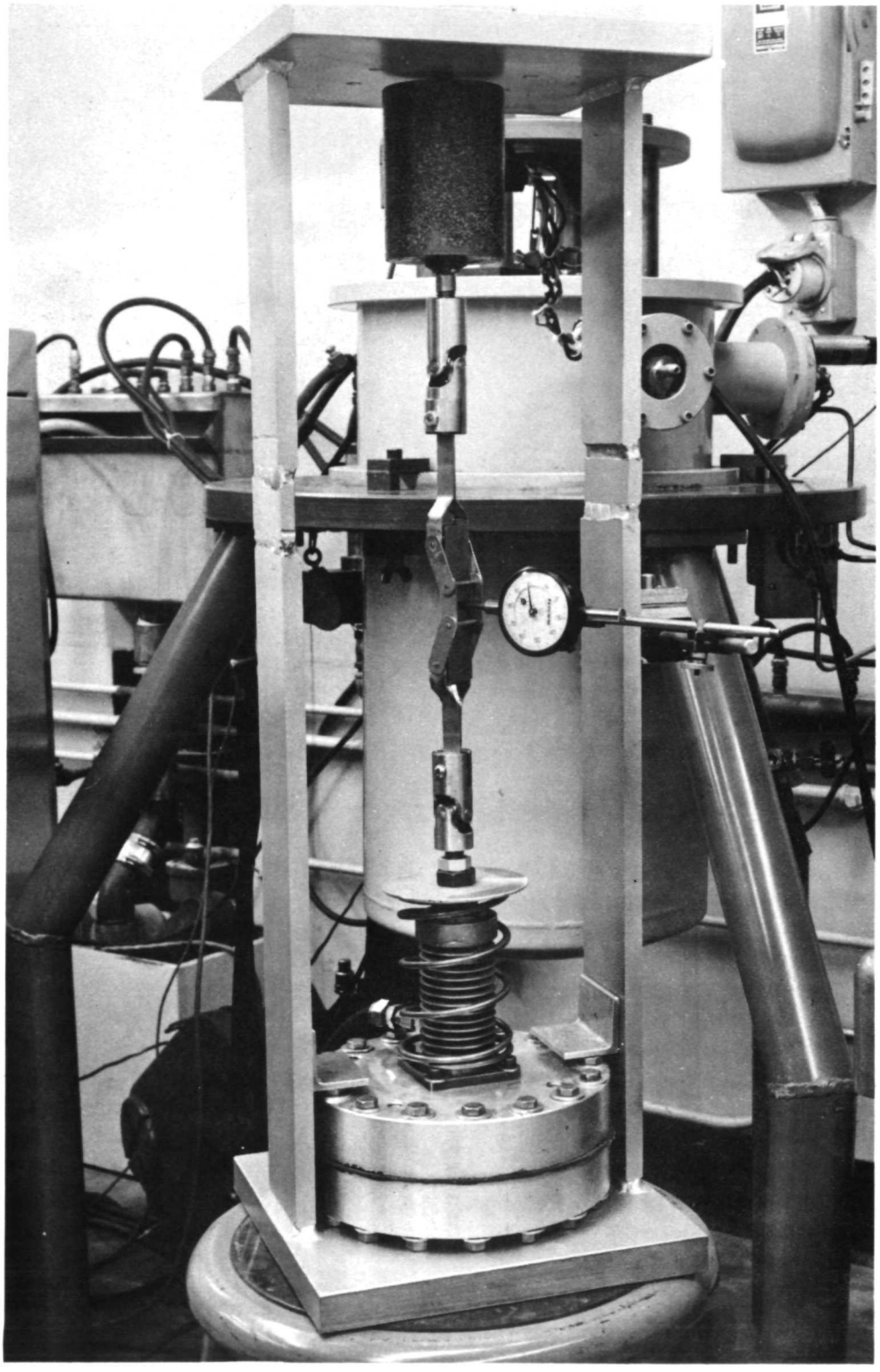

FIGURE 68. RE-ENTRY SIMULATOR LOADING MECHANISM

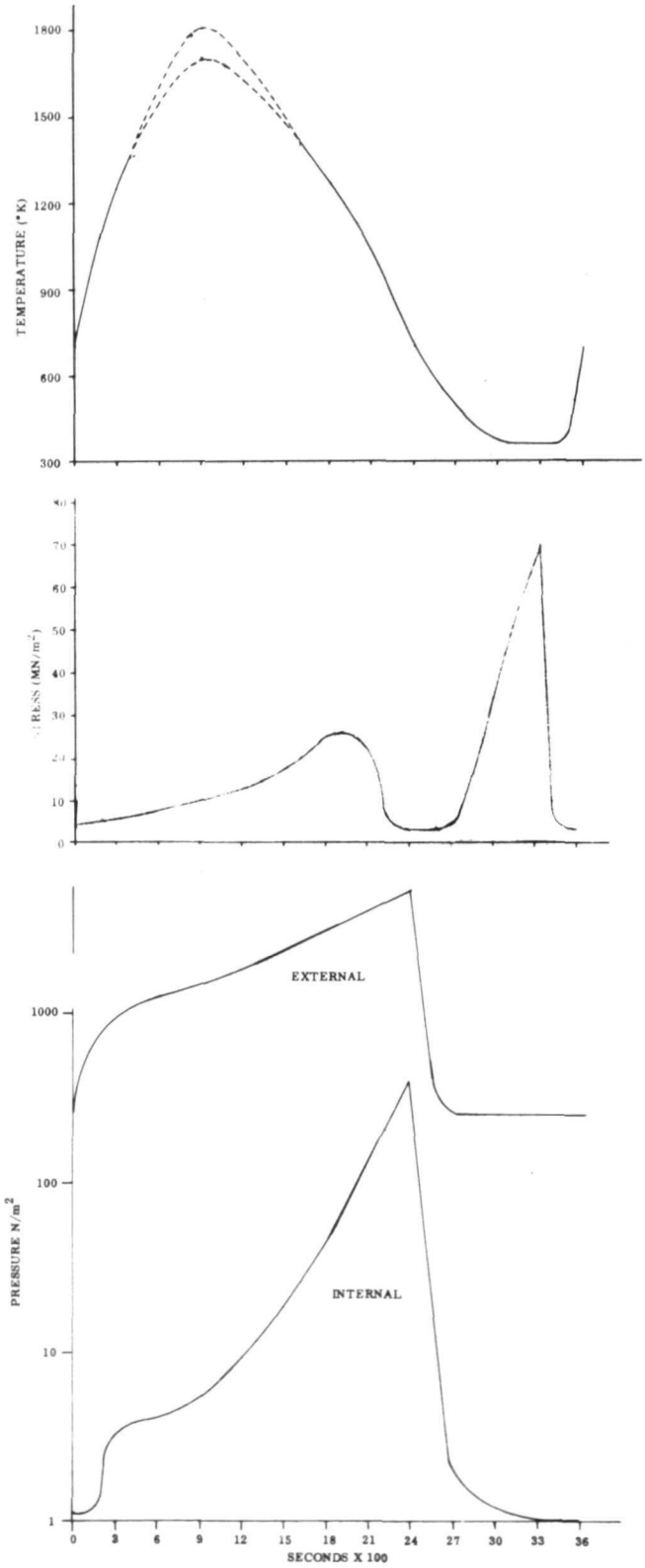

FIGURE 69. PRESSURE, STRESS AND TEMPERATURE VS TIME PROFILES FOR RE-ENTRY SIMULATOR

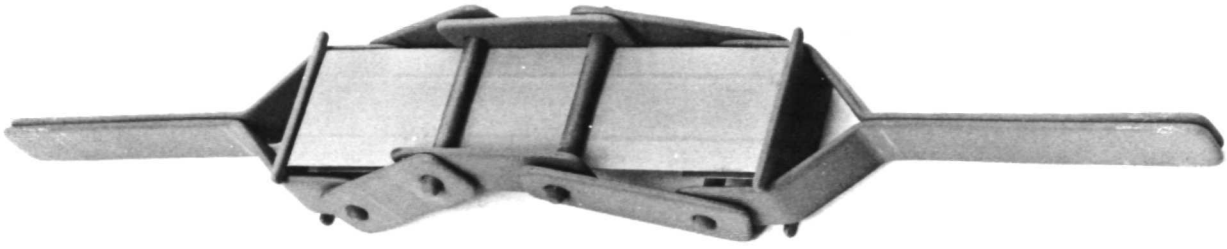

FIGURE 70. MHS PANEL IN FOUR-POINT LOADING FIXTURE

To determine the efficiency of the MHS panel loading system (losses due to fraction at the load points, etc.), a correlation was made between the actual bending stress in the outer fibers of the MHS panel and the applied load to the four-point bending fixture. This was accomplished by instrumenting a test panel with a strain gage and then straining the panel at room temperature. From the load-strain data it was possible to determine the room temperature proportional limit on the MHS panel. For the ascent load condition in this program, the panel was stressed to 77 percent of the room temperature proportional limit on the outer fibers of the panel.

Miniature Heat Shield Panel Fabrication

It was originally proposed that yield strength diffusion bonding be used to join all parts of the MHS panels. Initial experimental work indicated that this joining method was unsuitable. The continuous seam diffusion bonding process (CSDB) was tried and found to be both applicable and satisfactory. It proved beneficial to include a 25×10^{-6} meter thick pure tantalum foil in all joints to improve bonding characteristics. Inclusion of the tantalum foil complicated panel production by requiring that the excess foil be trimmed from each joint.

Tooling was modified to permit simultaneous bonding (CSDB) of five MHS panels per bonding run. Face sheets were bonded to both panel ribs during the first bonding pass. Inversion of the parts and insertion of locating spacers then permitted bonding of the tabs to the ribs. Panels were made slightly longer than required and were subsequently trimmed to the correct overall length.

Ribs were fabricated from 0.013-inch rather than 0.020-inch thick 90Ta-10W alloy for this program. A completed panel is shown in Figure 71, and the typical CSDB joint appearance is shown in Figure 72. The darker, central area is the tantalum interleaf used as an aid in bonding. No evidence for unbonded areas or "dirty" interfaces was indicated by the metallography.

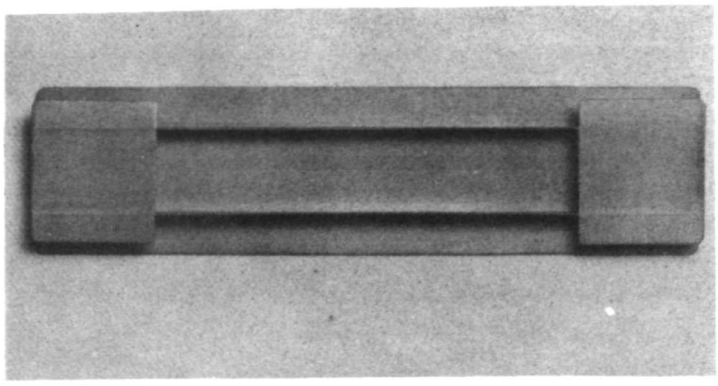

FIGURE 71. TYPICAL MHS PANEL APPEARANCE

MHS Panel Joint

Etchant: Unetched

Magnification: 1000X (oil)

Pure Tantalum Foil

FIGURE 72. MICROSTRUCTURE OF CSDB JOINT IN MHS PANEL

MHS Panel Coating

Dip coating experiments were initiated with the normal spraying slurry (0.5 kg powders, 0.4 ℓ vehicle, 3600 seconds ball milling) and standard bend test coupons. Withdrawal rates from 4×10^{-4} to 3×10^{-3} meter/sec were tried with completely unsatisfactory results. Only about 0.040 kg/m^2 of unevenly distributed coating could be deposited using this slurry. The desired slurry deposit was 0.300 to 0.340 kg/m^2.

A second slurry was prepared from 0.5 kg powders plus 0.24 ℓ of vehicle and was ball milled for 16 hours. The new slurry had an average particle size of 4.0×10^{-6} meter as compared with 5.5×10^{-6} meter for the 3600 second ball-milled slurry. Dip coating results were again very poor with deposits ranging from 0.144 to 0.560 kg/m^2.

for withdrawal rates of 4×10^{-4} to 3×10^{-3} meter/sec, respectively. Little edge coverage was obtained and severe coating sag occurred.

A thixotropic agent (MPA-60) supplied by Baker Castor Oil Company was obtained and incorporated into the SA-13 slurry to aid in particle suspension, viscosity stabilization and flow characteristics. Table LVII summarizes data for a number of slurries which were prepared and tested. Slurry 1 deposited a maximum of about 0.100 kg/m^2 of material and was discarded. Slurry 2 offered good end-to-end deposit uniformity but produced 0.400 to 0.440 kg/m^2 deposits for 8×10^{-4} to 2×10^{-3} meter/sec withdrawal rates. Compositions 3, 4, 5 and 6 were efforts to slightly decrease the deposition obtained from slurry 2. The combination designated number 6 was selected as the best system and was used to dip coat all MHS panels used during the program. A withdrawal rate of 1.25×10^{-3} meter/sec was found to produce a deposit of 0.290 ± 0.030 kg/m^2 and excellent end-to-end bisque uniformity. Edges and corners were found to be thinly coated and were supplemented by hand brushing. Panels experienced the normal SA-13 firing cycle but were supported on BN coated Al_2O_3 discs instead of rods.

TABLE LVII

SLURRY COMPOSITIONS

Designation	SA-13 Powders (kg)	Vehicle (ℓ)	MPA-60 (kg)	Ball-milling Time (hours)
1	0.5	0.40	0.032	1
2	0.5	0.24	0.020	16
3	0.5	0.27	0.022	18
4	0.5	0.25	0.020	17
5	0.5	0.27	0.021	1
6	0.5	0.23	0.018	1

Application of the 0.050 kg/m^2 vitreous overlay to all MHS panels was by spraying. Firing was as previously described: 1800 seconds at 1700° K and atmospheric pressure. Table LVIII contains coating weights for all MHS panels coated during the program.

Re-Entry Exposure

Miniature heat shield panels were exposed to both internal and external pressure conditions while being stressed and cycled to a maximum of 1700° K. One panel was

TABLE LVIII

MHS PANEL COATING AND FIRING DATA

Panel	Applied SA-13 (kg/m^2)	Fired SA-13 (kg/m^2)	Applied GN19D (kg/m^2)	Fired GN19D (kg/m^2)
A	0.388	0.295	NA	
B	0.403	0.330	NA	
C	0.354	0.290	NA	
D	0.390	0.280	NA	
E	0.420	0.340	NA	
F	0.397	0.330	NA	
G	0.398	0.330	NA	
H	0.396	0.330	NA	
I	0.380	0.300	0.120	0.135
J	0.355	0.280	0.085	0.101
K	0.390	0.320	0.068	0.083
L	0.407	0.330	0.070	0.081
M	0.438	0.360	0.057	0.070
N	0.355	0.280	NA	
O	0.321	0.250	NA	
P	0.329	0.260	NA	
Q	0.312	0.240	0.068	0.079
R	0.320	0.250	0.069	0.072
S	0.325	0.250	0.063	0.077
T	0.302	0.230	0.064	0.081
U	0.325	0.250	0.052	0.072
V	0.303	0.230	0.061	0.077
W	0.282	0.220	0.065	0.082
X	0.307	0.230	0.062	0.080
Y	0.308	0.230	0.052	0.070

NA = Not Applied

also exposed to the external pressure condition after being intentionally damaged with an 0.0063 meter diameter spot defect.

Re-entry exposure of the SA-13 coated panel "B" was performed using the 1700° K - external pressure conditions. Testing continued until structural failure occurred after 1800 seconds of the fifteenth cycle. Sixteen pressure-temperature profiles were completed before the panel was removed from the test facility.

Figure 73 shows the appearance of Panel "B" before, during and after the re-entry exposure. A typical range of brown tones was exhibited by the tested specimen with the facesheet being generally darker than the "inside" surfaces of the panel. No evidence for coating failure was visible except at the fracture site. Failure appears to have been initiated at the "inside" edge of one rib and to have progressed by oxidizing away a small wedge shaped section of that rib. It is probable that the rate of oxidation of the rib was enhanced by the application of stress during testing.

Verification of the mode of failure for Panel "B" was desired and a second panel (D) was, therefore, exposed at 1700° K and external pressure conditions. A

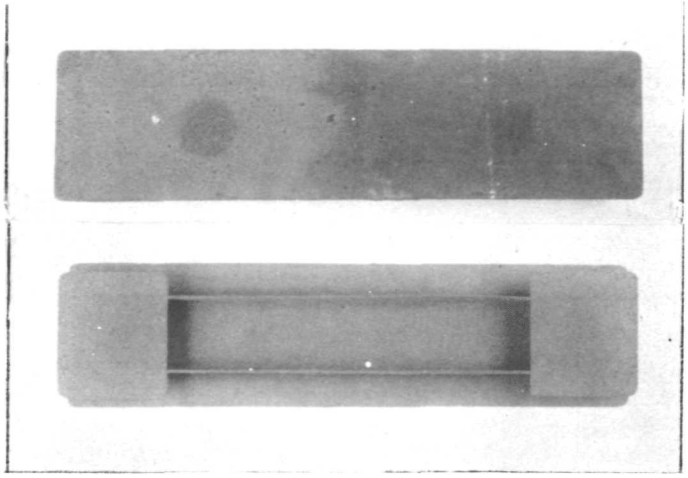

Pre-oxidized

Magnified: 0.75X

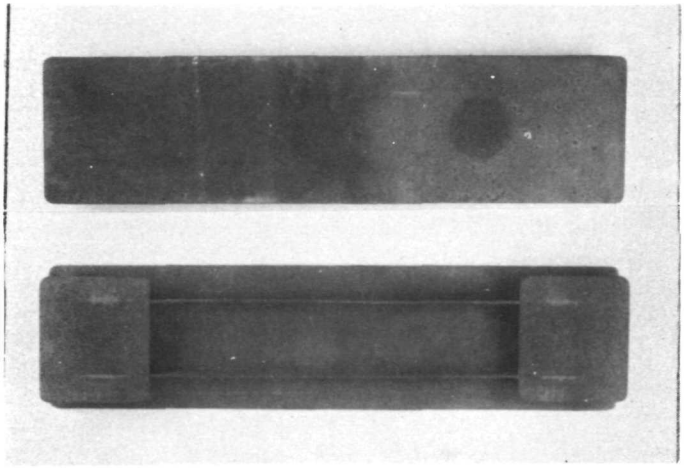

5 Re-entry cycles

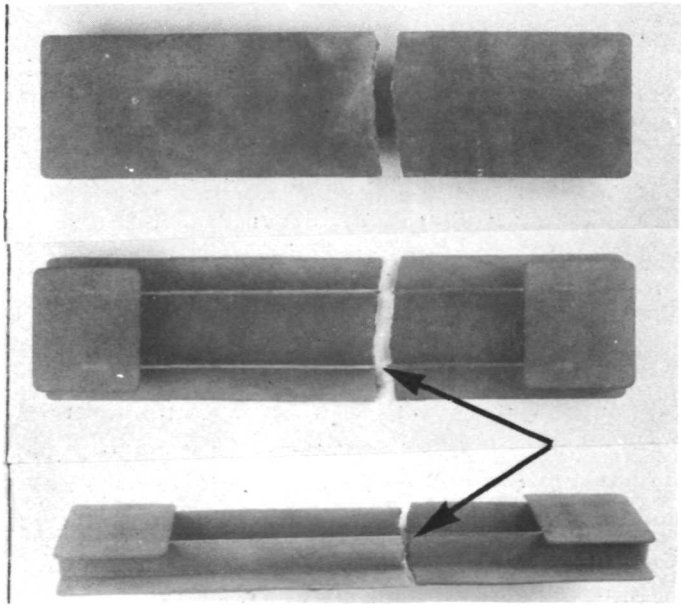

16 Re-entry cycles

FIGURE 73. SA-13 COATED MHS PANEL "B" APPEARANCE RECORD DURING 1700°K - EXTERNAL PRESSURE RE-ENTRY EXPOSURE

total of 48 simulated re-entry cycles were logged before Panel "D" was removed from test. In contrast to Panel "B", which fractured at 15 cycles, structural failure of Panel "D" did not occur. Testing was terminated because numerous facesheet and tab edge failures had occurred. Both ribs were free of edge and surface failures at the time exposure was halted. Figure 74 shows the macroscopic appearance of Panel "D" after various exposure levels. The pre-oxidized panel was golden-brown colored and had gained 0.022 kg/m^2 after the one-hour - 1700°K - atmospheric pressure proof cycle. Total weight gain measurements of 0.023 kg/m^2 and 0.030 kg/m^2 were obtained after 3 and 26 re-entry cycles, respectively. The first edge failure occurred sometime after 26 re-entry exposures and made subsequent weight measurements meaningless in terms of coating behavior. A typical golden-brown color was maintained throughout the test.

Panel "D" was exposed to the greatest number of test cycles of those panels coated with SA-13 and was also the only panel to exhibit significant permanent deformation without structural failure. Post-test measurements indicated a radius of curvature for the panel of 0.39 meter. The midpoint deflection (facesheet concave) averaged about 140 x 10^{-6} meter/re-entry cycle for the 48 test cycles performed.

Extensive metallographic work was performed on MHS panel "D" to determine the effects of simulated re-entry exposure on the SA-13 coating and underlying substrate. Figure 75 shows the general appearance and relative thickness of the tested SA-13 coating on different areas of MHS panel "D". Good, uniform edge, T-joint and surface coverage is indicated. The outer surface of the facesheet and the rib edges are seen to have been coated more heavily than other areas of the panel.

Figure 76 shows the coating appearance on top of and in the plane of a rib (A), on top of an across a rib (B) and on the facesheet just below a rib when sectioned parallel to the rib length (C). Part A of Figure 76 shows that placing the coating in tension during testing resulted in many oxidized coating cracks which paralleled the coating/substrate interface. These cracks appear more like compression than tension cracks. It is possible that accelerated oxidation occurred while cracks were held open (in tension) and that compressive cracking occurred during cooldown because the relatively large volume of oxide generated could not be accommodated. Such a mechanism could only occur if the compressive strength of the oxide were greater than the shear strength of the coating. Coated areas placed in compression (Fig. 76, Part C) during testing were noteworthy for smaller than normal cracks. Figure 77 shows the appearance of surface coating cracks when seen from the plane of the coating. This view was obtained by grinding into the surface of a slightly bent piece of a rib from MHS panel "D". The substrate, M_5Si_3, and outer zone of coating are shown. Cracks in the outer coating zone are seen to be wide and to contain oxides while cracks in the M_5Si_3 diffusion zone are quite narrow. The crack pattern in the coating appears unrelated to the grain structure of the substrate.

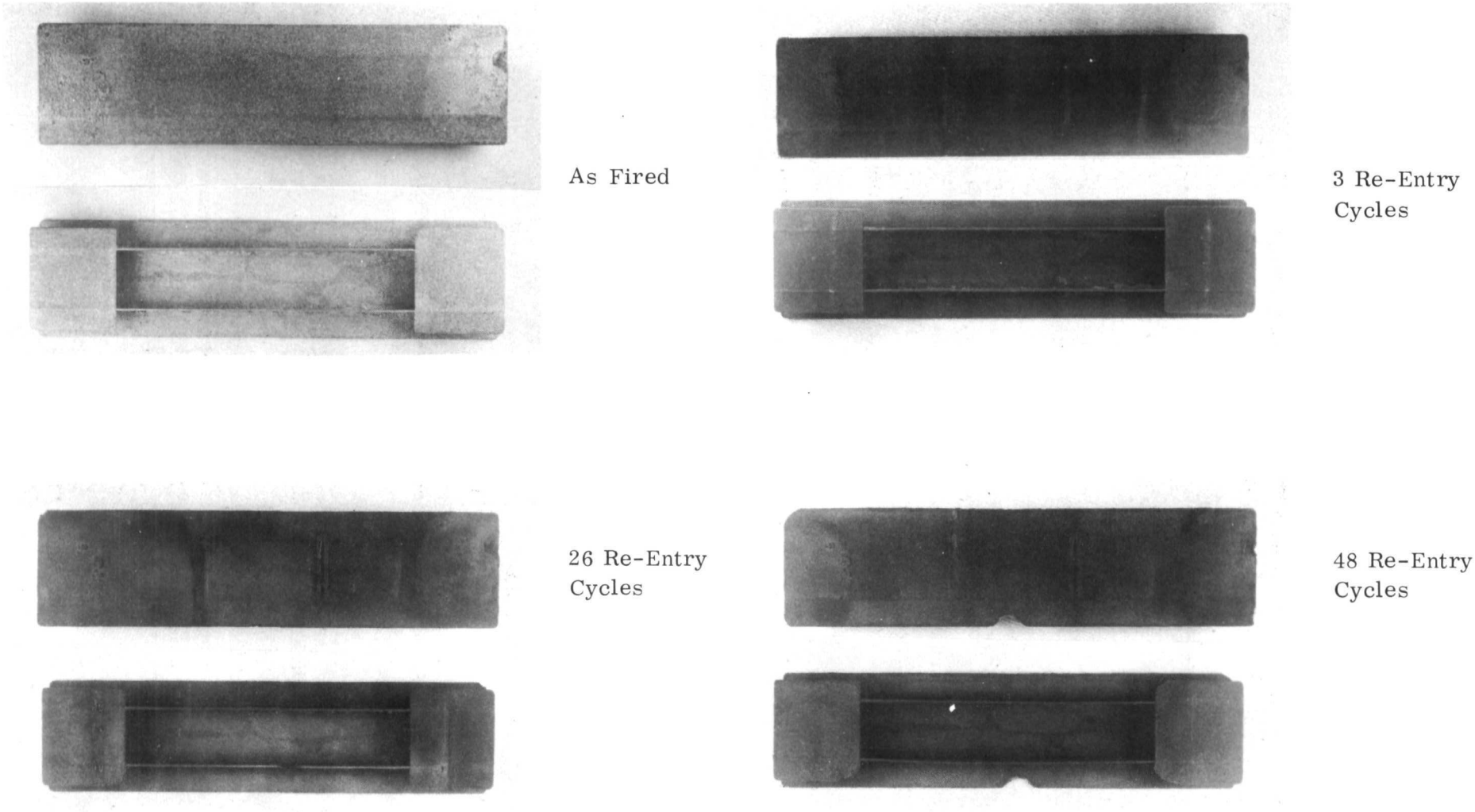

Magnification: 0.75X

FIGURE 74. SA-13 COATED MHS PANEL "D" APPEARANCE RECORD DURING 1700°K - EXTERNAL PRESSURE RE-ENTRY EXPOSURE

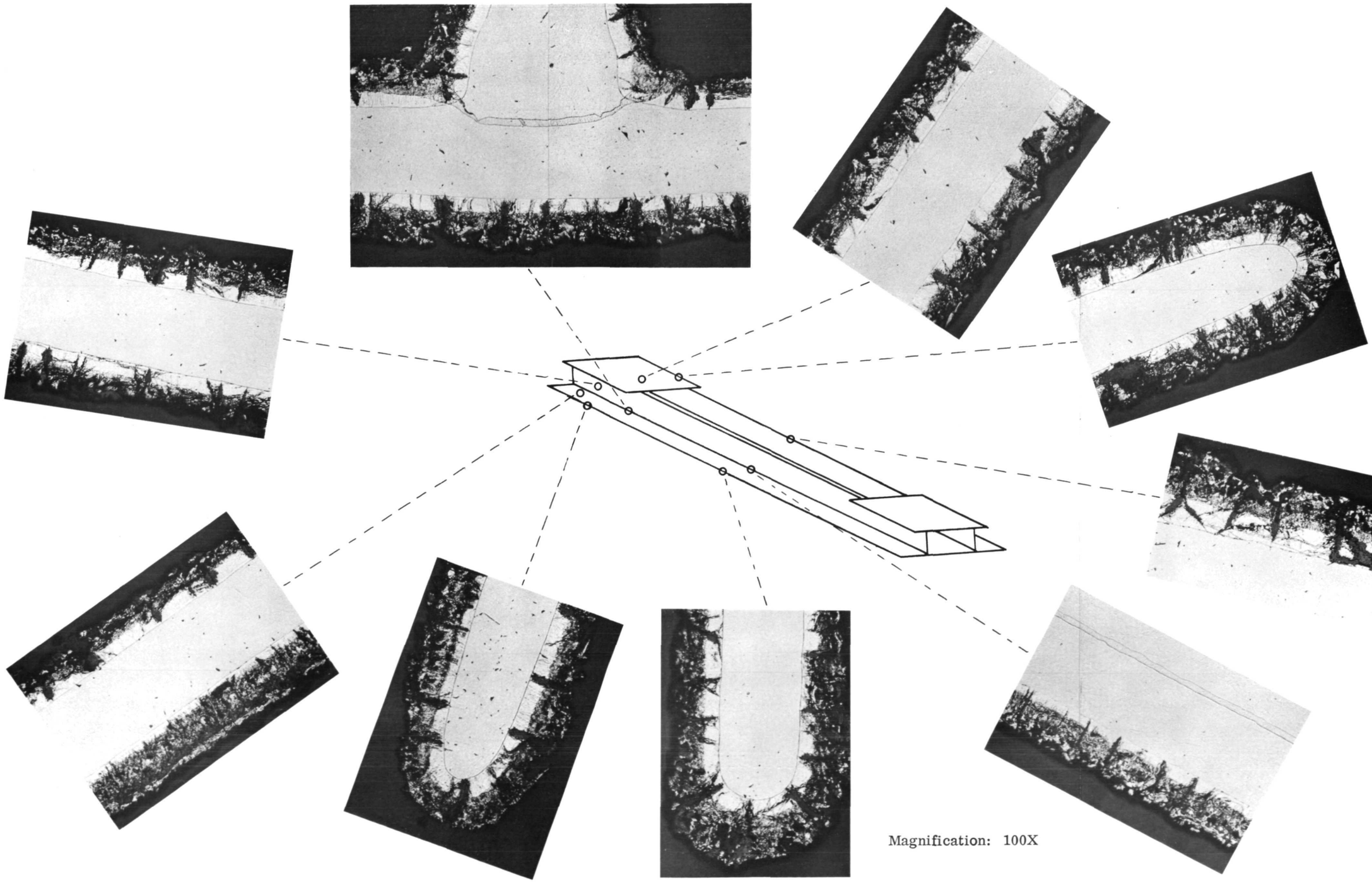

Magnification: 100X

FIGURE 75. COMPARISON OF COATING THICKNESS AND CONSUMPTION FOR VARIOUS LOCATIONS ON MHS PANEL "D" AFTER RE-ENTRY EXPOSURE

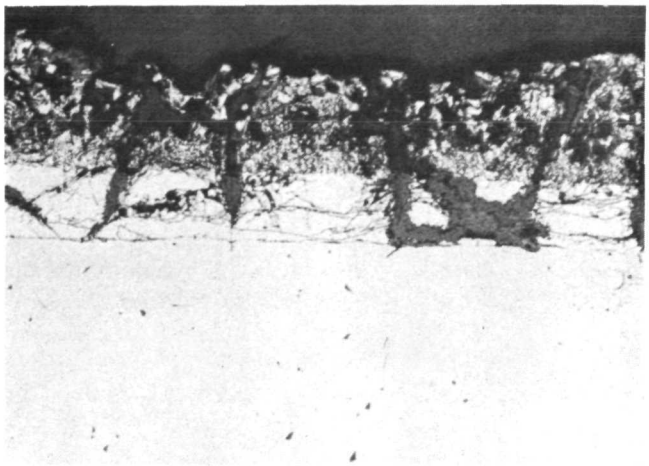

Part A

Coating on Top Edge of Rib, Sectioned in Plane of Rib

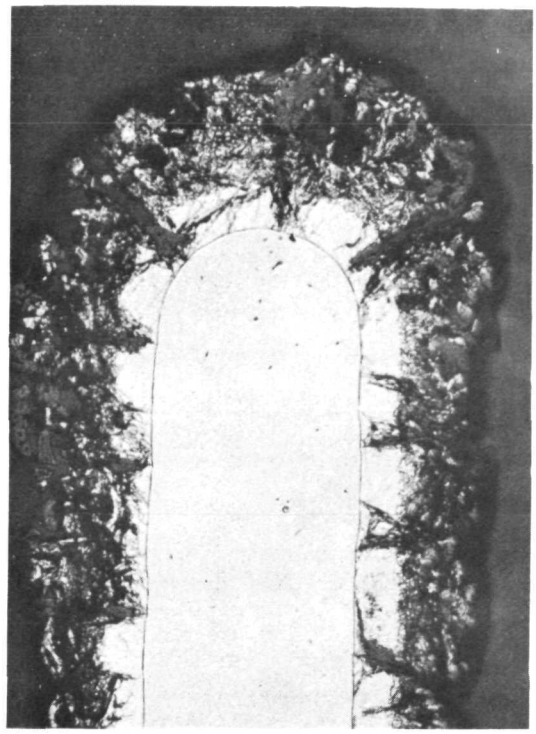

Part B

Coating on Top Edge of Rib, Sectioned Perpendicular to Plane of Rib

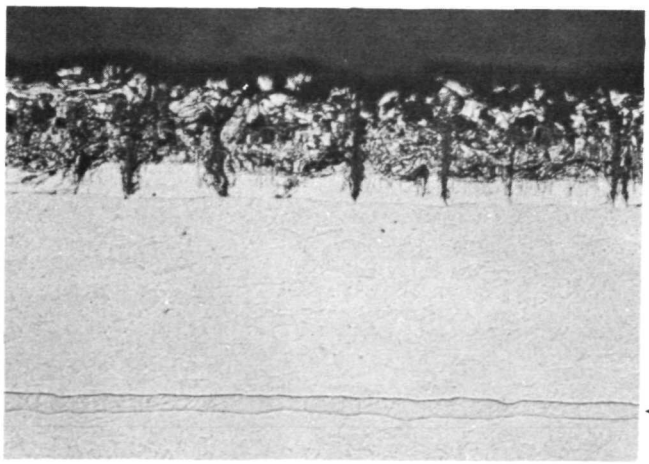

Facesheet to Rib Edge Diffusion Bond

Part C

Coating on Outside of Facesheet, Sectioned Parallel to Plane of Rib

Magnification: 125X

Etchant: HF-HNO_3-Lactic

FIGURE 76. EFFECTS OF STRESS ON SA-13 COATED MHS PANEL "D" AFTER 48 RE-ENTRY CYCLES - 1700°K AND EXTERNAL PRESSURE

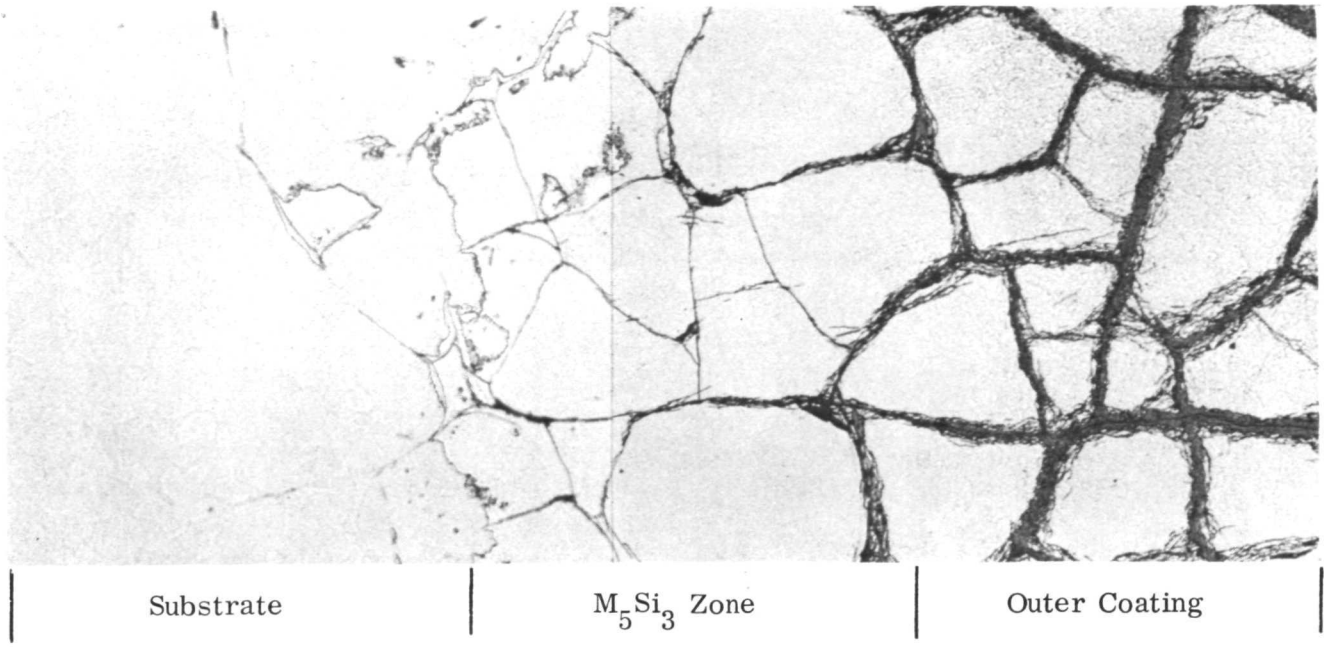

Magnification: 125X

Etchant: $HF-HNO_3$-Lactic

FIGURE 77. MICROSTRUCTURE OF SA-13 COATING SURFACE, PANEL "D", 48 RE-ENTRY CYCLES TO 1700°K AND EXTERNAL PRESSURE

A detailed view of the re-entry exposed coating is shown in Figure 78 together with substrate centerline hardness measurements. Coating consumption was possibly greater near the center of the panel than at the ends. The range of hardness values includes six individual data points spaced across the width of the facesheet. No obviously oxidized areas were present on either specimen in Figure 78. The wide range of hardness values measured at the midpoint of the panel presumably reflects the possibly greater coating consumption observed in this area and the effects of stress.

An SA-13 coated MHS panel ("C") was intentionally defected by grit blasting an 0.0063 meter diameter area of coating from the outer surface of the facesheet. This panel was subsequently exposed to the 1700°K - external pressure re-entry conditions until structural failure occurred during the 32nd minute of the 17th test cycle. Figure 79 traces the appearance of this panel from beginning to end of the re-entry testing. A typical milk-chocolate brown color was displayed by all surfaces except the facesheet which showed some dark brown regions.

Structural failure appears to have occurred after the intentionally introduced defect had spread beyond the rib/face sheet joint. Oxidation of the ribs occurred to a considerable depth before panel fracture occurred. A small section of facesheet did not break when the panel ribs failed. Two corners of one tab experienced coating

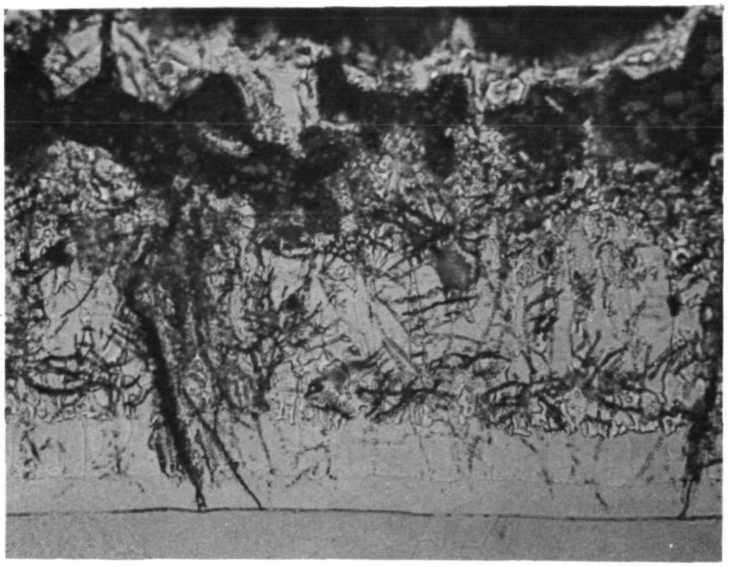

Outer Surface, Facesheet, 0.0064 Meter From End of Panel

Substrate ℄ Hardness:

286-323 KHN (100 g load)

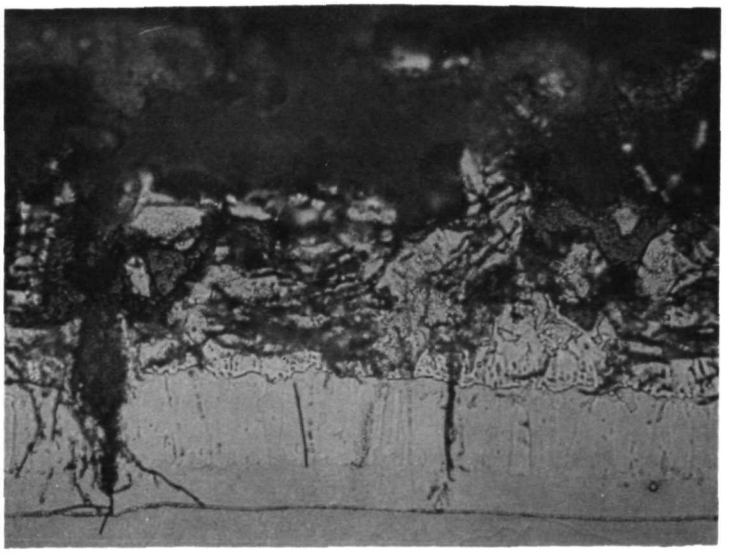

Outer Surface, Facesheet, Center of Panel

Substrate ℄ Hardness:

273-445 KHN (100 g load)

Magnification: 500X

Etchant: HF-HNO_3-Lactic

FIGURE 78. SA-13 MICROSTRUCTURE MHS PANEL "D", AFTER 48 RE-ENTRY CYCLES TO 1700°K AND EXTERNAL PRESSURE

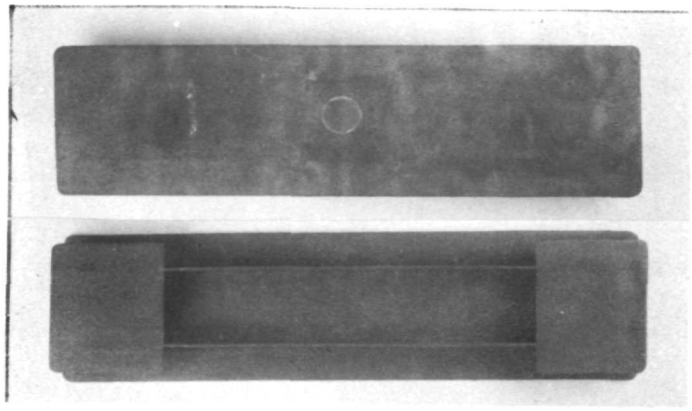

Pre-oxidized

Magnified: 0.75X

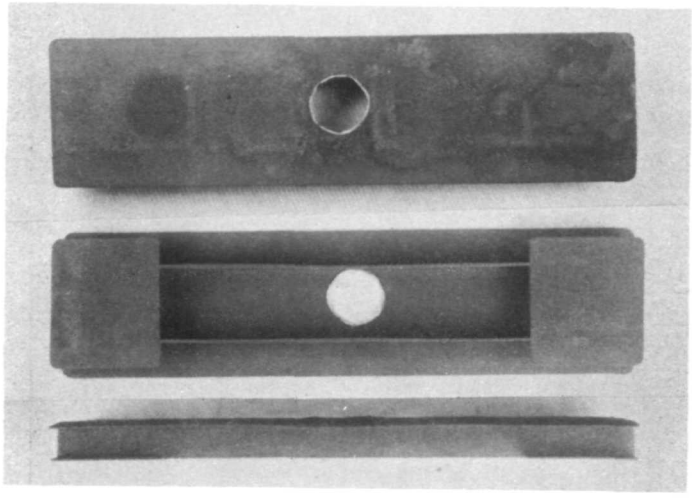

8 Re-entry cycles

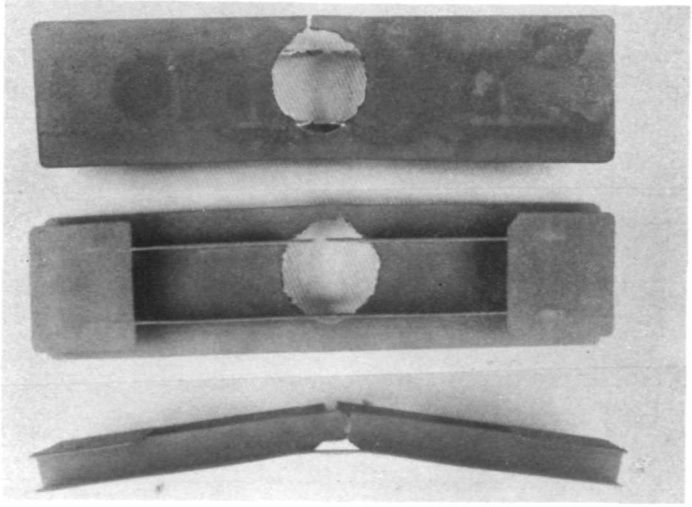

17 Re-entry cycles

FIGURE 79. INTENTIONALLY DEFECTED SA-13 COATED MHS PANEL "C" APPEARANCE RECORD DURING 1700° K - EXTERNAL PRESSURE RE-ENTRY EXPOSURE

failure and substrate recession between the 8th and 17th test cycles. No other coating failure sites were visually evident.

Re-entry exposure to the 1700° K - internal pressure profile was performed using MHS panel "E". A total of 42 re-entry cycles were completed before the panel was removed from test. Structural failure of this panel did not occur; however multiple edge failures were present and would certainly cause rapid structural failure if the outer panel surface had been exposed to the high mass flow, external pressure conditions experienced during re-entry. Figure 80 shows the general appearance of MHS panel "E" in the as-fired condition and after 3, 21 and 42 re-entry cycles. The pre-oxidized panel showed a mixture of green and brown tones and gained 0.011 kg/m^2 during the 1-hour - 1700° K proof cycle. Exposure to the 1700° K internal pressure test conditions promoted an immediate color change to charcoal black. Figure 81 traces the weight change behavior for the panel during test and includes an estimate of the coating changes based on the estimated volume of substrate consumed by oxidation. The general trend for the coating parallels that were observed for 1700° K - 13 N/m^2 exposure: an initial weight loss followed by a slow gain.

The diameter of a circular defect was estimated to increase at a rate of about 3×10^{-4} meter/re-entry cycle. This rate of growth was determined from measurements of failure site size as a function of exposure time.

As previously noted, MHS panel "E" did not bend during the 42-cycle - 1700° K - internal pressure exposure. No obvious differences between the coating on the tension and compression edges of a rib were observed. Overall panel coverage was similar to that depicted by Figure 75. Detailed views of the tested coating are shown in Figure 82 together with substrate centerline hardness values. Again, greater coating consumption was indicated near the center of the panel than near the ends. This observation also correlates with the higher range of measured hardness values observed at the center of the panel. A failed area of coating and substrate (edge, center of panel) accounted for the single data point at 612 KHN. Without this point, the range was 290-449 KHN.

Panel "M", coated with the SA-13 silicide and overlaid with the GN-19D glass, was exposed for a total of 49 re-entry cycles to the 1700° K - external pressure conditions. A photographic record of panel response is shown in Figure 83. The mottled appearance which is evident on the panel facesheet from 19 cycles onward was caused by vaporized tungsten oxide from failed quartz heating lamps in the simulator. This panel was removed from test after a failure developed at a rib end/facesheet edge intersection. Internal and external surfaces developed a medium tan color during exposure.

Panel "M" was the only panel besides "D" to exhibit any permanent deformation after testing. Measurements indicated a radius of curvature for the panel of about 3.0

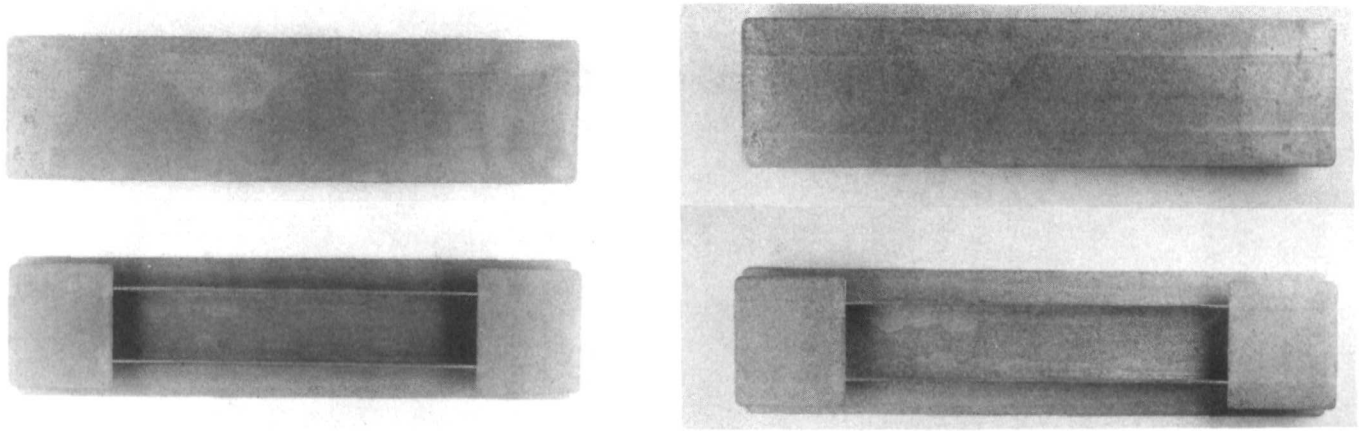

As Fired

3 Re-Entry Cycles

Magnification: 0.75X

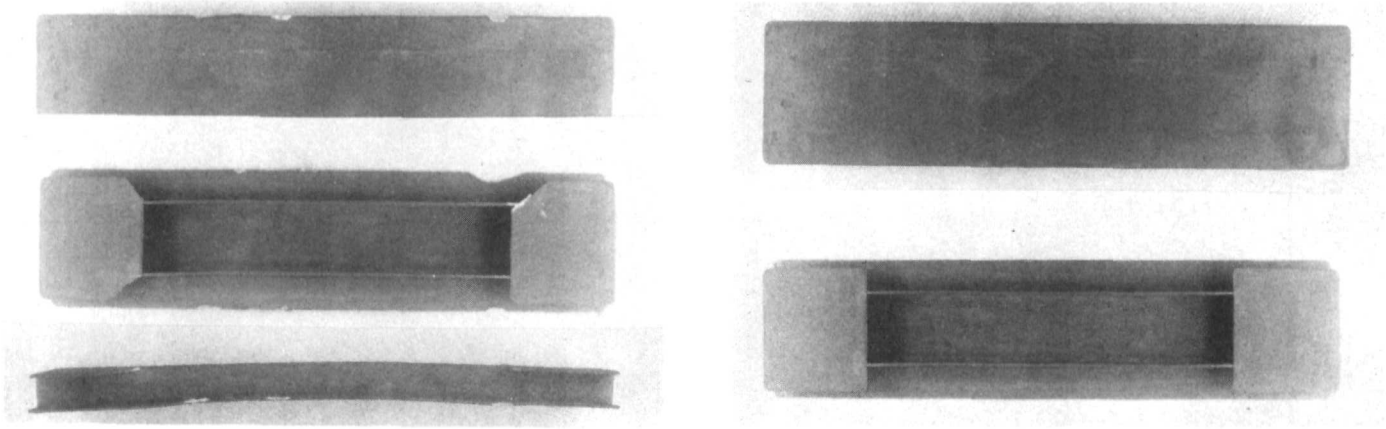

21 Re-Entry Cycles

42 Re-Entry Cycles

FIGURE 80. SA-13 COATED MHS PANEL "E" APPEARANCE RECORD DURING 1700°K - INTERNAL PRESSURE RE-ENTRY EXPOSURE

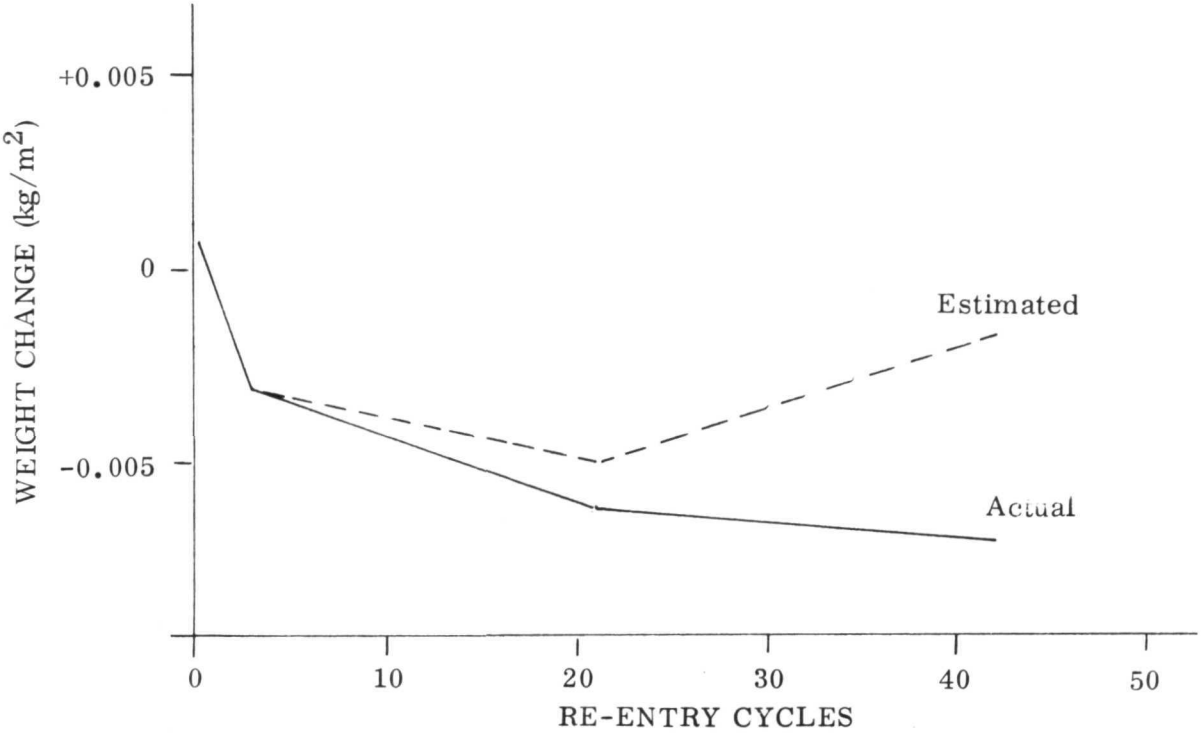

FIGURE 81. WEIGHT CHANGE DATA FOR MHS PANEL "E"
1700° K - INTERNAL PRESSURE RE-ENTRY EXPOSURE

meter. The total midpoint deflection (facesheet concave) was determined to be 4.4×10^{-4} meters.

Weight measurements on the panel indicated a gain of 0.018 kg/m^2 after 19 cycles and 0.040 kg/m^2 after 24 re-entries. These data may have been influenced by small quantities of tungsten oxide deposited on the panel each time a quartz heating lamp failed.

Microscopic examination revealed that some edges on panel "M" were more heavily coated than was intended (Fig. 84, Part A). Flat surfaces were found to be relatively uniformly coated. Figure 84, Parts B and C provide a coating thickness comparison between different areas on the facesheet. Greater substrate and coating consumption is shown for the central versus end regions of the panel. Substrate centerline hardness values, determined across the width of the facesheet and 0.0064 meter from the end, ranged from 279 to 341 KHN (100 g). Values of 264 to 314 were determined across the facesheet and at the panel center.

Another glass overlaid MHS panel, "K", was re-entry exposed for 58 cycles using the 1700° K - internal pressure re-entry profile. Figure 85 shows the appearance of this panel before and during testing. Lightly colored marks on the facesheet

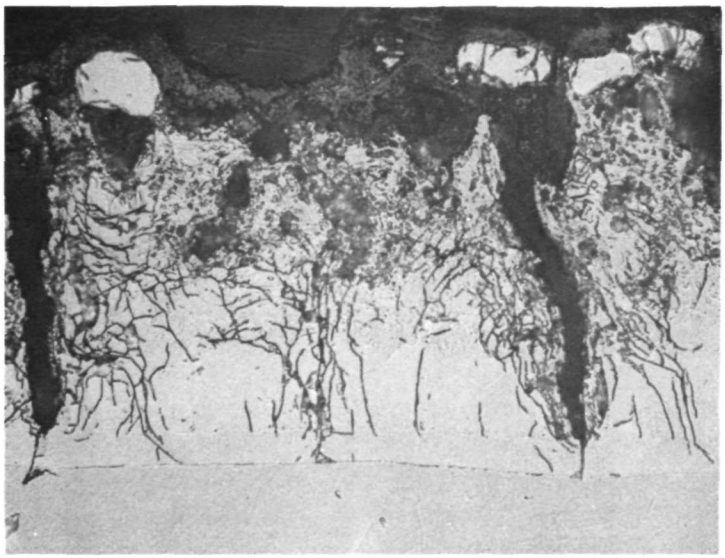

Outer Surface, Facesheet, 0.0064 Meter From Panel End

Substrate ℄ Hardness:

273-326 KHN (100 g load)

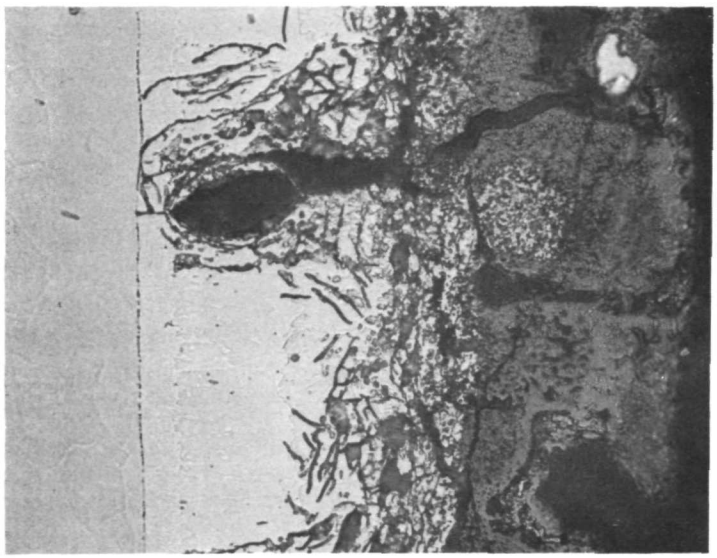

Outer Surface, Facesheet, Center of Panel

Substrate ℄ Hardness:

290-612 KHN (100 g load)

Magnification: 500X

Etchant: HF-HNO_3-Lactic

FIGURE 82. SA-13 MICROSTRUCTURE, MHS PANEL "E", AFTER 42 RE-ENTRY CYCLES TO 1700°K AND INTERNAL PRESSURE

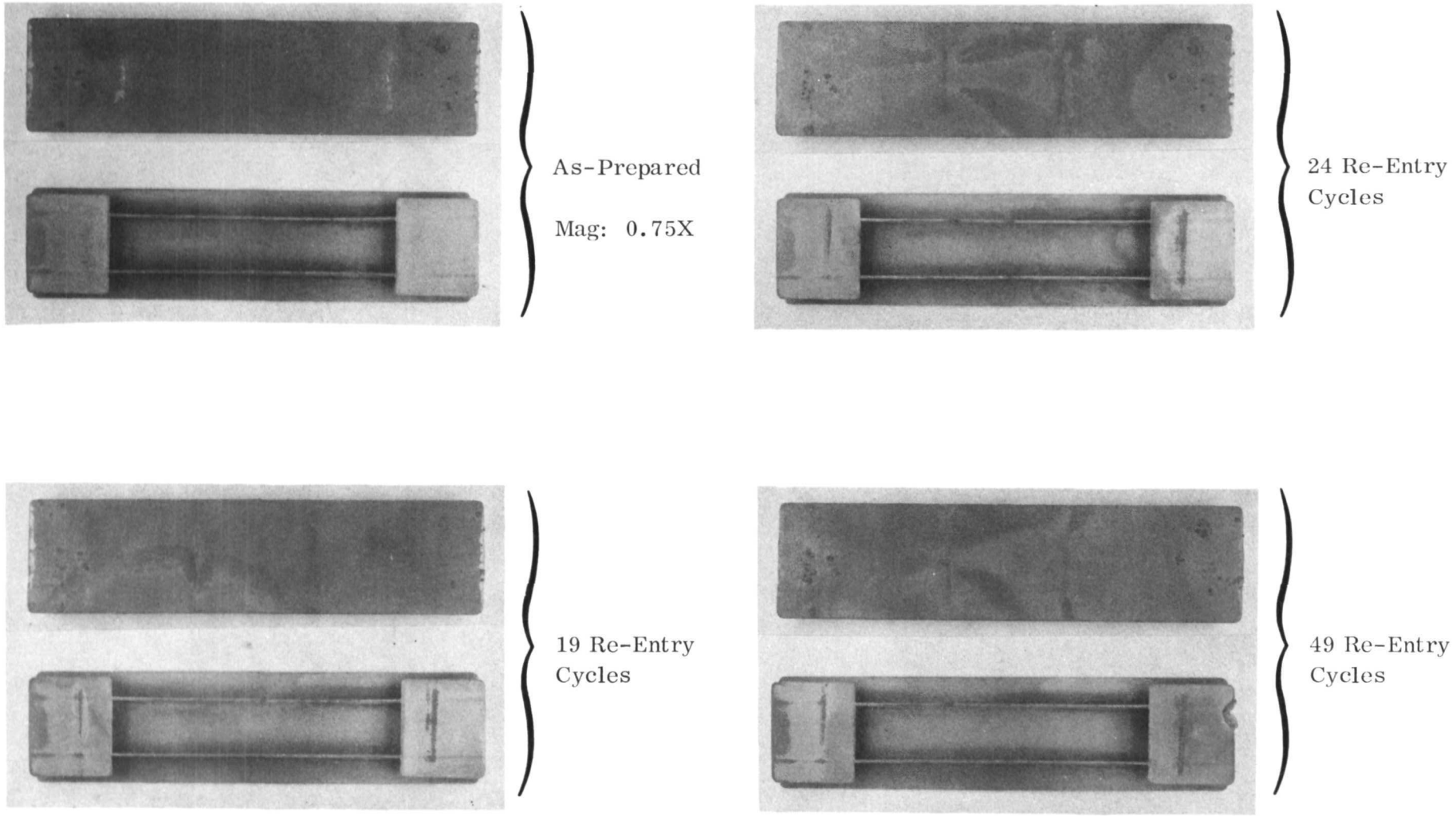

FIGURE 83. SA-13+GN19D COATED MHS PANEL "M" APPEARANCE RECORD DURING 1700° K-EXTERNAL PRESSURE RE-ENTRY EXPOSURE

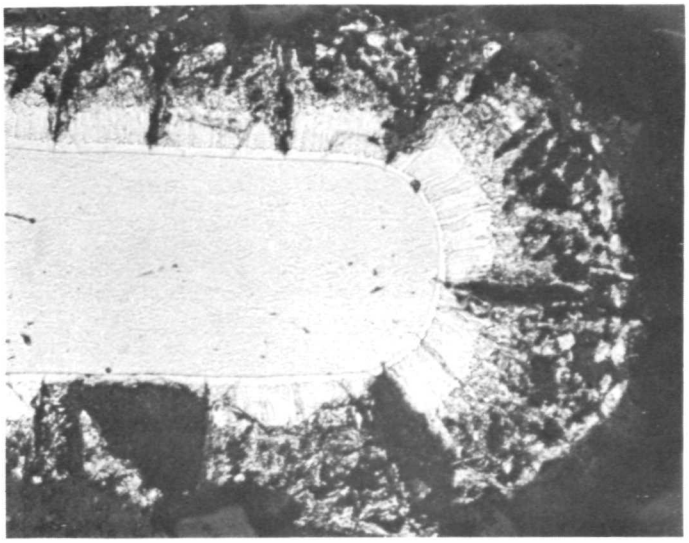

Part A

Rib Edge at Center of Panel

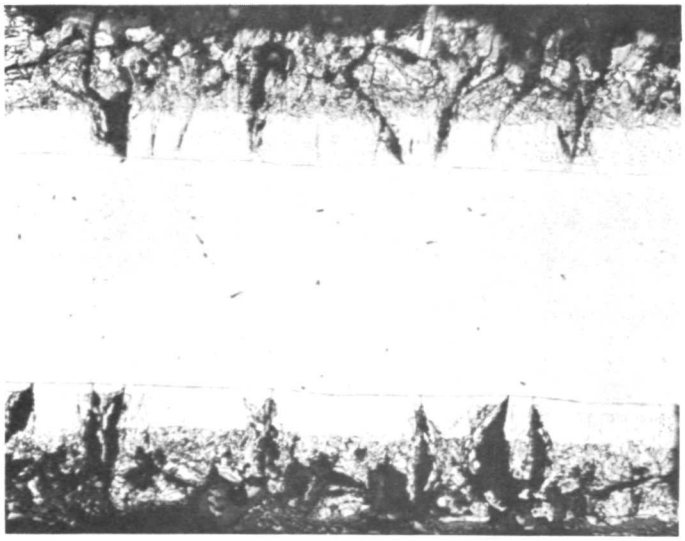

Part B

Facesheet at Center of Panel
Substrate ℄ Hardness: 264-314 KHN
(100 g load)

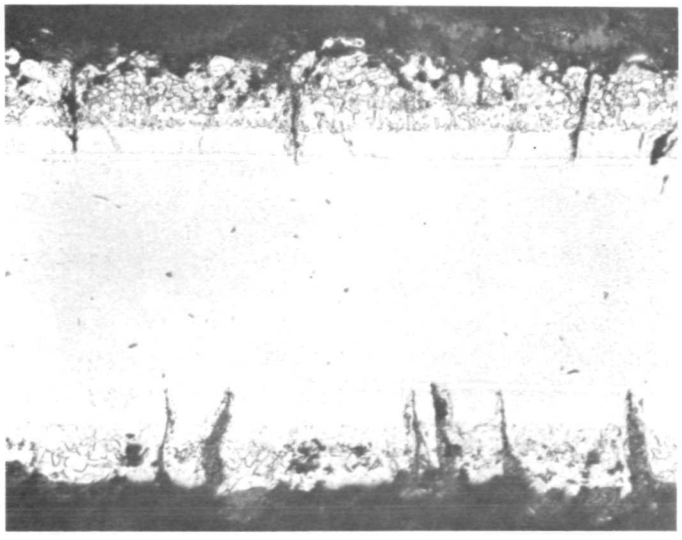

Part C

Facesheet, 0.0064 Meter From
End of Panel
Substrate ℄ Hardness: 279-341 KHN
(100 g load)

Etchant: HF-HNO_3-Lactic
Magnification: 125X

FIGURE 84. COMPARISON OF COATING THICKNESS AND SUBSTRATE CONSUMPTION FOR VARIOUS LOCATIONS ON MHS PANEL 'M" AFTER RE-ENTRY EXPOSURE

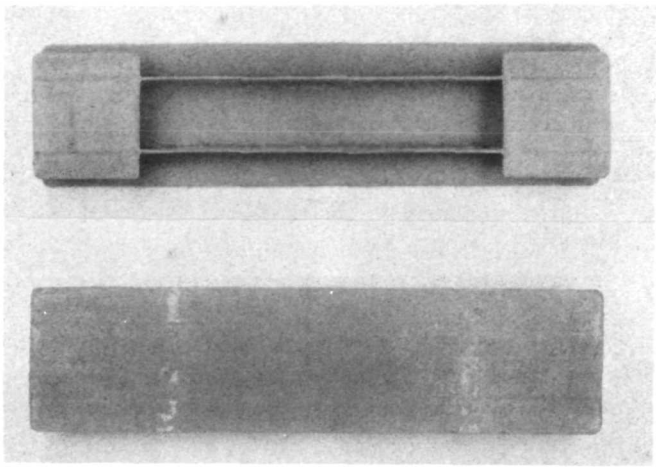

As Prepared

Magnification: 0.75X

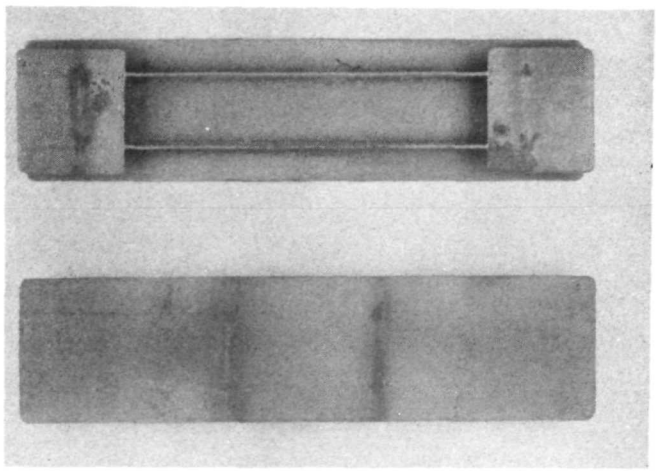

56 Re-Entry Cycles

FIGURE 85. SA-13+GN-19D COATED MHS PANEL "K" APPEARANCE RECORD DURING 1700° K - INTERNAL PRESSURE RE-ENTRY EXPOSURE

(as-prepared condition) are adherent dyna-quartz, the support media used during firing of the glass overlay. After-test color was slate gray. No coating failures were visually evident after 58 cycles; however some vitreous overlay had separated from the underlying silicide near the corner of one tab. This may have been the result of too thick a layer of glass in a localized area or of devitrification and subsequent spalling.

Panel "K" remained free from permanent deformation throughout the testing. Weight change measurements showed a gain of 0.026 kg/m^2 after 56 re-entries. Comparison with the 1700° K - 13 N/m^2 LP-SC data (Fig. 57) suggests that an overall weight loss might have been expected since the peak temperature during simulated re-entry occurred near a 10 N/m^2 pressure level (see Fig. 66).

As with previous parts, panel "K" was cross-sectioned at the center and at a point 0.0064 meter from an end (left side, Fig. 85). Figure 86 was prepared to show

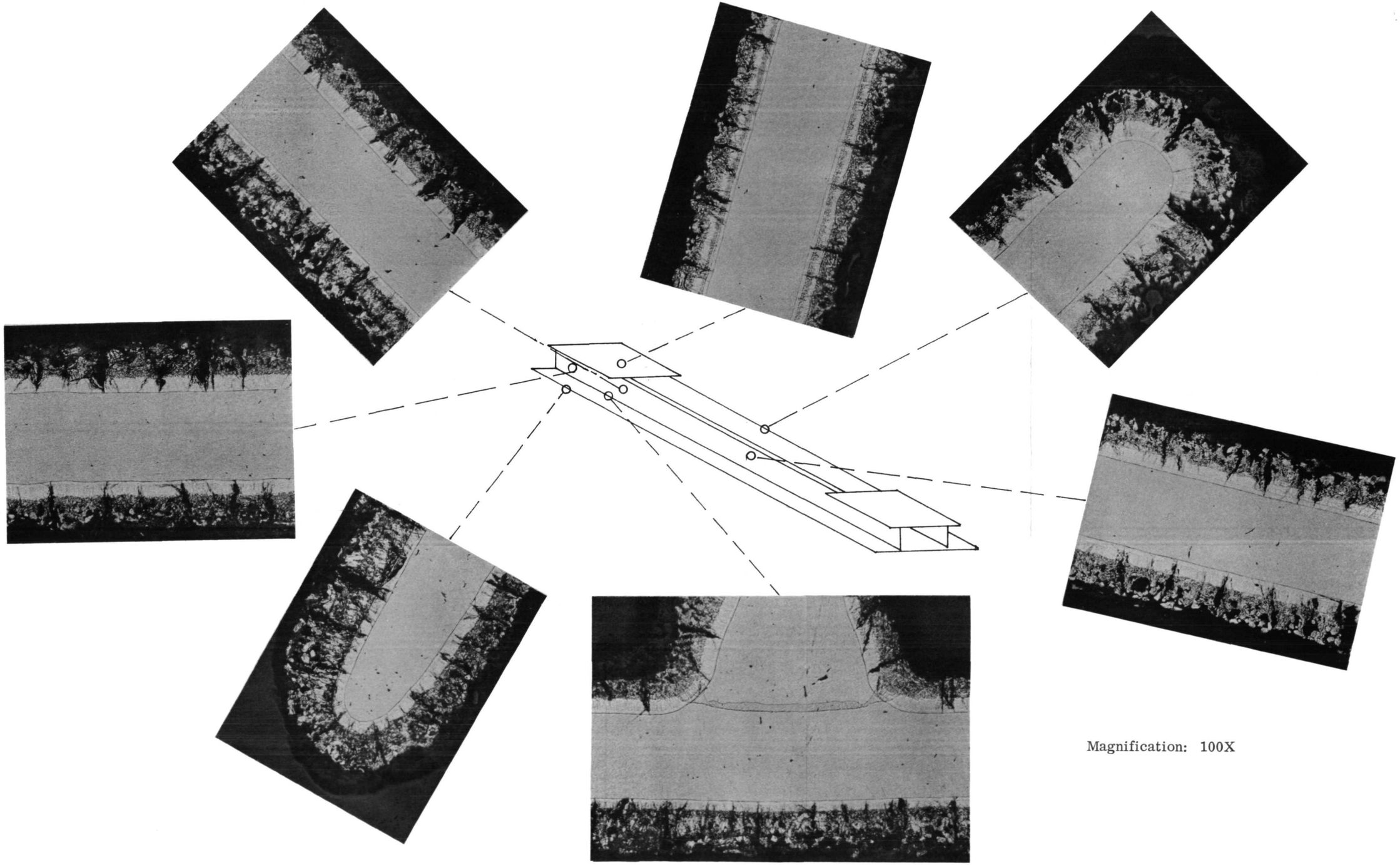

Magnification: 100X

FIGURE 86. COMPARISON OF COATING THICKNESS AND CONSUMPTION FOR VARIOUS LOCATIONS ON MHS PANEL "K" AFTER RE-ENTRY EXPOSURE

variations in coating thickness and structure after testing. The clear, colorless nature of the glass overlay makes this feature difficult to observe in many of the individual photomicrographs. Quite good thickness uniformity is indicated for all flat surfaces. Again, edges were coated more heavily than flat surfaces in many instances. This is a consequence of the brushing and striping techniques used to deposit additional slurry on edges after dip coating the entire part. Figure 87 provides a detailed view of the coating as present on the outer surface of the facesheet and at the panel center. Some glass is visible and exhibits at least two distinct phases.

Microhardness values (KHN, 100 g) for the centerline of the residual substrate varied from 255-290 across the facesheet and 0.0064 meter from the panel end. Values of 271 to 277 were found across the facesheet and at the panel center.

3.3.3 Elevated Temperature Tensile Tests

Tensile coupons were LP-SC exposed at 1700° K - 13 N/m^2, 1700° K - 1300 N/m^2 and 1810° K - 1300 N/m and were subsequently tensile tested in air in duplicate at room temperature, 1033 and 1700° K. Intentionally defected coupons (4T spot, center of gauge length) were LP-SC exposed for 1 cycle and subsequently tensile tested in air at room temperature and 1033° K. The coupons used for these tests had the same gauge length and dimensions as shown in Figure 18, but were lengthened one inch to facilitate gripping during high-temperature testing. Both the SA-13 and GN-19D overlaid SA-13 coating systems were prepared and evaluated.

Coating application methods and firing cycles were as previously described. SA-13 slurry was applied at the 0.350 ± 0.040 kg/m^2 level and GN-19D glass at the 0.050 ± 0.010 kg/m^2 level. Firing of SA-13 silicide yielded weight losses in the 12 to 23 percent range, considerably below the "normal" 20 to 28 percent span. Lower than normal weight losses are believed to have resulted from firing the specimens while more closely racked than usual. No appearance abnormalities were observed.

Tables LIX, LX and LXI contain LP-SC test results for the coatings when exposed to each of the three scheduled temperature-pressure combinations. Exposure levels for removal of each coating system at each test condition were selected to assure that multiple specimens would be available for tensile testing.

Appearance for all exposed coupons was normal in terms of color. SA-13 coated samples failed to develop sufficient glass to seal expansion cracks and failed prematurely when exposed at 1700° K and 1300 N/m^2. The lower than normal weight loss during firing may have caused this behavior by altering the coating composition. When overlaid with the GN-19D glass, equivalent SA-13 coated coupons achieved 30 and 100 test cycle levels without failure. Poorer reliability was again observed for the silicide vs glass overlaid silicide system when exposed at 1700° K and 13 N/m^2. No GN-19D overlaid coupon ever failed during the program when exposed for up to

FIGURE 87. SA-13 + GN-19D MICROSTRUCTURE, MHS PANEL "K" AFTER 58 RE-ENTRY CYCLES TO 1700°K AND INTERNAL PRESSURE

100 LP-SC's to 1700° K and 13 N/m^2 or 1300 N/m^2. Plain SA-13 coated coupons never quite achieved the 100-cycle level.

Exposure at 1810° K and 1300 N/m^2 reversed the relative performance of the two coatings. SA-13 coated samples developed a thin clear glass and a dark brown color. By contrast, the GN-19D overlaid specimens exhibited extensive glass mobility and a cloudy tan color. Application of a still more refractory glass overlay would probably tip the relative performances in favor of the overlaid system.

Tensile data for LP-SC exposed samples are shown in Tables LXII, LXIII and LXIV. Results are reported in terms of (1) original specimen substrate cross-section, (2) residual substrate cross-section after coating, (3) residual substrate cross-section after LP-SC, and (4) total specimen cross-section. Measurements on eight different SA-13 coated coupons showed that 38×10^{-6} meter/side of substrate was consumed during the coating operation. This value was used in calculating all "after coating" tensile properties. Figures 88 and 89 show the growth of the M_5Si_3 diffusion zone beneath the SA-13 coating as a function of the number of test cycles to 1700 or 1810° K. The 1700° K data were plotted to show the effect of GN-19D firing and SA-13 pre-oxidation as well as the subsequent LP-SC exposure. These diffusion data were determined from SA-13 and SA-13 + GN-19D coated and exposed specimens and were used to calculate tensile strengths after test exposure. Lines drawn through the data points were determined by a least squares analysis.

All specimens were strained at an 0.05 in/in/min rate until tensile failure occurred. Yield strength values were determined from load vs strain curves and are

TABLE LIX

1700° K - 13 N/m^2 LP-SC EXPOSURE OF THE SA-13 AND SA-13 + GN-19D COATINGS

Spec. No.	Coating	Cycles	Result
156T	SA-13	1	D, R
157T		1	D, R
158T		1	D, R
159T		1	D, R
160T		1	D, R
161T		1	D, R
307		21	R
311		21	R
313		21	R
316		21	R
322		23	R
334		23	R
292		43	F
293		44	F
298		44	R
302		44	R
304		44	R
305		44	R
194T	SA-13 + GN-19D	1	D, R
195T		1	D, R
196T		1	D, R
197T		1	D, R
198T		1	D, R
199T		1	D, R
294		23	R
333		23	R
335		23	R
336		23	R
338		23	R
339		23	R
320		100	R
321		100	R
326		100	R
327		100	R
328		100	R
334		100	R

R = Removed From Test
F = Failed
D = Intentionally Defected

TABLE LX

1700°K-1300 N/m^2 LP-SC EXPOSURE OF THE SA-13 AND SA-13 + GN-19D COATINGS

Spec. No.	Coating	Cycles	Result
150T	SA-13	1	D, R
151T		1	D, R
152T		1	D, R
153T		1	D, R
154T		1	D, R
155T		1	D, R
253		19	F
256		10	F
257		17	F
258		20	F
259		17	F
260		10	F
267		17	F
268		19	F
182T	SA-13 + GN-19D	1	D, R
183T		1	D, R
184T		1	D, R
185T		1	D, R
186T		1	D, R
187T		1	D, R
303		28	R
308		28	R
255		30	R
262		30	R
309		30	R
314		30	R
254		100	R
263		100	R
264		100	R
266		100	R
277		100	R
278		100	R

R = Removed From Test
F = Failed
D = Intentionally Defected

TABLE LXI

1810°K - 1300 N/m^2 LP-SC EXPOSURE OF THE SA-13 AND SA-13 + GN-19D COATINGS

Spec. No.	Coating	Cycles	Results
162T	SA-13	1	D, R
164T		1	D, R
165T		1	D, R
166T		1	D, R
167T		1	D, R
168T		1	D, R
273		20	R
280		20	R
282		20	R
287		20	R
290		20	R
291		20	R
269		40	R
271		40	R
274		40	R
276		40	R
279		40	R
284		40	R
188T	SA-13+GN-19D	1	D, R
189T		1	D, R
190T		1	D, R
191T		1	D, R
192T		1	D, R
193T		1	D, R
315		10	R
317		10	R
318		10	R
319		10	R
301		13	F
300		20	R
283		30	R
286		30	R
289		30	R
296		30	F
299		30	R

R = Removed From Test
F = Failed
D = Intentionally Defected

TABLE LXII

ROOM TEMPERATURE TENSILE TEST RESULTS

Specimen No.	Coating	Exposure (cycles/°K/N/m^2)	Yield Strength (MN/m^2)				Ultimate Strength (MN/m^2)				Elongation (%)
			A	B	C	D	A	B	C	D	
186	SA-13	-	417	532	-	-	474	605	-	-	16
189		-	432	560	-	-	496	644	-	-	13
156T		1/1700/13	-	-	-	-	345	447	482	-	2
158T		1/1700/13	-	-	-	-	370	491	515	-	1
322		23/1700/13	427	545	631	266	472	603	698	294	7
334		23/1700/13	426	547	640	233	487	625	730	267	8
293		44/1700/13	469	601	735	281	511	655	800	307	14
298		44/1700/13	439	568	700	-	477	618	783	-	11
154T		1/1700/1300	-	-	-	-	194	252	270	-	1
155T		1/1700/1300	-	-	-	-	207	267	288	-	1
258		20/1700/1300	478	617	714	283	516	666	770	295	10
268		19/1700/1300	485	625	724	295	519	670	774	316	14
162T		1/1810/1300	-	-	-	-	187	243	266	-	1
164T		1/1810/1300	-	-	-	-	185	238	262	-	1
280		20/1810/1300	453	585	775	273	491	633	839	296	13
290		20/1810/1300	456	586	783	272	497	640	853	297	11
276		40/1810/1300	447	574	840	279	488	626	917	304	12
279		40/1810/1300	454	584	851	274	489	628	916	295	16
341	SA-13 + GN-19D	-	443	567	-	280	496	635	-	314	18
342		-	476	614	-	257	545	703	-	295	13
194T		1/1700/13	-	-	-	-	328	427	460	-	2
195T		1/1700/13	-	-	-	-	304	394	423	-	2
294		23/1700/13	467	665	706	280	519	738	784	311	8
335		23/1700/13	445	575	668	261	498	644	748	292	7
320		100/1700/13	429	529	730	263	473	583	805	290	13
321		100/1700/13	395	509	672	244	425	547	713	262	8
182T		1/1700/1300	-	-	-	-	276	342	366	-	1
183T		1/1700/1300	-	-	-	-	335	431	461	-	1
303		28/1700/1300	477	618	735	294	534	691	823	329	13
308		28/1700/1300	475	636	755	289	504	675	801	306	12
254		100/1700/1300	472	610	825	229	499	645	871	242	11
263		100/1700/1300	454	584	786	254	494	635	856	276	11
189T		1/1810/1300	-	-	-	-	376	482	535	-	2
193T		1/1810/1300	-	-	-	-	288	375	410	-	2
315		10/1810/1300	456	591	738	270	467	605	745	276	9
317		10/1810/1300	422	540	650	264	454	570	699	284	9
283		30/1810/1300	448	576	805	270	465	598	835	281	9
295		30/1810/1300	451	569	800	283	481	607	852	302	11

A = Based on uncoated substrate cross section

B = Based on unaffected substrate cross section after coating

C = Based on unaffected substrate cross section after LP-SC exposure

D = Based on cross section of substrate plus applied coating

TABLE LXIII

1033°K TENSILE TEST RESULTS

Specimen No.	Coating	Exposure (cycles/°K/N/m^2)	Yield (MN/m^2)				Ultimate (MN/m^2)				Elongation (%)
			A	B	C	D	A	B	C	D	
190	SA-13	-	249	322	-	-	264	341	-	-	3
191		-	254	328	-	-	275	355	-	-	2
157T		1/1700/13	171	220	233	-	171	220	233	-	1
159T		1/1700/13	89	115	123	-	108	139	149	-	1
307		21/1700/13	194	263	292	-	280	380	422	-	4
311		21/1700/13	258	329	377	-	264	337	386	-	2
302		44/1700/13	201	259	320	-	208	268	330	-	2
304		44/1700/13	196	253	306	-	231	298	364	-	2
151T		1/1700/1300	24	31	33	-	26	34	36	-	1
152T		1/1700/1300	16	21	22	-	18	23	25	-	1
253		19/1700/1300	234	299	385	143	247	317	407	151	2
267		17/1700/1300	152	196	222	91	184	237	269	110	2
165T		1/1810/1300	*	-	-	-	*	-	-	-	*
166T		1/1810/1300	*	-	-	-	*	-	-	-	*
282		20/1810/1300	180	232	308	108	239	308	408	143	3
291		20/1810/1300	177	228	300	108	237	304	401	144	2
271		40/1810/1300	246	318	466	152	246	318	466	152	2
274		40/1810/1300	161	208	302	99	260	335	489	150	2
346	SA-13 + GN-19D	-	146	189	-	-	255	329	-	-	4
351		-	151	195	-	-	274	354	-	-	4
196T		1/1700/13	155	200	214	-	163	210	225	-	1
197T		1/1700/13	155	200	216	-	155	200	216	-	0
336		23/1700/13	231	298	353	142	263	340	402	162	4
338		23/1700/13	237	305	353	147	245	315	365	152	2
326		100/1700/13	177	227	303	110	229	294	392	142	2
327		100/1700/13	253	325	438	157	253	325	438	157	2
184T		1/1700/1300	129	167	189	-	129	167	189	-	1
185T		1/1700/1300	150	196	210	-	150	196	210	-	1
309		30/1700/1300	194	253	301	116	259	338	402	155	3
314		30/1700/1300	215	274	321	134	219	279	327	136	2
264		100/1700/1300	184	258	311	109	265	370	446	156	3
266		100/1700/1300	270	351	474	146	270	351	474	146	2
188T		1/1810/1300	36	46	50	-	36	46	50	-	1
190T		1/1810/1300	*	-	-	-	*	-	-	-	*
318		10/1810/1300	117	150	183	66	179	231	279	99	3
319		10/1810/1300	192	247	300	118	228	292	356	139	2
286		30/1810/1300	266	342	471	155	266	342	471	155	2
289		30/1810/1300	244	313	431	135	259	332	458	155	2

A = Based on uncoated substrate cross section

B = Based on unaffected substrate cross section after coating

C = Based on unaffected substrate cross section after LP-SC exposure

D = Based on cross section of substrate plus applied coating

* Broke during loading

TABLE LXIV

1700°K TENSILE TEST RESULTS

Specimen No.	Coating	Exposure (cycles/°K/N/m^2)	Yield Strength (MN/m^2)				Ultimate Strength (MN/m^2)				Elongation (%)
			A	B	C	D	A	B	C	D	
310	SA-13	-	143	184	-	-	147	180	-	-	22
312		-	151	195	-	-	162	209	-	-	16
313		21/1700/13	126	161	187	-	149	191	222	-	16
316		21/1700/13	129	164	189	-	156	198	229	-	9
305		44/1700/13	162	210	258	-	162	210	258	-	9
273		20/1810/1300	142	184	247	83	164	213	285	96	4
287		20/1810/1300	159	205	272	96	165	213	283	100	3
269		40/1810/1300	148	189	269	92	156	200	283	97	2
284		40/1810/1300	143	186	275	82	154	200	295	88	5
173T	SA-13 + GN-19D	-	146	188	-	-	152	196	-	-	13
174T		-	133	173	-	-	145	189	-	-	12
333		23/1700/13	132	170	198	71	189	243	283	102	2
339		23/1700/13	130	167	195	76	167	215	250	97	9
328		100/1700/13	142	183	246	88	146	189	253	91	12
334		100/1700/13	132	171	229	73	150	194	260	83	3
255		30/1700/1300	133	172	203	75	141	182	215	79	16
262		30/1700/1300	131	168	198	79	137	176	207	83	21
277		100/1700/1300	124	159	214	70	136	175	235	77	10
278		100/1700/1300	121	156	209	69	136	175	235	77	15
300		20/1810/1300	110	141	191	66	157	202	272	95	8

A = Based on uncoated substrate cross section

B = Based on unaffected substrate cross section after coating

C = Based on unaffected substrate cross section after LP-SC exposure

D = Based on cross section of substrate plus applied coating

for 0.2 percent offset. Room temperature elongation values were obtained with the aid of an extensometer attached to the specimen gauge section. Elevated temperature elongations were determined from recordings of load vs crosshead movement. It was assumed that all crosshead movement resulted in elongation with occurred within the heated gauge length section of the coupons. The facts that the specimen ends were three times as wide and were cold or very much cooler than the gauge section lends support to this supposition. Figure 90 diagrams the temperature gradients along a tensile coupon during testing. The ends of the furnace were closed with dyna-quarts plugs beyond the lowest noted temperatures.

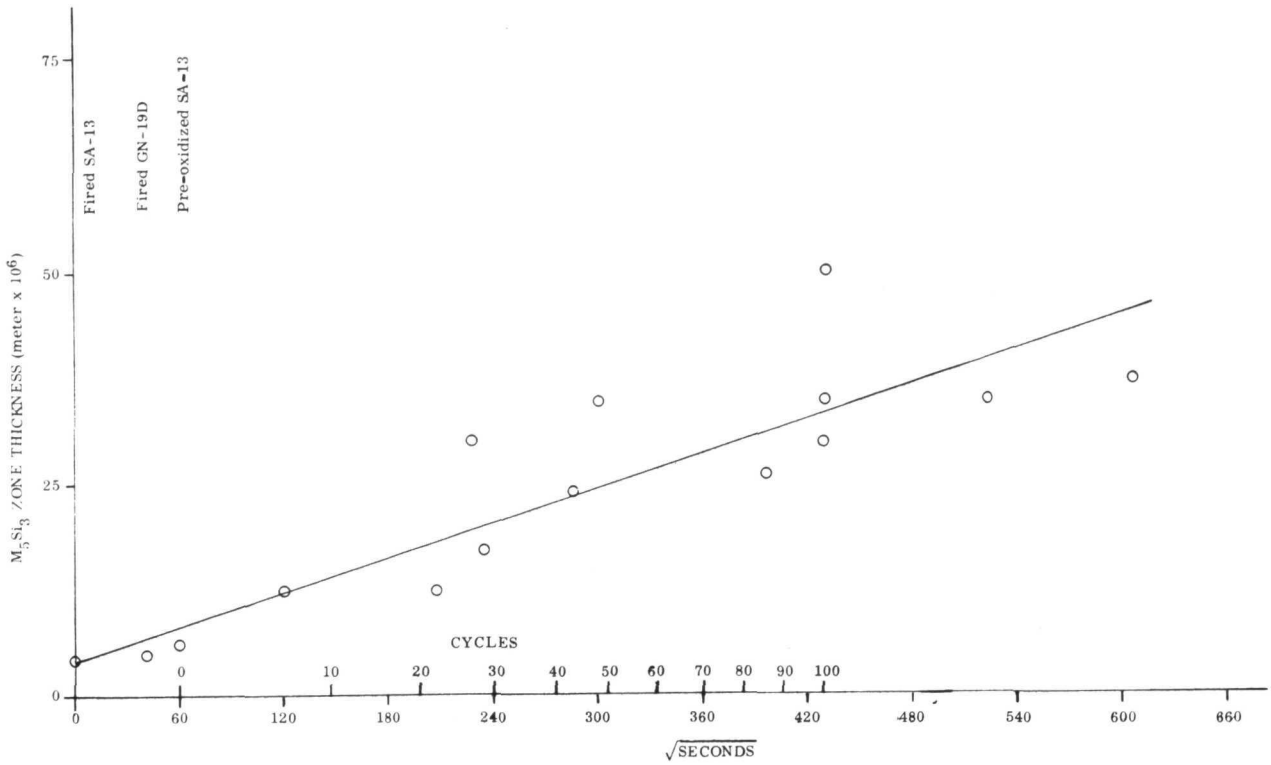

FIGURE 88. M_5Si_3 THICKNESS VS TIME AT 1700°K

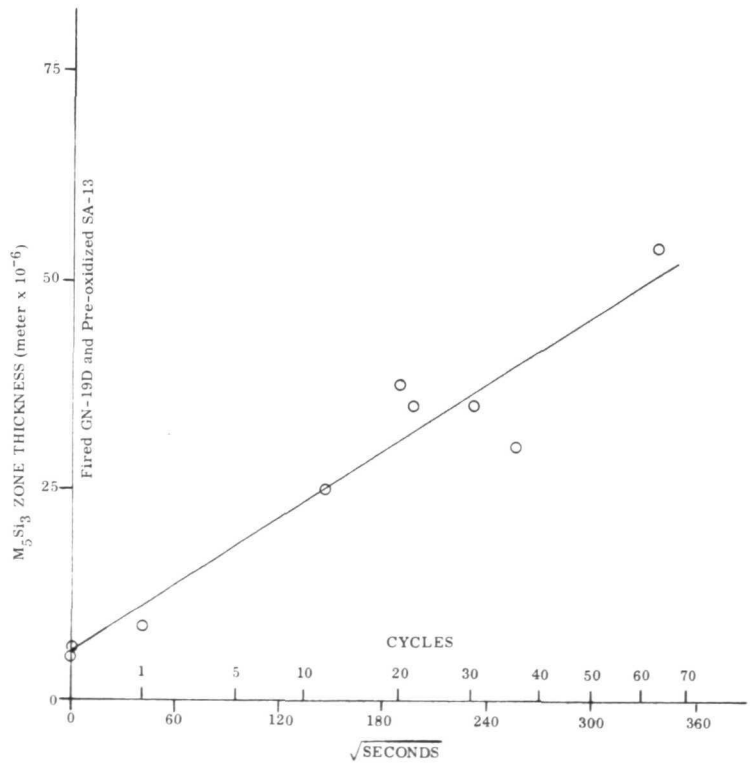

FIGURE 89. M_5Si_3 THICKNESS VS TIME AT 1810°K

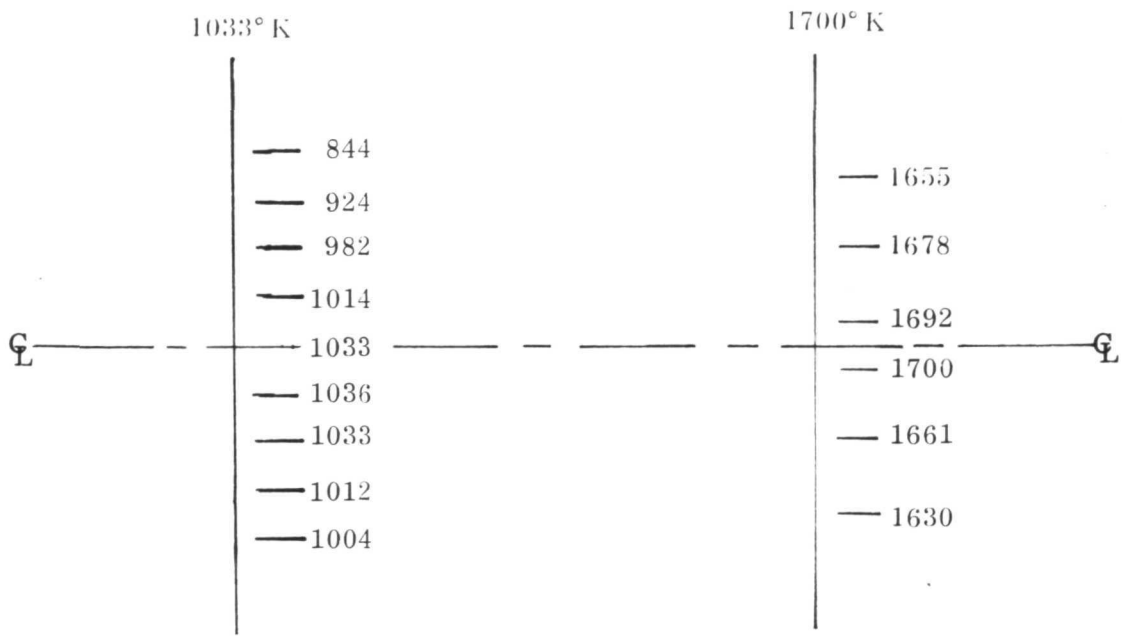

FIGURE 90. FURNACE TEMPERATURE GRADATION DURING TENSILE TESTS

Examination of Tables LXII, LXIII and LXIV revealed that yield or tensile strengths are notably different for various techniques for determining area. As an illustration, Figure 91 shows the yield strength at room temperature of coated and LP-SC tested specimens (data from Table LXII). The experimental results show that, within the normal life of the coating, the stress calculated on the unaffected substrate cross-sectional area after coating will provide strength values closely approaching test results for the uncoated alloy. Use of the residual cross-section after test gives a yield strength far above that known for 90Ta-10W alloy (Ref. 8). Use of the original cross-sectional area or total cross-sectional area gives a yield strength lower than the uncoated alloy.

The major deviation from uncoated alloy tensile properties occurred during the coating operation and the first few test cycles. Strengths were similar for both coatings and for all exposure conditions after about 10 LP-SC's.

An example of the surface and cross-sectional appearance of intentionally introduced, 4T spot defects is shown by Figure 92. Each specimen shown in this figure was exposed for one LP-SC at 1700° K. Exposure for one LP-SC at 1810° K and 1300 N/m^2 caused considerable damage and distortion in both SA-13 and SA-13 + GN-19D overlaid coupons. The SA-13 coated samples burned through at the defect; the GN-19D overlaid ones did not. Closer examination of glass overlaid coupons showed (Fig. 93) that the glass had definitely flowed or diffused across the defect and thereby provided a measure of protection to the substrate. Figure 93 shows the edge of an intentional defect and the continuous layer of glass which covered the entire defect after test.

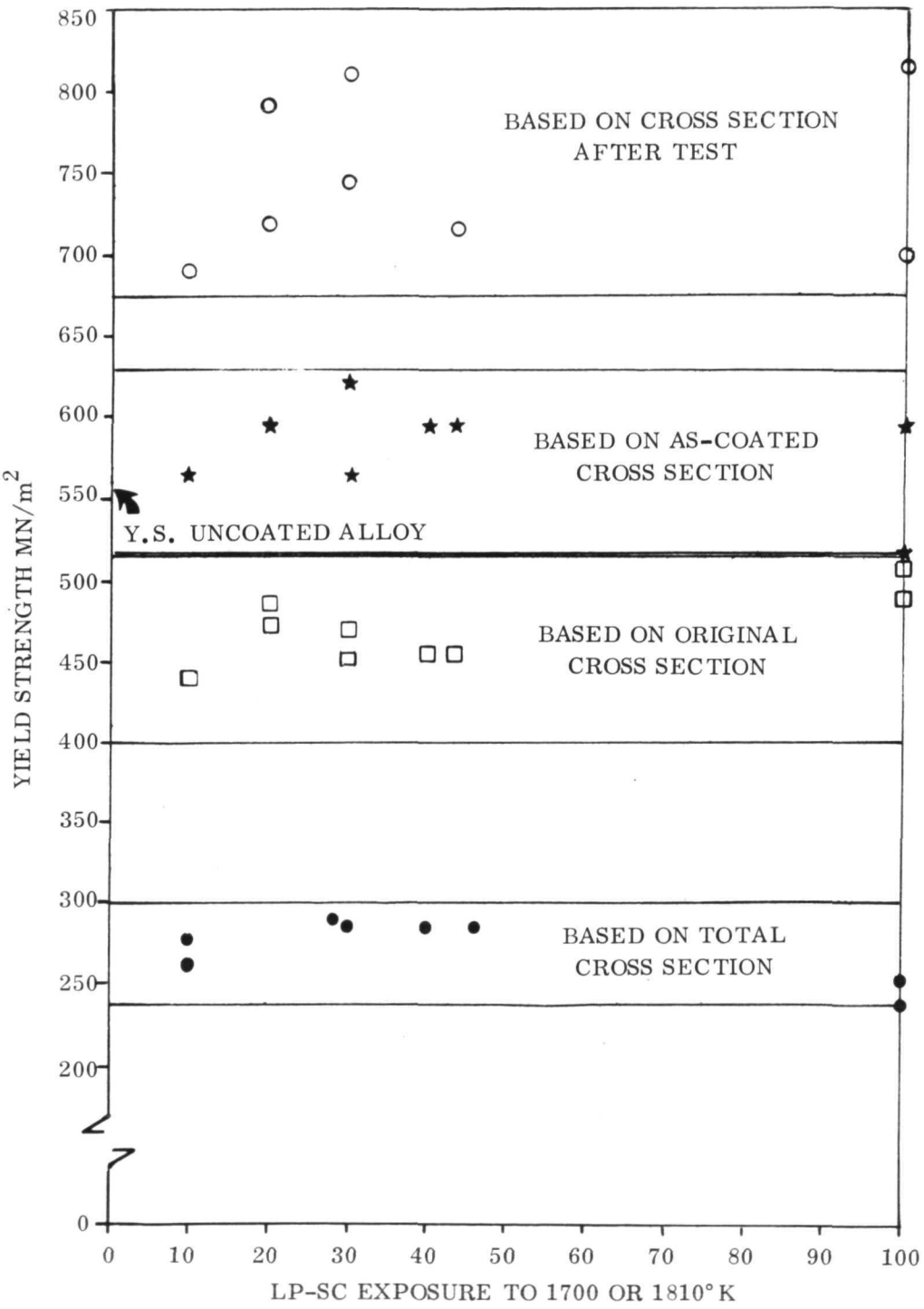

FIGURE 91. YIELD STRENGTH AT ROOM TEMPERATURE AFTER LP-SC EXPOSURE USING VARIOUS AREA EVALUATION TECHNIQUES

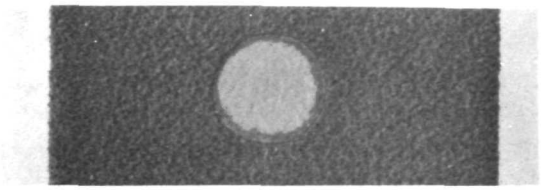

9X

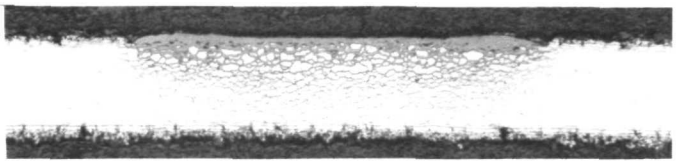

35X

SA-13, 13 N/m^2

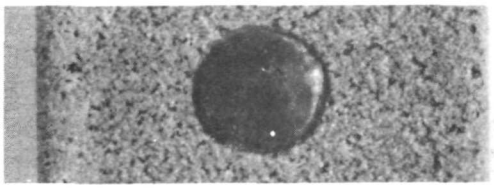

9X

35X

SA-13 + GN-19D, 13 N/m^2

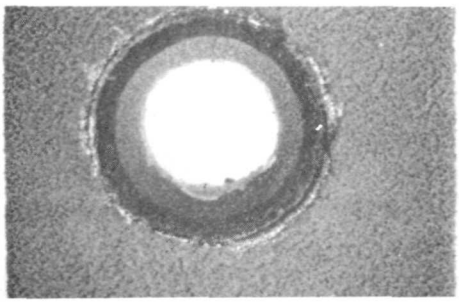

9X

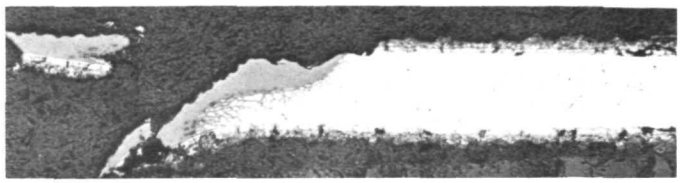

35X

SA-13, 1300 N/m^2

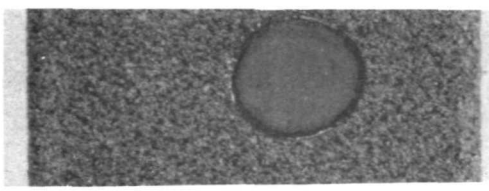

9X

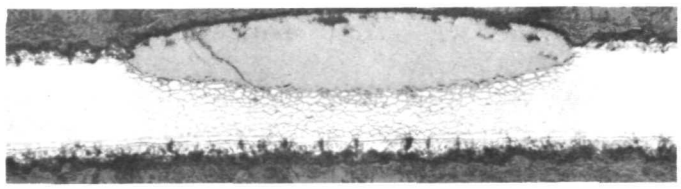

35X

SA-13 + GN-19D, 1300 N/m^2

FIGURE 92. MACRO AND MICROSCOPIC APPEARANCE OF 4T SPOT DEFECTED SPECIMENS AFTER 1 LP-SC TO 1700°K

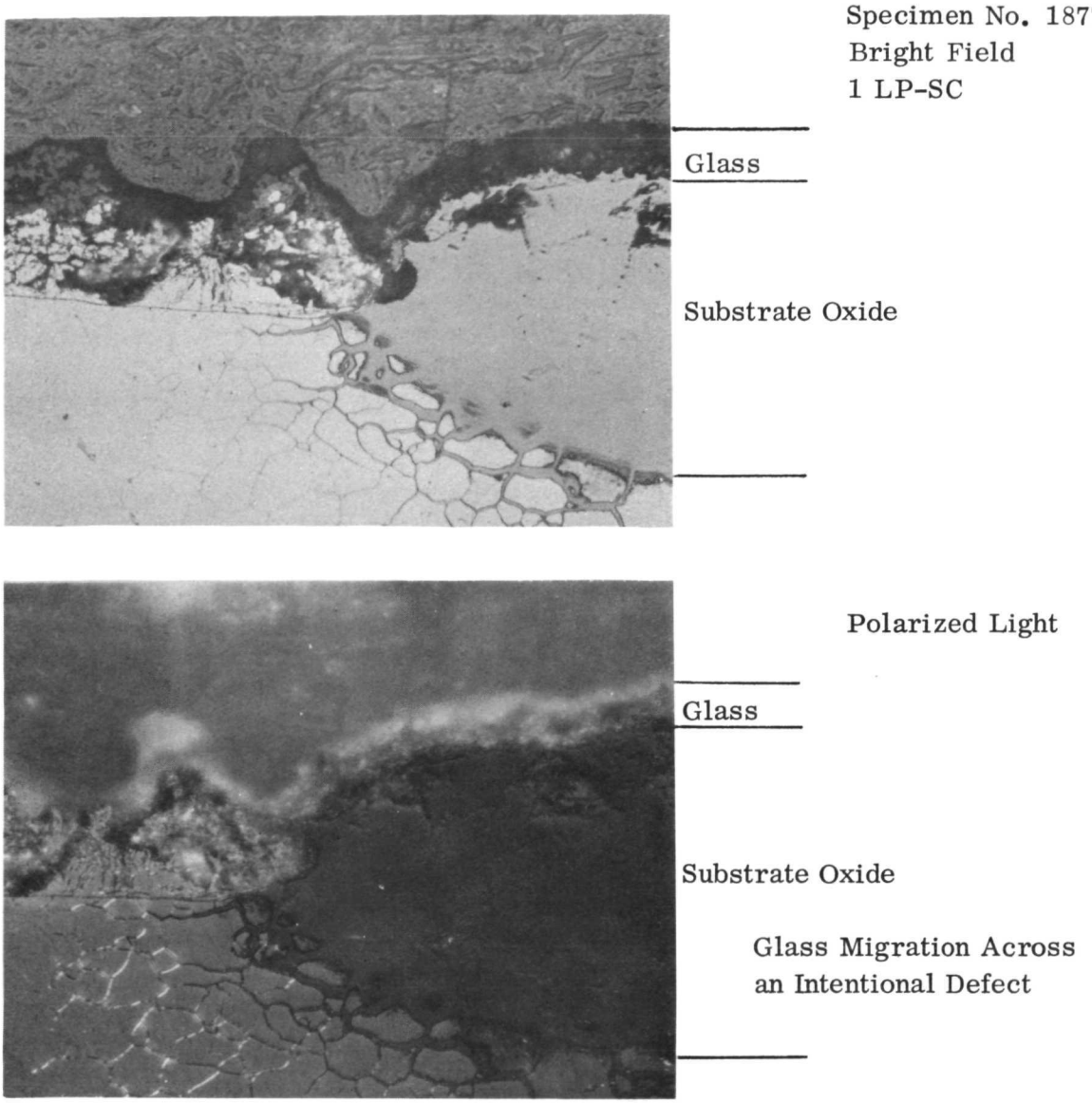

FIGURE 93. 4T SPOT DEFECTED SPECIMEN, SA-13 + GN-19D COATING, AFTER LP-SC EXPOSURE AT 1700° K AND 1300 N/m^2

A diagram of substrate microhardness vs distance from the defect is shown by Figure 94 for each specimen shown in Figure 92. Microhardness measurements (KHN, 100 g) were made every 250 x 10^{-6} meter and are shown to scale with respect to the original defect size. These data support the optical data (Fig. 93) which showed that GN-19D overlaid coupons were better able to resist defects than were plain SA-13 coated samples. The advantage of having the glass overlay appears less clearcut at 13 than at 1300 N/m^2.

Examples of 1700° K - 1300 N/m^2 LP-SC tested, GN-19D overlaid coupons are shown in Figure 95 after 28 and 100 cycles. Comparison with specimens exposed at

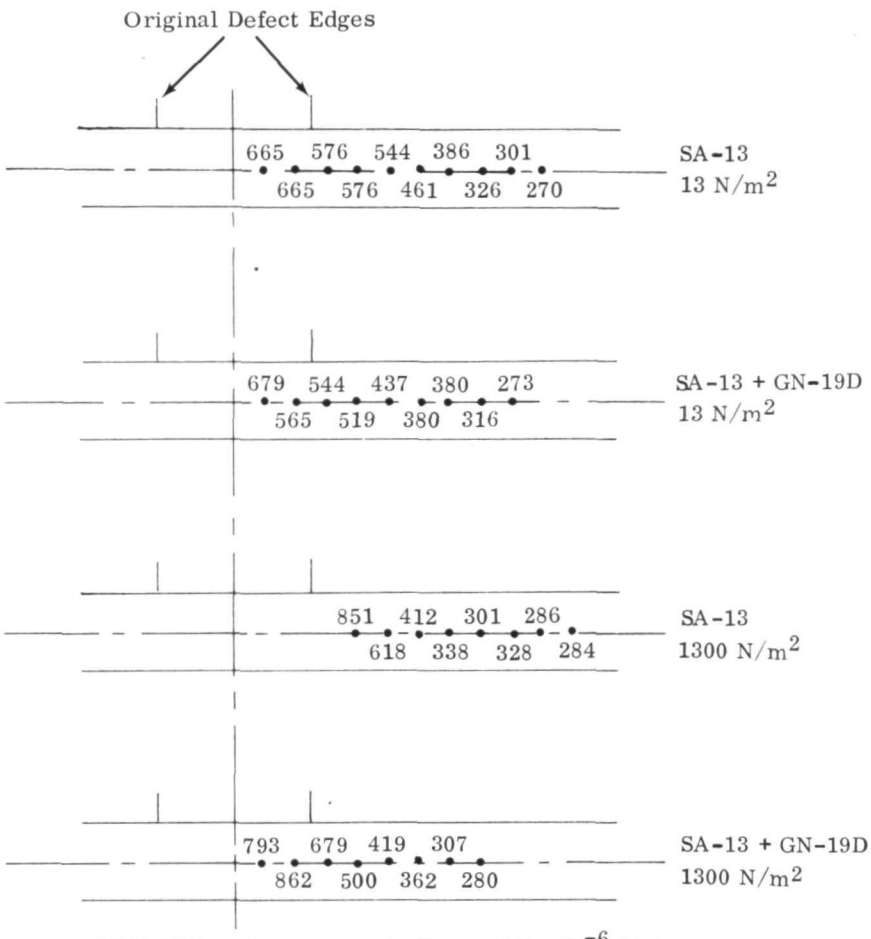

FIGURE 94. DIAGRAM OF MICROHARDNESS MEASUREMENTS FOR 4T SPOT DEFECTED SPECIMENS AFTER 1700°K - 13 OR 1300 N/m^2 LP-SC EXPOSURE

13 N/m^2 (Fig. 42) suggests a lower rate of silicide consumption (fewer voids) for 1300 than for 13 N/m^2 exposure. Appearance of the GN-19D overlaid coating is shown in Figure 96 after 1810°K - 1300 N/m^2 exposure. Considerable glass fluidity is evident from the very smooth outer surface.

Weight change data were recorded for 1700°K - 1300 N/m^2 exposed SA-13 + GN-19D coated coupons and are shown in Figure 97. An approximately 0.010 kg/m^2 gain was observed for each specimen during firing of the vitreous overlay (1800 seconds - 1700°K). This weight gain is comparable to that experienced by the plain SA-13 coating during pre-oxidation and was plotted as equivalent to one LP-SC (i.e., $\sqrt{\text{cycles}} + 1$ in Figure 97. Comparison with similar data for the plain SA-13 coating (Fig. 37) reveals that the glass overlaid coupons gained weight during LP-SC at about 50 percent of the rate for the plain silicide.

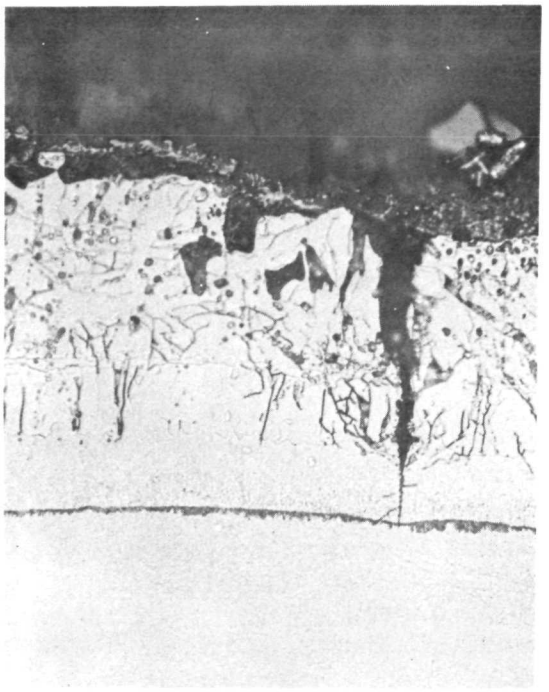

Spec. No. 308
28 LP-SC
Substrate ℄ Hardness = 259-286 KHN (100 g)

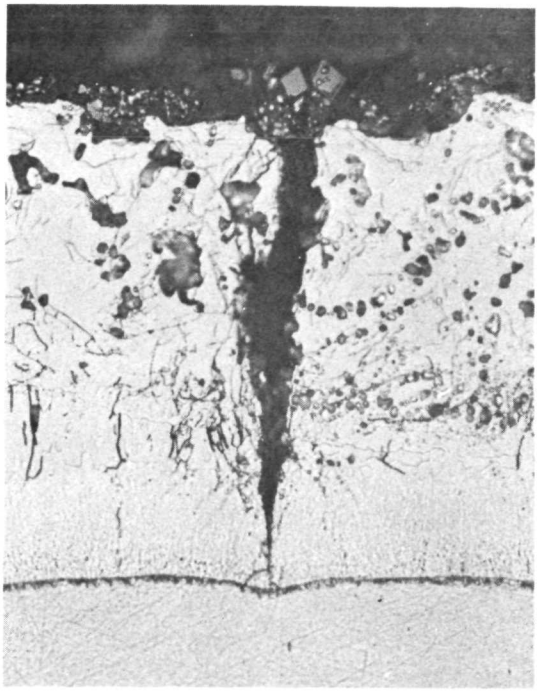

Spec. No. 263
100 LP-SC
Substrate ℄ Hardness = 262-309 KHN (100 g)

Etchant: $HF-HNO_3$-Lactic
Mag: 500X

FIGURE 95. SA-13 + GN-19D MICROSTRUCTURE AFTER LP-SC EXPOSURE AT 1700°K AND 1300 N/m^2

Substrate hardness measurements after 1700° K - 1300 N/m^2 LP-SC testing were about 30 points lower on the KHN (100 g) scale for glass overlaid than for plain SA-13 coated samples (compare Figs. 35 and 95). These data plus the kinetic, strength, metallographic and lifetime observations show conclusively that the glass overlay greatly enhances the ability of the SA-13 silicide to reliably protect 90Ta-10W alloy from oxidation at 1700° K and pressures as low as 13 N/m^2.

3.3.4 Total Hemispherical Emittance Measurements

Total hemispherical emittance values were determined for SA-13 coated specimens after LP-SC exposure at 1700° K - 13 N/m^2, 1700° K - 1300 N/m^2 and 1810° K - 1300 N/m^2, and for GN-19D overlaid coupons after LP-SC exposure at 1700° K and both 13 and 1300 N/m^2. These data are shown in Table LXV. For any single specimen, the emittance values were nearly constant over the 1256-1811° K temperature range. Most emittance values ranged near 0.71, with one specimen being significantly higher (0.78) and one noticeably lower (0.62). No appreciable

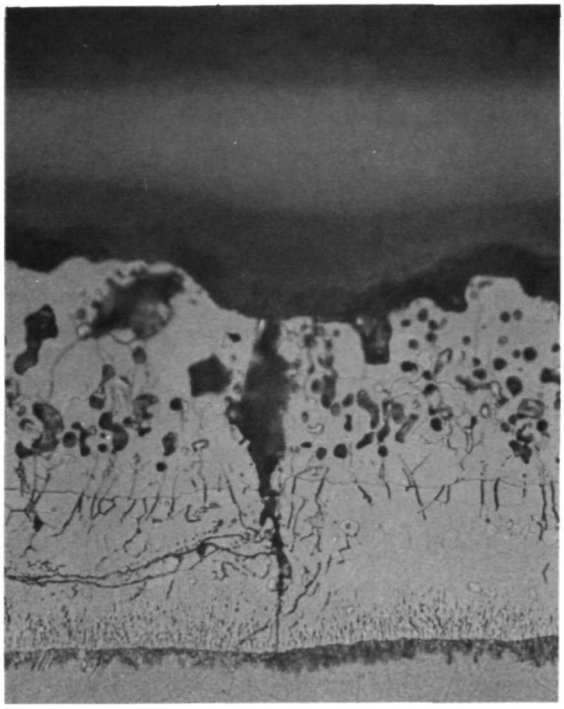

Specimen No. 295

30 LP-SC

Etchant: $HF-HNO_3$-Lactic

Magnification: 500X

FIGURE 96. SA-13 + GN-19D MICROSTRUCTURE AFTER LP-SC EXPOSURE AT 1810°K - 1300 N/m^2

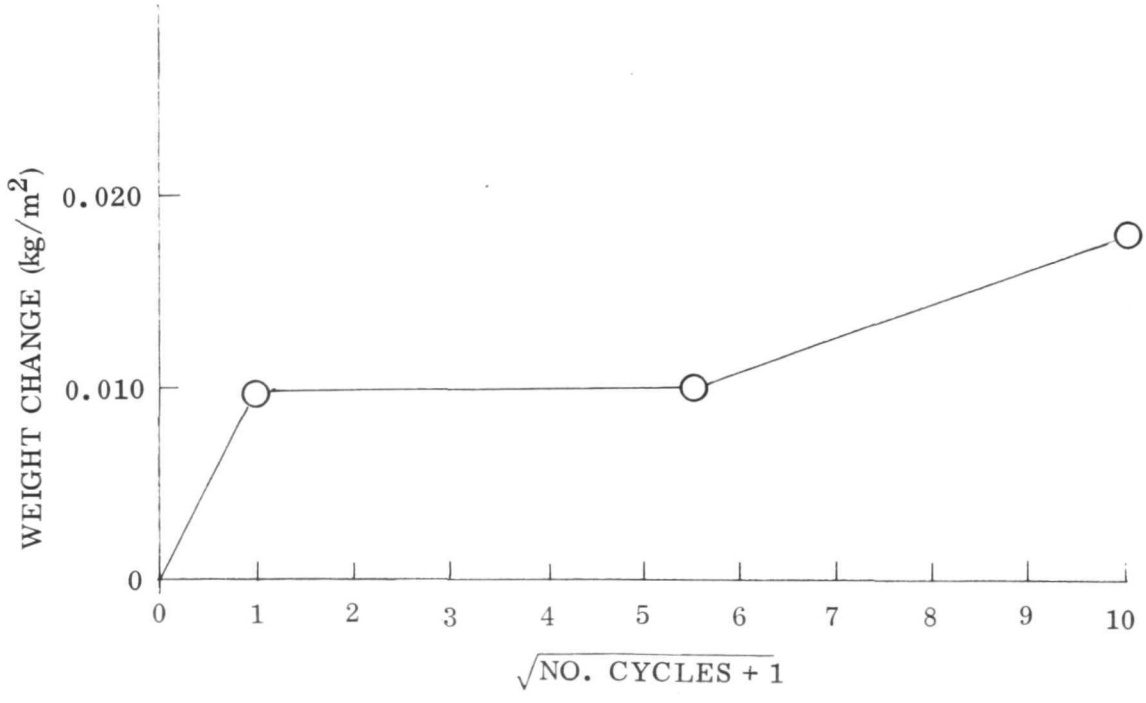

FIGURE 97. WEIGHT CHANGE DATA FOR 1700°K - 1300 N/m^2 LP-SC EXPOSED SA-13 + GN-19D COATING

TABLE LXV

TOTAL HEMISPHERICAL EMITTANCE VALUES AFTER LP-SC EXPOSURE OF THE SA-13 AND SA-13 + GN-19D COATINGS

Coating	Cycles	Temp. (°K)	Pressure (N/m^2)	$\epsilon_{H,T}$ at °K					
				1256	1367	1478	1589	1700	1811
SA-13	0	--	--	.711	.706	.702	.699	.696	.695
SA-13	1	1700	13	.718	.717	.718	.720	.723	.727
SA-13	21	1700	13	.715	.709	.706	.703	.703	.703
SA-13	98	1700	13	.689	.682	.672	.673	.671	.670
SA-13	1	1700	1300	.617	.623	.628	.633	.638	.642
SA-13	22	1700	1300	.698	.694	.692	.691	.690	.691
SA-13	86	1700	1300	.705	.701	.699	.698	.699	.699
SA-13	1	1811	1300	.712	.709	.707	.706	.705	.706
SA-13	25	1811	1300	.772	.774	.776	.778	.780	.782
SA-13	63	1811	1300	.734	.733	.732	.732	.732	.734
SA-13+GN-19D	0	--	--	.747	.745	.743	.742	.742	.742
SA-13+GN-19D	23	1700	13	.720	.718	.718	.716	.716	.718
SA-13+GN-19D	28	1700	1300	.711	.708	.704	.702	.700	.700

difference was observed for similarly exposed SA-13 and SA-13 + GN-19D coated coupons. The emittance values obtained do not correlate with weight change data for either coating at either exposure pressure. Following is a description of the method employed to generate the reported data.

Near normal spectral reflectance data were collected and used to determine spectral direction emittance by the equation

$$\epsilon_{\lambda,\theta} = 1 - \rho_{\lambda,\theta} \qquad (2)$$

where

$\rho_{\lambda,\theta}$ = directional reflectance at wavelength (λ) and direction θ = 12 degrees from surface normal

$\epsilon_{\lambda,\theta}$ = directional emittance at wavelength (λ) and direction θ = 12 degrees from surface normal.

Directional emittance (12 degrees) data were then integrated against blackbody functions of temperature (1256, 1367, 1478, 1589, 1700, 1811° K) to produce the total near normal emittance at temperature.

In order to do this, values of emittance data over the wavelength range 3×10^{-10} to 2×10^{-8} meter were used in the following equation:

$$\epsilon_{\theta T} = \frac{\int_{\lambda_1}^{\lambda_2} e_{b,\lambda,T}\, \epsilon_{\lambda,\theta}\, d\lambda}{\int_{\lambda_1}^{\lambda_2} e_{b,\lambda,T}\, d\lambda} \qquad (3)$$

where

$e_{b,\lambda,T}$ = Planck's blackbody function at wavelength λ and temperature T

$\epsilon_{\theta,T}$ = total near normal emittance at $\theta = 12$ degrees and temperature T

This wavelength range includes greater than 99.9 percent of all radiant energy for each temperature level. The values of total near normal directional emittance data were then adjusted to total hemispherical emittance ($\epsilon_{H,T}$) by electromagnetic theory for dielectric materials using the curves published in Reference 9. The data were collected and reduced by Convair Division of General Dynamics using a Cary Model 14 spectrometer, ellipsoidal directional reflectometers and a CDC 6400 computer.

Acquisition of total hemispherical data in the manner described above is justified by the observation that emittance at a discrete wavelength does not change with temperature (Ref. 9, p. 137). Further support of the technique is offered by comparison of total hemispherical emitance values obtained at Solar by the emission technique and by Ronald L. Nichols and Vaughn Yost of NASA, Huntsville, who measured room temperature reflectance values and calculated as described above. Both groups obtained total hemispherical emittance values of 0.86 at 533° K for a Solar developed and supplied high-emittance coating designated SP41MA-1.

3.3.5 Creep Measurement

The final experimental effort of the program was directed toward a determination of the time for 1 percent creep to occur for samples held at 1700 or 1810° K in air and stressed to 41.3 MN/m^2. Size limitations imposed by the available furnace and test fixture dictated use of the same specimen as was used for elevated temperature tensile measurements.

The experimental setup consisted of a support frame to hold a small Pt-20Rh resistance wire electric furnace and to anchor the top of a specimen. Attached to the lower end of the specimen was a grip and an extension rod which supported a container of lead shot. A linear potentiometer was attached to the extension rod and served to measure specimen elongation during testing. A recorder provided a record of time vs elongation during testing and a micro-switch was so located that specimen rupture shut off both a timer and the recorder. Specimens were loaded by slowly lowering a support jack under the lead shot container.

Measurements were made to determine the temperature distribution over the gauge length of a specimen during creep exposure. These data are diagrammed to scale in Figure 98 for both the 1700 and 1810° K conditions. Specimens had a one-inch gauge length and were centered within the furnace during exposure. Top and bottom openings to the furnace were closed with fitted dyna-quartz plugs.

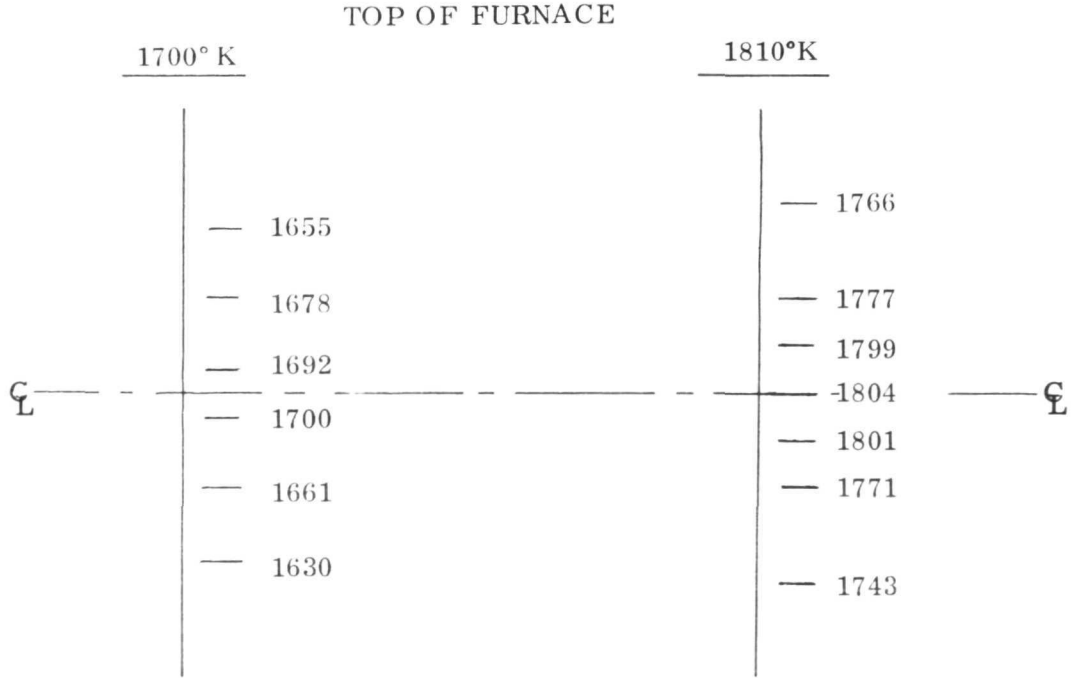

FIGURE 98. FURNACE TEMPERATURE GRADATION DURING CREEP TESTS

Four SA-13 + GN-19D coated tensile coupons were creep tested; two at 1700° K and two at 1810° K. Loads were calculated for each coupon so as to yield a 41.3 MN/m^2 stress on the residual substrate after coating. Table LXVI contains data for each specimen tested. Both specimens tested at 1700° K failed within the grip areas bec the coating was damaged during clamping. Sufficient data were recorded before failure occurred to permit extrapolation to the one percent creep level. No Stage 1 creep was observed after applying the load to any of the specimens. Essentially linear strain vs time data were observed for the 1700° K coupons until the onset of failure by oxidation in the grip area. Data for specimen 352 were precisely linear throughout the 1810° K exposure. A non-linear strain vs time response was observed for specimen 349. The reported time for one percent creep for this specimen is an average value for the total test time.

TABLE LXVI

TIME TO ONE PERCENT CREEP

Spec. No.	Temp. (° K)	Time for 1% Creep (sec.)*	Comment
347	1700	3.6×10^5 †	Failure in lower grip at 34.5 hours
350	1700	2.7×10^5 †	Failure in top grip at 75.5 hours
349	1810	2.52×10^4	Removed from test after 18 hours
352	1810	2.88×10^4	Removed from test after 18 hours

* Load = 41.3 MN/m^2

† Values obtained by extrapolation.

Ultimate appearance of the 1700° K creep tested samples was dark green and glazed. Both 1810° K exposed coupons assumed a medium brown color and, while glazed, were dull. No evidence for glass flow was observed on any of the specimens. Figure 99 shows macro and microscopic views of 1700 and 1810° K creep tested coupons together with microhardness values for the substrate at the center of the gauge length.

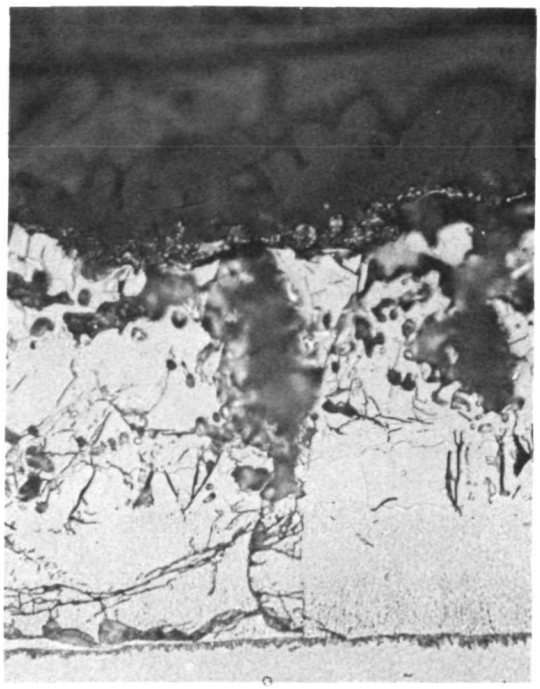

Spec. No. 350

2.7×10^5 sec. at 1700° K

Magnification: 0.75X
500X

℄ Hardness: 279-307
KHN(100 g)

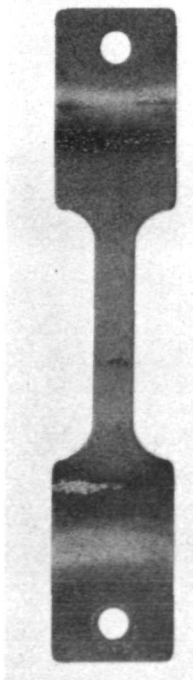

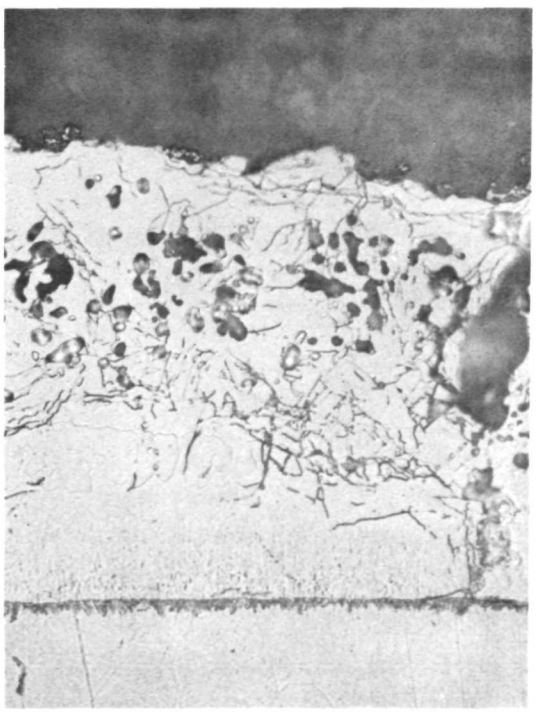

Spec. No. 352

2.88×10^4 sec. at 1810°K

Magnification: 0.75X
500X

℄ Hardness: 264-282
KHN(100 g)

FIGURE 99. MACRO AND MICROSTRUCTURE OF SA-13 + GN19D CREEP TESTED COUPONS

4

DISCUSSION

The original program goal was to develop a fused slurry silicide coating which could provide protection to 3.3×10^{-4} meter thick 90Ta-10W alloy for up to 100 atmospheric re-entries at 1810° K. Within the limits imposed by thermodynamics, kinetics, substrate creep rates and available test equipment, this objective was achieved. Low-pressure, slow-cycle lifetimes at 1700° K and either 13 or 1300 N/m^2 pressures consistently exceeded 100 test cycles. No failures were ever observed for SA-13 +GN-19D coated coupons when tested at these conditions. Simulated re-entry exposure of miniature heat shield panels yielded lifetimes of about 50 re-entries for the glass overlaid SA-13 silicide. Test conditions included a simultaneous variation of temperature, pressure, and stress as a function of time. Both internal and external pressure conditions were simulated. A combination of the effects of stress and of the much more complex test sample accounts for the shorter lifetimes observed in simulated re-entry than during low-pressure, slow-cycle testing.

Exposure of the SA-13 silicide at 1810° K and 1300 N/m^2 produced consistent low-pressure, slow-cycle lifetimes of 25 cycles, probable lifetimes near 40 cycles and a maximum observed lifetime of 63 cycles. Vitreous overlaid SA-13 coated coupons did not perform as well as SA-13 silicide coated coupons because the applied glass overlay was not sufficiently refractory for use at 1810° K. That glass which naturally formed over the SA-13 silicide was immobile at 1810° K; whereas the applied glass overlay became quite fluid when exposed at 1810° K. Slight modifications to the GN-19D overlay composition and firing cycle could produce a glass suitable for use to 1810° K.

Neither the plain nor overlaid SA-13 silicide was able to withstand the 1810° K - 13 N/m^2 low-pressure, slow-cycle test condition. Examination of thermodynamic data (Ref. 2, 5) shows that these parameters are well within the pressure/temperature region where the most stable refractory metal silicides are unstable with respect to reactions such as

$$MSi_2 + SiO_2 \rightarrow MSi + 2SiO\ (g)$$

$$5MSi_2 + 7SiO_2 \rightarrow M_5Si_3 + 14SiO\ (g)$$

$$5MSi + 2SiO_2 \rightarrow M_5Si_3 + 4SiO\ (g)$$

$$3M_5Si_3 + 4SiO_2 \rightarrow 5M_3Si + 8SiO\ (g).$$

Reactions such as are shown above would consume any silica formed during pre-oxidation or applied as an overlay. In addition, insufficient oxygen is present at 13 N/m^2 to permit formation at 1810° K of a condensed SiO_2 phase on the silicides.

In contrast with the developed coatings, the existing coating systems used for comparison (R512A, C, K) were unable to provide protection for the 90Ta-10W alloy beyond about 10 low-pressure, slow-cycles to either 1700 or 1810° K. Of these three Sylvania applied systems, R512A offered the longest apparent lifetimes, but still failed to preserve the substrate mechanical properties.

Post-test mechanical and physical property determinations included: (1) tensile strength, (2) elongation, (3) ductile-brittle bend transition temperature, (4) microhardness values, (5) time to yield one percent creep, and (6) total hemispherical emittance. As previously noted, tensile strengths based on the residual substrate cross-sectional area were consistently higher than for the uncoated or as-coated alloy when measured in air at 300, 1033 and 1700° K. This indicates either a coating/substrate interaction or strengthening due to contamination with oxygen. Microhardness values tended to slowly increase with increased exposure times for the SA-13 coating but to remain constant for the GN-19D overlay system. These hardness values were shown to be related to the substrate oxygen content. Some coating/substrate interaction is indicated by the facts that (1) GN-19D overlaid coupons exhibited no change in substrate hardness when exposed at 1700° K, and (2) both GN-19D overlaid and SA-13 coated specimens became stronger with increased exposure times.

Substrate ductility, as measured by tensile elongation values, was observed to decrease as a result of any test exposure, but not as a function of increasing test exposure. Uncoated alloy elongated 20-25 percent at room temperature (300° K). The act of coating reduced the 300° K elongation values to the 13-18 percent range. Low-pressure, slow-cycle exposure at 1700° K and either 13 N/m^2 or 1300 N/m^2 further reduced elongation values to the 7-14 percent, essentially the same as for 1700° K test exposure.

Evidence for a ductility minimum near 1033° K is shown by the 2-4 percent elongation values determined for both as-coated and asptested specimens when tensile tested at 1033° K. No relationship between exposure length or temperature ductility was observed. Reference 5 shows data which suggest a ductility minimum, but provides no specific data near 1033° K.

Elongation values determined during 1700° K tensile tests were inconsistent, ranging from 3-21 percent for 1700° K exposed coupons. The data suggest better elongation after 1300 than 13 N/m^2 LP-SC exposure, just the reverse of what might be anticipated. Ductility at 1700° K after 1810° K - 1300 N/m^2 exposure fell within the 2-8 percent range and appeared to be consistently lower than for 1700° K exposure.

All elongation values were based on the assumption that the strain was uniformly distributed along the one-inch gauge length. The presence of a temperature gradient (approximately 45° K) along the specimen gauge length may invalidate this assumption and mean that the measured strain actually occurred over a shorter distance. This effect could be especially pronounced during 1700° K tensile testing and may explain some of the inconsistencies noted among these data. Lack of an extensometer for use at 1700° K required that elongation be determined from crosshead movement. This may also have contributed to the observed data inconsistencies.

Intentionally defected coupons regularly displayed 0-3 percent elongation regardless of the LP-SC exposure level or test temperature. In line with other observations (metallography), GN-19D overlaid coupons produced values near the top of this range, while SA-13 coated samples yielded the lower values.

Throughout the program, ductile-brittle bend transition temperatures of 200° K or lower were consistently noted for SA-13 or glass overlaid SA-13 coatings after all LP-SC test exposures. Many intentionally defected coupons also exhibited a DBBTT of 200° K or lower. This indicated that some useful substrate remained after at least one LP-SC to any of the various temperature/pressure combinations employed.

Microhardness values for the as-received 90Ta-10W alloy ranged from 261-281 KHN for a 100 g load. Application of the SA-13 silicide increased these values to the 285-322 range. Substrate microhardness values after LP-SC exposure were generally lower than for the as-prepared specimen but were found to slowly increase as a function of 1300 N/m^2 test exposure time for SA-13 coated samples. The maximum hardness value observed for an LP-SC exposed (1300 N/m^2), unfailed, SA-13 coated sample was 340 KHN. Slight softening relative to the as-received alloy hardness was observed for all SA-13 coated and 1700° K - 13 N/m^2 LP-SC exposed samples. Glass overlaid (GN-19D) specimens were consistently a few hardness points softer than comparably exposed SA-13 coated samples. Again, specimens exposed at 13 N/m^2 were slightly softer than similarly tested 1300 N/m^2 coupons. Comparison of substrate hardness values determined at the center of MHS panel facesheets revealed that the GN-19D overlay greatly improved protectiveness of the coating system during simulated re-entry. Glass overlaid MHS panel substrates exhibited no hardening relative to the as-received alloy while SA-13 coated panels showed substrate hardening of up to 150 points (100 g KHN scale) after re-entry exposure. Further, the GN-19D overlaid panels were exposed to a greater number of test cycles than were the plain SA-13 coated parts.

Total hemispherical emittance data generated during the program ranged near 0.72 and indicated the possible need for a coating modification to increase the re-radiative capabilities of the coating system. No distinct trend of emittance values versus LP-SC exposure was observed. Where comparable data were available, little

difference existed between the SA-13 and the glass overlaid SA-13 systems. A small addition to the GN-19D overlay could be formulated so as to increase the re-radiative properties of the protective system.

If one percent creep is assumed to be the maximum permissible deformation for a heat shield panel, the 90Ta-10W alloy appears capable of use at 41.3 MN/m^2 loading for greater than 100 re-entries at 1700° K. Time to creep one percent at 1810° K and 41.3 MN/m^2 was about 2.7×10^4 seconds and would probably limit heat shield panel reuse to about 15 re-entry cycles (assume 1800 seconds at 1810° K/cycle). Provided the ambient pressure was 1300 N/m^2 or greater, the developed coatings appear capable of preserving the substrate mechanical properties for this number of re-entries to near 1800° K.

Some of the initial coatings investigated in the program (SA-5, DAM + DAS) were found to be extremely sensitive to processing conditions. For instance, only small weight loss during firing differences between SA-5 coated coupons resulted in vastly different test responses. SA-13 proved the least sensitive to weight loss during firing of any tested coating. The preferred weight loss range for a 0.350 kg/m^2 thick SA-13 slurry was found to be 20-32 percent. Low-pressure, slow-cycle lifetimes for SA-13 at 1700° K and 1300 N/m^2 were, however, reduced to only about 10-20 cycles by weight loss during firing values of about 18 percent or less. Low weight losses evidently changed the final silicide composition in a manner which inhibited glass formation during 1700° K exposure. Exposure at 1810° K and 1300 N/m^2 was not obviously influenced by firing variations encountered during the program.

Material losses during the fusion of SA-13 were principally a function of

(1) applied slurry weight thickness

(2) time above 1500° K during the fusion cycle

(3) specimen arrangement on support fixture

That weight loss would be a function of the applied slurry weight thickness is logical because vaporization is a function of surface area. Heavier coatings applied over the same surface area and fired through the same cycle will incur smaller percentage weight losses than equivalent but lighter coatings. Though observed, this was not a major source of coating composition variation for specimens used during the program because a standard quantity of slurry was always applied.

Experimental work during the early part of the program showed that most coating element vaporization occurred above about 1500° K. As a consequence, firing cycles were conducted so as to maintain a uniform length of time above 1500° K during SA-13 fusion cycles.

Specimen-to-specimen and layer-to-layer distances on the firing rack were found to significantly influence coating weight losses during fusion. For the size coupons used throughout the program, a one-half inch specimen-to-specimen and a one-inch layer-to-layer arrangement was found to yield acceptable SA-13 weight losses during fusion. Closer spacing and heavy furnace loading were responsible for the lower than desired weight losses encountered during preparation of the final set of SA-13 coated tensile coupons.

Intentional defects including 1T and 4T diameter surface and 4T hole defects were introduced into specimens prior to LP-SC testing (T = material thickness = 330 x 10^{-6} meter). A coating surface defect of 0.0064 meter diameter was also placed in an MHS panel before exposure to external pressure re-entry conditions. One T surface defects on either the SA-13 or SA-13 + GN-19D coating generally filled with a dark oxide during the first LP-SC exposure at either 13 or 1300 N/m^2 and showed no further change within about 5 test cycles. Some lifetime observations on 1T surface defects were open to question because it was very difficult to establish before testing that all coating had been removed from the substrate. The 4T surface defects responded differently to the various temperature/pressure conditions used. Exposure at 1700° K and 13 N/m^2 produced no obvious tantalum oxide and no specimen deformation in up to six test cycles, regardless of which coating was present. The 1700° K - 1300 N/m^2 test condition resulted in substrate burn-through of a 4T surface defect in an SA-13 coating during the first exposure cycle. By contrast, only an oxide pimple was formed on a similarly exposed glass overlaid coupon. Metallographic analysis showed a thin layer of glass covering the defected area when the GN-19D overlay was present. A single 1810° K - 1300 N/m^2 cycle converted a 4T surface defect in a SA-13 coating to a hole of about 2500 x 10^{-6} meter diameter. Equivalent exposure of a GN-19D overlaid sample produced only a black oxide pimple at the surface defect site.

From the work of previous investigators of coatings for tantalum alloys (Ref. 1,3,10,11), it can be concluded that titanium and molybdenum or tungsten were apparently the most effective silicide modifiers. Both tantalum and tungsten were included in pack or fused slurry applied coatings because coating/substrate reaction and interdiffusion occurred during processing. Sintered slurry coatings included tungsten as a modifier element but were essentially free from tantalum.

Nearly all successful silicide coatings for tantalum alloys have been shown to generate vitreous silica (SiO_2) and rutile (TiO_2) as a part of the developed coherent oxide. No tantalum oxide, Ta_2O_5, is observed for protective coatings. Presence of a glassy oxide over the complex silicide layer is required to: (1) seal cracks due to coating/substrate expansion rate mismatches, and (2) control the transfer of oxygen from the gas phase to the silicide phase.

The best overall slurry composition evolved during this program (SA-13) contained appreciable quantities of chromium and titanium and smaller amounts of

molybdenum, tungsten and vanadium. Fusion of the SA-13 composition onto the 90Ta-10W alloy introduced major amounts of tantalum and considerable additional tungsten into the final coating. Vapor pressure data and calculated vaporization rates indicate that only chromium and silicon were likely to be lost during fusion of the applied SA-13 slurry. If it is assumed that chromium and silicon each accounted for one-half of the observed weight loss during fusion and that 0.680 kg/m^2 of 90Ta-10W alloy were consumed during fusion by 0.350 kg/m^2 of slurry, then the final coating composition is approximated by

Element	Weight Percent
Tantalum	66
Silicon	17
Tungsten	8.8
Titanium	3.8
Chromium	2.8
Molybdenum	1.5
Vanadium	0.8

More than sufficient silicon is present to convert all of the above tungsten, titanium and molybdenum to disilicides, all tantalum to Ta_5Si_3 and all chromium to Cr_3Si, the compounds determined by X-ray diffraction. Electron microprobe data from LP-SC exposed specimens indicated the presence of tantalum disilicide in the coating. The presence of other unidentified compounds was indicated by the XRD work. Presumably these were mixed silicides and would not appreciably influence the results of the above calculation.

X-ray diffraction analysis showed the possible presence of cristobalite (SiO_2), Cr_2O_3, Ta_5Si_3 and some unidentified compounds after long LP-SC exposure at 1700° K and 13 N/m^2. Noteworthy for its absence was TiO_2. As expected from vapor pressure data, no evidence for molybdenum or tungsten oxides was observed.

Other diffraction data showed cristobalite (SiO_2) and rutile (TiO_2) definitely present and Cr_2O_3, $TiSi_2$ and Ti_5Si_3 probably present after extensive LP-SC exposure at 1810° K and 1300 N/m^2. Microprobe and metallographic work also indicated the presence of SiO_2, TiO_2 and Cr_2O_3 at the specimen surface. Some evidence for dissolved tantalum oxide in the vitreous SiO_2 was also noted. No EMP evidence for titanium silicides was found after 1810° K - 1300 N/m^2 exposure; however residual disilicides of tantalum, tungsten and molybdenum were apparently present just below the glassy surface layer.

An X-ray diffraction analysis of a GN-16C overlaid specimen disclosed only a very weak cristobalite (SiO_2) pattern after LP-SC exposure at approximately 1840° K and 1300 N/m^2. The presence of small amounts of all silicide constituents except

vanadium and of all glass constituents was indicated by an X-ray fluorescent scan of the specimen surface.

The above analytical data and the observed coating lifetimes provide support for the observation by Kolodney and Graff (Ref. 12) that a protective coating need not develop a substantially pure silica layer such as is observed for the oxidation of molybdenum and tungsten disilicides above about 900° K. It is, however, important that the metal oxides be compatible with SiO_2 to the extent that they do not promote rapid conversion of vitreous SiO_2 to crystalline SiO_2 (cristobalite) or physically disrupt the vitreous silica film.

The selection of potential silicide coating compositions for use on tantalum alloys has been largely emperical in the past. Inclusion of various quantities of groups IV, V and VI metals in a coating was known to produce complex and refractory silicides which might oxidize to produce a continuous and protective surface layer of SiO_2. The inclusion in the coating of such potential glass forming elements as cobalt, iron and manganese (Ref. 13) has been shown to greatly enhance the glass forming tendencies of some compositions. Outstanding lifetimes have been achieved with these coatings at temperatures up to about 1700° K. Unfortunately, the metal oxide/SiO_2 systems for iron, manganese and cobalt display eutectic temperatures of 1453, 1524 and 1655° K, respectively, and may limit use of such a coating to low velocity conditions at temperatures much above the respective oxide eutectic temperatures. Considerable mobility for iron-containing glasses was observed in the early phases of this work.

A solution to the above potential problem and a method for reducing consumption of the disilicide was achieved in the present program when highly refractory and stable glasses were developed for application over silicide coatings. Outstanding protection and reliability were achieved by a glass overlaid silicide coating when tested at 1700° K and over the 13 N/m^2 to atmospheric pressure range. Visual absence of opaque oxide phases (TiO_2, Cr_2O_3) in the applied glass layer, plus slower oxidation kinetics and greater MSi_2 retention for vitreous overlaid vs plain silicide coated samples showed that the glass overlay decreased the silicide coating response to the test conditions.

The initial products of oxidation of a coating are determined by the original coating surface composition and will, therefore, include nonvolatile metal oxides. The general reaction is

$$MSi_2 + O_2 \rightarrow M_xO_y + SiO_2$$

and necessarily consumes some disilicide.

Once a coherent SiO_2 film has formed, disilicide is consumed at a rate controlled either by inward oxygen diffusion through the silica layer or by outward silicon

diffusion through a developing subsilicide (M_5Si_3) layer between the MSi_2 and SiO_2. The great benefit derived from an intentionally applied glass overlay on a silicide coating is the elimination of the rapid MSi_2 oxidation which occurs before a silica film can be established and grown to a substantial thickness. In effect, the kinetics normally observed only after long-term exposure are immediately impressed on the coating. A further benefit is that the presence of metal oxides included or dissolved in the developing silica layer is reduced. This offers the possibility for reducing the rate of oxygen diffusion through the silica film. Metallographic and X-ray diffraction analyses confirmed that fewer coating metal oxides were present in the applied than in the "natural" glass layer.

5

CONCLUSIONS

The program goal was development of a fused slurry silicide coating which could protect the 90Ta-10W alloy through 100 atmospheric re-entries to 1700 or 1810° K. Following are specific conclusions relative to the coating system performance:

- It was necessary to develop a coherent glassy oxide over the silicide coating in order to achieve significant protection at 1700° K.
- The glass overlaid silicide coating exceeded 100 low-pressure, slow cycles to 1700° K at a pressure of either 13 or 1300 N/m^2. No specimen with a glass overlay experienced a failure in less than 100 cycles.
- At 1700° K and at both pressure levels, the SA-13 silicide coating without glass overlay was able to provide a range of lives from 20 to 98 cycles.
- Neither the plain nor overlaid SA-13 silicide coating was able to withstand the 1810° K, 13 N/m^2 low-pressure, slow-cycle test conditions.
- At 1810° K, 1300 N/m^2, the SA-13 coatings have a probable life average of near 40 cycles, while the overlaid silicide lives were much less.
- Vitreous overlaid silicides provided protection for a miniature heat shield panel for 50 simulated atmospheric re-entries at 1700° K and either internal or external pressure conditions.
- Post-test tensile strengths based on residual substrate area were equal to or greater than values for the unexposed alloy.

REFERENCES

1. Shoemaker, H. E. and Stetson, A. R., "Silicide Coatings for Tantalum and Columbium Alloys", NASA-Lewis Research Center, NASA-Cr-72519, August 1969.

2. High-Temperature Oxidation-Resistant Coatings, prepared by Committee on Coatings, National Materials Advisory Board, Div. of Engineering, National Research Council, National Academy of Sciences/National Academy of Engineering, Washington, D.C., 1970.

3. Priceman, S. and Sama, L., "Development of Fused Slurry Silicide Coatings for the Elevated Temperature Oxidation Protection of Columbium and Tantalum Alloys", Technical Report AFML-TR-68-210, December 1968.

4. Fitzgerald, B. G., "Fused Slurry Silicide Coatings for Columbium Alloy Re-Entry Heat Shields", Seventh Quarterly Technical Progress Narrative, NAS3-14307, April 1972.

5. Schmidt, F. F., Tantalum and Tantalum Alloys, DMIC Report 133, July 25, 1960.

6. Bartlett, R. W., "Investigation of Mechanisms for Oxidation Protection and Failure of Intermetallic Coatings for Refractory Metals - Part III", Technical Report ASD-TDR-63-753 (Sept. 1965).

7. Lynch, J. F., Ruderer, G. G., and Duckworth, W. G., "Engineering Properties of Ceramics", Air Force Materials Laboratory Technical Report, AFML-TR-66-52 (June 1966).

8. Siegal and Howell, NASA-S.P. 164, Vol. I, pg. 115.

9. Bracco, D. J., Lublin, P., and Sama, L., "Identification of Microstructure Constituents and Chemical Concentration Profiles in Coated Refractory Metal Systems", AFML TR-66-126 (May 1966).

10. Wimber, R. T., and Stetson, A. R., "Development of Coatings for Tantalum Alloy Nozzle Vanes", NASA CR-54529 (July 1967).

11. Kolodney, M. and Graff, R. A., "Fundamentals of the Oxidation Protection of Columbium and Tantalum", NASA Grant NGR 33-013-017, October 1968.

12. Packer, C. M., "Fused Slurry Silicide Coatings for Tantalum Reentry Heat Shields", Eighth Quarterly Technical Progress Narrative, NAS3-14316 (July 1972).

DISTRIBUTION

NASA Headquarters
600 Independence Avenue, S. W.,
Washington, D.C. 20546
Attn: Mr. G. Deutsch (RW)
Mr. J. Maltz (RWM)
Dr. A. O. Tishler (RP)
Mr. N. Peil (MN)
Mr. D. Gilstad (RV-2)
Mr. J. Gangler (RWM)
Mr. F. J. Demeritte (RV-1)
Mr. M. Rosch (RV-2)
Mr. J. Malament (MTG)

National Technical Information Service
Springfield, VA 22151

NASA-Lewis Research Center
21000 Brookpark Road
Cleveland, OH 44135
Attn: Contracts Section B (MS 500-313)
Library (MS 60-3)
Patent Counsel (MS 500-311)
Report Control Office (MS 5-5)
Technology Utilization (MS 3-19)
Mr. G. M. Ault (MS 3-13)
Mr. J. P. Merutka (MS 49-1)
Mr. W. D. Klopp (MS 105-1)
Mr. S. S. Manson (MS 49-1)
Mr. R. W. Hall (MS 105-1)
Mr. S. J. Grisaffe (MS 49-1)
Mr. N. T. Saunders (MS 105-1)

NASA Representative
Scientific and Technical Information
Facility
Box 33
College Park, MD 20740

NASA-Langley Research Center
Langley Field, VA 23365
Attn: Dr. J. Buckley (MS 206)
Dr. R. A. Anderson (MS 188)
Mr. B. Stein (MS 188-A)
Library (MS 185)

Mr. W. Reihl
S+E-ASTN-MX Bldg. 4612
Marshall Space Flight Center
Huntsville, AL 35812

Mr. C. E. Cataldo
S+E-ASTN-M
Marshall Space Flight Center
Huntsville, AL 35812

Library
NASA-Marshall Space Flight Center
Huntsville, AL 35812

Library-22-3. Reports
NASA - Ames Research Center
Moffett Field, CA 94035

Library
NASA-Goddard Space Flight Center
Greenbelt, MD 20771

Library
NASA Flight Research Center
P. O. Box 273
Edwards, CA 93523

Library/Acquisitions
Jet Propulsion Laboratory
4800 Oak Grove Drive
Pasadena, CA 91102

DISTRIBUTION (Cont'd)

Technical Library, Code JM6
NASA-Manned Spacecraft Center
Houston, TX 77058

Mr. E. Bartlett
Battelle Memorial Institute
505 King Street
Columbus, OH 43201

Mr. N. Geyer
AFML/LLP
Headquarters
Wright Patterson AFB, OH 45433

Mr. L. K. Crockett
Space Division
North American Rockwell
12214 Lakewood Blvd.,
Downey, CA 90241

Mr. J. R. Williamson
AFM/LLP
Wright-Patterson AFB, OH 45433

Mr. R. A. Nau
General Dynamics Corporation
P. O. Box 1128
San Diego, CA 92112

Mr. L. Mead
Grumman Aerospace Corporation
Plant 25
Bethpage, NY 11714

Mr. C. S. Deneen
Martin-Marietta Corporation
815 Connecticut Ave., N. W.
Washington, DC 20006

Mr. R. Perkins
Lockheed Palo Alto Research Laboratory
3251 Hanover Street
Palo Alto, CA 94304

Mr. E. F. Styer (MS/8K-93)
The Boeing Company
P. O. Box 3999
Seattle, WA 98124

Mr. B. Black (MZ 641-30)
Convair Aerospace Division
P. O. Box 1128
San Diego, CA 92112

Mr. S. Musikant, U1237
General Electric Company
P. O. Box 8555
Philadelphia, PA 19101

Dr. J. Colwell
Aerospace Corporation
P. O. Box 95085
Los Angeles, CA 90045

Mr. L. A. Harris
Space Division
North American Rockwell
12214 Lakewood Blvd.,
Downey, CA 90241

Mr. L. G. St.Leger, ES-8
Bldg. 13, Room 116
NASA-Manned Spacecraft Center
Houston, TX 77058

DISTRIBUTION (Cont'd)

Mr. H. K. Larson, MS 234-1
NASA-Ames Research Center
Moffett Field, CA 94035

Mr. W. H. Goesch
AFDL, Code FDTS
Wright Patterson AFB, OH 45433

Mr. T. P. Brooks (E-231)
McDonnell Douglas Corporation
P. O. Box 516
St. Louis, MO 63166

Dr. C. O. Ong
Bellcomm, Inc.,
955 L-Enfant Plaza
North, S. W.
Washington, DC 20024

Mr. L. Hjelm
AML
Wright-Patterson AFB, OH 45433

Mr. G. M. Ecord
SMD-Material Tech.
NASA-Manned Spacecraft Center
Houston, TX 77058

Mr. C. E. Tharratt
Chrysler-Space Division
P. O. Box 29200
New Orleans, LA 70129

Mr. B. Fitzgerald
McDonnell Douglas, East
McDonnell Douglas Corporation
St. Louis, MO 63166

Mr. S. J. Gerardi, Coating Engineer
Vac-Hyd. Processing Corporation
928 Engracia Avenue
Torrance, CA 90501

Technical Information Center
Aerojet Liquid Rocket Company
Sacramento, CA 95613